EARLY AGE SHRINKAGE MONITORING OF HIGH PERFORMANCE CEMENTITIOUS MIXTURES USING MONOLITHIC AND COMPOSITE PRISMS SPECIMENS

LADO RIANNEVO CHANDRA
(B.Eng)

A THESIS SUBMITTED
FOR DEGREE OF DOCTOR OF PHILOSOPHY
DEPARTMENT OF CIVIL ENGINEERING
NATIONAL UNIVERSITY OF SINGAPORE
2011

ACKNOWLEGMENTS

I would like to express my sincere thanks and appreciation to my supervisor, Associate Professor Gary Ong Khim Chye, for his invaluable guidance, constructive discussions, patience, and support throughout the course of this study.

I also like to thank my former lecturers especially Ms. Han Aylie for her valuable comments, supports and encouraging words to pursue this graduate study.

Gratification is also addressed to all the technologists of the Structural and Concrete Laboratory for their indispensable assistance in ensuring the successful completion of all laboratory experimental works.

I would also like to thank my family for their love, moral support, and encouragement throughout my life. And to my wife, Lily Setyaningsih, for her kind understanding and continuous support throughout the wonderful years of my graduate study.

Finally, I gratefully acknowledge the National University of Singapore for the opportunity and the award of research scholarship to pursue this graduate study.

May, 2011

Lado Riannevo Chandra

TABLE OF CONTENT

CHAPTER 6 CONCLUSIONS AND RECOMMENDATIONS

ABSTRACT

For the last three to four decades, the early age shrinkage of high performance cementitious mixtures has become a concern among engineers. Despite this fact, information about early age shrinkage is still not well documented in the literature. This thesis firstly focused on issue pertaining to the selection of the starting point or the "time zero" value (i.e. TZV) to be used for early age shrinkage monitoring of high performance cementitious mixtures cured under sealed and unsealed curing conditions.

Following the issue of TZV for early age shrinkage monitoring, an improved image analysis technique capable of monitoring early age shrinkage strains with respect to the depth from the top surface of cementitious prism specimens during the first 24 hours after adding water to the mixture was described in the present study. The improved image analysis technique can be applied for either sealed prism specimens (generally used for autogenous shrinkage monitoring) or unsealed prism specimens (typical of those used for early age drying shrinkage monitoring) with acceptable accuracy.

Once the improved image analysis technique was established, the technique was used to investigate the influence of some constituent materials and mixture properties such as superplasticizers, water-to-cementitious ratio, aggregate volume, and silica fume on the development of shrinkage strains within prism specimens exposed to a dry environment from an early age.

With the knowledge of early age shrinkage strains monitored on monolithic prism specimens, the study was extended to investigate the influence of substrate preparation on the early age shrinkage strains and cracking (de-lamination) during the first 24 hours after adding water to the mixture of newly cast cementitious materials in composite prism specimens. The findings provide a better understanding of early age shrinkage of high performance cementitious mixtures cast either as a monolithic or as a two layer composite prism specimen.

Keywords: Early age shrinkage at various depths, Time zero value, Image analysis, Bonded-concrete overlay, High performance cementitious mixture, Cracking, De-lamination

LIST OF TABLES

LIST OF FIGURES

Chapter 1 INTRODUCTION

1.1 Background and Motivation

Over the last three to four decades, many improvements have been made in concrete technology in order to meet the increasing demands of material performance, one of which is the introduction of enhanced cementitious mixtures also known as High Performance Cementitious Mixtures (HPCM) or High Performance Concrete (HPC). The advantages of using High Performance Cementitious Mixtures are widely acknowledged. The use of HPC in high rise buildings will increase the lateral stiffness and reduce the deflection of these buildings, thus providing more comfort level for the occupants. In addition, the use of HPC on building construction is also preferable due to the higher strength/weight ratio. A reduction in overall building weight makes it possible to build on soils with marginal load-carrying capacities.

Despite these advantages, durability issues of high performance cementitious mixtures have become a concern among engineers. Both practical and laboratory studies have shown that high performance cementitious materials are more susceptible to cracking during the early ages. This early age cracking may greatly compromise the performance of a concrete structure, both aesthetic performance and overall service life performance. While the cause of such early age cracking can be numerous, for example improper design and overloading during the early ages, one major cause of this early age cracking is early age shrinkage. Studies have shown that a significant amount of shrinkage strains was generated during the early ages after casting of such high performance cementitious mixtures [Aïtcin (2001)]. The relatively significant amount of early age shrinkage strains in conjunction with several factors, such as high degree of restraint and other relevant material properties, might cause early age cracking. In addition, it is widely known that the cracking risk of cementitious elements increases when they are exposed to a dry environment at an early age. Although it is generally accepted that the influence of drying at early ages can be eliminated by proper handling and curing techniques, it is often difficult to provide an ideal curing environment for cementitious materials in practice. This phenomenon is

also important in the case of high performance cementitious mixtures. A typical high performance cementitious mixture is expected to be more susceptible to early age cracking when exposed to a dry environment at an early age.

With increasing awareness of early age shrinkage, some issues are still contentious. These include disagreement on a globally accepted standard procedure and on the starting point or the time zero "value" (i.e. TZV) for commencement of early age shrinkage monitoring. On top of this, early age shrinkage is also of concern when high performance cementitious mixtures are utilized as overlays in repair work. In the following section, brief descriptions relating to some of these contentious issues are presented. More detailed literature review relevant for the specific issue of early age shrinkage monitoring of high performance cementitious mixtures is provided at the beginning of each chapter.

1.1.1 Early Age Shrinkage of Cementitious Material

The exact interpretation of "early age" for the whole range of cementitious materials may vary tremendously depending on the context and the purpose of study. With reference to early age shrinkage, the term "early age shrinkage" of cementitious material may refer to volume changes occurring immediately after placing of the cementitious mixture up to about 24 hours thereafter [Holt and Leivo (1999), Kyaw (2007)]. This period of time, as shown in *Figure 1.1* and *Figure 1.2*, includes the time when the cementitious material is still fluid and workable (i.e. plastic stage), the transition stage when it experiences stiffening and initial hardening due to cement hydration, and finally the hardening stage when appreciable mechanical strength continues to develop in the cementitious material [Mehta and Monteiro (1993), Schindler (2004)].

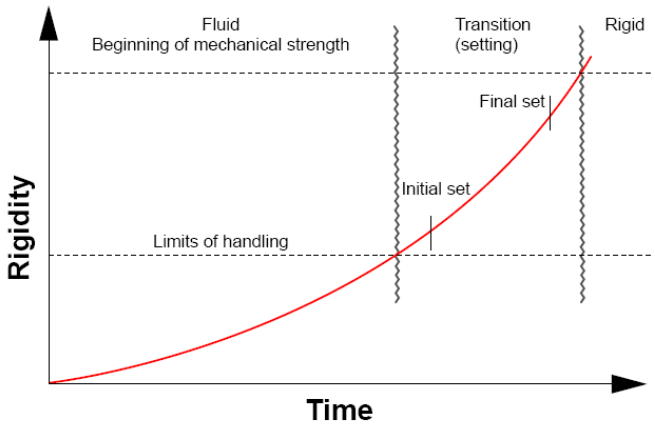

Figure 1.1 Early age stages of cementitious material according to Mehta and Monteiro (1993)

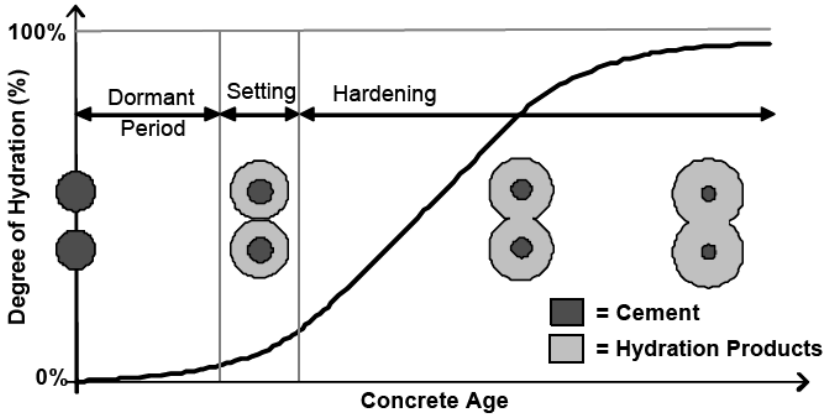

Figure 1.2 Early age stages of cementitious material based on the assessment of degree of hydration [Schindler (2004)]

Volume change of cementitious material itself consists of many types; chemical shrinkage, autogenous shrinkage, early age settlement, drying shrinkage, plastic shrinkage, and thermal deformation. Among these volume changes, autogenous shrinkage, drying shrinkage (i.e. plastic shrinkage), and thermal deformation are the most common types of volume changes encountered during the early ages. Autogenous shrinkage is generally defined as apparent volume change due to hydration process while drying shrinkage or plastic shrinkage is defined as apparent volume change due to moisture loss to the environment. Thermal deformation, on the other hand, is defined as volume changes that occur when the cementitious mixture undergoes temperature fluctuations. It is important to note that these volume changes can occur simultaneously and the effect of these volume changes may affect and mutually interact with

each other during the early ages. Hence, some researchers often resort to referring early age shrinkage strains monitored in a test specimen as "total early age shrinkage strains" of the cementitious material being tested. [Holt and Leivo (1999), Kyaw (2007)].

1.1.2 Time Zero Value

As mentioned previously, the starting point or the "time zero" value (i.e. TZV) to be used for early age shrinkage monitoring is not well defined in the literature [Weiss (2002), Kyaw (2007)]. In most early age shrinkage studies, the TZV used would depend on either the purpose of the study or on the limitations of the testing equipment utilized. As a result, different TZV are used and a meaningful comparison between different materials and between various studies for seemingly similar cementitious mixture is difficult to be performed. Thus a rational approach to identify a suitable TZV for use especially for early age shrinkage monitoring of high performance cementitious mixtures is needed.

1.1.3 Technique for early age shrinkage monitoring

For shrinkage monitoring of cementitious materials, standard apparatus and procedure for long-term shrinkage strain monitoring are well defined in ASTM-C490-04 (2004) and ASTM-C157/C157M-04 (2004) respectively. On the other hand, in the case of early age shrinkage monitoring, various researchers had used a number of different specimen sizes, shapes and gauge lengths [Holt (2001), Al-Amoudi et al. (2006), Jensen and Hansen (1996), Ishikawa et al. (2000)]. In addition, early age drying shrinkage monitoring of cementitious mixtures is also prone to difficulties associated with instrument limitations. It is important to note that early age drying shrinkage has been reported to exhibit behavior similar to long term drying shrinkage in that it varies with depth from the exposed surface [Neville (2003), Ong and Kyaw (2006)]. Despite this fact, most of the linear measurement technique in use at present time can only provide an "average" value of the early age drying shrinkage strain across the whole cross section of the specimen. This is likely to compromise quantitative comparison between results reported by a number of researchers dealing with early age shrinkage measurement.

1.1.4 Early age drying shrinkage monitoring

As mentioned previously, the loss of moisture from the cementitious mixtures due to evaporation would increase early age shrinkage of such high performance cementitious mixtures. For a typical cementitious specimen, the moisture loss usually start from the top exposed surface and progresses into the interior of the high performance cementitious mixtures depending on the inherent mixture properties and the relative humidity, temperature, wind speed prevailing in the surrounding environment. This loss of moisture is expected to cause different shrinkage strains to be registered along the depth of the specimen with higher shrinkage strains being monitored at the surface. This situation may eventually increase the risk of cracking of such mixtures.

A review of available studies shows that research on the variation of shrinkage strain with respect to the depth from the top exposed surface of cementitious specimens during the first 24 hours after adding water to the mixture is very limited, particularly those cast using high performance cementitious mixtures. The variation of shrinkage strains within the cementitious specimens were typically monitored after having undergone a period of curing [Kim and Lee (1998), Al-Saleh and Al-Zaid (2006)]. Thus technically they miss out monitoring of shrinkage strains developed during the first 24 hours after adding water to the mixture.

1.1.5 Early age shrinkage of composite system

As mentioned previously, casting a new cementitious layer on the top of old concrete substrate is frequently applied in the area of concrete repair and retrofitting. In such composite systems, unlike typical monolithic systems, the differences in the shrinkage strains that develop near the top surface and at the interface between the hardened substrate and newly cast cementitious layer may result in tensile stresses being developed within the newly cast cementitious layer. These stresses may lead to cracking of the newly cast cementitious layer or delamination (i.e. debonding) at the interface between the hardened substrate and the newly cast cementitious layer. Although performance of composite systems has been studied extensively in

the literature [Wall and Shrive (1988), Austin et al. (1995), Xu (1999), Climaco and Regan (2001; Kyaw (2007), Bisschop and van Mier (2002), Kim and Weiss (2003), Pease et al. (2004), Kyaw (2007), Banthia and Gupta (2009)], the development of early age shrinkage strains occurring during the first 24 hours after adding water to the mixture of the newly cast cementitious mixtures cast on top of the hardened substrate has not been fully explored and investigated.

1.2 Objectives and Contribution

The objective of this thesis is to obtain a better understanding of early age shrinkage of high performance cementitious mixtures monitored through tests conducted on monolithic and composite prism specimens. Several issues dealing with early age shrinkage of high performance cementitious mixtures are addressed. More specifically, the objectives of this study are:

1. To provide an overview pertaining to the selection of TZV and to recommend a rational approach to select a suitable TZV for early age shrinkage monitoring of high performance cementitious mixtures under two test conditions; sealed and unsealed conditions.
2. To review the existing techniques for monitoring early age shrinkage strain with emphasis on early age drying shrinkage in order to provide a better understanding of early age shrinkage development of cementitious materials particularly within the first 24 hours after water is added to the mixture.
3. To investigate and quantify the early age shrinkage strains in high performance cementitious mixtures with respect to the depth during the first 24 hours after adding water to the mixture, especially for specimens exposed to early age drying conditions. Several key parameters that affect early age shrinkage strain including: the water-to-cementitious ratio of the mixtures, the inclusion of chemical admixtures, the aggregate volume, and the inclusion of supplementary cementitious materials (SCMs) will be indentified for tests conducted on prism specimens.

4. To investigate the effect of substrate preparation on the early age shrinkage strains and cracking (i.e. delamination) during the first 24 hours after adding water to the mixture of newly cast cementitious materials in composite prism specimens.

The finding of this research is expected to provide better understanding of early age shrinkage of high performance cementitious mixtures both in monolithic or composite systems. Moreover, the results could provide useful information for the estimation of stress and cracking due to early age shrinkage strains.

The research presented here is limited to high performance cementitious mixtures cast with normal Type I OPC used in relatively thin concrete specimens. Although the effects of early age shrinkage are also important in thick / mass concrete structures, they are not within the scope of the present study.

1.3 Organization of Thesis

This thesis consists of 6 chapters. As mentioned previously, a brief introductory section associated with the early age shrinkage monitoring, including the objectives of the present investigation was presented in Chapter 1. More detailed literature review relevant for the specific issue of early age shrinkage monitoring of high performance cementitious mixtures is provided at the beginning of each chapter.

In Chapter 2, a rational approach for selecting the starting time for early age shrinkage monitoring or the "time zero" value (i.e. TZV) was reviewed. The TZV determination based on assessment of the S-wave reflection loss at the interface between steel plate and cementitious materials was also presented in this chapter along with an assessment of stiffening time with respect to the depth from the top surface of both sealed and unsealed mortar specimens.

Chapter 3 discussed the technique for monitoring early age shrinkage strain with emphasis on plastic or early age drying shrinkage monitoring. Several techniques were reviewed and an improved image analysis technique for monitoring early age shrinkage with respect to

the depth from the top surface during the first 24 hours after adding water to the mixture was presented in this chapter.

In Chapter 4, an experimental study on the effect of several mixture constituents on the development of early age shrinkage strains with respect to the depth from the top exposed surface during the first 24 hours after adding water to the mixture was presented and discussed.

Chapter 5 presents an investigation of early age shrinkage strains of a newly cast cementitious layer in composite prism specimens during the first 24 hours after adding water to the mixture. The influence of substrate surface preparation and its moisture condition on the new cementitious layer was investigated along with an assessment of early age cracking and de-lamination by means of an image analysis approach.

Finally, a summary of the main findings in this investigation along with the suggestions for future research were given in Chapter 6.

Chapter 2 TIME ZERO VALUE FOR EARLY AGE SHRINKAGE MONITORING BASED ON S-WAVE REFLECTION LOSS MEASUREMENT

2.1 Introduction

During the past two decades, the importance of early age shrinkage in high performance cementitious materials have been reported in numerous studies [Springenschmidt et al. (1994), Jensen and Hansen (1996), Tazawa and Miyazawa (1999), Holt (2001), Aïtcin (2001), Weiss (2002), Zhang et al. (2003), Bjøntegaard and Sellevold (2004), Kaufmann et al. (2004), Ong and Kyaw (2006), Sant et al. (2006), Esping (2007), Kyaw (2007), Wong et al. (2007)]. Along with the acknowledgment of the importance of early age shrinkage, one important issue that still remains open for discussion is the starting point or the "time zero" value (i.e. TZV) to be used within the timeline along which early age shrinkage occurs. Earlier studies by Aïtcin (1999), Weiss (2002), and Sant et al. (2006) showed that the actual starting time used could influence the measured response and may substantially underestimate the magnitude of shrinkage strains monitored. Moreover, Weiss (2002) also reported that the difference in the TZV used is likely to account for the disparity in the magnitude of the early age shrinkage strains for seemingly similar cementitious mixtures reported in the literature.

Currently, there is no general agreement on the time from which early age shrinkage monitoring should start [Weiss (2002), Kyaw (2007)]. Some researchers such as Tazawa and Miyazawa (2001) and Bjøntegaard et al. (2004) followed the Japan Concrete Institute's (JCI) recommendation to use the initial setting time obtained by the penetration test as the TZV for shrinkage measurement. Others, depending on the capability of the test set-up used, specify the "time zero" value either at a suitable time (e.g. 30 minutes after adding water to the mix, time just after placing, etc.) [Jensen and Hansen (1996), Kaufmann et al. (2004), Ong and Kyaw (2006), Sant et al. (2006), Esping (2007), Wong et al. (2007)] or at the time when quantifiable strains are being registered in the measurement sensors. Examples of the latter include

restrained shrinkage test set-up [Springenschmidt et al. (1994)] and free shrinkage monitoring using embedded strain transducers [Zhang et al. (2003)].

The difference in the TZV used makes comparison between various studies difficult to perform. Therefore, the present study aims to provide an overview of the selection of TZV and to recommend a suitable TZV for early age shrinkage monitoring of high performance cementitious mixtures under two test conditions; sealed and unsealed conditions.

According to earlier studies by Holt (2001) and Kyaw (2007), two possible TZV can be adopted, based on whether the emphasis is on a "materials" or "structural" perspective. From the "materials" perspective it is preferable to start the early age shrinkage monitoring as soon as mixing is completed or from the onset of hydration. On the other hand, from the "structural" perspective, it is generally agreed that early age shrinkage measurements are meaningful only when the shrinkage strains lead to quantifiable stresses induced within the cementitious specimens (i.e. the time when the cementitious materials start to set or stiffen).

In the determination of TZV for early age shrinkage monitoring from both the "materials" and "structural" perspective, it is necessary to examine the cementitious material's setting and hardening development with time. As far as the setting and hardening behavior of cementitious materials is concerned, a number of techniques for monitoring the setting of cementitious materials have been investigated over the years [Weiss (2002)]. However, it is important to note that each technique has its own advantages and disadvantages in describing the stiffening time of cementitious materials during the early ages. The following sections will discuss several techniques used to monitor the stiffening time of cementitious materials, noting each advantage and disadvantage, as well as its ability to pinpoint the TZV for early age shrinkage monitoring.

2.2 Various Techniques Available for Monitoring Stiffening Behavior of Cementitious Materials

2.2.1 Penetration Resistance Test

The penetration tests ASTM-C191 (2004) and ASTM-C403/403M (2008) for cement paste and concrete mortar respectively) are the most widely used method for determining the setting time of cementitious materials. In the penetration resistance test (i.e. ASTM-C403/403M (2008)), the setting and hardening time of cementitious materials are specified based on the change in the penetration resistance of cementitious specimen with respect to time. The setting known as the initial setting time is regarded as the time at which the penetration resistance reaches a value of 3.4 MPa (500 psi). While the hardening time, also known as the final setting time, occurs when the penetration resistance reaches a value of 27.6 MPa (4000 psi).

Despite the standardization of the penetration resistance test, some differences on concrete stiffening time were addressed by various researchers. For example, The British Standard Institute BS 5075 defined the limit for placing and compacting of concrete at 0.5 MPa (72 psi). Another study by Abel and Hover (2000) observed that the time to begin finishing operations, which in practice was determined as the time when the boot of an adult male left an imprint approximately 6 mm deep in a fresh concrete surface, occurred at a penetration resistance of approximately 0.1 MPa (15 psi). In addition, Bury et al. (1994) observed that a finishing operations on concrete slabs performed using finishing machine were understood to start as soon as the measurable values of penetration resistance were obtained on companion mortar specimen. These evidences suggest that stiffening time started sooner than the time corresponding to the initial setting time as specified by ASTM-C403/403M (2008). Based on several evidences aforementioned, the initial and final setting time can be accepted as arbitrary points that only serve as a convenient reference points for determining the relative rates of hardening of mortars from different concretes both at the early and later stages [Christensen (2006)]. Although these points are useful for determining the effect of variables such as temperature, type of cement, mixture proportions, and an addition of admixtures upon the time of setting and hardening characteristic of the mortar; these points might not give the exact time

at which cementitious material develop its stiffness. Another major drawback of the penetration resistance test is the need to perform wet-sieving process in order to obtain the mortar phase from the concrete mixtures. The mortar phase sieved might have slightly different setting behavior from the corresponding concrete mixtures. In addition, the mortar fraction wet-sieved from concrete does not have a common initial stiffness which varies with the w/c ratio and sand content. Thus, these point might not suitable for pinpoint the "time zero" value for early age shrinkage measurement.

2.2.2 Heat Evolution Method

Hydration process of cement is an exothermic process which heat is liberated by the system. The typical rate of heat liberated by cement hydration is shown in *Figure 2.1*. Based on the rate of heat evolution, five stages have been defined in the literature.

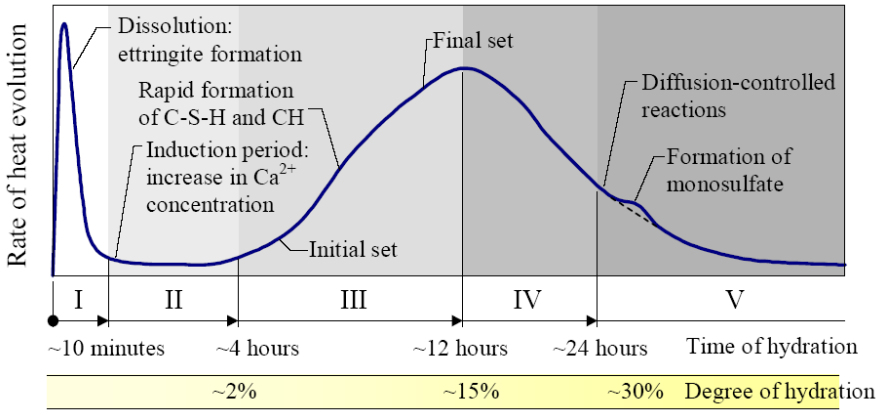

Figure 2.1 Schematic representation of heat evolution during hydration of cement and water, based on Gartner et al. (2001).

In the heat evolution method, it is generally assumed that the stiffening time corresponds closely with a point that occurs near the transition between dormant (stage II) to acceleration period (stage III). While the hardening time (final setting time), is considered to occur somewhere around the peak experienced in acceleration (stage III) and deceleration periods (stage IV). Instead using calorimeter, the simplest approach to assess the heat evolution in cementitious materials is by monitoring the temperature development as a function of time through a thermocouple embedded inside the cementitious specimen. Using this temperature

development, Christensen (2006) and Meddah et al. (2006) pointed out the correlation between the derivatives of temperature development to the setting or the stiffening time of the tested cementitious materials. Christensen (2006) found that the peak in the second derivative occurs earlier than the initial setting time monitored by ASTM-C403/403M (2008) and it seems to correlate better with the time when the penetration test achieving a value of 1.25 MPa (200 psi). While Meddah et al. (2006), on the other hand, correlates the peak in the first derivative to the solid percolation or the stiffening time of the tested concrete mixture. Despite this correlation, Weiss (2002) pointed out that although the heat evolution method provides information regarding the hydration kinetics; it is not specifically related to a measure of structural properties.

2.2.3 Volume Change Measurement

Other methods for determining the TZV for early age shrinkage monitoring is by performing volume change measurement. Currently two approaches are adopted. The first approach is based on the free shrinkage measurement, while the second approach is based on the stress development in the restrained shrinkage measurement.

On the first approach, the TZV for early age shrinkage monitoring is determined from the measurement of chemical and autogenous shrinkage. Chemical shrinkage is defined as the reduction in the absolute volume of the final product due to hydration reaction while autogenous shrinkage is defined as the reduction of the external (i.e. apparent) volume of cementitious materials. Hammer (1999), Boivin et al. (1999) and Holt (2002) have independently illustrated that at early age the chemical shrinkage and autogenous shrinkage measurements are reasonably similar. As the cementitious material hydrates and forms solid skeleton, the autogenous shrinkage starts to deviate from the chemical shrinkage. The time at which the deviation starts to occur corresponds to the "suspension-solid transitions" as well as the TZV for early age shrinkage measurement. Although this approach is appealing, a major drawback of this approach is that the measurement of the chemical shrinkage can only be performed on cement or binder paste without the inclusion of aggregates.

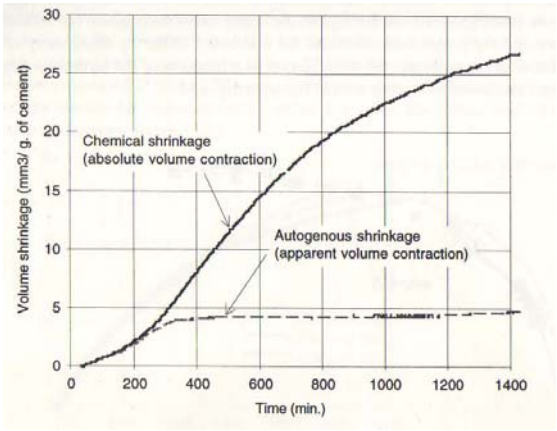

Figure 2.2 Comparison of chemical shrinkage and autogenous shrinkage (Boivin et al. (1999))

As mentioned previously, the second approach to define the TZV for early age shrinkage monitoring is by measuring the stress development in the restrained shrinkage test. On the restrained shrinkage test, a load required to bring back the cementitious specimen into its original length is monitored with time. Thus based on the load (i.e. stress) monitored, the TZV for early age shrinkage monitoring is determined to the time at which the compressive or tensile stresses started to develop in the cementitious specimen. Nevertheless, Weiss (2002) noted two difficulties for using the restrained shrinkage test for determining the TZV. The first difficulty deals with the mass of the test frame, friction and slip at the end grips due to a relatively soft concrete at the early ages. The second difficulty corresponds to the treatment of bleed water. Previous study by Bjøntegaard and Sellevold (2000) showed that the removal or addition of bleed water to the system can significantly alter the autogenous shrinkage.

2.2.4 Mechanical Properties Development and Degree of Hydration

Another method to observe the stiffening behavior of cementitious materials is by monitoring the development of mechanical properties such as Young's modulus, compressive strength, or tensile strength. At the early ages, shrinkage strains will cause internal stresses when appreciable magnitude of Young's modulus has developed. Thus the TZV for early age shrinkage monitoring is taken as the time at which the Young's modulus starts to increase. In order to facilitate this approach, the relationship between the Young's modulus and degree of

hydration is taken into account. An earlier study by Olken and Rostasy (1994) showed that the development of mechanical properties (i.e. Young's modulus) may begin at a critical degree of hydration (i.e. α_0). The same approach can also be used for early age shrinkage monitoring. The time at which the critical degree of hydration (α_0) occurred within the cementitious materials is considered as the TZV for early age shrinkage monitoring.

2.2.5 Electrical Technique

For the past two decades, the use of electrical method as a way to provide information regarding chemical reaction, microstructure, and chemical transport has increased significantly. An earlier work by Perez-Pena and Roy (1989) reported on the correlation between the electrical conductivity, the heat development, and microstructure changes. On the other hand, instead of monitoring the conductivity of cementitious materials, Calleja (1953) studied the correlation between the stiffening process and the electrical resistance on Portland cement and high alumina cement respectively. More recently, an improvement in the electrical resistivity measurement by using non-contacting equipment has been reported by Li et al. (2003), Wei and Li (2005), and Xiao and Li (2008). It is also interesting to note that study by Xiao and Li (2008) met with some success in measuring the bulk electrical resistivity of fresh concrete using the new apparatus. In addition, Xiao and Li (2008) also measured the cementitious pore solution resistivity with respect to time. Comparing the resistivity of bulk cementititous materials with that of the pore solution, Xiao and Li (2008) suggested that a change in the electrical resistivity during this early age is due to changes in porosity and connectivity of the cementitious materials.

Based on these studies, the development of setting and hardening in the cementitious material can be marked by two characteristic points. The first characteristic point is the onset of the hydration process as indicated by the maximum conductivity or the minimum resistivity occurring in the cementitious materials. The second characteristic point from electrical testing is the time when the change in the rate gain of electrical conductivity and resistivity occurs. It is postulated that the change in the rate gain corresponds to the rapid changes taking place in the

microstructure of the cementitious materials resulting particularly in an increase in cementitious material's stiffness.

Although the electrical testing may provide an information regarding the setting behavior of cementitious materials, it is still questionable whether the specifically identifiable points on electrical curves correspond directly with "time zero" for early age shrinkage measurement.

2.2.6 Ultrasonic Method

Similar to electrical testing, numerous studies [Keating et al. (1989),Reinhardt and Grosse (1996),Grosse and Reinhardt (2001),Rapoport et al. (2000),Voigt and Shah (2003),Subramaniam et al. (2005)] have been published on the use of ultrasonic waves to monitor the setting and hardening process of cementitious materials. Some of the techniques rely on the propagation of ultrasonic waves through the specimen while others utilize the reflection of the ultrasonic waves. For either transmission or reflection methods, a longitudinal wave (i.e. compression wave / P-wave) or a transverse wave (i.e. shear wave / S-wave) can be used.

In the transmission method, the pulse velocity and the energy of the ultrasonic waves propagating through the cementitious sample is monitored. In an earlier study on cement slurries, Keating et al. (1989) pointed out that the increase in the solid phase connectivity will determine the change in velocity of the cement paste at an early age. Further study by Reinhardt and Grosse (1996) proposed an ultrasonic device capable of monitoring the development of ultrasonic wave velocity as early as after the placing of the cementitious mixtures in the mould. This technique has been successfully used in the investigation of the setting and hardening of concrete [Grosse and Reinhardt (2001)].

On the other hand, the reflection method is based fundamentally on the phenomenon that an ultrasonic wave will be partially reflected and partially transmitted when traveling through a medium upon encountering a boundary between two mediums with different acoustic impedances. By monitoring the change in the reflection coefficient over time, previous works

by Rapoport et al. (2000), Voigt and Shah (2003), and Subramaniam et al. (2005) have demonstrated the sensitivity of wave reflection to a change in cementitious microstructure.

In ultrasonic testing techniques, similar to other techniques, the TZV for early age shrinkage based on the ability of ultrasonic techniques to determine the setting or the stiffening time of the cementitious materials. So far, two recommendations of the stiffening time based on ultrasonic assessment have been made. The first recommendation suggests that setting occurs when a specific ultrasonic wave velocity is reached within the cementitious materials, while the second recommendation relates the change in the P-wave or S-wave responses to the setting of the cementitious materials. Nevertheless, it should be noted that these times have not been used to establish the suitable TZV for early age shrinkage monitoring.

2.3 The Determination of TZV: Material and Structural Point of View

As mentioned previously, the determination of TZV for early age shrinkage monitoring can be determined based on whether the emphasis is on a "materials" or structural perspective. Comparing the TZV from the "materials" and the "structural" perspective, the latter seems more appealing due to the following:

- **Equipment capability.** Shrinkage monitoring from the onset of hydration requires the use of equipment that is sufficiently sensitive to be able to measure the small volume changes especially during the first hour or so after mixing.
- **Time Consideration.** The onset of hydration as monitored by electrical testing typically occurs within the first hour or so, sometimes as early as 20 minutes after adding water to the mixtures [Wei and Li (2005), Li et al. (2007)]. Thus there is a possibility that early age shrinkage monitoring might not be possible given the lead time needed to complete all preparatory works beforehand (i.e. time for mixing, casting, finishing and placing the specimen into the exposure chamber and experimental set-up). Moreover, when larger specimens are involved, the preparation works may take even longer time to finish.

- **Early age settlement**. During early ages when the cementitious mixture is still fluid and workable, the cementitious mixture may also register early age settlement under gravity. This early age settlement may affect the early age shrinkage measurement especially in techniques that involve the monitoring of strains along the length of specimens cast in rigid molds.

- **Stress and Cracking Development**. During the early ages, before the cementitious mixture sets or stiffens, the cementitious mixture is free to deform without inducing any appreciable stresses. However, as the cementitious mixture hardens and shrinks due to cement hydration, the rigidity (i.e. stiffness) of the cementitious mixture also begins to increase. Once a certain degree of stiffness has developed, the development of shrinkage strains may result in appreciable stresses which may lead to cracks developing. In this regards, starting early age shrinkage monitoring from the stiffening time is more preferable since this stiffening time may be used to indicate when appreciable stresses will begin to develop within the cementitious mixture caused by shrinkage effects.

2.4 Technique for Determining the Stiffening Time

Determining the stiffening time requires the selection of an appropriate technique. Two main considerations apply. First, the technique should be able to determine the stiffening time through direct access to the material or specimens without any additional procedural requirements that may affect setting and hardening behavior. Thus extracting the mortar component of a concrete mixture for stiffening time tests may not be desirable. Second, the technique should take into consideration the exposure conditions of the test specimens, which means the technique should be applicable for a variety of casting and curing conditions since early age shrinkage monitoring may be required to be performed under a range of exposure conditions, e.g. sealed or unsealed conditions.

Table 2.1 summarizes the recommendation on the stiffening time of cementitious materials based on different techniques mentioned earlier (i.e. penetration resistance test, heat measurement, volume change measurement, mechanical properties development, electrical

testing, and ultrasonic technique). It can be seen that several techniques are clearly inappropriate when benchmarked against some of conditions existing in practice. The penetration test, for example, has been reported to be operator sensitive [Christensen (2006)]. The heat measurement method is also questionable due to its lack of correlation with the development of mechanical properties of the cementitious material being tested [Weiss (2002)]. In the same way, the determination of stiffening time based on restrained volume change measurement may also be questionable due to the possible loss of grip and friction during the early ages [Weiss (2002)]. Among this list of techniques, ultrasonic testing seems to have some inherent advantages. First, ultrasonic testing offers the possibility for determining the stiffening time non-destructively and is conducted directly on the actual sample of cementitious mixture. Second, it is also possible to conduct ultrasonic testing on test samples under both sealed and unsealed curing conditions. Third, the setup of ultrasonic testing is deemed to be simpler and the method is easier to conduct under both laboratory and site conditions. Nevertheless, a number of disadvantages in the ultrasonic testing have also been reported in the literature [Popovics et al. (1990), Keating et al. (1989), Sayers and Dahlin (1993), and Aggelis and Philippidis (2004)]. Therefore, it is important that an appropriate ultrasonic technique test methodology be selected for determining stiffening time.

As mentioned previously, currently there are two recommendations to obtain stiffening time based on ultrasonic assessment. The first suggests that stiffening time occurs when a specified ultrasonic wave velocity is reached within the cementitious materials [Reinhardt and Grosse (1996), Lee et al. (2004)], while the second recommendation relates to the change in the P-wave or S-wave response when the cementitious material sets [Pessiki and Carino (1988), Boumiz et al. (1996), and Voigt et al. (2005)]. The significance of these two recommendations will be discussed in the following section.

Table 2.1 Recommendation on Stiffening Time based on various methods

Specific Stiffening Time pointed out	**Advantages**	**Disadvantages**
Penetration test ((ASTM-C191 (2004), ASTM-C403/403M (2008)))		
Initial setting time at 3.4 MPa (500 psi)	Easy to perform	1. There is a need for the wet sieving process to obtain the mortar phase. This may slightly change the stiffening behavior. 2. Reference points are arbitrary defined
Heat Evolution (Mindess et al. (2003), Meddah et al. (2006))		
1. The stiffening of cementitious materials is assumed to occur near the transition from induction (i.e. dormant) period to acceleration period. (Mindess et al. (2003)) 2. Maximum of Thermal Flux (Meddah et al. (2006))	Can be performed on paste, mortar, and concrete mixtures.	1. Provide the information on hydration kinetics but not specifically related to mechanical properties (Weiss (2002)) 2. The exact stiffening time is not well defined.
Mechanical Properties and Degree of hydration (Olken and Rostasy (1994))		
Critical degree of hydration (α_0) (Olken and Rostasy (1994))	Provides information regarding the structural / mechanical properties development.	1. The assessment of mechanical properties is often very difficult to perform, especially at early ages. 2. The assessment of degree of hydration is typically performed on paste, without the inclusion of aggregates.
Early Age Volume Change: 1. Free shrinkage test (Hammer (1999), Boivin et al. (1999) and Holt (2002))		
The stiffening time is selected to be the time when the autogenous shrinkage start to deviate from chemical shrinkage	May provide the time when the "solid skeleton" develops within the cementitious materials	Chemical shrinkage measurement may only be performed on thin paste only.
Early Age Volume Change: 2. Restrained shrinkage test (Springenschmidt et al. (1994))		
The stiffening time is assumed to be the time when compressive or tensile stresses start to occur within the specimen.	May provide the exact time when the stresses are induced within the materials.	Friction and loss of grip during the early ages are possible. (Weiss (2002))
Electrical (Li et al. (2003), Wei and Li (2005), and Xiao and Li (2008))		
1. Maximum conductivity or minimum resistivity is regarded as the beginning of hydration process. 2. Stiffness of cementitious materials is expected to develop rapidly when the rate gain of conductivity or resistivity is increased	1. May provide the exact time when the hydration process starts. 2. Non-destructive in nature 3. Can be applied for various types of cementitious materials	1. Considered difficult to perform 2. The rapid change in the rate of conductivity or resistivity typically occurs after the final setting time.
Ultrasonic : P-wave (Pessiki and Carino (1988), Reinhardt and Grosse (1996), Lee et al. (2004), Popovics et al. (1990), Keating et al. (1989), Sayers and Dahlin (1993), Aïtcin and Neville (2003), Aggelis and Philippidis (2004))		
1. The stiffening time is regarded as the time when the P-wave start to increase. (Pessiki and Carino (1988)) 2. The stiffening time corresponds to the time when specific P-wave velocity is achieved. (Reinhardt and Grosse (1996), Lee et al. (2004))	1. Non–destructive in nature 2. Can be applied for various types of cementitious materials 3. Can be used for various exposure conditions 4. Widely available	P-wave velocities may be affected by several factors, such as: 1. Internal densification due to aggregate settlement 2. Wave attenuation 3. The extensive use of chemical admixtures.
Ultrasonic : S-wave (D'Angelo et al. (1995), Boumiz et al. (1996), Rapoport et al. (2000), Voigt et al. (2005))		
1. The stiffening time is regarded as the time when the first S-wave can be transmitted through the cementitious materials. (Boumiz et al. (1996)) 2. The stiffening time is regarded as the time when the reflection of S-wave starts to decrease. (Voigt et al. (2005))	1. Shear wave does not propagate through liquid or gas; only propagate through solid medium 2. Can be applied for various types of cementitious materials 3. Can be applied for various exposure conditions	May be affected by the wave attenuation.

From the perspective of the first recommendation in the ultrasonic testing technique, specifying a certain wave velocity to indicate setting of the cementitious material needs to take into account the wave propagation in the cementitious mixture progressing from a fresh state to a hardened state. It is well known that cementitious materials are considered as dispersive mediums in which the ultrasonic wave velocity is affected by many parameters, such as: ultrasonic frequency, air content, aggregate content, and aggregate size. A study by Popovics et al. (1990) reported that ultrasonic waves with higher frequency attenuated more in cementitious materials, especially at early ages. Other studies by Keating et al. (1989) and Sayers and Dahlin (1993) showed that the presence of air bubbles have a significant effect in reducing the longitudinal ultrasonic waves velocity. A more recent study by Aggelis and Philippidis (2004) also reported that sand content and size significantly influence the ultrasonic wave velocity in cementitious materials especially during a fresh state. Moreover, it is important to note that the specific ultrasonic velocity to be used to indicate the stiffening time is based on correlations with the initial setting time obtained via the penetration test which is rather operator sensitive. Thus selecting a value of ultrasonic wave velocity for benchmarking might not be appropriate as a reliable indicator of stiffening time of the cementitious material being tested especially if the exposure environment is not constant.

The second recommendation in ultrasonic testing technique utilizes the change in the P-wave or S-wave responses to indicate setting of the cementitious materials. This can be when an increase in the ultrasonic P-wave velocity occurs [Pessiki and Carino (1988)], when the ultrasonic S-wave is first detected [Boumiz et al. (1996)], or when an increase in the S-wave reflection loss is noted [Voigt et al. (2005)]. In the case of monitoring an increase in the ultrasonic P-wave velocity, available data in the literature suggest that this approach faces several challenges. First, the time when the P-wave velocity starts to increase is sometimes difficult to identify due to severe wave attenuation when propagating through fresh cementitious materials [Pessiki and Carino (1988)]. Second, the increase in the P-wave velocity during the first few hours after adding water to the mixture can only be attributed to the formation of ettringitte and calcium hydroxide that may have little or no influence on the stiffening process

[Aïtcin and Neville (2003)]. Third, internal settlement of the solid particles (e.g. cement particles and sand) due to gravity may also create a denser microstructure without significant bond between the individual particles which may provide a path for the ultrasonic waves to propagate [Voigt et al. (2005)]. Fourth, identification of the time when the P-wave velocity increases is sometimes difficult especially in the case of low water-to-cementitious ratio mixtures with added high-range water reducing admixture (HWRA) [Lee et al. (2004)]. The shorter distance between solid particles (i.e. cement and aggregates) in low water-to-cementitious ratio mixes with significant retardation effect due to HWRA causes a rather slow, gradual and prolonged increase in P-wave velocities without a clear transition point.

Instead using the P-wave, some researchers have study the relation between ultrasonic S-wave and the setting of cementitious materials [Rapoport et al. (2000), Boumiz et al. (1996), D'Angelo et al. (1995)]. Earlier work by D'Angelo et al. (1995) in the monitoring of S-wave propagation through cementitious materials reported that the S-wave is more sensitive than P-wave to solid particles connectivity. However, precise monitoring of the S-wave onset time is also prone to attenuation problem. Boumiz et al. (1996) stated that although the cementitious materials develop non-zero shear modulus at the solid percolation boundaries, the severe wave attenuation when propagating through the fresh cementitious materials might mask detection of the very first shear waves. On the other hand, monitoring the S-wave development via reflection technique as reported by Rapoport et al. (2000) seems to be more promising. Since S-wave does not propagate through a fluid or gaseous media, during the period of time which cementitious material is still fluid and workable, the S-wave transmitted will be fully reflected and reflection loss would be equal to zero. As hydration proceeds, the bonds between cement particles occur within the cementitious material. Consequently, the S-wave starts to propagate through the inter-connected solid particles (i.e. cement particles and aggregates) and simultaneously, the S-wave reflection loss starts to increase.

In summary, the S-wave reflection loss technique is a suitable for determining the time when the bonding of the cementitious particles occur (i.e. stiffening time) especially for low w/c ratio mixtures. Considering several criteria that have been mentioned earlier, the S-wave

reflection loss can be applied directly on various cementitious materials being tested from paste to concrete mixtures. In addition, it is also possible to extend the S-wave reflection loss technique to obtain stiffening time to be used as the TZV within the timeline along which early age shrinkage of cementitious materials occurs under both sealed and unsealed curing conditions.

2.5 Shear Wave Reflection Loss

Earlier application of the S-wave reflection technique was reported by Stepisnik et al. (1981). The reflection coefficient of S-wave was shown to be a sensitive indicator of the hydration behavior of the cement paste at early ages. Further study by Rapoport et al. (2000) and Subramaniam et al. (2005) attempted to investigate the correlation between the S-wave reflection coefficient and the setting time via the penetration resistance test. More recently, more comprehensive studies on the use of S-wave reflection loss to describe the chemical and physical parameters of cementitious materials was reported by Voigt et al. (2005).

2.5.1 Principles of Shear Reflection Loss

The S-wave reflection technique is principally based on the phenomenon that the S-wave will be partially reflected and partially transmitted upon encountering a boundary between two mediums with different acoustic impedances. In the S-wave reflection technique, the reflection coefficient of ultrasonic S-wave at the interface between buffer material and the corresponding cementitious material monitored. The schematic measurement of S-wave reflection coefficient is shown in *Figure 2.3*.

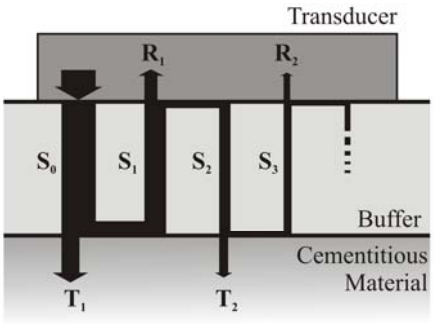

Figure 2.3 Schematic measurement of S-wave reflection coefficient [Voigt (2005)]

As can be seen in *Figure 2.3*, S_0 is an ultrasonic wave that is transmitted from the transducer into the buffer material. At the moment this ultrasonic wave encounters the interface between the buffer and cementitious materials, a part of the ultrasonic wave is transmitted into the cementitious material (i.e. T_1) and another part is reflected back to the transducer (i.e. S_1). When the ultrasonic wave encounters the buffer-transducer interface, a part of ultrasonic wave is received by the transducer (i.e. R_1) and another part is reflected back into the buffer material (i.e. S_2). This process repeats until the ultrasonic wave attenuates.

In a typical signal analysis, the reflection coefficient (i.e. r) is calculated based on the amplitude of the first and the second reflections (i.e. A_1 and A_2 in Eq. 2.1). The amplitudes A_1 and A_2 can be measured both in time or frequency domain.

$$r = \frac{A_2}{A_1} \qquad \textit{Eq. 2.1}$$

In the calculation of S-wave reflection coefficient, it is important to emphasize that the reflection coefficient is not only influenced by the transmission losses at the interface between the buffer material and the cementitious material, but also influenced by transmission loss between the transducer and the buffer material, as well as the geometric losses while transmitting through the buffer material. This is schematized in *Figure 2.4*

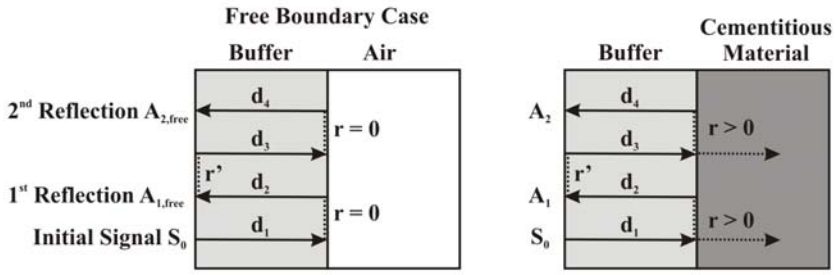

Figure 2.4 Analytical procedure for calculating the reflection coefficient [Voigt (2005)]

In order to eliminate the transmission losses, a procedure that initially developed by Ozturk et al. (1999) was adopted. The procedure uses the amplitudes derived from the frequency domain. However, the procedure can also be applied to reflection calculation in the time domain. Based on the procedure, the first and the second reflection loss can be written as:

$$A_1 = S_0 \times d_1 \times r \times d_2 \qquad \textit{Eq. 2.2}$$

$$A_2 = S_0 \times d_1 \times r \times d_2 \times r' \times d_3 \times r \times d_4 \qquad \textit{Eq. 2.3}$$

A_1 and A_2 : the amplitude of the first and the second reflection in the time domain respectively;

S_0 : the incident wave including the variables due to coupling;

r : the reflection coefficient at interface between the buffer material and the cementitious materials;

r' : the reflection coefficient at interface between the transducer and buffer material;

d_1, d_2, d_3, d_4 : the variables to express the signal losses when the S-wave propagate through the buffer material.

Calculating the ratio of A_2/A_1 is not sufficient to determine the reflection coefficient since the variables d_3 and d_4 remain in the expression. In order to isolate the variables d_3 and d_4, a measurement on a free boundary must be performed. In the case of free boundary case, the

reflection coefficient at the interface of the buffer and air is equal to zero since the S-wave can not travel through air.

Thus the ratio of the second reflection to the first reflection in the free boundary case results in:

$$\frac{A_{2,free\ boundary}}{A_{1,free\ boundary}} = \frac{S_0 \times d_1 \times d_2 \times r' \times d_3 \times d_4}{S_0 \times d_1 \times d_2} = d_3 \times r' \times d_4 \qquad \textit{Eq. 2.4}$$

And finally, the reflection coefficient (r) can be isolated with Eq. 2.6, where the ratio derived in Eq. 2.5 is divided by the ratio for the free boundary case (Eq. 2.4).

$$\frac{A_2}{A_1} = \frac{S_0 \times d_1 \times r \times d_2 \times r' \times d_3 \times r \times d_4}{S_0 \times d_1 \times r \times d_2} = d_3 \times r \times r' \times d_4 \qquad \textit{Eq. 2.5}$$

$$\frac{A_2 / A_2}{A_{2,free\ boundary} / A_{1,free\ boundary}} = \frac{d_3 \times r \times r' \times d_4}{d_3 \times r' \times d_4} = r \qquad \textit{Eq. 2.6}$$

2.5.2 Reflection loss

The reflection coefficient is usually measured in decibel, known as reflection loss (i.e. R_L). The conversion of reflection coefficient into reflection loss can be done according to Eq. 2.7.

$$R_L(t) = -20log\left[r(t)\right] \qquad \textit{Eq. 2.7}$$

Where $r(t)$ and $R_L(t)$ are the reflection coefficient and the reflection loss at a given time t, respectively.

2.5.3 Mathematical Determination of Stiffening Time based on Shear Reflection Loss

Using steel as the buffer material, the typical curve of S-wave reflection loss versus time at the interface between steel and cementitious materials is shown in *Figure 2.5*

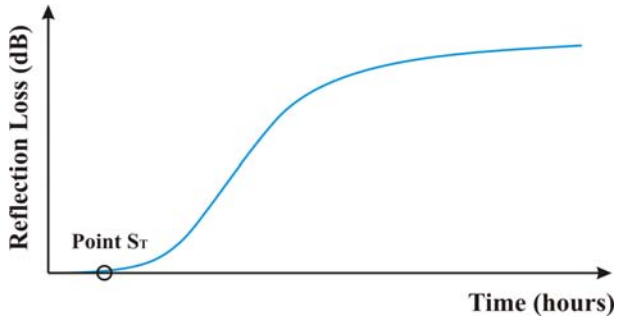

Figure 2.5 Typical curve of S-wave reflection loss with steel buffer

Based on this curve, a critical point (i.e. S_T) representing the stiffening time is determined. According to an earlier study by Rapoport et al. (2000), the procedure for determining the critical point S_T involves calculating the first derivative of the S-wave reflection loss and setting a threshold value at which the stiffening time is expected to occur. In the present study, a widely adopted numerical procedure for differentiating experimental data was followed. The procedure included to fit a set of polynomial or spline curves to the data and then to differentiate these curves analytically to obtain the required derivatives (Wahba (1990),Dierckx (1993)). More specifically, a widely used Savitzky-Golay (SG) method was used to obtain the first derivative of the S-wave reflection loss in the present study (Savitsky and Golay (1964)).

The threshold value adopted in the present study was based on the free boundary case. In the free boundary case, the S-wave reflection loss at the interface between steel and air is measured and the first derivative of S-wave reflection loss is calculated. Based on the calculated first derivative of S-wave reflection loss, an upper bound value corresponding to 98% confidence interval is set as the threshold value for determining the stiffening time of the cementitious materials.

2.6 Methodology and Materials

2.6.1 Assessment of the Stiffening Time

In order to assess the stiffening time of high performance cementitious materials, both the penetration resistance test and ultrasonic techniques (i.e. P-wave and S-wave) were used. The penetration resistance test was conducted according to ASTM-C403/403M (2008). The experimental test set-up for measuring the ultrasonic P-wave velocity was made by following Reinhardt and Grosse (1996). As shown in *Figure 2.6*, the mould was made from Perspex walls on which ultrasonic transducers were attached. P-wave ultrasonic transducers with central frequency of 150 kHz and 54 kHz were used for the mortar and concrete mixtures respectively. The sample thickness was adjusted according to the cementitious material being considered. The sample thickness was 30 mm and 100 mm for the mortar and concrete mixtures respectively. A commercial UPV (i.e. Ultrasonic Pulse Velocity) device with a resolution of 0.1 μs was used to monitor the travel time of the ultrasonic P-wave through the cementitious sample. The first P-wave velocity reading was taken immediately after casting and successive readings were taken at intervals 5-minutes during the first 24 hours after adding water to the mixture.

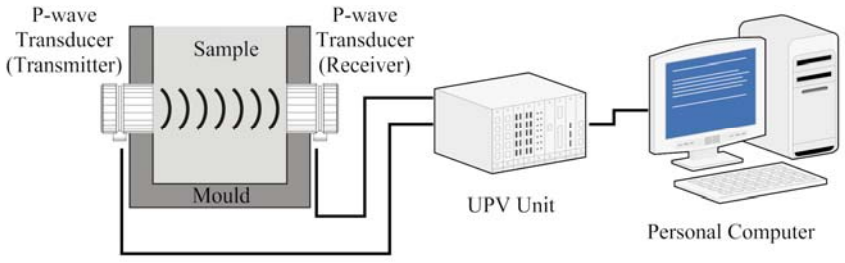

Figure 2.6 P-wave velocity testing arrangement [Reinhardt et al. (2000)]

Figure 2.7 shows the S-wave reflection loss test set-up. The test set-up was constructed based on earlier studies conducted by Rapoport et al. (2000) and Voigt and Shah (2003). The test set-up consists of a personal computer, a digitizer card, a pulser/receiver unit, a transducer, a perspex container, and a steel plate on which S-wave transducer with a frequency of 2.25 MHz was fixed. The S-wave transducer was connected to the digitizer card via the pulser/receiver

unit. The pulser/receiver unit excited the transducer and transmitted the analog signal of the received reflections to the digitizer card. The analog signal was digitized and stored in the personal computer for further analysis. The measurement of the reflection signal was recorded at 5-minutes intervals during the first 24 hours after adding water to the cementitious mixture.

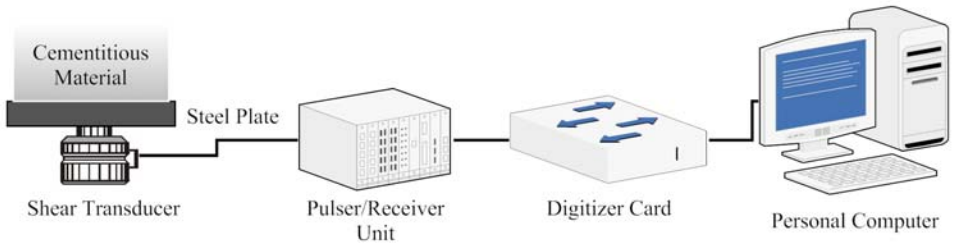

Figure 2.7 Shear wave reflection loss test arrangement [Rapoport et al. (2000)]

In the present study, to investigate the possibility of using the S-wave reflection loss for monitoring the stiffening time with respect to the depth of the specimens, the shear transducer was fixed at three different depths; 10 mm, 50 mm, and 100 mm from the top surface of the specimens. The test configuration can be seen in *Figure 2.8***.** Two surface treatments were considered in the present study; sealed or unsealed top surface. The former is representative of autogenous shrinkage while the latter is representative of early age drying shrinkage. In the case of sealed specimens, the top surface of the specimen was sealed with a layer of plastic wrap as soon as the casting was completed. On the other hand, the specimen with top surface unsealed was exposed to a dry environment (i.e. temperature of 30 ± 0.5 ^{0}C and relative humidity of 65 ± 2 %) as soon as casting was completed.

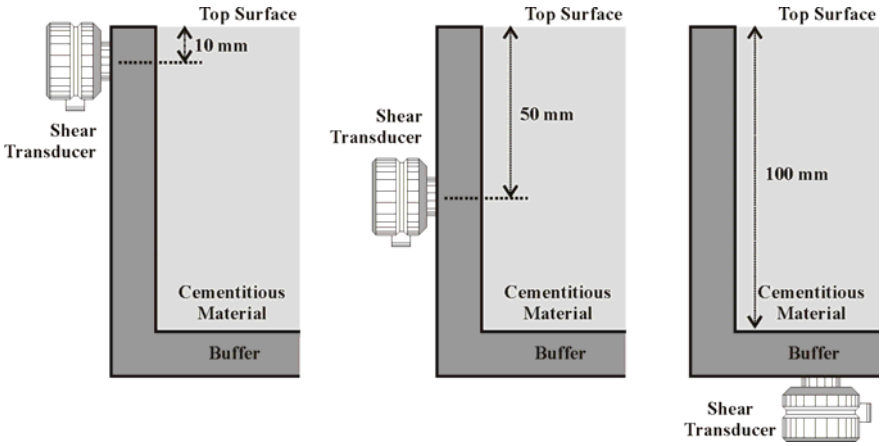

Figure 2.8 Shear wave test arrangement for monitoring the shear reflection loss at different depths from the top surface.

2.6.2 Materials

In the present study, OPC mortar and concrete mixtures with water-to-cementitious ratio of 0.20, 0.25, 0.30, 0.35, or 0.45 were prepared. In addition, concrete mixtures containing silica fume were cast with water-to-cementitious ratio of 0.30. Four replacement levels of silica fume were considered; 0%, 5%, 10%, and 15%. These mixtures proportions were selected as a representative of high performance cementitious mixtures (i.e. low w/c ratio with or without silica fume) and normal strength cementitious mixtures (i.e. high w/c). The mortar and concrete mix proportions are summarized in *Table 2.2*.

In all mortar and concrete mixtures, ASTM Type I normal OPC was used. In the case of silica fume concrete mixtures, densified silica fume with specific gravity of 2.2 was used. The fine aggregates used was natural sand with fineness modulus and specific gravity of 2.8 and 2.6 respectively. Crushed granite with maximum size of 12.5 mm was used as coarse aggregates in all concrete mixtures having water-to-cementitious ratio of 0.25, 0.35, or 0.45. For concrete mixtures cast with a water-to-cementitious ratio of 0.30, crushed granite with maximum size of 19 mm was used as coarse aggregates. The proportion of fine aggregates was kept at 50% by volume for the mortar mixtures. For the concrete mixtures, the total proportion of fine and coarse aggregates was kept at 65% by volume.

In all mortar and concrete mixtures, a polycarboxylate type high range water-reducing admixture (i.e. HWRA) was used to achieve the target workability. The target workability was determined based on flow test (ASTM-C1437-07 (2007)) and slump test (ASTM-C143/C143M-09 (2009)) for the mortar and concrete mixtures respectively. The target flow for mortar was approximately 110%. While the target slump for the concrete mixture was about 100 to 150 mm. The amount of liquid from the HWRA was accounted for in the mixture proportions.

Table 2.2 Mix Proportions

Mixture	w/c	Agg. Vol. %	Water, kg/m^3	Cement, kg/m^3	Silica Fume, kg/m^3	Fine Agg. Kg/m^3	Coarse Agg. Kg/m^3	HRWRA		Work-ability
								lt/m^3	by binder mass (%)	
M20	0.20	50%	155	906	-	1300	-	40.83	1.80	110 %
M25	0.25	50%	211	843	-	1300	-	5.28	0.25	140 %
M30	0.30	50%	233	776	-	1300	-	2.34	0.12	110 %
M35	0.35	50%	251	718	-	1300	-	1.26	0.07	90 %
M45	0.45	50%	281	625	-	1300	-	-	0.00	110 %
C25	0.25	65%	147	588	-	790	900	4.42	0.30	110 mm
C35	0.35	65%	175	501	-	790	900	1.88	0.15	165 mm
C45	0.45	65%	196	436	-	790	900	0.66	0.06	90 mm
C30-SF0	0.30	65%	157	539	-	790	900†	2.50	0.18	80 mm
C30-SF5	0.30	65%	157	500	26	790	900†	3.60	0.27	165 mm
C30-SF10	0.30	65%	155	476	52	790	900†	5.10	0.39	165 mm
C30-SF15	0.30	65%	154	436	77	790	900†	6.00	0.47	200 mm

Note : † 19 mm MSA

2.7 Results and Discussion

2.7.1 Threshold value for S-wave Reflection Loss

As mentioned previously, the threshold value for the S-wave reflection loss was determined based on the first derivative of S-wave reflection loss measurement in the free boundary case. *Figure 2.9(a)* and *Figure 2.9(b)* shows the results of three measurements in the free boundary case. Theoretically, the S-wave reflection loss and its first derivative in the free boundary case should be equal to zero. However, due to random noise in the actual experiment, the S-wave reflection loss and its first derivative may not be equal to exactly zero. As shown in *Figure 2.9(b)*, based on 98% confidence interval, the upper bound value of the first derivative of

the S-wave reflection loss results was about 0.028. This upper bound value was later adopted as the threshold value to determine the stiffening time of the cementitious materials tested in the present study.

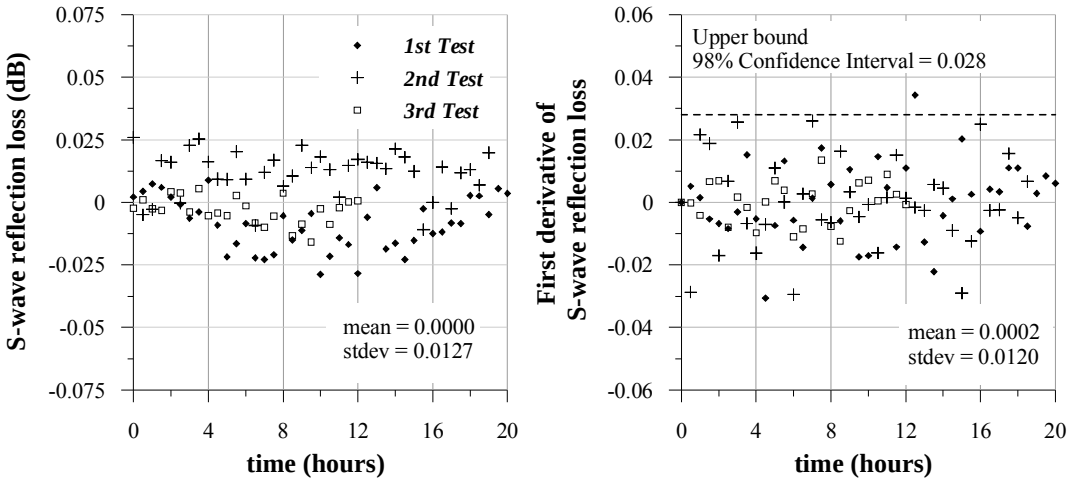

Figure 2.9 (a) S-wave reflection loss in the free boundary case; (b) the corresponding first derivative of S-wave reflection loss in the free boundary case

2.7.2 Stiffening time measured via Penetration resistance test and Ultrasonic Technique

As mentioned previously, two ultrasonic techniques and penetration resistance test were conducted for monitoring the stiffening time of mortar and concrete mixtures. The experimental results are summarized in *Table 2.3*. The results of penetration test, P-wave velocity, and S-wave reflection loss for cementitious mixtures tested in the present study are shown in *Figure 2.10* to *Figure 2.14*.

As shown in *Table 2.3* and *Figure 2.10*, the penetration resistance test showed that the initial setting time of the mortar and concrete mixtures was delayed with a decrease in water-to-cementitious ratio and with an increase in the silica fume content. This retardation can be attributed to the higher dosage of HWRA used in the tested cementitious mixtures. The corresponding P-wave velocity of the cementitious mixtures tested also showed good agreement with that of the penetration resistance test. It can be seen in *Figure 2.11* that the time when the P-wave starts to increase was delayed with a reduction in water-to-cementitious ratio, as well as with an increase in silica fume content. The present results also showed that the assessment of

the stiffening time through S-wave reflection loss showed good agreement with that of the penetration resistance test and P-wave velocity monitoring. It can be seen in *Figure 2.12*, *Figure 2.13*, and *Figure 2.14* that an increase in the stiffening time was observed with a reduction in water-to-cementitious ratio, as well as with an increase in silica fume content.

Table 2.3 Stiffening Time of Cementitious Mixtures Tested

Mixture	w/c	P-wave velocity increase (hr)	Stiffening time via S-wave reflection loss (hr)	Penetration test Initial set (hr)
M20	0.20	5	11.1	12.8
M25	0.25	0.75	4.0	5.7
M30	0.30	1.50	2.9	4.5
M35	0.35	1.25	2.7	3.2
M45	0.45	1.25	1.9	3.6
C25	0.25	6.5* / 2.25	4.6	5.2
C35	0.35	5.2* / 2.80	3.1	4.8
C45	0.45	3.5*	2.4	3.8
C30-SF0	0.30	3.6*	2.3	3.8
C30-SF5	0.30	4.2*	3.3	5.1
C30-SF10	0.30	4.8*	4.2	6.1
C30-SF15	0.30	5.9*	5.4	6.9

Note: * old testing set-up

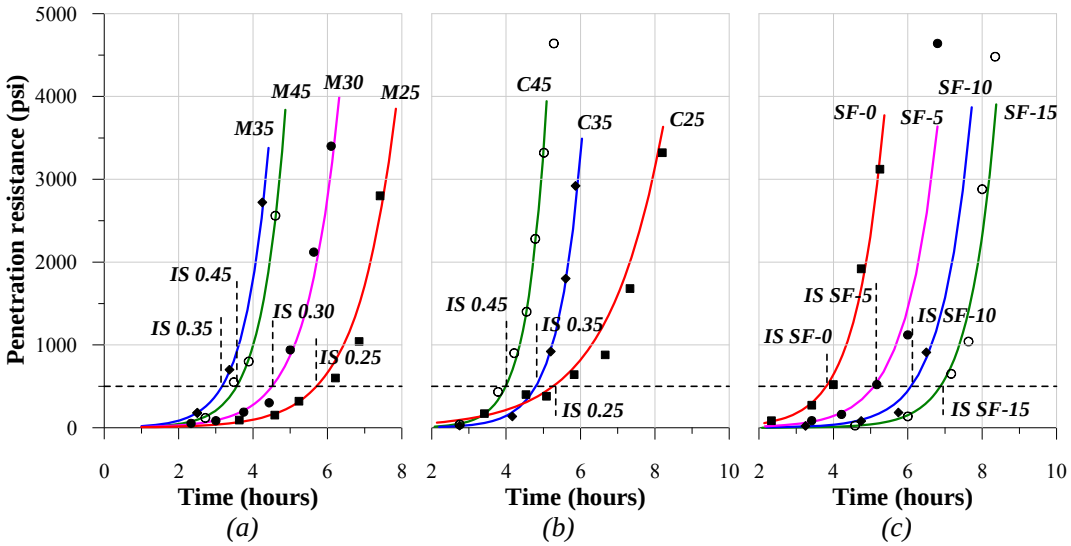

Figure 2.10 Setting time via penetration test for (a) Mortar mixtures with different water-to-cementitious ratios; (b) Concrete with different water-to-cementitious ratios; and (c) Concrete with different silica fume contents

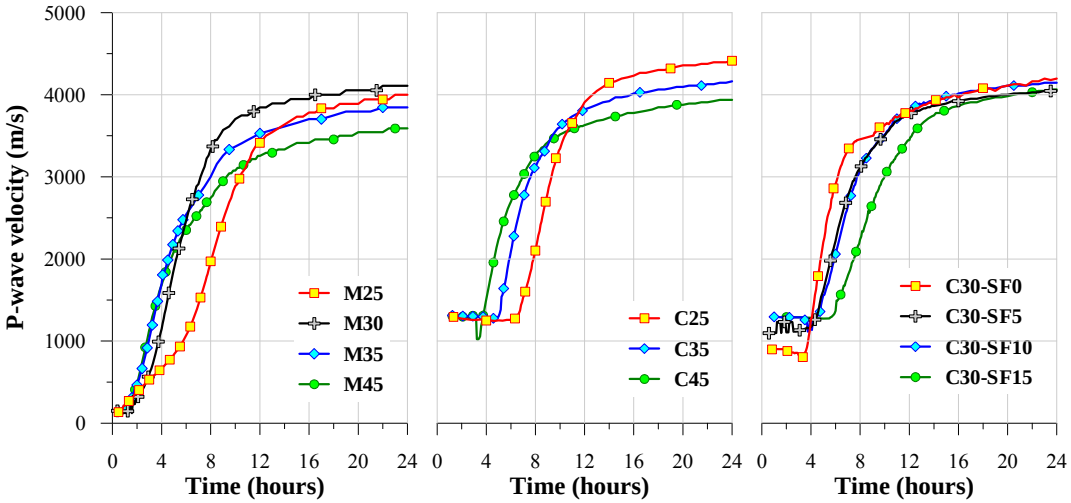

Figure 2.11 P-wave velocity for (a) Mortar mixtures with different water-to-cementitious ratios; (b) Concrete with different water-to-cementitious ratios; and (c) Concrete with different silica fume contents

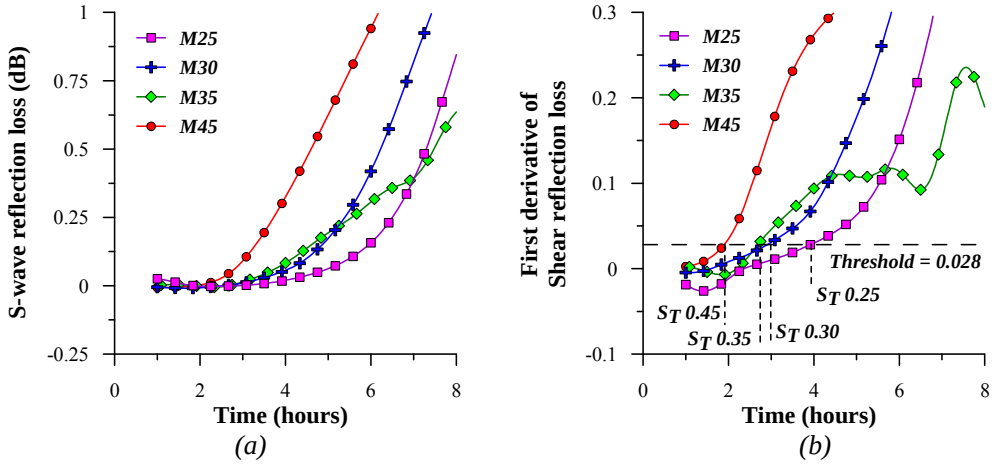

Figure 2.12 (a) S-wave reflection loss; and (b) First derivative of S-wave reflection loss for mortar mixtures with different water-to-cementitious ratios

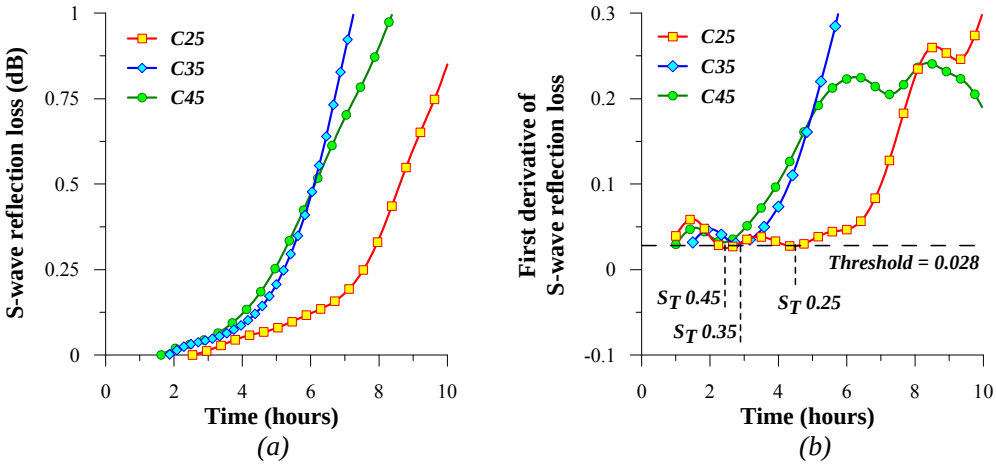

Figure 2.13 (a) S-wave reflection loss; and (b) First derivative of S-wave reflection loss for concrete mixtures with different water-to-cementitious ratios

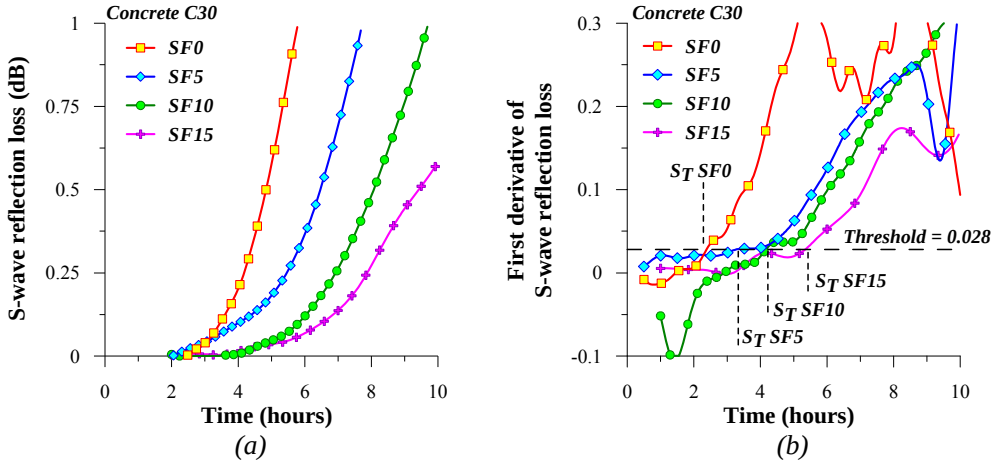

Figure 2.14 (a) S-wave reflection loss; and (b) First derivative of S-wave reflection loss for concrete mixtures with different silica fume contents

Comparison between the results of penetration resistance test, P-wave velocity and S-wave reflection loss showed that for the mortar mixtures cast with water-to-cementitious ratio in the range of 0.25 to 0.45, the P-wave velocity started to increase very early, approximately at 0.75 to 1.50 hours after adding water to the mixtures. The results were consistent with the earlier study by Aïtcin and Neville (2003) which suggested that the formation of early age hydration products (i.e. ettringitte and calcium hydroxide) significantly affects the ability of mortar mixtures to transmit the P-wave in the early ages. The stiffening time, on the other hand, was occurred between the time when P-wave velocity started to increase and the time when the initial setting obtained via penetration resistance test. In the case of mortar mixtures tested, the stiffening time occurred between 2.0 and 4.6 hours after adding water to the mixture, while the corresponding initial setting time via the penetration test occurred later, between 3.2 and 5.7 hours after adding water to the mixture. In the mortar mixture cast with water-to-cementitious ratio of 0.20 (i.e. M20), a similar trend was observed, the P-wave started to increase at 5 hours after adding water to the mixture, while the stiffening time via S-wave reflection loss and the initial setting time via penetration resistance test occurred at 11.2 and 12.8 hours after adding water to the mixture respectively.

In the case of concrete mixtures cast with either different water-to-cementitious ratios or different dosages of silica fume, as can be seen in *Table 2.3*, similar trends in the results were

also obtained. The stiffening time obtained via S-wave reflection loss occurred before the initial setting time obtained via the penetration test conducted on companion mortar cubes. The stiffening time occurred between 2.3 and 5.6 hours after adding water to the mixtures, while the initial setting time via the penetration resistance test occurred between 3.8 and 6.9 hours after adding water to the mixtures. Nevertheless, the corresponding P-wave velocity measurement showed a contradicting result; the P-wave velocity started to increase at much later time than the stiffening time. This could be attributed to the testing set-up used in the present study. As mentioned earlier, the testing set-up for monitoring the P-wave velocity was different for the mortar and concrete mixtures. In the present study, a specimen with thickness of 30 mm was used for mortar mixtures. While in the case of concrete mixtures, due to the inclusion of coarse aggregates, it was necessary to use a thicker specimen (i.e. 100 mm thick). As shown in *Figure 2.15(a)*, the present testing setup was capable to measure the P-wave velocity on mortar mixtures as low as 300 m/s at the beginning of the test. However, using the test set-up for the concrete specimens, the testing setup registered a P-wave velocity of 1300 m/s at the beginning of the test. This value was much higher than that reported by Lee et al. (2004) of about 500 m/s at the beginning of the test. Therefore, in the P-wave testing set-up for concrete mixture, it is possible that the P-wave propagates through the mold during the early hours. Only after hydration products have filled the empty pore space and a certain degree of stiffness has developed which allows P-wave to transmit through the concrete mixture, the increase in the P-wave velocity can be measured properly. This assumption was verified by repeating the measurement on the modified testing set-up. As can be seen in *Figure 2.15(a)* and *Figure 2.15(b)*, using the modified testing set-up, the P-wave velocity of approximately 200 m/s was registered for concrete mixtures at early ages. Moreover, similar to that of the mortar mixtures tested, it can be seen that the P-wave velocity started to increase at much earlier time that the stiffening time via the S-wave reflection loss.

In the case of concrete mixtures with different dosages of silica fume, as can be seen in *Table 2.3*, similar trends in the results were also obtained. The stiffening time obtained via S-wave reflection loss occurred before the initial setting time obtained via the penetration test

conducted on companion mortar cubes. The stiffening time occurred between 2.3 and 5.6 hours after adding water to the mixtures, while the initial setting time via the penetration resistance test occurred between 3.8 and 6.9 hours after adding water to the mixtures.

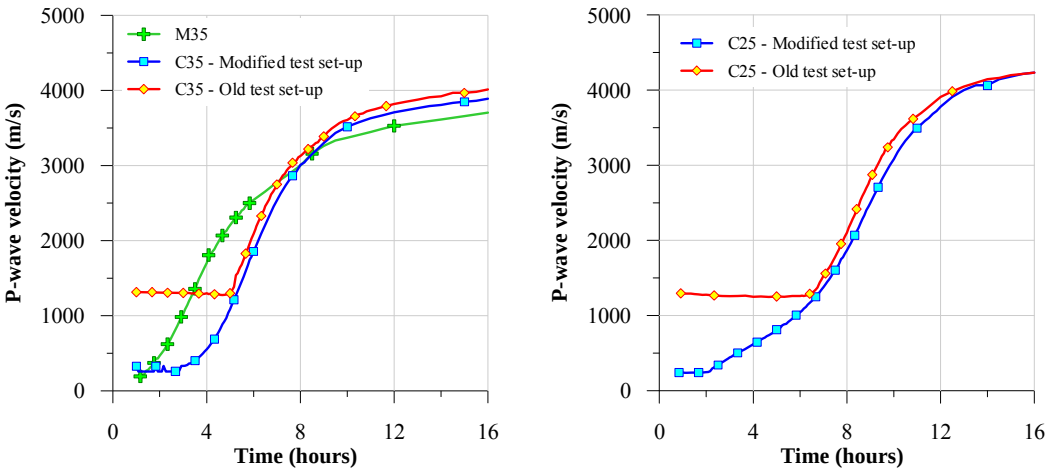

Figure 2.15 (a) P-wave velocity of mortar and concrete cast with w/c ratio of 0.35; and (b) P-wave velocity of concrete cast with w/c ratio of 0.25

2.7.3 Stiffening time of mortar mixtures cured under sealed and unsealed conditions

As mentioned previously, the technique for determining stiffening time should also be applicable for a variety of casting and curing conditions since early age shrinkage monitoring can be performed on either sealed or unsealed specimens. For a 100-mm thick mortar specimens tested in the present study, when sealed curing is applied on the top surface of a freshly cast cementitious materials, the stiffening time is expected to occur at about the same time throughout the depth of the specimens. On the other hand, when the top surface of a freshly cast cementitious material is exposed to a drying environment at an early age, moisture loss to the environment (i.e. evaporation) may affect microstructural development of the cementitious material, as well as the stiffening time. As shown in *Figure 2.16*, at the beginning just after mixing, spaces between cement particles and aggregates form a system of interconnected pores which is completely filled with water **(A)**. Due to evaporation and hydration (i.e. self-desiccation), water is drawn from the system until water menisci finally start to form between

cement particles near the exposed surface. When the water menisci form, the curvature of these water menisci causes a negative pressure that consolidates the microstructures especially at the surface layer **(B)** [Brinker and Scherer (1990), Lura et al. (2007)]. As evaporation continues to remove the water from the surface of the cementitious mixtures, two scenarios are possible; the surface layer may be unaffected by the drying and stiffen at the same time as the interior (i.e. $\mathbf{C_1}$) or it may stiffen earlier (i.e. $\mathbf{C_2}$). In the former scenario, as shown in stage $\mathbf{C_1}$, interior of cementitious material may able to supply water to the surface layer through the interconnected pore system. Simultaneously, this process may also consolidate the microstructure of the interior, causing the cement particles and aggregates to move closer to each other. As the distance between the cement particles in the interior is decreased due to water migration, a subsequent hydration process may produce enough hydration products to bridge the gap between these cement particles. As a result, a similar stiffening time may occur in the interior layers. In the latter scenario, as shown in stage $\mathbf{C_2}$, it is also possible that below a critical water-to-cementitious ratio, the water loss from the exposed surface may significantly affects the distance between the cement particles near the top exposed surface. Since the initial distance between cement particles decreases with a reduction in the water-to-cementitious ratio, a relatively shorter distance between cement particles may cause significant negative pressures to build-up near the exposed surface from where the water is removed through evaporation and hydration process. The high negative pressure may significantly consolidate both the cement particles and aggregates, causing these particles to be in contact to each other, and creating a "skin layer" near the exposed top surface. In addition, it is possible that once the "skin layer" is formed near the exposed top surface, this "skin layer" may also act as a surface barrier thus the stiffening time in the interior may be less affected by evaporation. As shown in stage **D**, as evaporation continues, the drying front recedes into the interior of the cementitious material. Simultaneously, as hydration products fill the spaces between solid particles, the interconnected pore system may become discontinuous and the interior may not be able to replenish the water that is lost from the surface layer. As a result, further hydration near the exposed top surface may be hindered due to the lack of the available free water.

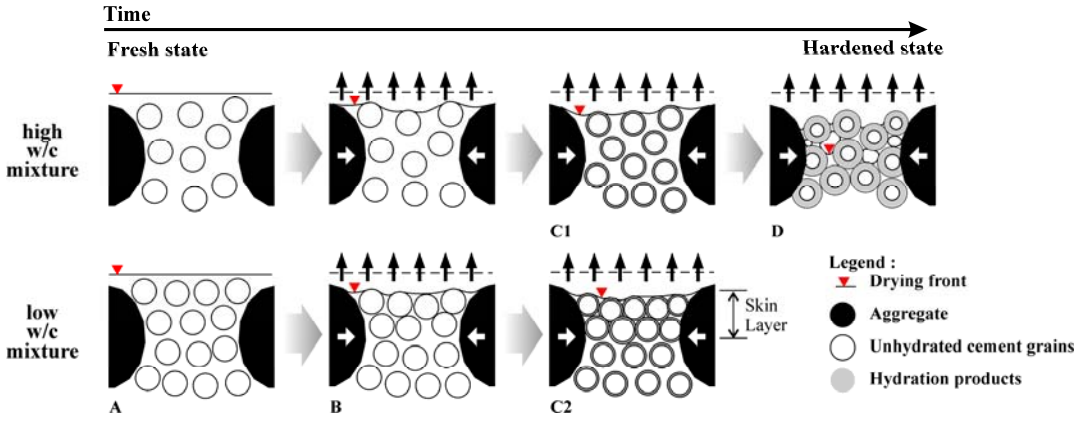

Figure 2.16 Drying sequence for mortar mixture when exposed to drying environment at early ages

2.7.3.1 Stiffening time at different depths of sealed mortar specimens

As mentioned previously, the S-wave reflection loss was monitored at three different depths; 10 mm, 50 mm, and 100 mm depth from the top surface of the mortar specimens. The results of S-wave reflection loss of the sealed mortar specimens cast with different water-to-cementitious ratios are shown in *Figure 2.17* to *Figure 2.21*. The corresponding stiffening time determined from the first derivative of the S-wave reflection loss is summarized in *Table 2.4*.

The results showed that the sealed mortar specimens registered a lower S-wave reflection loss at a depth of 10 mm and 50 mm from the top surface. The corresponding results of the stiffening time of the sealed mortar specimens showed that a similar stiffening time was monitored at a depth of 50 mm and 100 mm from the top surface, while a slight earlier stiffening time was monitored at a depth of 10 mm especially on sealed mortar specimens cast with water-to-cementitious ratio of 0.25, 0.35, and 0.45. Although the results are unexpected, some possible causes for this can be attributed to localized bleeding, as well as an increase in local porosity due to slight moisture loss experienced by the sealed mortar specimens.

If isolated bleeding occurs near the top surface of the specimens, the presence of bleed water is expected to increase the water content at the surface locally. This increase in the water-to-cementitious ratio would result in a reduction in the "absolute" S-wave reflection loss value monitored [Voigt and Shah (2003)]. If this is the case then an increase in the local water-to-

cementitious ratio should result in lower S-wave reflection loss values during the first few hours after casting, accompanied simultaneously by a longer stiffening time. This however was not observed in the results reported herein.

On the other hand, an increase in mortar porosity due to moisture loss especially near the top surface may contribute to a reduction in S-wave reflection loss and the earlier stiffening time observed near the top surface. It has been reported that an increase in the cementitious porosity was accompanied by a reduction in the shear wave velocity [Lafhaj et al. (2006)]. Similarly, since the S-wave reflection loss is affected by the density and the shear velocity of the cementitious materials [Rose (1999)], a lower shear wave velocity would result in a decrease in the S-wave reflection loss. As shown *Figure 2.22*, the weight loss monitored on the M25 and M45 mortar specimens showed a slight moisture loss in the sealed mortar specimens during the first 24 hours after adding water to the mixture. This loss of moisture, although it was not as severe as that monitored in the case of unsealed mortar specimens, may also contribute to an increase in the local porosity as well as the earlier stiffening time observed in the surface layer. Based on the results obtained, ignoring the earlier stiffening time observed at 10 mm depth from the top surface, the results obtained at 50 mm and 100 mm depth from the top surface showed that the stiffening time was similar throughout the depth of the sealed mortar specimens..

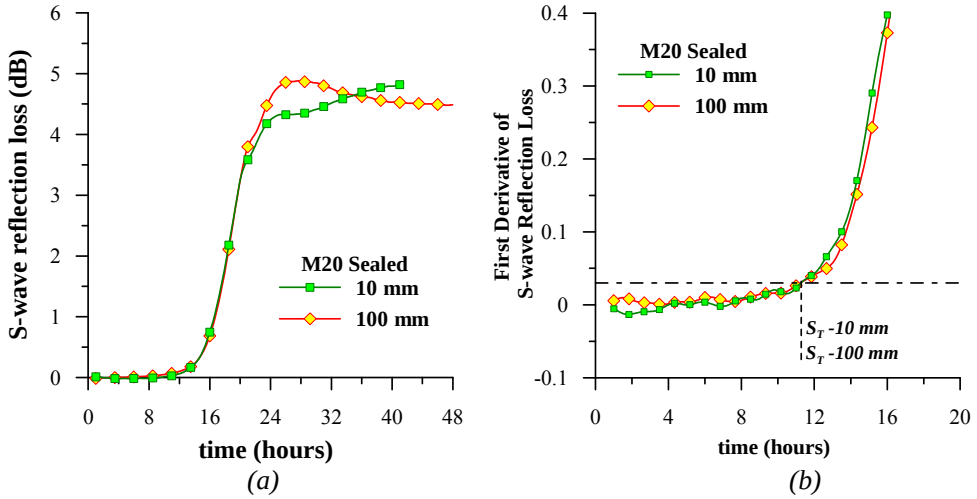

(a) *(b)*

Figure 2.17 (a) S-wave reflection loss at different depths; and (b) The corresponding first derivative of S-wave reflection loss for sealed mortar mixtures cast with water-to-cementitious ratio of 0.20

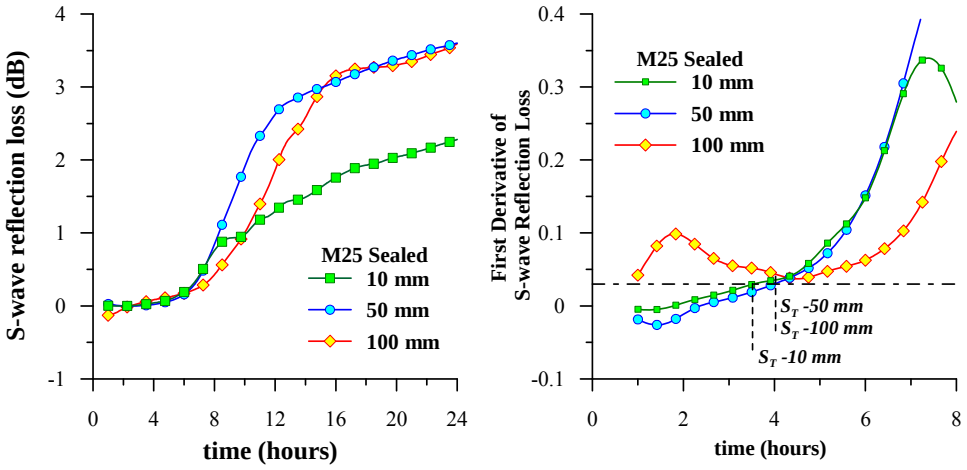

(a) *(b)*

Figure 2.18 (a) S-wave reflection loss at different depths; and (b) The corresponding first derivative of S-wave reflection loss for sealed mortar mixtures cast with water-to-cementitious ratio of 0.25

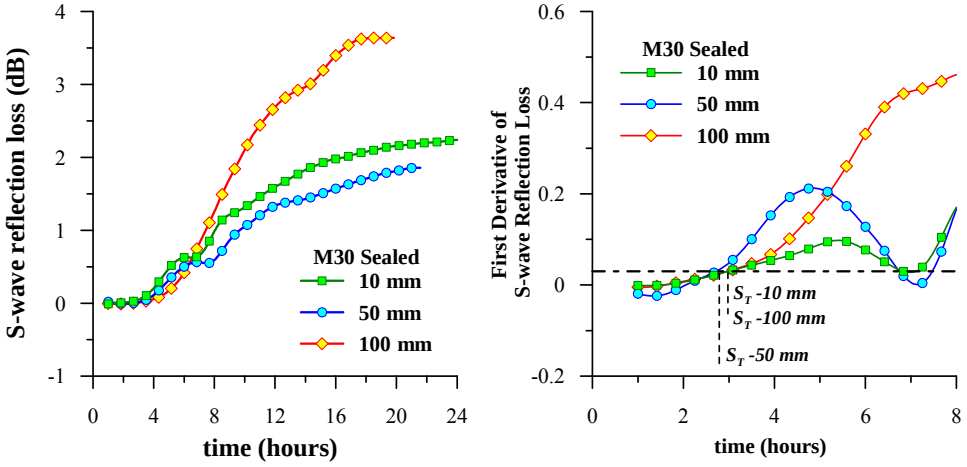

(a) *(b)*

Figure 2.19 (a) S-wave reflection loss at different depths; and (b) The corresponding first derivative of S-wave reflection loss for sealed mortar mixtures cast with water-to-cementitious ratio of 0.30

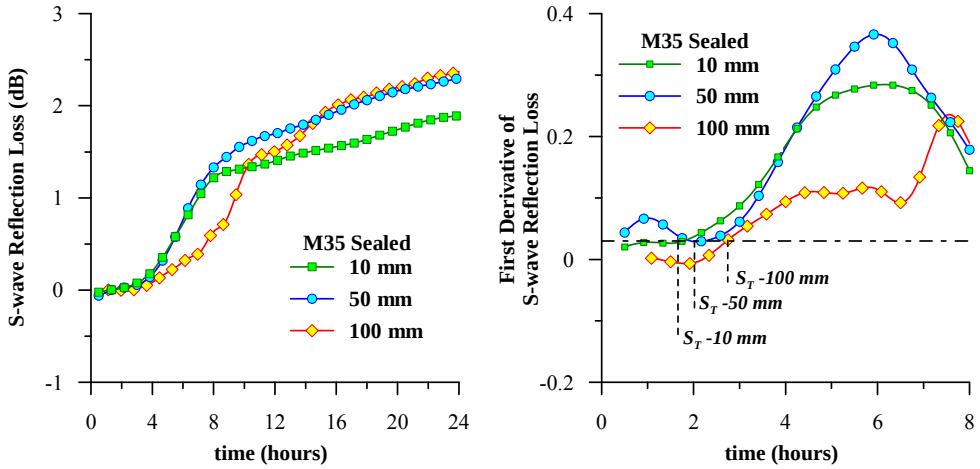

(a) *(b)*

Figure 2.20 (a) S-wave reflection loss at different depths; and (b) The corresponding first derivative of S-wave reflection loss for sealed mortar mixtures cast with water-to-cementitious ratio of 0.35

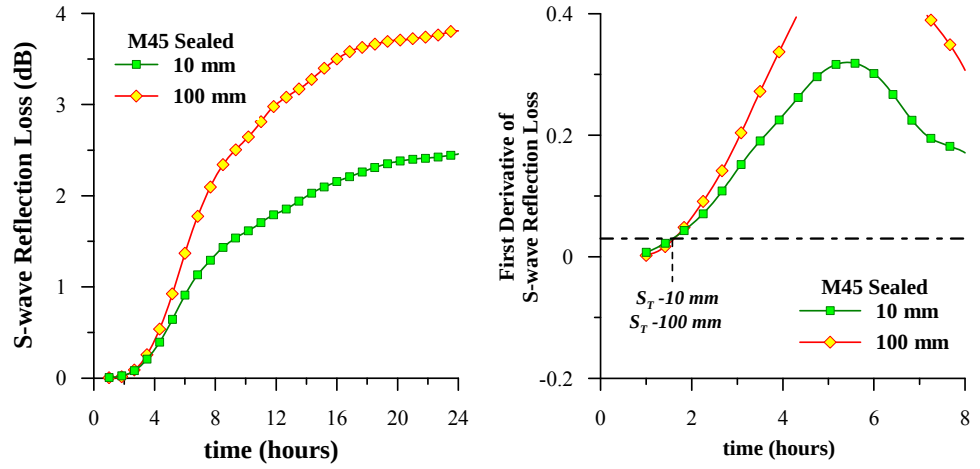

(a) *(b)*

Figure 2.21 (a) S-wave reflection loss at different depths; and (b) The corresponding first derivative of S-wave reflection loss for sealed mortar mixtures cast with water-to-cementitious ratio of 0.45

Table 2.4 Stiffening time at different depths on sealed mortar specimens

Mortar	Stiffening Time – S-wave Reflection Loss (hours)		
	Depth 10 mm	Depth 50 mm	Depth 100 mm
M20	11.2	-	11.1
M25	3.5	3.9	4.0
M30	2.9	2.7	2.9
M35	1.7	2	2.7
M45	1.6	-	1.6

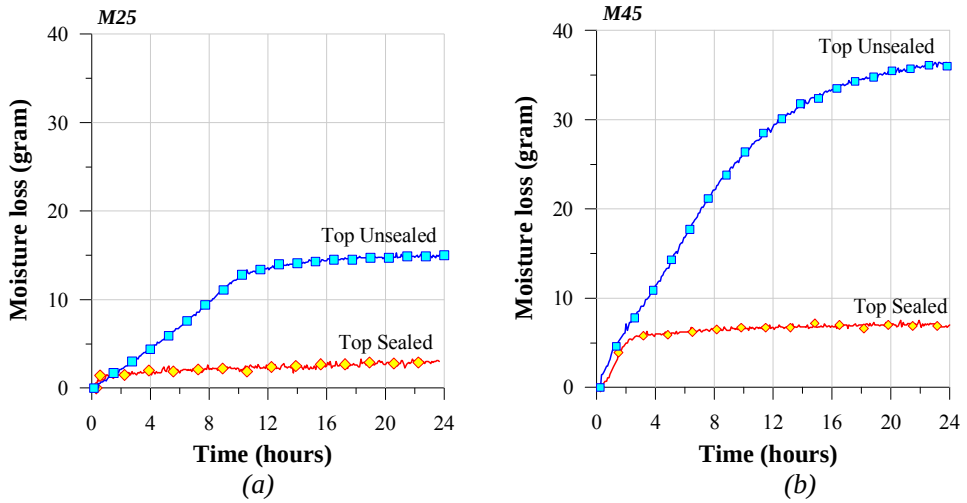

Figure 2.22 Moisture loss monitored on mortar mixture cast with water-to-cementitious ratio of (a) 0.25 and (b) 0.45 starting from 30 minutes after adding water to the mixture

2.7.3.2 Stiffening time at different depths of unsealed mortar specimens

In the case of the unsealed mortar specimens tested, as expected, the results showed that the S-wave reflection loss varied with depth from the top exposed surface. The plots of S-wave reflection loss-versus-time also showed that the development of S-wave reflection loss at different depths was similar during the first few hours after adding water to the mixture. After that, a more gradual increase in the S-wave reflection loss was monitored near the top exposed surface before the plots of the S-wave reflection loss flatten with time. A comparison of S-wave reflection loss monitored at a depth of 10 mm from the top surface between the sealed and unsealed mortar specimens showed that higher S-wave reflection losses were monitored in the sealed mortar specimens, with the exception of M25 and M30 mortar specimens. The higher S-wave reflection loss monitored in the unsealed M25 and M30 mortar specimens could be attributed to consolidation brought about by the evaporation. As the evaporation draws water out from the mortar mixtures, the negative pore pressure consolidates the cement particles and aggregates near the top surface. Consequently, as the hydration products fill the gaps between these cement particles, the solid networks allows more S-waves to be transmitted through the mortar mixtures. As a result, the S-wave reflection loss increases.

The corresponding results of the stiffening time showed that the two possible scenarios mentioned previously were observed in the unsealed mortar specimens tested. The unsealed mortar specimens cast with water-to-cementitious ratio of 0.25, 0.30, 0.35, and 0.45 showed similar stiffening times at different depths. On the other hand, a much earlier stiffening time near the exposed top surface was observed on the unsealed mortar specimen cast with a water-to-cementitious ratio of 0.20. The stiffening time at 10 mm depth from the top exposed surface occurred approximately at 3.7 hours after adding water to the mixture while in the interior (i.e. 50 mm and 100 mm depth from the top exposed surface), the stiffening time occurred between 17.0 and 17.5 hours after adding water to the mixture. The results confirm that when the top surface is exposed at such early ages, a migration of water from the interior may influence the stiffening time of the mortar specimens. The latter consolidates the microstructure of the interior, and with hydration products fill the gap between cement particles and aggregates, a similar stiffening time occurs in the interior. Nevertheless, once the water-to-cementitious used becomes too low and reaches a critical value, a "skin layer" forms within the exposed top surface of the mortar specimens as indicated by the much earlier stiffening time monitored via S-wave reflection loss.

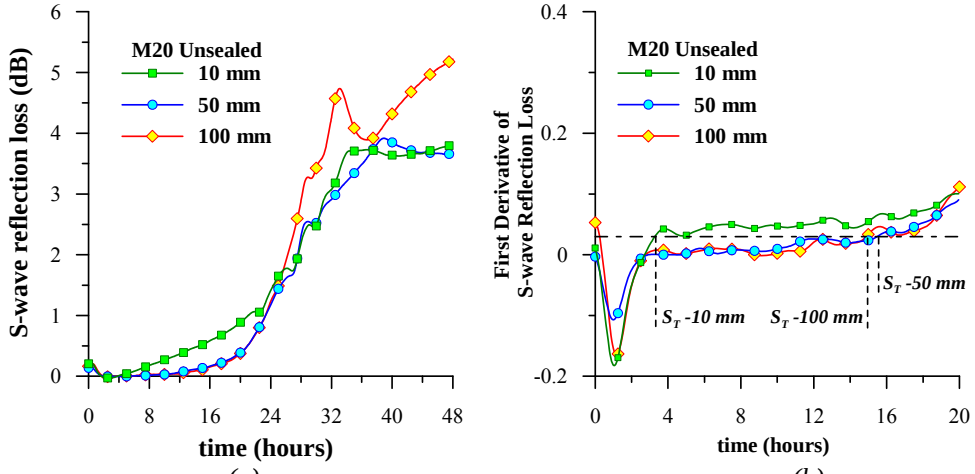

Figure 2.23 (a) S-wave reflection loss at different depths; and (b) The corresponding first derivative of S-wave reflection loss for unsealed mortar mixtures cast with water-to-cementitious ratio of 0.20

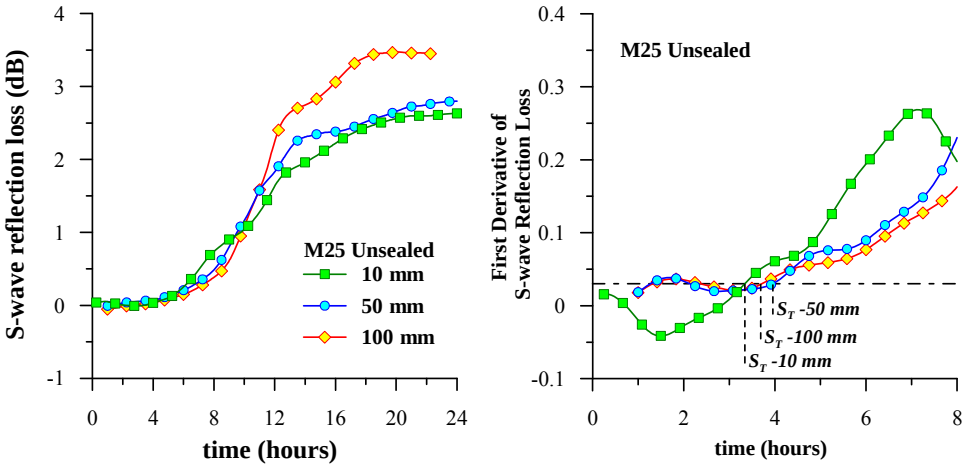

(a) *(b)*

Figure 2.24 (a) S-wave reflection loss at different depths; and (b) The corresponding first derivative of S-wave reflection loss for unsealed mortar mixtures cast with water-to-cementitious ratio of 0.25

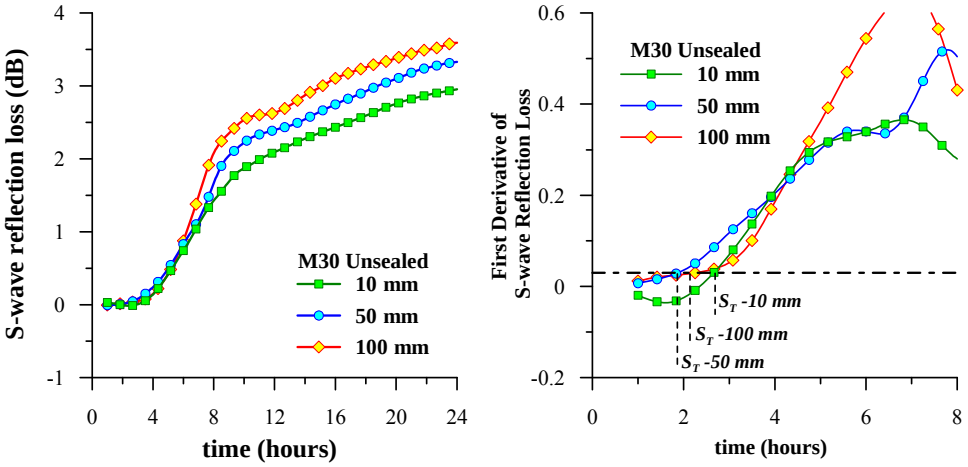

(a) *(b)*

Figure 2.25 (a) S-wave reflection loss at different depths; and (b) The corresponding first derivative of S-wave reflection loss for unsealed mortar mixtures cast with water-to-cementitious ratio of 0.30

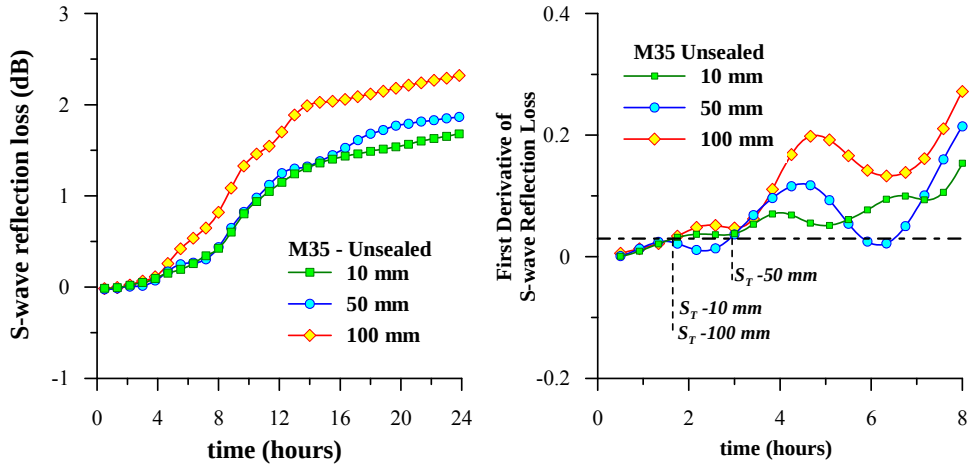

(a) *(b)*

Figure 2.26 (a) S-wave reflection loss at different depths; and (b) The corresponding first derivative of S-wave reflection loss for unsealed mortar mixtures cast with water-to-cementitious ratio of 0.35

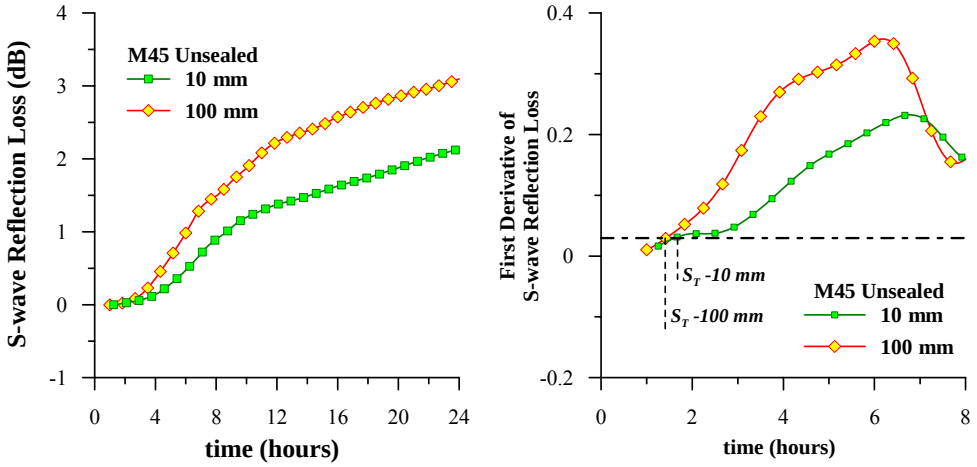

(a) *(b)*

Figure 2.27 (a) S-wave reflection loss at different depths; and (b) The corresponding first derivative of S-wave reflection loss for unsealed mortar mixtures cast with water-to-cementitious ratio of 0.45

Table 2.5 Stiffening time at different depths on unsealed mortar specimens

Mortar	Stiffening Time – S-wave Reflection Loss (hours)		
	10 mm Depth	50 mm Depth	100 mm Depth
M20	3.7	15.4	14.8
M25	3.3	3.9	3.7
M30	2.7	1.8	2.1
M35	1.6	2.9	1.6
M45	1.6	-	1.4

2.8 Summary and Conclusion of TZV for early age shrinkage monitoring

In early age shrinkage monitoring, the selection of an appropriate "time zero" value or TZV is still a contentious issue. Motivated by this fact, this chapter specifically aims to provide a means to select an appropriate TZV for use in early age shrinkage monitoring of high performance cementitious mixtures with low water-to-cementitious ratios. Based on the results obtained, although the penetration resistance test (i.e. ASTM C403) has been used in the standard method for monitoring autogenous shrinkage (i.e. ASTM C1698-09), the initial and the final setting time might not give the exact time at which cementitious material develop its stiffness. Another major drawback of the penetration resistance test is the need to perform wet-sieving process in order to obtain the mortar phase from the concrete mixtures. The mortar fraction sieved might have slightly different setting behavior from the corresponding concrete mixtures. In addition, the mortar fraction does not have common initial stiffness which varies with the w/c ratio and sand content. Thus, these point might not suitable for pinpoint the "time zero" value for early age shrinkage measurement. On the other hand, S-wave reflection loss is deemed to be an appropriate method for selecting TZV as it able to detect solid particles connectivity - the time when the cementitious mixture starts to develop its stiffness. The S-wave reflection loss can also be applied directly on various cementitious materials being tested from paste to concrete mixtures. Furthermore, it is also possible to extend the S-wave reflection loss technique to obtain stiffening time to be used as the TZV within the timeline along which early age shrinkage of cementitious materials occurs under both sealed and unsealed curing conditions.

The results of mortar specimens tested in the present study implied that in the case of sealed conditions, a similar stiffening time occurred throughout the depth of the mortar specimens. On the other hand, in the case of unsealed mortar specimens, it was found that the stiffening time may vary with depth depending on the water-to-cementitious ratio used. Based on results obtained, when the water-to-cementitious ratio of 0.20 was used, the mortar specimens registered a much earlier stiffening time especially near the top exposed surface. It is postulated that the water migration within the specimen as well as the formation of a "skin

layer" may significantly affect the occurrence of the stiffening time within the unsealed mortar prism specimens tested. This may affect the selection of an appropriate TZV for use in autogenous and early age drying shrinkage monitoring of high performance cementitious mixtures. However, it is important to note that the findings obtained are based on prism specimens cast using low water-to-cementitious ratio mixtures. Other cementitious mixtures with other types of binders and incorporating different mineral and chemical admixtures should also be tested. In addition, since only prism specimens with thicknesses up to 100 mm were tested, the numerical values reported may not apply in the case of specimens with other geometric dimensions.

Chapter 3 TECHNIQUE FOR EARLY AGE SHRINKAGE MONITORING

3.1 Introduction

3.1.1 Standardization in early age shrinkage monitoring

In the shrinkage monitoring of cementitious materials, the standard apparatus and procedure for monitoring long-term shrinkage strains are well defined in ASTM-C490-04 (2004) and ASTM-C157/C157M-04 (2004) respectively. The standard specimens are 75×75×285 mm and 100×100×285 mm for aggregates passing 25 mm and 50 mm sieve respectively. Shrinkage strain is then calculated based on the length change monitored using comparator with a recommended gauge length of 250 mm. Paradoxically in the case of early age shrinkage monitoring, numerous monitoring techniques have been developed around the world. Study of literature showed that various researchers used a number of specimen sizes, shapes and gauge lengths in their early age shrinkage tests [Holt (2001), Al-Amoudi et al. (2006), Jensen and Hansen (1996), Ishikawa et al. (2000)]. This situation creates a stumbling block in quantifying and comparing the results of numerous studies on early age shrinkage measurement.

Earlier studies on the early age shrinkage monitoring showed that specimen size and shape may produce significant effect on early age shrinkage monitored. In the autogenous shrinkage monitoring, earlier study by Miyazawa and Tazawa (2001) reported that the rate of autogenous shrinkage increased with an increase in specimen size. This could be attributed to the acceleration in hydration process due to higher temperature rise on larger specimens. On the other hand, in the early age drying shrinkage monitoring, earlier study by Slowik et al. (2004) showed that the early age drying shrinkage was nearly independent of the specimen size during the first few hours (i.e. approximately within the first 6 hours after water was added to the mixture). However, as the evaporation proceeded, smaller specimen shrank faster. Another study by Wong et al. (2007) tested two specimens with a volume-to-exposed surface area or V/S ratio of 25 mm and 75 mm. The results showed that during the early ages, the specimen with lower V/S ratio registered a higher shrinkage strains compared to the specimen with higher V/S

ratio. Despite the extensive study on the effect of specimen sizes and shapes, the effect of gauge length on early age shrinkage strain has not been comprehensively explored and quantified in the literature. A review of available studies [Holt (2001), Al-Amoudi et al. (2006), Jensen and Hansen (1996), Ishikawa et al. (2000), Glišić and Simon (2000), Slowik et al. (2004)] showed that the gauge length used typically the longest available gauge length which may depend on the test set-up and the specimen size. Some of the shrinkage measurements utilized a fixed gauge length (e.g. embedded strain gauge) [Ishikawa et al. (2000)] or due to the nature of the instrumentation, a relatively small gauge length vis-a-vis the length of the specimen was used (e.g. when fiber optic sensors or large specimens are used) [Glišić and Simon (2000), Slowik et al. (2004)]. Moreover, as only one gauge length is adopted by each method, a meaningful comparison of the effects of adopting a different gauge length other than the one adopted in a particular study is not possible. In this regard, by utilizing the image analysis technique to quantify early age shrinkage strains, it is possible to use various gauge lengths on the same specimen and to observe the effect of gauge lengths on the early age shrinkage strains monitored.

3.1.2 General Technique for Monitoring Early Age Shrinkage Strain

In the monitoring of early age shrinkage of cementitious materials, emphasis has been placed on monitoring either autogenous shrinkage strains or early age drying shrinkage strains. For both autogenous and early age drying shrinkage monitoring, several techniques reported in the literature can be classified as being either volumetric or linear-based measurement techniques. Volumetric measurements are often performed by casting a fresh batch of cementitious material encased in a membrane, e.g. rubber balloon that is submerged in a fluid. The volume change of the specimen is calculated based on the buoyancy principle (i.e. the variation of the weight of the submerged sample with time) [Tazawa and Miyazawa (1995), Holt and Leivo (1999), Loukili et al. (2000)]. On the other hand, linear-based measurements are frequently performed by casting the cementitious materials in a low friction rigid mold and recording the length change with respect to time [Holt (2001), Jensen and Hansen (1996),

Takada et al. (1999), Hammer (1999), Bjøntegaard et al. (2004), Zhang et al. (2003), Glišić and Simon (2000), Slowik et al. (2004), Ong and Kyaw (2006), JCI (1999), Morioka et al. (1999), Ishikawa et al. (2000), Esping (2007)]. Based on data available in the literature, most of the testing techniques that measure shrinkage linearly can be grouped as follows:

- Testing techniques that use "cast in nails" through a hole at the end of specimen with nail heads embedded in the cementitious materials [JCI (1999)].
- Testing techniques that use moveable endplates with plugs [Hammer (1999), Bjøntegaard et al. (2004), Morioka et al. (1999)].
- Testing techniques that use horizontal transverse bars cast within the cementitious materials [Takada et al. (1999)]
- Testing techniques that use vertical cast-in-bars [Holt (2001), Ong and Kyaw (2006)]
- Testing techniques that use embedded strain sensors [Zhang et al. (2003), Glišić and Simon (2000), Slowik et al. (2004), Ishikawa et al. (2000)]
- Testing techniques that make use of corrugated plastic moulds [Jensen and Hansen (1996), Esping (2007)]

Monitoring linear shrinkage strains at an early age is faced with several instrumental challenges that can generate ambiguous results. The difficulty of providing a firm anchorage at monitoring locations prior to setting, problems arising from mould friction, settlement problems, and problems with the rigidity of strain sensors have been reported in the literature [Holt and Leivo (1999), Kyaw (2007)].

Early age drying shrinkage is a complex phenomenon incorporating a range of deformations that occur immediately after casting. Autogenous shrinkage and shrinkage due to evaporation typically govern early age drying shrinkage [Radocea (1994)]. On top of this, during the early stage of a cementitious material, thermal dilation due to exothermic hydration and subsequent effects of cooling must also be accounted for in the measurement of early age

drying shrinkage. Typically most early age drying shrinkage monitoring techniques used at present time are rather similar to those used in monitoring linear autogenous shrinkage. Aside from taking into account temperature rise due to heat of hydration, the difference between autogenous shrinkage and early age drying shrinkage monitoring lies in whether there is moisture exchange between the specimen and the environment. In the former, the top surface is usually sealed by diffusion-tight plastic or aluminium foils immediately after casting to prevent any evaporation. While in the latter, the top surface may be left exposed to the environment as soon as the casting process is completed. It is important to note that early age drying shrinkage has been reported to exhibit similar behavior to long term drying shrinkage in that it varies with depth from the exposed surface [Neville (2003)]. This indication of variation on early age drying shrinkage was also mentioned by Ong and Kyaw (2006). It stated that: "… *it is reasonable to expect that the pins would move along with the specimen as it shrinks; the pins, due to their small diameter, may adopt an inclined position if shrinkage varies with the depth of the specimen. Because the water loss is expected to be highest from the exposed trowelled surfaces, it is likely that in the present test setup, shrinkage is not as high in parts of the specimen near the base of the mold*'. Despite this fact, most of the linear measurement techniques in use at present seem to be monitoring an "average" value of the early age drying shrinkage strain across the whole cross section of the specimens.

An earlier attempt to directly measure the shrinkage strains at different depths was reported by Hammer (2002) and Slowik et al. (2004). The early age drying shrinkage strains were measured at 5 mm and 50 mm below the top exposed surface by using either "cast-in-nails" screwed into IDT (inductive displacement transducers) through a hole at each end of the specimens [Hammer (2002)] or FBGs (fiber Bragg gratings) sensors [Slowik et al. (2004)]. In using the first method, it is important to note that there is a possibility of loss of grip in the "cast-in-nails" used. In addition, the inherent rigidity of the IDT in comparison to the still soft cementitious materials may also affect the accuracy of some of the early age shrinkage readings [Kyaw (2007)]. The use of FBGs sensors may solve the aforementioned problem. However, with the rather complicated experimental test setup, fragility and high cost of the sensors; such

limitations may become major drawbacks for the use of FBGs in the monitoring of early age drying shrinkage [Slowik et al. (2004),Wong et al. (2007)].

3.2 Methodology

In the light of the aforementioned, the effect of gauge length used on the early age shrinkage strains monitored was studied by using the image analysis technique. In addition, the following section also describes a technique capable of monitoring shrinkage development at different depths from the top surface of newly cast cementitious materials with acceptable accuracy. The proposed technique is based on the image analysis technique developed previously by by Ong and Kyaw (2006). In the present study, the image analysis technique has been extended to allow capturing of images of targets mounted on the side of the prism specimens. The proposed technique enables early age shrinkage monitoring to be conducted on prism specimens which are expected to register differences in shrinkage with depth from the top surface.

3.2.1 Image Analysis Technique

3.2.1.1 Principles of Image Analysis

As mentioned previously, the image analysis technique used for monitoring early age shrinkage is based on earlier work reported by Ong and Kyaw (2006). This technique goes some way in overcoming some of the difficulties associated with the fixing and placing of measurement gauges for early age shrinkage monitoring on fresh cementitious mixtures starting from before the mixture sets. The method reported is able to monitor shrinkage strains as early as 30 minutes after adding water to the mixture. Another advantage of the image analysis technique include its flexibility to be used with a number of specimen configurations, viz. slabs or prisms, specimen with different cross section, as well as composite specimens comprising freshly cast cementitious materials on a hardened concrete substrate. A flowchart of the image analysis technique is shown in *Figure 3.1*. This technique comprises embedding targets into the

cementitious materials, capturing the image of the targets, analyzing the position of the targets on an image database, and finally evaluating the shrinkage strains.

Figure 3.1 Flowchart of image analysis technique

3.2.1.2 Targets used for Image Analysis Technique

As shown in *Figure 3.2***,** the present study utilized a similar light-weight target used by Ong and Kyaw (2006). The targets were made from steel pins 75 to 125 mm long and 1.5 mm in diameter. These pins were topped with plastic discs, 6 mm in diameter. A 4 mm square inked target was glued on the top of the plastic disc. Each of these targets weighs about 1.3 to 2.6 gram. Pairs of these 4 mm squares were used as targets for monitoring shrinkage of the cementitious test specimen.

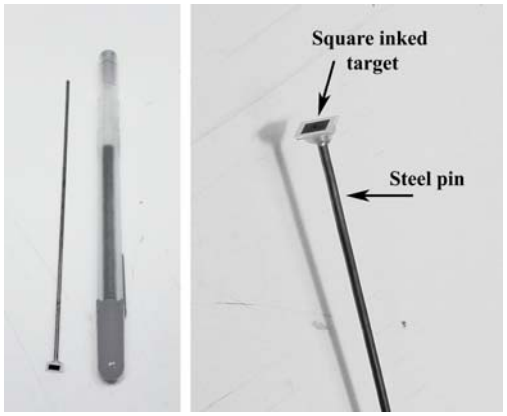

Figure 3.2 Target pin used in image analysis technique for monitoring early age shrinkage strains

3.2.1.3 Image Capturing

The image analysis technique relies on the use of high resolution Digital Single-Lens Reflex (DSLR) cameras to capture the movement of targets embedded in the cementitious specimens. Three DSLR cameras with a maximum resolution of 6.3, 10.1, and 12.4 megapixels

were used in the present study. In the image analysis technique, it is important to capture a sharp image of the targets thus necessary precautions are emphasized to reduce vibration that might affect the results of the image captured. These include securing the cameras on a tripod or a fix platform and controlling the cameras remotely. In addition, in order to minimize the effect of lens distortion, a specific focal length must be maintained during the entire testing period. A more detailed treatment on the effects of lens distortion, as well as the influence of the distance between targets and the lens on accuracy of the image analysis technique are available in previous work reported by Kyaw (2007).

The initial reading (i.e. the first image captured) was taken approximately 30 minutes after water was added to the mixture. The subsequent images of these targets were taken at specified time intervals, e.g. 5-minute intervals. Using the aforementioned equipments, the size of each image captured using the current test set-up was either 3072×2048 pixels, 3888×2592 pixels, or 4288×2848 pixels. According to previous study reported by Kyaw (2007), the sensitivity of the image analysis can be improved by resizing the image to approximately three times of its original size. Therefore, similar procedure was also implemented in the present study. After the resizing process, a series of images captured were compiled into one database, ready to use as the input for the image analysis process.

3.2.1.4 Image Analysis Process

To analyze the image database, commercially available image analysis software[1] was used in the present study. There are several steps in the image analysis process. These include segmentation, tracking, and coordinate-correction algorithm.

3.2.1.4.1 Segmentation/Threshold

The targets embedded in cementitious materials are the key information of the cementitious deformation. Therefore, image segmentation (i.e. separating targets from the

[1] Image Pro 6 was used due to the availability of image analysis software. Any brands of image analysis software could be used for the image analysis technique; provided that the software is capable of performing tasks mentioned in this thesis.

background) is a fundamental process. The simplest approach to do image segmentation is by conducting a thresholding. The important factor in the thresholding process is the choice of the threshold value. Several methods for choosing threshold value are available; it can be manually or automatically picked. In the present study, the threshold value is manually determined from the colour intensity values. *Figure 3.3* shows the target used with the corresponding red channel intensity values for the target and background. The threshold value was manually calculated based on *Eq. 3.1***.** In this approach, the threshold value was picked based on a mean intensity value of object (i.e. targets) and the background. As the present study used a RGB color image (i.e. Red Green Blue color space) on its analysis, the same procedure was performed for each color channel.

$$Threshold\ value = \frac{A - B}{2} \qquad Eq.\ 3.1$$

Where: A is the average pixel value of the background

B is the average pixel value of the object / target

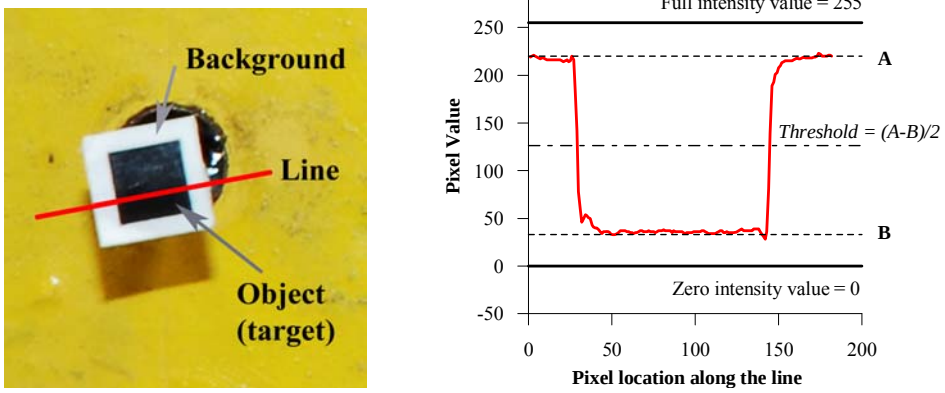

(a) *(b)*

Figure 3.3 (a) original image of the target; and (b) corresponding pixel value along the line marked in the original image

3.2.1.4.2 Tracking

After the targets are separated from the background, the next step is tracking process. In the tracking process, the program tracks the "same" target in the subsequent images. In the present study, the interest was to determine the variation X-Y coordinates with time (i.e. *X(t)* and *Y(t)*) of the targets embedded in the cementitious materials.

3.2.1.4.3 Coordinate Correction Algorithm

In the image analysis technique, coordinate correction algorithm is also important. As mentioned previously, necessary precautions were emphasized to reduce a vibration that might affect the results of the image captured. Nevertheless, a slight vibration during the experiment was still possible to occur. This unwanted vibration may induce additional variation in the target's coordinate computed in the previous step. Therefore, to compensate an error due to the unwanted vibration, a coordinate correction algorithm was employed as follows:

$$\begin{aligned} X(t) &= X(t,original) - \left[x(t) - x(0)\right] \\ Y(t) &= Y(t,original) - \left[y(t) - y(0)\right] \end{aligned} \qquad \textit{Eq. 3.2}$$

Where:

X(t) and *Y(t)* are the X-Y coordinate of specific target at time t after the correction

X(t,original) is the X coordinate of specific target at time t before the correction

Y(t,original) is the Y coordinate of specific target at time t before the correction

x(t) and *y(t)* are the X-Y coordinate of reference point at time t

x(0) and *y(0)* are the X-Y coordinate of reference point at time 0

3.2.1.5 Shrinkage Strains Evaluation

In the image analysis, the shrinkage strain is calculated based on a length change (i.e. a change in the number of pixels) between a pair of targets embedded in the cementitious materials (i.e. *Eq. 3.3*). The original distance between the two targets is calculated at the time zero value (i.e. TZV) adopted. At certain time t, the distance between this pair of targets is

recomputed. The shrinkage strain is obtained by dividing the length change with the original length. Given the present testing arrangement, the resolution of the image analysis technique is approximately ± 12 με [Ong and Kyaw (2006)].

$$Shrinkage\ strain = \frac{L(0) - L(t)}{L(0)} \qquad Eq.\ 3.3$$

Where:

L(t) is the number of pixels between the two targets at time t

L(0) is the number of pixels between the two targets at TZV

3.2.2 Image analysis for monitoring the early age shrinkage strains

Figure 3.4 shows the measurement schematic and the actual equipment set-up used in the present study. Shrinkage monitoring was carried out using cameras focused on two faces; the top trowelled surface of the specimens (i.e surface shrinkage) and the side of the specimens (i.e. shrinkage strains with respect to depth from the top exposed surface).

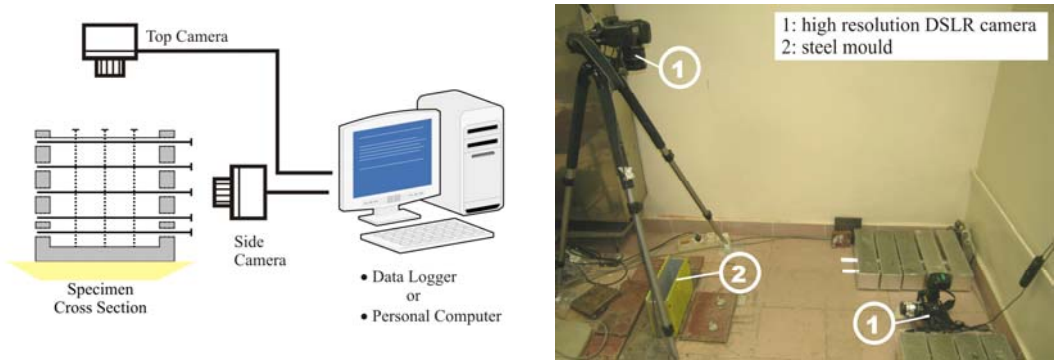

(a) *(b)*

Figure 3.4 (a) schematic of shrinkage measurement; and (b) the actual testing arrangement for monitoring shrinkage strains from the top and side faces.

In the present study, two sizes of molds were used. Steel molds with inner dimensions of 75 mm width by 75 mm depth and 285 mm length were used for mortar specimens, while steel molds with inner dimensions of 100 mm width by 100 mm depth and 400 mm length were

used for concrete specimens. The steel molds were lined with 1 mm thick Teflon sheets to reduce friction. A lining of plastic wrap was also used between the mortar mixture and the Teflon sheets to prevent leakage of the freshly placed cementitious mixture. During casting, the fresh cementitious mixture was placed in the molds and compacted on a vibration table. The exposed top surface was trowelled smooth and the targets for shrinkage monitoring from the top surface were inserted into the freshly cast specimen. In the case of autogenous shrinkage monitoring, the pins pierced through the plastic wrap that was placed over the top surface immediately after trowelling. Based on several preliminary tests, the effect of piercing the plastic wrap on the evaporation or shrinkage strains monitored was negligible. The targets on the top surface did not settle as the pins penetrated through the full depth of the specimens. The pins were firmly bonded to the surrounding mortar. Although it is reasonable to expect that the bond between the pin and the freshly placed mortar might not be robust during the initial one to two hours or so, once the mortar mixture stiffens, the pins were expected to move along with the mortar as it hardened and shrunk. This was confirmed by Ong and Kyaw (2006) by comparing the shrinkage strains monitored using laser sensor and image analysis. Both image analysis and laser sensor registered comparable shrinkage magnitudes after the initial setting time.

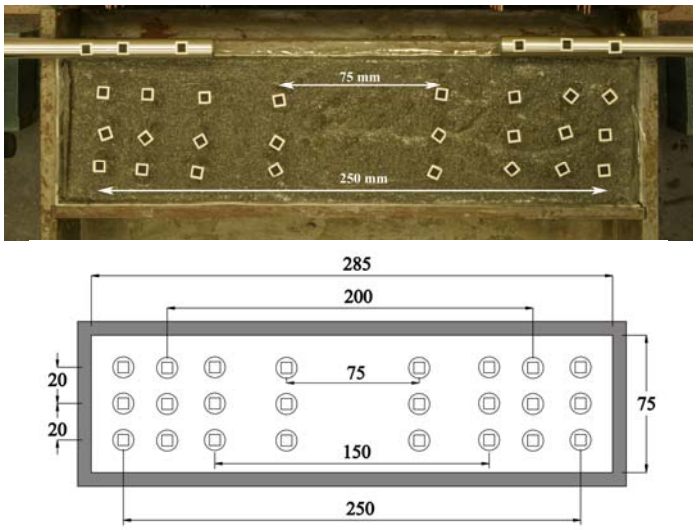

Figure 3.5 The arrangement of targets on top surface for gauge length experiment, mm

For studying the effect of gauge length on the shrinkage strains monitored, numerous pairs of targets were arranged so that the desired number of gauge lengths could be accommodated on the 285 mm long prism specimens**.** *Figure 3.5* shows the nominal gauge length (i.e. distance between selected pairs of targets) on the top surface of the specimen. The longest nominal gauge length was 250 mm and the shortest was 75 mm. The actual distance in pixel values between selected pairs of targets was used to compute the shrinkage strains in the present study.

As mentioned previously, the shrinkage monitoring was carried out from the top surface and at one side of each specimen. While the targets for shrinkage monitoring on the top surface were inserted into the freshly cast specimen just after casting was completed, the targets for shrinkage monitoring on the side of the specimen were positioned in the steel mold prior to casting. As shown in *Figure 3.6*, the early age shrinkage strains on the sides of the prism specimen were monitored using pairs of targets placed at different depths. In the case of 75×75×285 mm steel mold, the targets were placed at depths of 3, 20, 40, and 60 mm from the trowelled surface of the specimen. While for the 100×100×400 mm steel mold, the targets were placed at depths of 3, 20, 40, 60, and 80 mm from the trowelled surface of the specimen.

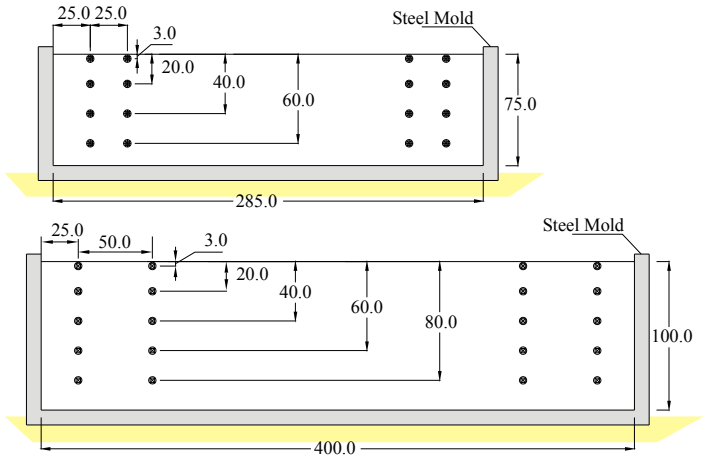

SIDE VIEW

Figure 3.6 The arrangement of targets on the side face of mould for two types of prisms used in the present study, mm

As shown in *Figure 3.7(a)*, 6 mm diameter holes were predrilled through both sides of the steel mold. Corresponding holes were also made in the Teflon sheets lining the interior faces of the steel mold. *Figure 3.7(b)* shows a layer of plastic wrap was used between the mortar mixture and the Teflon sheets to prevent leakage of the freshly placed cementitious mixture. A grease lubricant was also applied at locations where the pins pierced the plastic wrap to further minimize the possibility of leakage. As shown in *Figure 3.7(c)*, to hold the pins in position before and during casting, two semicircular rubber pieces were fitted into the 6 mm diameter holes after the pins were inserted through the plastic wrap lining the sides of the steel mold. The cementitious mixture was placed, compacted on the vibration table, and transported to the environmental chamber with the rubber pieces left in-place. These rubber pieces were removed prior to the start of early age shrinkage monitoring. The removal of the rubber pieces did not lead to leakage of any material from the still soft cementitious mixture due to the presence of the plastic wrap and viscous grease lubricant. As shown in *Figure 3.7(d)*, the monitoring of the targets started as soon as the specimen was placed in the environmental chamber, approximately 30 minutes after adding water to the mixture and monitored continuously for 24 hours. A temperature of 30 ± 0.5^{0}C [86 ± 0.9^{0}F] and a relative humidity of 65 ± 2% were maintained in the environmental chamber for the entire duration of the experiment. The temperature and relative humidity were selected to simulate environmental conditions prevailing under Singapore's tropical climate.

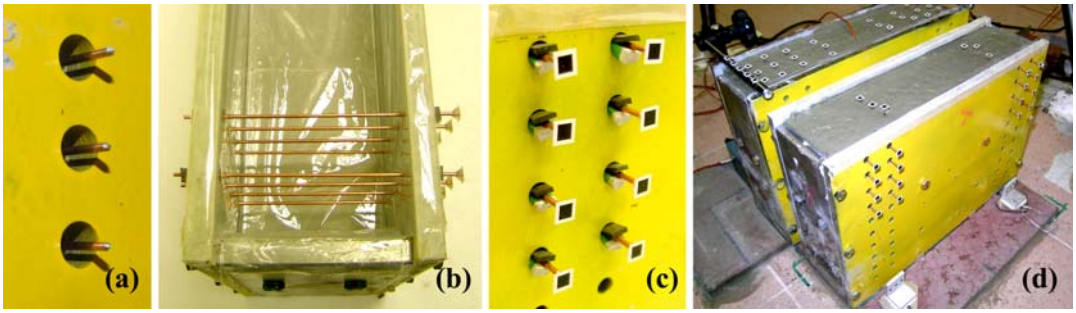

Figure 3.7 Specimens preparation for monitoring early age shrinkage with depth from the top surface

3.2.3 Laser technique

Besides the image analysis technique, the laser technique was also used for determining the length change of the cementitious specimens. The early age shrinkage strain monitored using the laser technique is typically referred as the "average" shrinkage value over the entire specimen's cross section. The laser testing set-up was made based on an earlier work by Morioka et al. (1999). As shown in *Figure 3.8(a)*, the laser sensors[1] with a resolution of 5 μm were fixed onto base plates to ensure the stability with the time. The cementitious deformation was measured via the reflection of laser beams from the surfaces of the reflection plate attached at both ends of the specimen. The reflection plate used for the laser sensor was made from 3 mm thick Perspex plate. Each plate was attached to 25 mm long 3 mm diameter threaded screw. The gauge length was taken as the distance between innermost ends of the screws attached to the reflection plates.

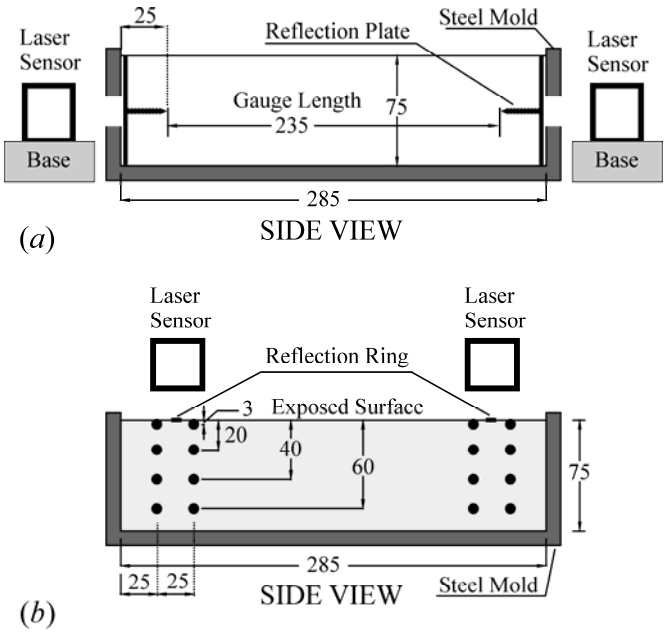

Figure 3.8 (a) Test set-up for early age shrinkage monitoring using laser sensors [Morioka et al. (1999)], and (b) test set-up for monitoring early age settlements of mortar prism specimens [Kaufmann et al. (2004)], mm

[1] Micro laser sensors, LM10 - ARN 1150 series, Nais, Matsushita Electronic Works Pte. Ltd

In addition to the early age shrinkage monitoring, the laser sensors were also used for monitoring the settlements of mortar prism specimens. As shown in *Figure 3.8(b)*, the settlements of mortar specimens were measured via the reflection of laser beams from a 6 mm diameter reflection ring located on the top surface of the mortar specimen. The reflection ring was made from PE plastic with metallic coating. The thickness of this reflection ring is about 0.02 mm and its weight is 0.0086 gr. This light-weight ring was placed directly on the top surface of the mortar specimen as soon as casting was completed [Kaufmann et al. (2004)].

3.2.4 Materials used

To study the effect of gauge lengths on the early age shrinkage strain monitored as well as to assess the capability of the image analysis technique for monitoring early age shrinkage with respect to the depth from the top surface, several mortar and concrete mixtures with water-to-cementitious ratio ranging from 0.25 to 0.35 were prepared. In all the mixtures, ASTM Type I normal OPC was used together with natural sand as the fine aggregate. The natural sand had fineness modulus and specific gravity of 2.8 and 2.6 respectively. Crushed granite with a maximum size of 12.5 mm and a specific gravity of 2.6 was used as coarse aggregates. Both coarse and fine aggregates were prepared according to the requirements specified in ASTM-C33-08 (2008).

Table 3.1 Mix porportions

Mixture	w/c	Agg. Vol. %	Water, kg/m^3	Cement, kg/m^3	Silica Fume, kg/m^3	Fine Agg. Kg/m^3	Coarse Agg. Kg/m^3	HRWRA	
								lt/m^3	by cement mass (%)
M25	0.25	50%	208	843	-	1300	-	5.28	0.25
M30	0.30	50%	231	776	-	1300	-	2.34	0.12
M35	0.35	50%	250	718	-	1300	-	1.26	0.07
C25	0.25	65%	144	588	-	790	900	4.42	0.30
C35	0.35	65%	175	501	-	790	900	1.88	0.15

In the case when a high range water-reducing admixture[1] was used, the amount of liquid was accounted for in the mix proportion calculation based on its liquid volume fraction of about 64.5%. *Table 3.1* shows the summary of the mortar and concrete mixtures proportion used in the present investigation.

3.3 Results and Discussion

3.3.1 The effect of gauge length on early age shrinkage strains monitored

As shown previously in *Figure 3.5*, the arrangement of targets on the top surface allowed shrinkage strains to be monitored based on nominal gauge lengths of 75, 150, 200 or 250 mm. Early age shrinkage strains of mortar mixtures cast with water-to-cementitious ratio of 0.25, 0.30, and 0.35 monitored from as early as 30 minutes up to 24 hours after adding water to the mixtures are shown in *Figure 3.9* to *Figure 3.11* respectively. In this thesis, the early age shrinkage strains reported refer to the total shrinkage strains experienced by the cementitious materials. No thermal or temperature correction was made to the results as this requires accurate determination of CTE (i.e. Coefficient of Thermal Expansion) at such very early ages. Results of early age shrinkage monitoring showed that the shape of strain-time curve for both sealed and unsealed specimens monitored by different gauge lengths is very similar. In the sealed mortar specimens tested, there was no significant difference in "absolute" shrinkage strains value monitored. However, in the unsealed mortar specimens, especially on M30 and M35 mortar mixtures, a reduction in the "absolute" value of shrinkage strain at 24 hours after adding water to the mixture was observed with shorter gauge lengths.

[1] ADVA 181N, W.R. Grace Pte. Ltd. Singapore

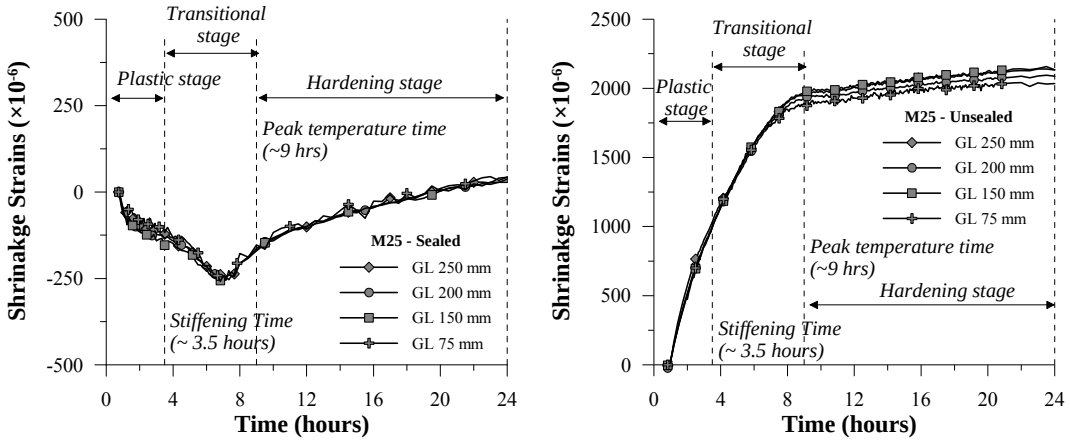

Figure 3.9 Early age shrinkage strains of (a) the sealed, and (b) the unsealed mortar specimens cast with water-to-cementitious ratio of 0.25 monitored based on different gauge lengths.

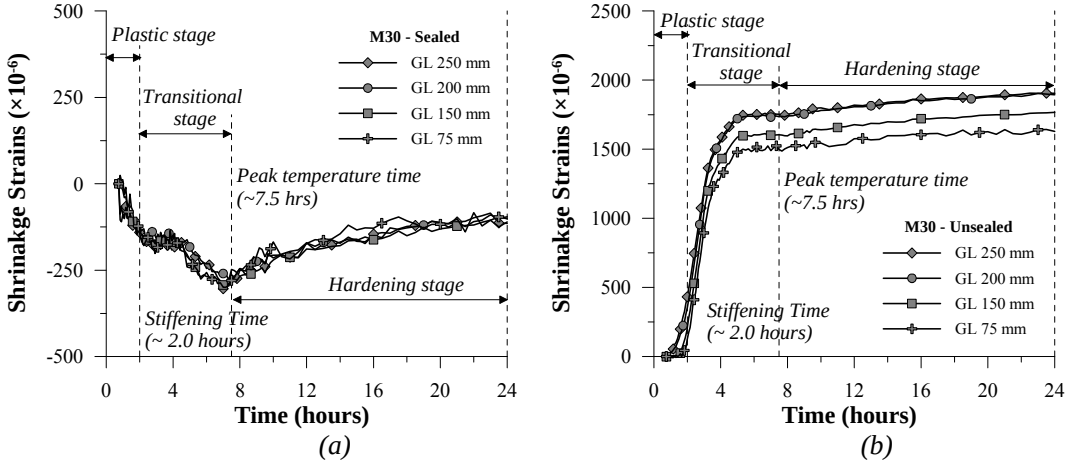

Figure 3.10 Early age shrinkage strains of (a) the sealed, and (b) the unsealed mortar specimens cast with water-to-cementitious ratio of 0.30 monitored based on different gauge lengths.

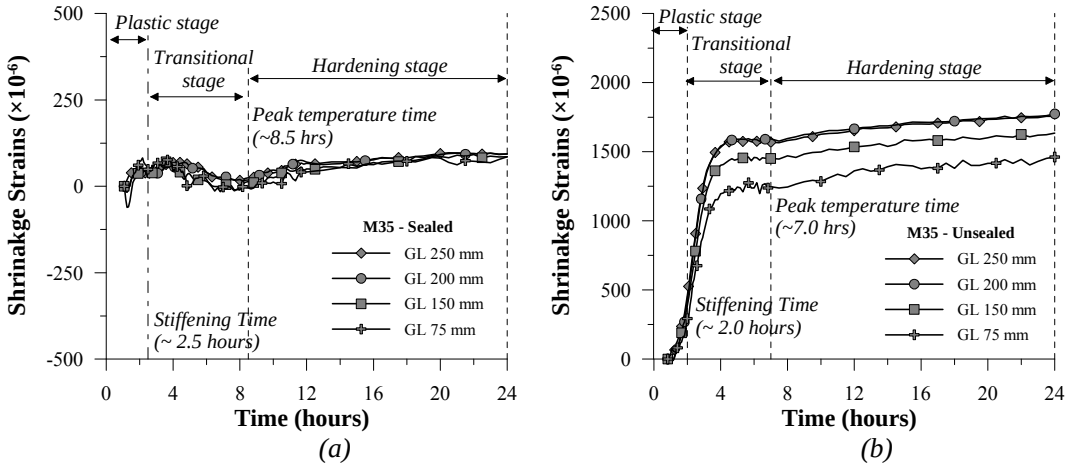

Figure 3.11 Early age shrinkage strains of (a) the sealed, and (b) the unsealed mortar specimens cast with water-to-cementitious ratio of 0.35 monitored based on different gauge lengths.

In order to investigate the effect of gauge length more clearly, the shrinkage-time curves were divided into three stages: plastic, transitional, and hardening stage. The stiffening time, as discussed in Chapter 2, was used as the boundary between plastic stage and transitional stage. In a similar approach with the heat evolution assessment, the peak temperature time was selected as the beginning of hardening stage. The amounts of shrinkage strains developed during these stages are shown in *Figure 3.12* and *Figure 3.13* for the sealed and unsealed mortar specimens respectively. As three measurements for each gauge length are possible, a range of results for each gauge length was also noted on the top of each bar.

In the sealed mortar specimens tested, considering the variation of the test results, there was no significant effect of gauge length on the shrinkage strains monitored at different stages. During the plastic stage, as shown in *Figure 3.12*(a), the "absolute" early age expansion values of 110, 140, 130, and 120 με were monitored in M25 mortar specimens using nominal gauge lengths of 75, 150, 200, and 250 mm respectively. While during the transitional stage, the "absolute" expansion values of 70, 40, 60, and 70 με were monitored using nominal gauge lengths of 75, 150, 200, and 250 mm respectively. Similarly, during the hardening stage, the "absolute" shrinkage strain values of 210, 220, 220, and 230 με were monitored using nominal gauge lengths of 75, 150, 200, and 250 mm respectively. In the case of M30 and M35 mortar specimens, similar trends were also observed.

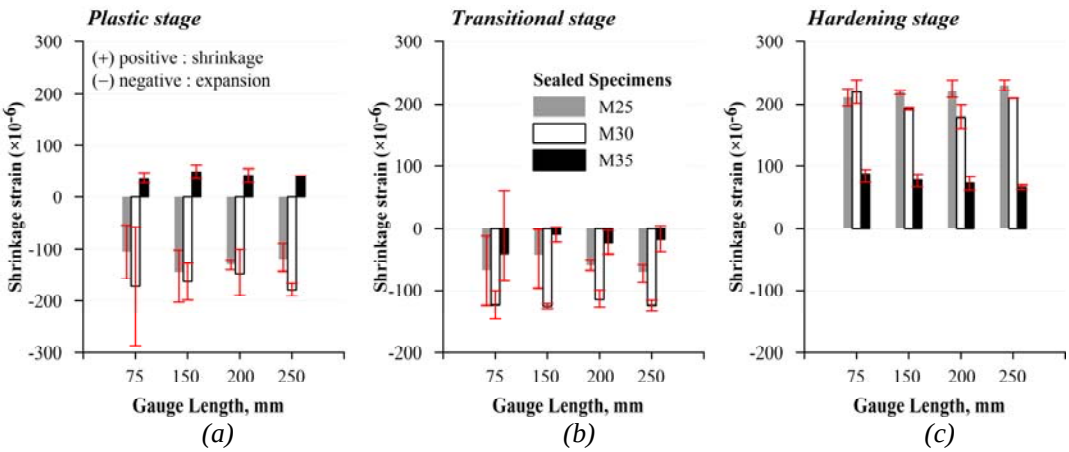

Figure 3.12 Comparison between shrinkage strains monitored based on different gauge lengths on the sealed mortar specimens during (a) plastic stage; (b) transitional stage; and (c) hardening stage

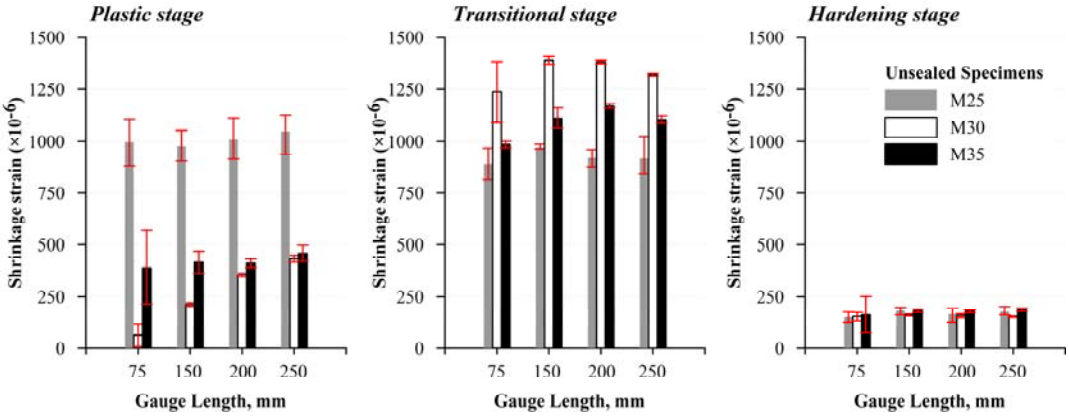

Figure 3.13 Comparison between shrinkage strains monitored based on different gauge lengths on the unsealed mortar specimens during (a) plastic stage; (b) transitional stage; and (c) hardening stage

In the case of the unsealed mortar specimens, as shown in *Figure 3.13*, the reduction in the early age shrinkage monitored using different gauge length was more prominent at early ages. As shown in *Figure 3.13(a)*, during the plastic stage, results showed that the M30 mortar specimen registered lower shrinkage strain values when the nominal gauge length used was less than 200 mm. On the other hand, the M25 mortar specimens showed that there was no significant decrease in shrinkage strain values using different sets of gauge lengths. During the transitional stage, as shown in *Figure 3.13(b)*, the M25 and M30 mortar specimens showed no reductions in the shrinkage strain values with shorter gauge lengths. In fact, slightly higher shrinkage strains were observed with shorter gauge lengths. On the other hand, the M35 mortar specimens showed a reduction in the shrinkage strain values when the gauge length used was less than 150 mm. Finally, during the hardening stage, as shown in *Figure 3.13(c)*, no significant reduction in the "absolute" shrinkage strain values was monitored for all the mortar specimens tested. It can be seen that comparable "absolute" shrinkage strain values were monitored for the M25, M30, and M35 mortar specimens, regardless of the gauge length used. Present results showed that for the unsealed mortar specimens tested, the "absolute" shrinkage strains value monitored was affected by the gauge length used. The reduction monitored on shorter gauge lengths mainly occurred during the plastic stage, prior to the stiffening time. After the stiffening time was reached, the "absolute" shrinkage strains value was less affected by the

gauge length used. Present results also showed that rather similar "absolute" shrinkage strains values for unsealed mortar specimens can be achieved using nominal gauge lengths of either 200 mm or 250 m. Although gauge lengths of more than 250 mm were not tested in the present study, shrinkage strains were expected to be similar to those based on 250 mm nominal gauge length.

Based on the present results, shorter gauge lengths may be used for monitoring early age shrinkage strains on sealed specimens. On the other hand, shorter gauge lengths may not be appropriate for unsealed specimens if the early age shrinkage strains that develop during plastic and transition stages are included in the measurement. In this regard, it is recommended to use longer gauge lengths (i.e. 200 or 250 mm) for typical prism specimens used for early age shrinkage monitoring. In the present study, for further analysis of results, a nominal gauge length of 250 mm will be the norm used.

3.3.2 Early age shrinkage strain with depth from the top surface of prism specimen

3.3.2.1 Settlement of the target monitored from the side of the prism specimen

In the present study, one objective is to demonstrate that the image analysis technique is capable of measuring settlements and early age shrinkage strains from one side of the prism specimen without any ambiguity in results. One potential issue concerns settlement of the target pins under its own weight. This "additional" settlement of the targets may affect the shrinkage strains monitored. In order to address this issue, settlement checking was conducted. The settlements of the targets located at different depths from the top exposed surface were compared to the settlements of the mortar specimens measured using laser sensors. As shown previously in *Figure 3.8*, laser sensors measured the settlement of mortar specimens through the reflection of laser beams from a 6 mm diameter reflection ring located on the top surface of the mortar specimens.

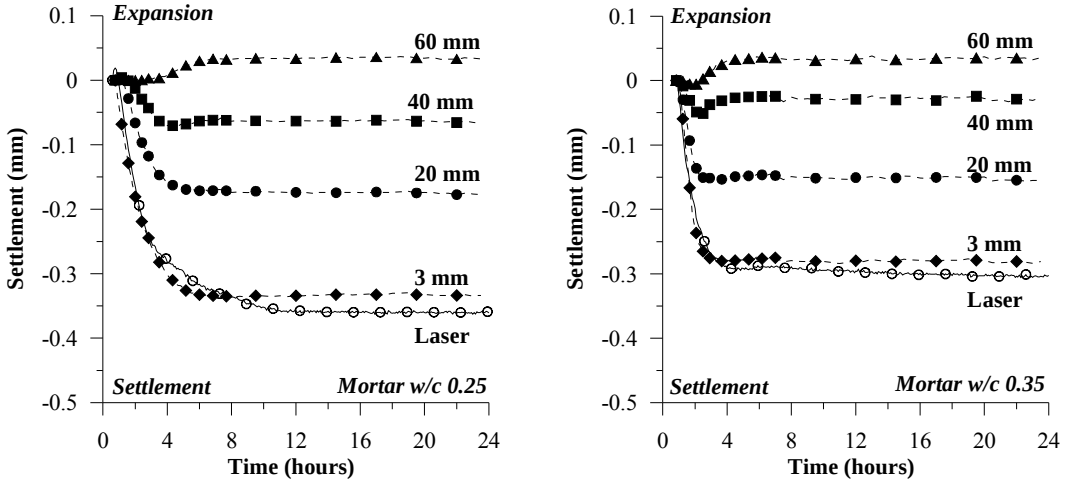

Figure 3.14 A comparison between settlements monitored using image analysis technique and laser sensor on mortar mixtures cast with water-to-cementitious ratio of (a) 0.25, and (b) 0.35 respectively.

Figure 3.14(a) and *Figure 3.14(b)* show the settlements measured using the image analysis technique and laser sensors on mortar specimens cast with a water-to-cementitious ratio of 0.25 and 0.35 respectively. As expected, during the first 24 hours after adding water to the mixture, the settlement readings of targets located at different depths showed that settlement of mortar specimens reduced with depth from the top exposed surface. The targets located near the top exposed surface registered higher "absolute" settlement values compared to that monitored near the base of the specimen. It can be seen also that the targets nearest to the base of the mould registered negligible settlements; in fact a slight "expansion" was registered. The results also showed that up to 4 hours after adding water to the mixture, the targets located at a depth of 3 mm from the top exposed surface registered settlement readings comparable to that monitored using laser sensors. At the end of the testing period (i.e. 24 hours after adding water to the mixtures) the laser sensors registered a slightly higher settlement compared to that measured using the image analysis technique. This however is not unexpected since the reflection ring used for the laser sensors was located directly on the surface of the mortar specimen, thus is expected that the reflection ring will settle more than the targets used in image analysis. Based on the results obtained, the self-weight of the targets used in the image analysis technique seemed to have a negligible effect to the settlement monitored. Thus the target movements

monitored from the side of the cementitious specimen correspond to the actual movement of the cementitious material in which the targets are embedded.

3.3.2.2 Early age shrinkage strains with depth in sealed mortar and concrete prism specimens

Figure 3.15(a) and *(b)* show the early age shrinkage strain monitored at various depths from the top surface of the sealed mortar specimens cast with a water-to-cementitious ratio of 0.25 and 0.30 respectively. The early age shrinkage strains were plotted from approximately 30 minutes after water was added to the mixture. It can be seen that the shrinkage-time curve of shrinkage strains monitored from the side of the sealed mortar specimens were rather similar. However, while total shrinkage strains monitored during the first few hours after adding water to the mixture showed primarily positive values (i.e. shrinkage), those monitored on the top surface registered negative values (i.e. expansion). When the total shrinkage strains for the same specimens were plotted using the stiffening time as the TZV, as shown in *Figure 3.16(a)* and *Figure 3.16 (b)*, it was observed that all the total shrinkage strains plotted including those monitored form the side of the specimens registered negative values (i.e. expansion) during the first few hours followed by positive values (i.e. shrinkage) at the later ages. In addition, the magnitudes of shrinkage strains monitored from both top surface and from the side of the specimens are largely similar. This phenomenon could be explained by examining in more detail the total shrinkage versus time values during the first 10 hours as plotted in *Figure 3.17* to *Figure 3.19*. In addition to the total shrinkage values, the settlements of the targets are also plotted. As mentioned previously, the settlements were obtained by tracking the vertical movement of the targets with time. It may be noted that upon closer inspection, the difference monitored for the shrinkage measurement from the top and from the side of the specimen occurred mainly during the plastic stage when the mortar is still fluid and workable. Moreover, the results also showed that the difference in the total shrinkage strain with time monitored during the plastic stage may be partially attributed to the difference in the water-to-cementitious ratio of the mixture being investigated. It can be seen that in the case of mortar specimens cast

using the mixture with a water-to-cementitious ratio of 0.25, the settlements measurement registered an expansion at a depth of 3 mm from the top surface during the plastic stage. Simultaneously, the corresponding shrinkage strains monitored from the top surface (i.e. "surface") also showed expansion during this stage. In the case of mortar specimens cast using a water-to-cementitious ratio of 0.35, settlements measurement showed no expansion was monitored. The corresponding shrinkage strains monitored from the top surface also showed no expansion during this stage. In the case of M30 mortar specimens cast using a mixture with a water-to-cementitious ratio of 0.30, it is expected that its behavior would be in between that monitored for the M25 and the M35 mortar specimens. The shrinkage strain monitoring from the top surface of the M30 mortar specimens showed a similar result to that of the M25 mortar specimens. The shrinkage strains monitored from the top surface of the specimens registered an expansion during this plastic stage. Based on the results obtained, it seemed that in the mortar specimens tested, this early age expansion during the plastic stage may contribute to the difference observed between the early age shrinkage strains monitored from the top surface (i.e. "surface") and from the side of the mortar specimens. As shown in *Figure 3.20*, when early age shrinkage is monitored from the top surface of the prism specimens, movement of the targets towards the camera lens (i.e. expansion) would result in a reduction in distance between the target and the camera lens. This may be registered as an increase in the number of pixels between the two targets embedded on the top surface. The reverse occurs in the event of a settlement. On the other hand, when the early age shrinkage measurement is carried out from the side of the prism specimens, the distance between the target and the camera lens does not change when there is settlement of the cementitious material. Even if there is settlement, the movement of the targets towards the base of the prism mold can be used to monitor the amount of settlement taking place.

The results, as shown in *Figure 3.17* to *Figure 3.19*, also showed that the shrinkage strains measurement from the side of the specimen seems to be less sensitive to the early age expansion or settlement of the mortar specimens during the plastic stage. It can be seen that the shrinkage trains monitored at a depth of 3 mm from the top surface registered comparable

absolute values to that monitored at a depth of 60 mm from the top surface of the sealed mortar specimens tested.

The results of early age shrinkage strains monitored using the image analysis technique was also compared with that monitored using laser sensors. Both tests were performed on the same specimens. The results for sealed mortar specimens cast with a water-to-cementitious ratio of 0.35 is shown in *Figure 3.19*. The result showed that during the plastic stage, the laser sensors registered a significant amount of shrinkage strains compared to that observed using the image analysis technique. The results implied that the shrinkage strains monitored using laser sensors were significantly affected by the settlement of mortar specimens, especially during the plastic stage. During this stage, mortar specimens are most likely to experience early age settlement as there is no solid skeleton to resist the volumetric deformation. This early age settlement may exert a force on the reflection plate attached on both ends of the mortar prism, causing the laser sensors to register shrinkage strains. Nevertheless, the results showed that after the stiffening time was reached, the shrinkage strains monitored using the image analysis technique and the laser sensors were rather similar in trend and magnitude.

In the case of concrete specimens, the results of early age shrinkage monitoring from sealed concrete specimens cast with a water-to-cementitious ratio of 0.25 and 0.35 are shown in *Figure 3.21(a)* and *Figure 3.21(b)* respectively. It can be seen that similar to that monitored on the sealed mortar prism specimens tested; the results showed that similar shrinkage strains were obtained at the various depths of the sealed concrete prism specimens. In a completely sealed specimen, shrinkage was not expected to show any major differences with depth. However, some minor variations were noted in the sealed concrete specimens tested, most probably due to a minor moisture loss from the sealed top surface and due to the resolution of the present test set-up.

The repeatability of early age shrinkage measurements conducted on two sealed mortar specimens each cast with a water-to-cementitious ratio of 0.25 and 0.30 are shown in *Figure 3.22(a)* and *Figure 3.22(b)* respectively. It can be seen that the variability is small. Repeated tests on other batches of mortar cast with the same water-to-cementitious ratio under the same

test conditions showed almost identical results. This implied that after the stiffening time is reached, image analysis technique could be used for monitoring early age shrinkage strains of the sealed mortar specimens with acceptable accuracy.

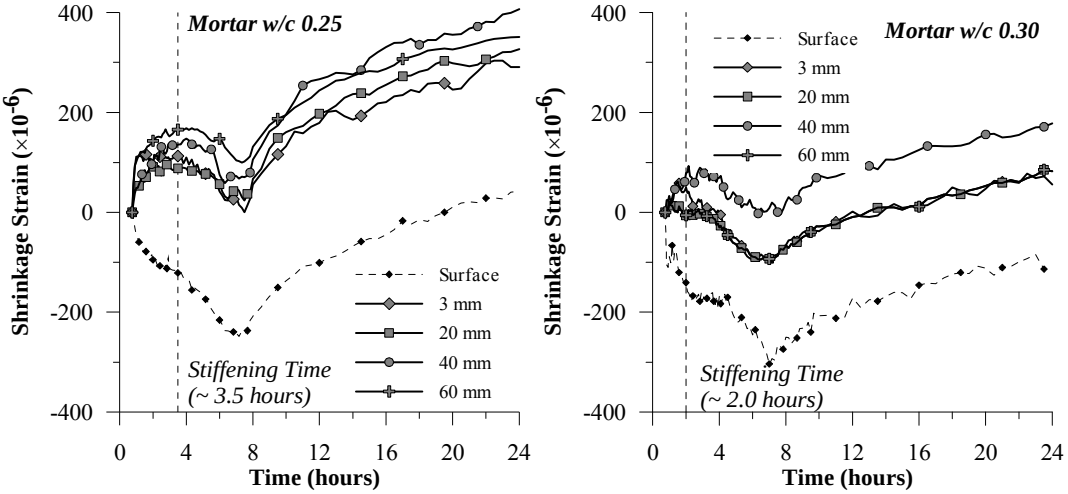

(a) *(b)*

Figure 3.15 Early age shrinkage strain with respect to the depth from the top surface on sealed mortar specimens cast with water-to-cementitious ratio of (a) 0.25 and (b) 0.30 starting from 30 minutes up to 24 hours after adding water to the mixture.

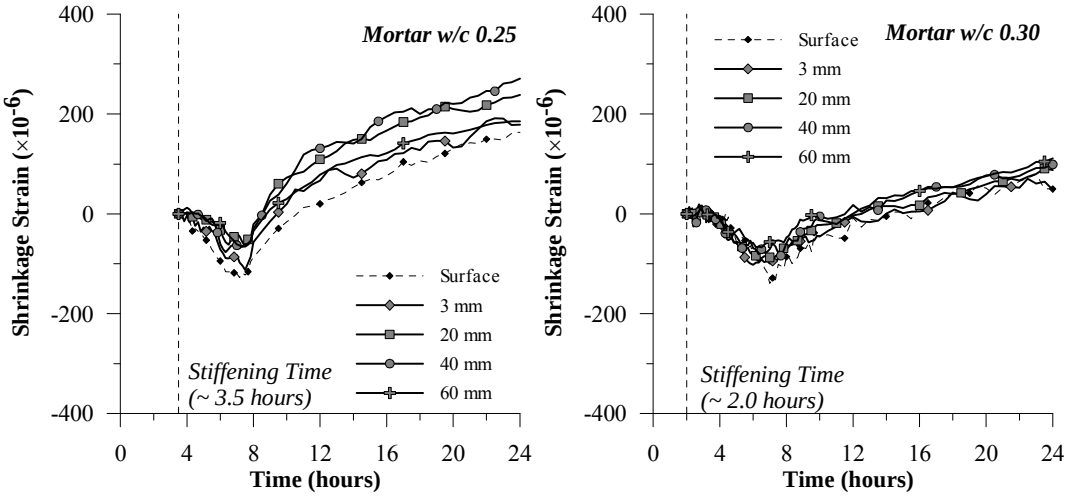

(a) *(b)*

Figure 3.16 Early age shrinkage strain with respect to the depth from the top surface on sealed mortar specimens cast with water-to-cementitious ratio of (a) 0.25 and (b) 0.30 starting from stiffening time up to 24 hours after adding water to the mixture.

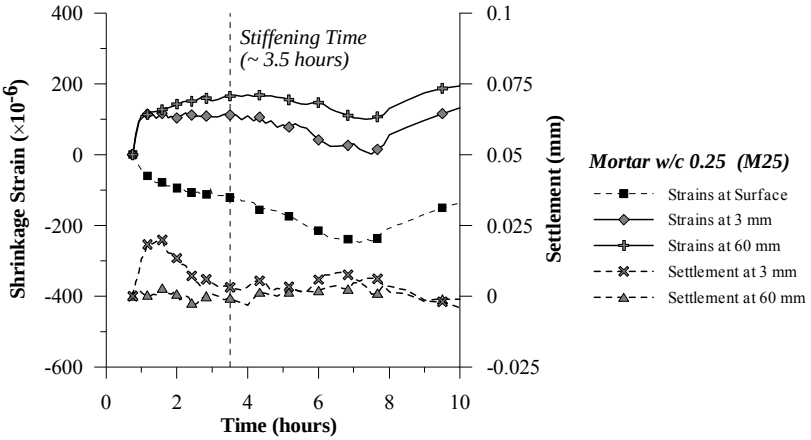

Figure 3.17 Early age shrinkage strains and settlements monitored using image analysis on sealed mortar specimens cast with water-to-cementitious ratio of 0.25, starting from 30 minutes up to 10 hours after adding water to the mixture.

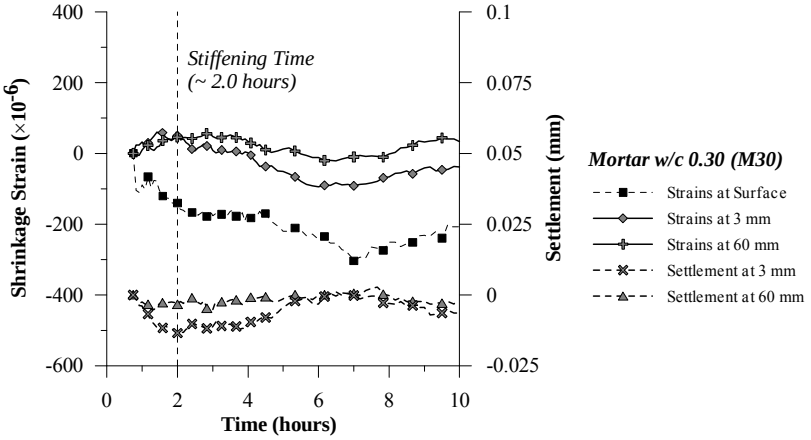

Figure 3.18 Early age shrinkage strains and settlements monitored using image analysis on sealed mortar specimens cast with water-to-cementitious ratio of 0.30, starting from 30 minutes up to 10 hours after adding water to the mixture.

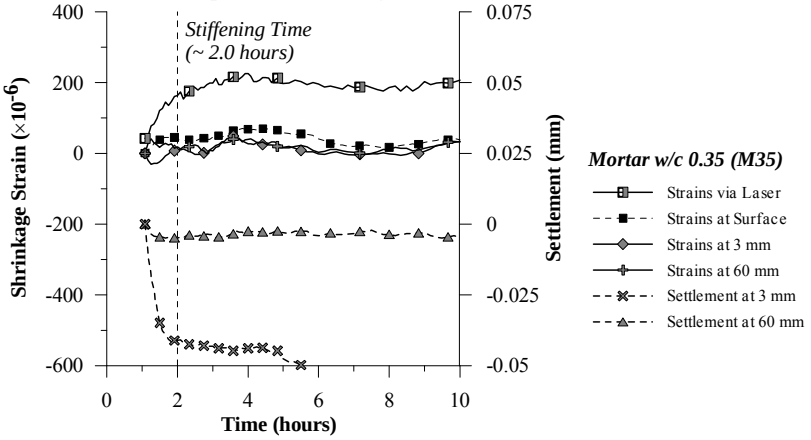

Figure 3.19 Early age shrinkage strains and settlements monitored using image analysis and laser sensors on sealed mortar specimens cast with water-to-cementitious ratio of 0.35, starting from 30 minutes up to 10 hours after adding water to the mixture.

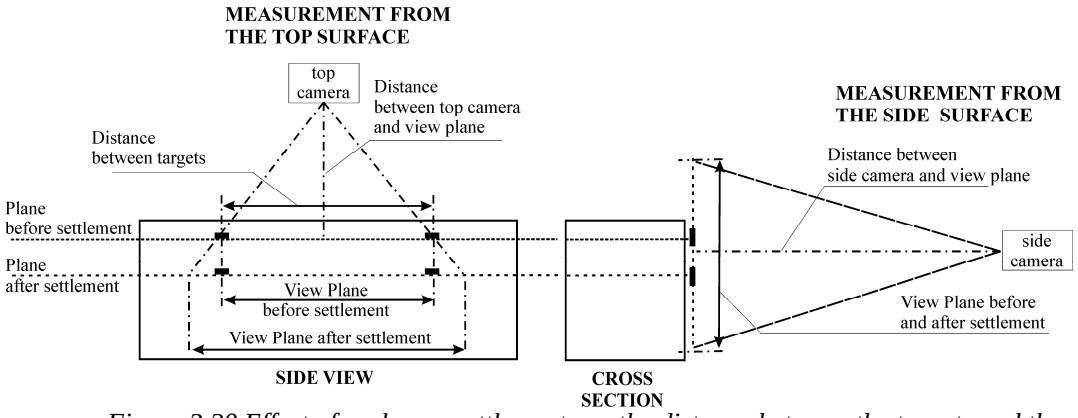

Figure 3.20 Effect of early age settlements on the distance between the targets and the camera mounted on the top and on the side of the prism specimen [modified from Kyaw(2007).

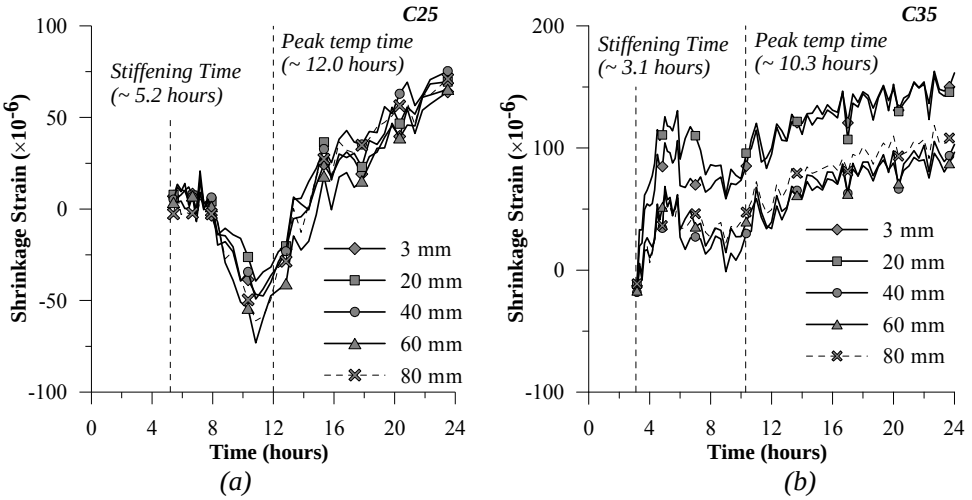

(a) *(b)*

Figure 3.21 Early age shrinkage strains monitored using image analysis on sealed concrete specimens cast with a water-to-cementitious ratio of (a) 0.25 and (b) 0.35 starting from stiffening time up to 24 hours after adding water to the mixture.

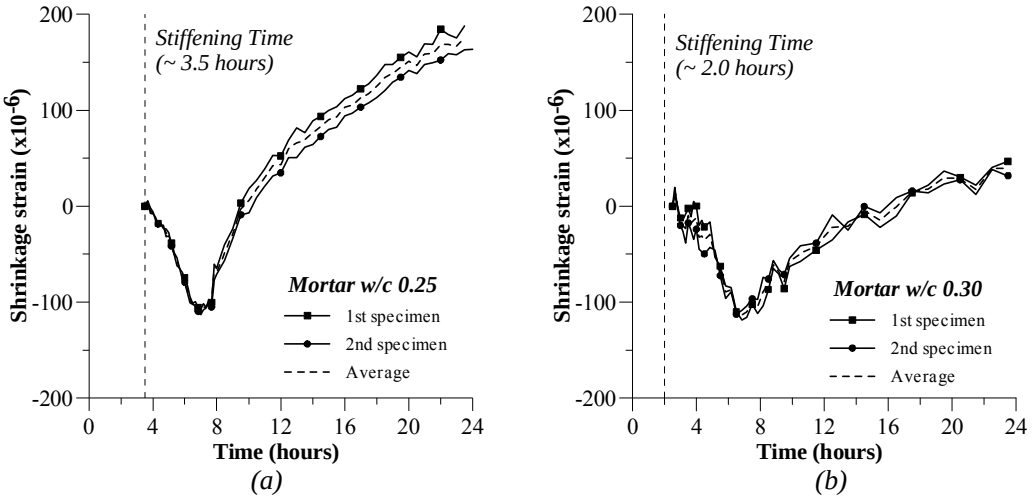

Figure 3.22 Repeatability of early age shrinkage measurement on sealed mortar specimens cast with a water-to-cementitious ratio of (a) 0.25 and (b) 0.30 starting from the stiffening time respectively

3.3.2.3 Early age shrinkage strains with depth in unsealed mortar and concrete prism specimens

Results of early age shrinkage monitoring from the top and the side of unsealed mortar specimens cast with water-to-cementitious ratio of 0.30 and 0.35 are shown in *Figure 3.23* and *Figure 3.24* respectively. The results clearly showed that different shrinkage strains at different depths were monitored in the unsealed mortar specimens. Starting either from 30 minutes after water was added to the mixture or from the stiffening time, the plots of the early age shrinkage strain at various depths versus time were rather similar one to another. However, "absolute" values of shrinkage strain decreased with depth from the top surface. A comparison of the shrinkage strains monitored on the top surface and from the side of the specimens showed that the targets inserted from the top surface registered the highest early age shrinkage strain. In the mortar specimens cast with water-to-cementitious ratio of 0.30, as shown in *Figure 3.23(a)*, starting from about 30 minutes up to 24 hours after water was added to the mortar mixture, the targets inserted into the top surface registered an "absolute" shrinkage strain value of 2350 με. The corresponding targets located at depths of 3 mm and 60 mm registered "absolute" shrinkage strain values of 2260 με and 1050 με respectively. Similarly, plotting with the TZV set at the stiffening time, as shown in *Figure 3.23(b)*, differences in the "absolute" shrinkage strain values

were also observed. An "absolute" shrinkage strain value of 1690 με was observed from the targets inserted into the top exposed surface, while at depths of 3 mm and 60 mm, the "absolute" shrinkage strain values were about 1420 με and 940 με respectively.

Figure 3.25(a) shows the development of early age shrinkage strains on mortar specimens cast with water-to-cementitious ratio of 0.35 during the first 6 hours after water was added to the mixture. It can be clearly seen that the shrinkage strain near the exposed surface started earlier. As shown in *Figure 3.25(b)*, at 1.5 hours after water was added to the mixture, the targets located at 3 mm depth from the top exposed surface already registered "absolute" shrinkage strain value of 250 με. As the evaporation continued, the shrinkage strains progressed into the interior of the mortar specimens. At the time when the stiffening time occurred, the "absolute" shrinkage strain values of 770 με and 125 με were observed at the depth of 3 mm and 60 mm respectively.

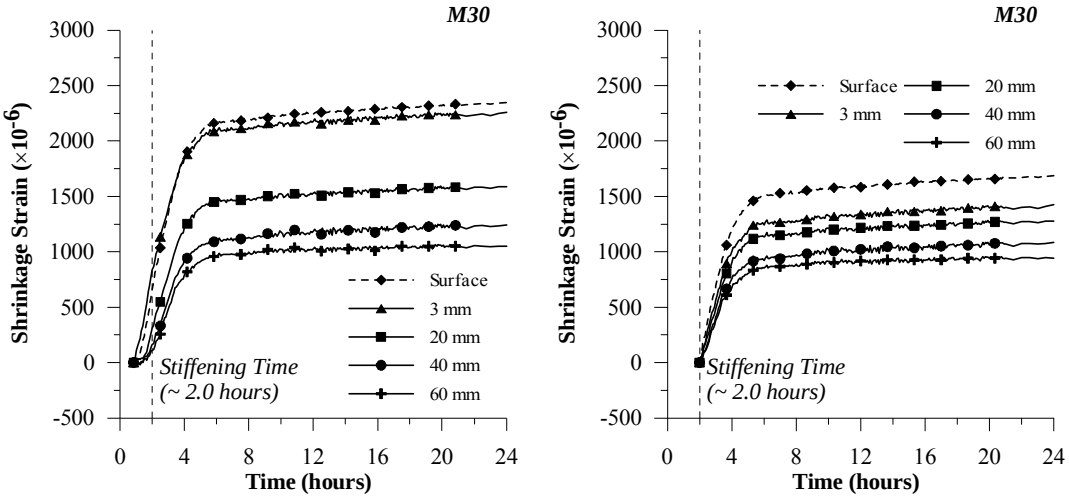

Figure 3.23 Early age shrinkage strain with respect to the depth from the top surface on unsealed mortar specimens cast with water-to-cementitious ratio of 0.30 starting from (a) 30 minutes after water was added to the mixture, and (b) stiffening time respectively.

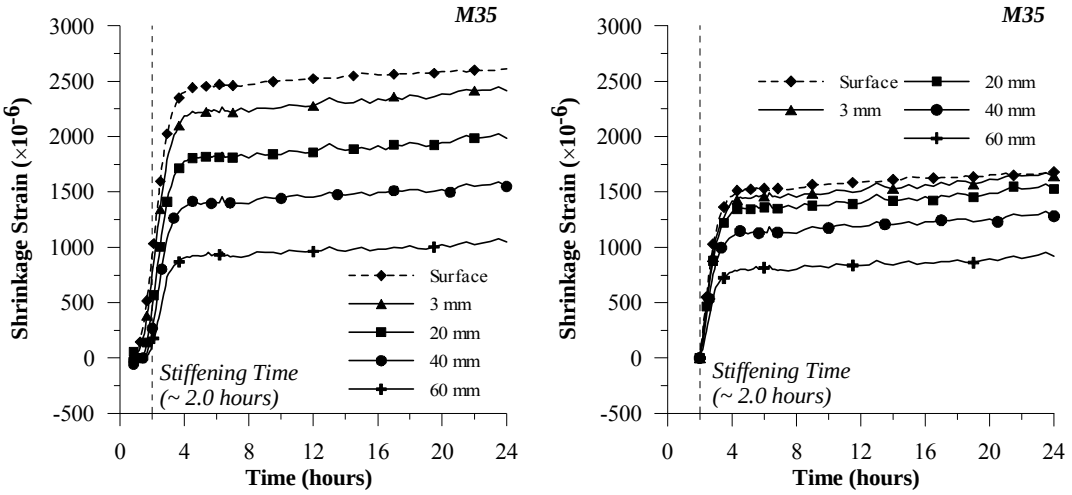

(a) *(b)*

Figure 3.24 Early age shrinkage strain with respect to the depth from the top surface on unsealed mortar specimens cast with water-to-cementitious ratio of 0.35 starting from (a) 30 minutes after water was added to the mixture, and (b) stiffening time respectively.

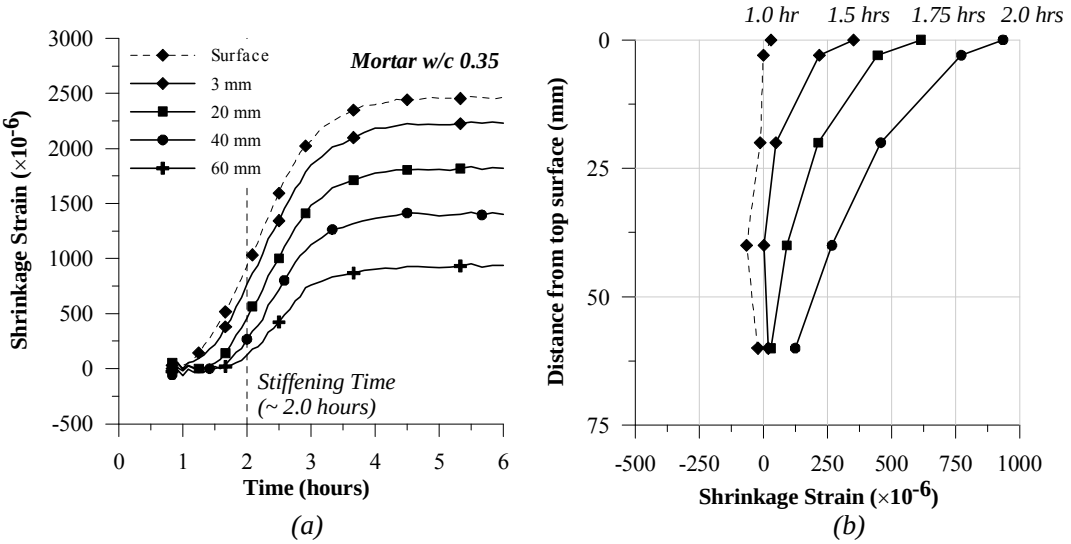

(a) *(b)*

Figure 3.25 (a) Early age shrinkage strain with respect to the depth from the top surface on unsealed mortar specimens cast with water-to-cementitious ratio of 0.35 starting from 30 minutes up to 6 hours after water was added to the mixture; (b) Early age shrinkage strain of unsealed mortar specimens as a function of depths from the top exposed surface during the paste-suspension phase.

The repeatability of early age shrinkage measurement was also conducted on two unsealed mortar specimens. *Figure 3.26* shows two sets of test results of early age shrinkage strains with depth from the top surface on two unsealed mortar specimens cast with a water-to-cementitious ratio of 0.30. It can be seen that both sets of test results were almost identical

except for that monitored at a depth of 60 mm. Nevertheless, the results imply that variability between specimens is relatively small.

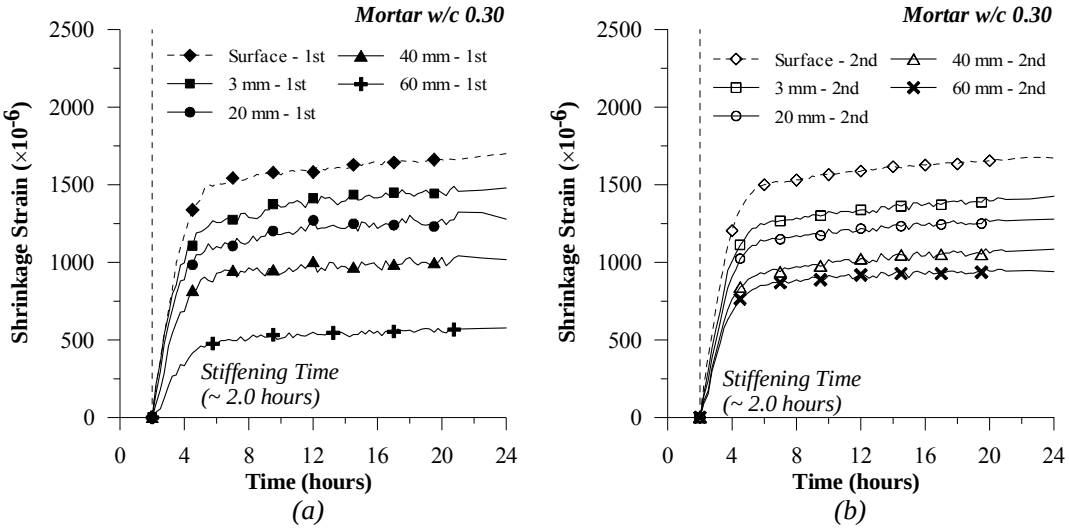

Figure 3.26 Early age shrinkage measurements on (a) first and (b) second unsealed mortar specimens cast with a water-to-cementitious ratio of 0.30 starting from the stiffening time respectivel

The early age shrinkage strains monitored using the image analysis technique on unsealed mortar specimens was also correlated with that measured using laser sensors. As shown in *Figure 3.27* and *Figure 3.28*, the results showed that during the plastic stage, the shrinkage strains monitored using laser sensors were lower than that monitored on the top surface. On the other hand, the development of shrinkage strains monitored using laser sensors was comparable to the average value of the shrinkage strains monitored from the side of the specimens, especially in the case of mortar specimens cast with a water-to-cementitious ratio of 0.25. It is also clear that after the stiffening time was reached, the shrinkage strains monitored using laser sensors were more in agreement with the average value of the shrinkage strains monitored from the side of the specimens.

In the case of concrete specimens, the results of early age shrinkage monitoring from unsealed concrete specimens cast with a water-to-cementitious ratio of 0.25 and 0.35 are shown in *Figure 3.29(a)* and *Figure 3.29(b)* respectively. It can be seen clearly that different shrinkage strains values were monitored at different depths from the top exposed surface of the unsealed

concrete prism specimens. A more detailed discussion dealing with early age drying shrinkage of unsealed mortar and concrete specimens is elaborated in the Chapter 4 of the present thesis. Based on the present study, the results showed that the image analysis can be conveniently used for monitoring early age shrinkage strains with respect to the depth from the top surface of both unsealed mortar and concrete prism specimens respectively.

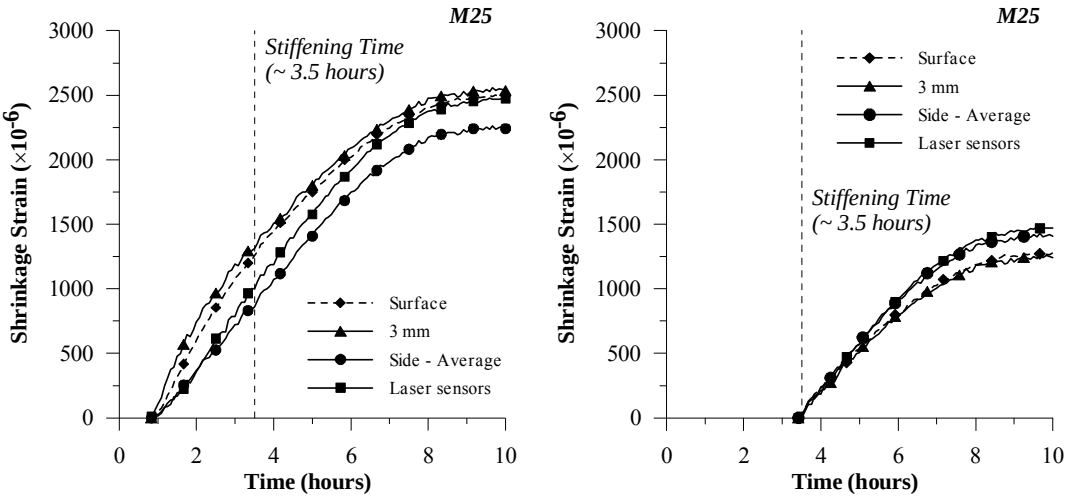

Figure 3.27 Early age shrinkage strain monitored using image analysis and laser sensors on unsealed mortar specimens cast with water-to-cementitious ratio of 0.25; starting from (a)30 minutes after adding water to the mixture, and (b) the stiffening time respectively.

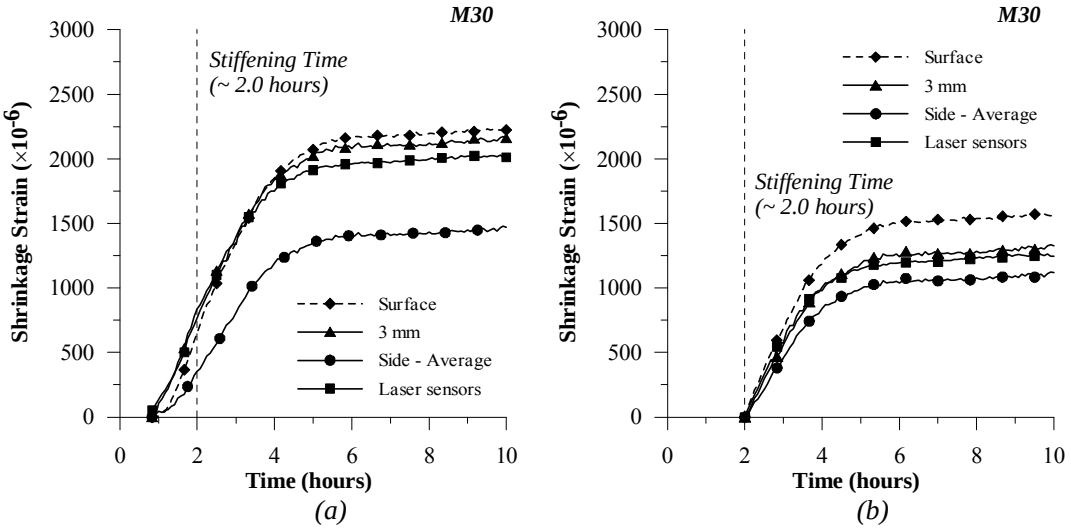

(a) *(b)*

Figure 3.28 Early age shrinkage strain monitored using image analysis and laser sensors on unsealed mortar specimens cast with water-to-cementitious ratio of 0.30; starting from (a) 30 minutes after adding water to the mixture, and (b)the stiffening time respectively.

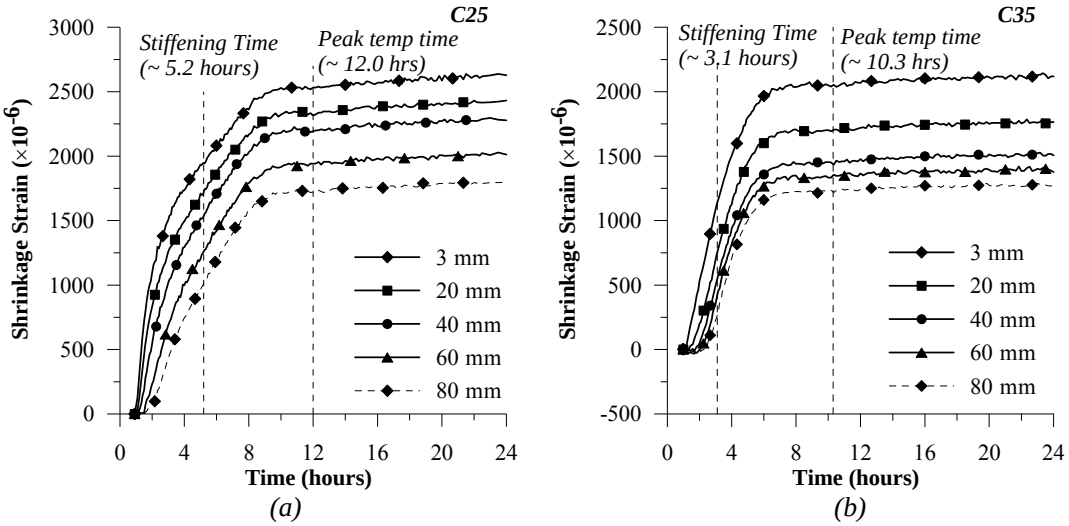

Figure 3.29 Early age shrinkage strains monitored using image analysis on unsealed concrete specimens cast with a water-to-cementitious ratio of (a) 0.25 and (b) 0.35 starting from 30 minutes up to 24 hours after adding water to the mixture.

3.4 Summary

This chapter discussed several issues related to the measurement of early age shrinkage strains in a typical cementitious prism specimen. Based on experimental studies carried out, the following conclusions could be drawn:

1. The gauge length used in early age shrinkage may affect the "absolute" value of shrinkage strains monitored. For several gauge lengths tested (i.e. 75, 150, 200, and 250 mm), the results showed that in the case of sealed prism specimens tested, a gauge length less than 200 mm could be used for monitoring early age shrinkage strains without any significant difference in the "absolute" shrinkage strains value monitored. On the other hand, a gauge length of less than 200 mm may not be suitable for unsealed prism specimens. The corresponding "absolute" shrinkage strain values were found to be lower than those obtained based on a nominal gauge length of 250 mm. The reduction in the "absolute" shrinkage strain values monitored when using shorter gauge lengths primarily occurred during the plastic stage, prior to the occurrence of the stiffening time. After the stiffening time, the "absolute" shrinkage strains value was less affected by the gauge length used. In this regard, it is recommended that gauge lengths in the order of 200 to 250 mm be used for early age shrinkage monitoring of typical prism specimens, especially unsealed prism specimens.

2. The present study also showed that image analysis technique may be used to monitor early age shrinkage strains with respect to the depth from the trowelled surface of monolithic mortar and concrete prisms specimens starting as early as 30 minutes after adding water to the mixture with acceptable accuracy. This technique can be applied for either sealed prism specimens (generally used for autogenous shrinkage monitoring) or unsealed prism specimens (typical of those used for early age drying shrinkage monitoring).

3. Based on the early age shrinkage strain monitoring using image analysis and laser sensors performed on sealed mortar prism specimens, the results showed that early age shrinkage readings using laser sensors and image analysis from the top surface of the specimens were affected by early age settlements or expansions during the plastic stage. On the other hand, the early age shrinkage readings from the side of the specimens seemed to be less affected by this early age settlements or expansions. The present results also showed that after the stiffening time is reached within the mortar specimens, comparable early age shrinkage strains were monitored using the image analysis technique either on the top surface or on the side of the specimens, as well as those monitored using laser sensors. Furthermore, as expected with the sealed mortar and concrete prism specimens, the early age shrinkage strain is relatively uniform across the whole cross section of the specimen.

4. The applicability of image analysis technique for monitoring early age shrinkage strains with respect to the depth from the top surface starting from approximately 30 minutes after adding water to the mixture was also demonstrated on the unsealed mortar and concrete prism specimens. As expected, the early age shrinkage strains vary significantly with depth from the exposed top surface of the mortar and concrete specimens especially when adopting a chronologically earlier TZV. A comparison between early age shrinkage strains monitoring using image analysis technique and laser sensors also showed that shrinkage strains monitoring using laser sensors is likely to provide an “average” value of shrinkage strain that develop across the whole cross section of the prism specimens.

Chapter 4 EARLY AGE SHRINKAGE STRAINS VERSUS DEPTH OF HIGH PERFORMANCE CEMENTITIOUS MIXTURES

4.1 Introduction

Early age drying shrinkage of cementitious materials is a parameter that affects the durability of concrete structures, including those made with high performance cementitious mixtures. To minimize the risk of cracking due to early age drying shrinkage, adopting adequate and proper curing processes starting from an early age is essential. Many techniques are available, including water-ponding, water-fogging, plastic sheeting, or wet burlap. Besides the aforementioned techniques, many construction practitioners also rely on the use of curing compounds for the proper curing of concrete. Unfortunately, the effectiveness and suitability of curing compounds depends largely on the concentration of volatile organic compounds (VOC), which has become the focus of the environment regulations. A study by Whiting and Snyder (2003) reported that the effectiveness of curing compounds decreases with a reduction in the VOC concentration. The reduction in the effectiveness of curing compounds as well as the difficulty to ensure that the environment is ideal curing in practice may eventually increase the possibility of fresh cementitious mixtures being exposed prematurely to a drying environment at an early age.

When curing is delayed or inadequate, the loss of moisture to the environment significantly increases the magnitude of early age shrinkage strains in such mixtures [Almusallam (2001)]. The loss of moisture generally starts from the exposed surface and progresses into the interior of the high performance cementitious mixtures depending on the inherent mixture properties and environmental conditions such as relative humidity, temperature, prevailing wind speed, etc. Since moisture loss varies with the depth from the exposed surface of a cementitious material, a non-uniform distribution of shrinkage strains within the cementitious material will develop [Neville (2003)]. An earlier study by Shin and Lange (2004) showed that in some cases of overlays, this non-uniform shrinkage strains may become one of

the major factors giving rise to surface cracking or debonding at the interface between the overlay and substrate layer. In addition, the variation of early age shrinkage with respect to the depth from the top surface of cementitious mixtures may also play an important role in early age cracking observed. The non-uniform shrinkage strains in conjunction with a high early age shrinkage strains experienced by most high performance cementitious mixtures may also increase the risk of cracking in such cementitious material.

In reality, the loss of moisture due to delayed or inadequate curing can occur very early and studies on the variation of shrinkage strain with respect to the depth from the top surface of high performance cementitious mixtures during the first 24 hours after adding water to the mixture is very limited. A review of available studies shows that the variation of shrinkage strains within cementitious specimens tested were typically monitored by assessing the changes in internal relative humidity [Shin and Lange (2004), Grasley et al. (2006)] or by direct monitoring of shrinkage strains at various depths [Kim and Lee (1998), Hammer (2002), Al-Saleh and Al-Zaid (2006)]. The direct monitoring of shrinkage strains at various depths reported in available literature is extremely rare. Some of these studies started measurements only after a period of curing has elapsed, thus very early age shrinkage strains developed during the first 24 hours after adding water to the mixture are not available [Kim and Lee (1998), Al-Saleh and Al-Zaid (2006)].

As mentioned previously in Chapter 3, earlier attempts to monitor the development of shrinkage strains at different depths have been reported by Hammer (2002) and Slowik et al. (2004). Results by Hammer (2002) showed that higher and earlier shrinkage strains developed near the exposed surface of concrete mixtures cast with a water-to-binder ratio of 0.30 when the top surface was exposed to an environment with 50% RH immediately after casting. A study by Slowik et al. (2004) on 60 mm thick cement paste with water-to-cementitious ratio of 0.45 showed that there was no significant difference in early age shrinkage strains monitored at depth of 5 mm and 50 mm. Only after about 1 day, the FBG sensor near the exposed surface started to register higher shrinkage strains compared to those located near the bottom of the specimens.

In this chapter, the development of early age shrinkage strains with respect to the depth from the top exposed surface by means of direct measurement was investigated. The influence of several mixture parameters to the variation of early age shrinkage strains within the specimen cross section was studied. The mixture parameters that were varied included the water-to-cementitious ratio, the aggregate volume proportion, and the addition of chemical or mineral admixtures.

4.1.1 Effect of High-range water reducing admixture (i.e HRWRA / superplasticizer)

High-range water-reducing admixtures or superplasticizers play an important role in today's high performance cementitious mixtures. As it is common to use low water-to-cementitious ratio cast with or without any addition of supplementary cementitious materials in such high performance cementitious mixtures, the use of high-range water reducing admixtures or superplasticizers is inevitable to achieve the desired workability. Earlier studies by Al-Amoudi et al. (2006) and Kyaw (2007) reported that the effect of superplasticizers on early age shrinkage is dependent on the type of superplasticizer used. Al-Amoudi et al. (2006) reported that the cementitious mixtures cast with Sulfonated naphthalene polymer (SNP) type superplasticizers registered higher early age shrinkage strains compared with other types of superplasticizers (i.e Modified lignosulfate polymer (MLP), Sulfonated naphthalene formaldehyde (SNF), and Polycarboxylic ether (PCE)). A more recent study by Kyaw (2007) reported that the cementitious mixtures cast with naphthalene formaldehyde type superplasticizer registered higher early age shrinkage strains compared with those cast with Polycarboxylate based superplasticizers. This higher early age shrinkage was attributed to the excessively longer retardation experienced by concrete mixtures with naphthalene formaldehyde based superplasticizers.

4.1.2 Effect of aggregate content

In a typical cementitious mixture, the aggregate particles may occupy 30% to 75% of the overall volume. These aggregate particles often act as a form of internal restraint that resists

movements and deformation, thus reducing the shrinkage strain monitored. An earlier study by Hobbs (1974) showed that the important influencing parameters pertaining to aggregates that affect the shrinkage of concrete are aggregate volume fraction and shrinkage of the aggregates themselves. In high performance cementitious mixtures, it has been reported that the stiffness of the aggregate could also affect the shrinkage response. Generally as the stiffness of the aggregate increased, the shrinkage strain monitored is reduced. Overall, the effect of aggregate in restraining the shrinkage strains monitored is substantial, as the shrinkage of a cement paste may be almost ten times higher than the shrinkage of a concrete (Neville (2003)).

4.1.3 Effect of water-to-cementitious ratio

The water-to-cementitious ratio is also regarded as an important parameter that influences the early age shrinkage of cementitious material. In high performance cementitious materials, in the absence of water curing, the autogenous shrinkage develops very rapidly and intensively due to its finer porosity. Studies by Tazawa and Miyazawa (1999) and Zhang et al. (2003) has clearly shown that the autogenous shrinkage of concrete increased with a reduction in the water-to-cementitious ratio. Similarly, when the top surface is exposed to dry environment at early ages, an increase in the early age shrinkage with a reduction in the water-to-cementitious ratio is noted especially during the first few hours after adding water to the mixture (Kyaw (2007)).

4.1.4 Effect of silica fume

The effect of silica fume on early age shrinkage is still controversial. An earlier study by Hammer (2001) tested for early age shrinkage starting just after the casting of concrete mixtures with a water-to-cementitious ratio of 0.40 and with 5, 10, or 15% silica fume replacement. It is reported that there was no significant effect of silica fume replacement on the early age shrinkage strains monitored. On the other hand, Al-Amoudi et al. (2004) reported that silica fume replacement increased the plastic shrinkage strains of concrete mixtures cast with a water-to-cementitious ratio of 0.45. Similar increase in the early age shrinkage strains of

concrete mixtures cast with a water-to-cementitious ratio of 0.30 or 0.35 and with 7 or 15% silica fume replacement was reported by Kyaw (2007). The increase in the early age shrinkage strains was more prominent during the first few hours after adding water to the mixture. The higher hydration rate and the lesser amount of bleed water available in the concrete mixtures with silica fume replacement were deemed as the cause for an increase in the early age shrinkage strains monitored.

4.2 Methodology and Mix Compositions

In this investigation, the image analysis technique as described in Chapter 3 was used for monitoring the variation of early age shrinkage strain with respect to the depth from the top surface of the prism specimens. The moisture loss with respect to time was monitored during the testing period by weighing the prism specimens on a digital scale with 0.1 g sensitivity. The first reading was taken immediately after casting and successive readings were taken automatically using data acquisition software. The moisture loss was computed by subtracting $w_{(i)}$ (weight at i-th hours) from $w_{(i-1)}$ (weight at (i-1)-th hours). Simultaneously, temperature readings were monitored on the same specimen using a thermocouple via an automatic data logger with a sensitivity of 0.1^0C. The workability of mortar and concrete mixture were determined via the flow test method (ASTM-C1437-07 (2007)) and the slump test method (ASTM-C143/C143M-09 (2009)) respectively. The flow of the mortar mixture or the slump of the concrete mixture was measured just after mixing was completed (i.e. within 10 to 15 minutes after water was added to the mixture). The assessment of stiffening time was performed by using the S-wave reflection technique as discussed previously in Chapter 2. In addition, the initial setting and the final setting time were also determined via the penetration test (ASTM-C403/403M (2008)) on companion mortar cubes. All the specimens were tested in the temperature and humidity controlled room with ambient temperature and relative humidity of 30 ± 0.5^0C and 65 ± 2 % respectively for the entire duration of the experiment.

The mortar and concrete mixtures tested with water-to-cementitious ratio ranging from 0.20 to 0.45 are shown in *Table 4.1*. Type I Portland cement with a Blaine fineness of 365 m^2/kg

was used in all cementitious mixtures. Crushed granite with a maximum size of 19.0 mm or 12.5 mm and a specific gravity of 2.60 was used as coarse aggregates. The smaller maximum aggregate size was used since it has less inherent defect as compared to the larger maximum aggregate size. In addition, study by Aïtcin (2001) also showed that larger MSA may lead to weaker transition zones containing more micro-cracks. Nevertheless, when the parent rock (from which the aggregate is derived) is sufficiently strong and homogeneous, 20 or 25 mm MSA can also be used without adversely affecting the workability and strength of the concrete [Aïtcin (2001)]. The fine aggregates used was natural sand with fineness modulus and specific gravity of 2.80 and 2.60 respectively. Both coarse and fine aggregates were prepared according to the requirement specified in ASTM-C33-08 (2008).

Table 4.1 Mixture proportion of mortar and concrete mixtures

Mixture	w/c	Agg. Vol. %	Water, kg/m^3	Cement, kg/m^3	Silica Fume, kg/m^3	Fine Agg. Kg/m^3	Coarse Agg. Kg/m^3	HRWRA	
								lt/m^3	by binder mass (%)
M30-SP 0	0.30	36%	291	952	-	942	-	0	0.00
M30-SP 0.08	0.30	36%	290	952	-	942	-	2.20*	0.08
M30-SP 0.18	0.30	36%	288	952	-	942	-	4.50*	0.18
M30-SP 0.28	0.30	36%	286	952	-	942	-	6.70*	0.28
M20	0.20	50%	155	906	-	1300	-	40.83	1.80
M25	0.25	50%	208	843	-	1300	-	5.28	0.25
M30, M30-SF0 M30-AG50	0.30	50%	231	776	-	1300	-	2.34	0.12
M35	0.35	50%	250	718	-	1300	-	1.26	0.07
M45	0.45	50%	281	625	-	1300	-	-	0.00
M30-SF5	0.30	50%	229	724	38	1300	-	4.39	0.23
M30-SF7.5	0.30	50%	227	701	57	1300	-	4.74	0.25
M30-SF10	0.30	50%	223	677	75	1300	-	8.10	0.43
M30-AG36	0.30	36%	300	1000	-	942	-	1.75	0.07
M30-AG45	0.30	45%	256	857	-	1170	-	2.15	0.10
M30-AG55	0.30	55%	205	694	-	1430	-	5.21	0.30
C25	0.25	65%	144	588	-	790	900	4.42	0.30
C35	0.35	65%	175	501	-	790	900	1.88	0.15
C45	0.45	65%	196	436	-	790	900	0.66	0.06
C30-SF0	0.30	65%	156	539	-	790	900†	2.50	0.18
C30-SF5	0.30	65%	155	500	26	790	900†	3.60	0.27
C30-SF10	0.30	65%	153	476	52	790	900†	5.10	0.39
C30-SF15	0.30	65%	149	436	77	790	900†	6.00	0.47

Note : * ADVA 108
† 19 mm MSA

Commercially available high-range water-reducing admixtures[4] were used in the cementitious mixtures to achieve the target workability. These chemical admixtures conform to ASTM-C494/C494M-08a (2008) as type F or G (retarding) admixtures. ADVA 108 and ADVA 181N have a specific gravity of 1.07 and 1.125 respectively. The solid content of these admixtures is about 35.5% by weight.

The mineral admixture used was commercially available densified microsilica with a specific gravity of 2.2. The SiO_2 content according to the product specification is 92.4%.

4.3 Results and Discussion

4.3.1 Effect of HRWRA

The effect of different dosage of HRWRA / superplasticizer was studied on mortar specimens cast with a water-to-cementitious ratio of 0.30. Four different dosages of superplasticizer, i.e. 0%, 0.08%, 0.18%, and 0.28%, were used. As can be seen in *Table 4.2*, the resulting workability based on the flow method was 40%, 80%, 100%, and 155% respectively. Results also showed that the stiffening time, the initial setting, and the final setting time were delayed with the addition of superplasticizer. The retardation became more prominent in mortar specimens with a higher dosage of the superplasticizer.

Table 4.2 Mixture properties of mortar with different dosages of surperplasticizer

Mixture	w/c	Agg. vol.	Workability	Stiffening time (hrs)	Initial set (hrs)	Final set (hrs)	Peak temp time (hrs)
M30-SP 0	0.30	36%	40%	1.0	2.5	3.8	7.8
M30-SP 0.08	0.30	36%	80%	1.6	3.1	4.6	8.5
M30-SP 0.18	0.30	36%	100%	2.5	4.0	5.7	9.5
M30-SP 0.28	0.30	36%	155%	3.7	5.2	7.3	11.5

The temperature development of mortar specimens cast with different dosages of superplasticizer during the first 24 hours after adding water to the mixture is shown in *Figure 4.1*. The results showed that the addition of superplasticizer did not change the peak temperature

[4] ADVA-108 and ADVA-181N, W.R. Grace Pte. Ltd. Singapore

reached. However, the peak temperature time was delayed with the addition of superplasticizer. This delay in the temperature rise was consistent with the delay in the stiffening time or the setting time as tested in the companion mortar cube.

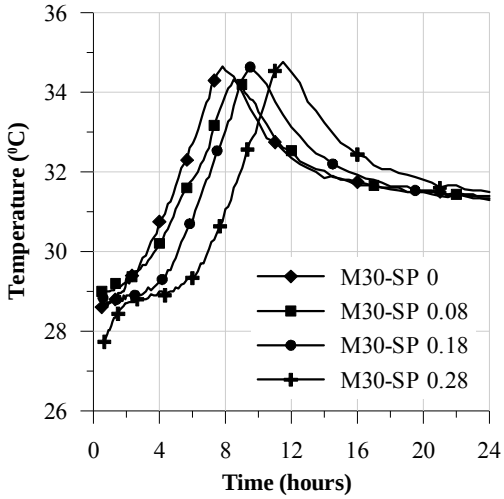

Figure 4.1 Temperature development of mortar mixtures with different dosages of HRWRA

The moisture loss measurement for these mortar specimens starting either from 30 minutes after adding water to the mixture or from the stiffening time up to the 24 hours after adding water to the mixture are shown in *Figure 4.2(a)* and *Figure 4.2(b)* respectively. Starting from 30 minutes after adding water to the mixture, the results of moisture loss measurement showed that the total moisture loss increased with an addition of superplasticizer. During the first few hours after adding water to the mixture, the total moisture loss was similar for all the mortar specimens. At about 8 hours after adding water to the mixture, the total moisture loss for the mortar specimens with lower superplasticizer dosages started to increase more gradually compared to those mortar specimens with higher superplasticizer dosages. At the end of the testing period (i.e. 24 hours after adding water to the mixture), the total moisture loss was about 62.3 gram and 72.3 gram for the mortar specimens without any superplasticizer (i.e. M30-SP 0) and with a superplasticizer dosage of 0.28% (i.e. M30-SP 0.28) respectively. The increase in the total moisture loss for the mortar specimens with higher superplasticizer dosages can be attributed to the retardation effect of the superplasticizer. As the stiffening time of the mortar

mixtures was delayed; evaporation would take place for a longer duration. As shown in *Figure 4.2(b)*, if the results were plotted starting from the stiffening time, the total moisture loss decreased with the addition of superplasticizer. This can be attributed to the fact that some portion of the mixing water present in the mortar mixture has already lost prior to the stiffening time, and as a part of the water became chemically bound due to cement hydration, less water became available for further evaporation.

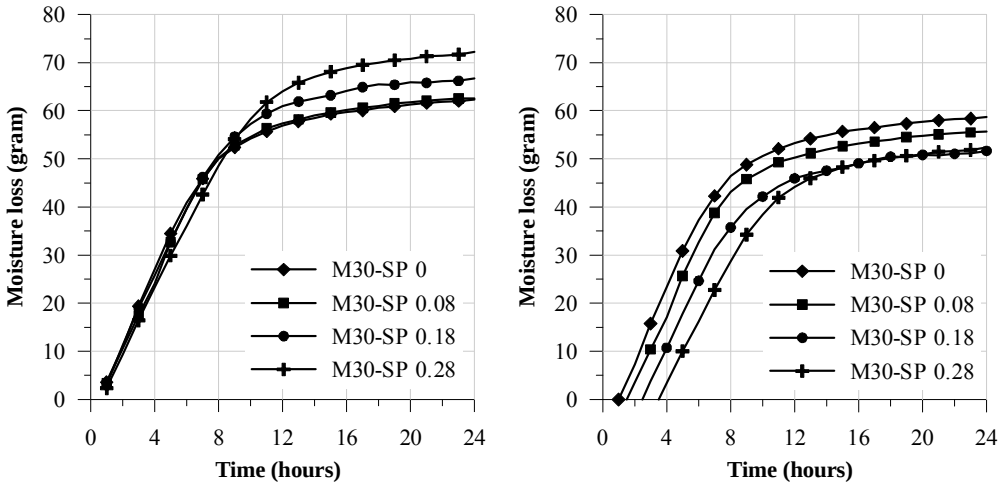

Figure 4.2 Moisture loss measurement for mortar specimens with different dosages of superplasticizer starting from (a) 30 minutes after adding water to the mixture, and (b) stiffening time up to 24 hours after adding water to the mixture

The early age shrinkage monitored at different depths from the top exposed surface of mortar specimens cast with different dosages of superplasticizer starting either from approximately 30 minutes after adding water to the mixture or from the stiffening time up to 24 hours after adding water to the mixture are shown in *Figure 4.3* to *Figure 4.6*. The results clearly showed that in the case of inadequate curing, moisture loss affected the shrinkage strains throughout the depth of the mortar specimens. Starting either from 30 minutes after adding water to the mixture or from the stiffening time, the shapes of the shrinkage strains-versus-time plots at different depths were similar and decreased rapidly with depth from the top surface. Plots of "absolute" shrinkage strains value-versus-distance from the top surface of the mortar specimens at 24 hours after adding water to the mixture with starting time either from 30

minutes after adding water to the mixture or from the stiffening time are shown in *Figure 4.7(a)* and *Figure 4.7(b)* respectively. Starting from 30 minutes after adding water to the mixture, as shown in *Figure 4.7(a)*, the results showed that the addition of superplasticizer increased the "absolute" shrinkage strains value monitored at all depths due to its "side effect" of delaying the stiffening time as well as prolonging the transitional stage of the cementitious mixture being investigated.. The increase in the "absolute" shrinkage strains value became more significant at higher dosages of superplasticizer. At a depth of 3 mm from the top exposed surface, the mortar mixture with superplasticizer dosage of 0%, 0.08%, 0.18% and 0.28% registered "absolute" shrinkage strain values of 2370 με, 2240 με, 3250 με, and 4830 με respectively.

On the other hand, plotting shrinkage strains from the stiffening time, as can be seen in *Figure 4.7(b)*, the results showed more gradual decrease in the "absolute" shrinkage strain value with depth from the top exposed surface. The addition of superplasticizer also increased the "absolute" value of shrinkage strain at all depths. An average increase of about 7%, 44%, and 110% in the "absolute" shrinkage strain value was registered by mortar specimens with superplasticizer dosage of 0.08%, 0.18%, and 0.28% respectively. This increase in the "absolute" shrinkage strains is observed even though the results of moisture loss assessment (i.e. *Figure 4.2(b))* showed that starting from the stiffening time, the total moisture loss decreased with the addition of superplasticizer. The increase in the shrinkage strains with the addition of superplasticizer may be due to longer transitional stage (i.e. period between the stiffening time and the peak temperature time) in the mixture with higher dosage of superplasticizer. It can be seen that the transitional stage of the mortar specimens with superplasticizer dosage of 0%, 0.08%, 0.18%, and 0.28% was about 6.8 hrs, 6.9 hrs, 7.0 hrs, and 7.8 hrs respectively. During this prolonged transitional stage, more gradual refinement of the mortar specimen's microstructure and porosity networks may occur. Simultaneously, as the evaporation draws water out from the mortar specimen, higher shrinkage strains could be induced within the mortar specimen.

Based on the results obtained, it seems that the use of HWRA with prolonged retarding effect would be detrimental in the case where early age shrinkage and cracking is important.

Nevertheless, in order to get a firm conclusion, we also need information on the development of mechanical properties of the mortar mixtures, such as its elastic modulus. Even though the shrinkage strains might be higher, if the elastic modulus of the mortar is low, then the resultant stresses generated within the mortar mixtures are also low. On the contrary, even though the shrinkage strains are lower, but if the elastic modulus of the mortar is quite high, then the resultant stresses are also high. In addition, in order to conclude whether the resultant stresses are high enough to cause cracking within the mortar mixture, then the tensile resistance/capacity as well as its creep or tensile relaxation of the mortar mixture needs to be taken into account. As long as the resultant stresses are lower than the mortar' tensile capacities, then the cracks will not occur.

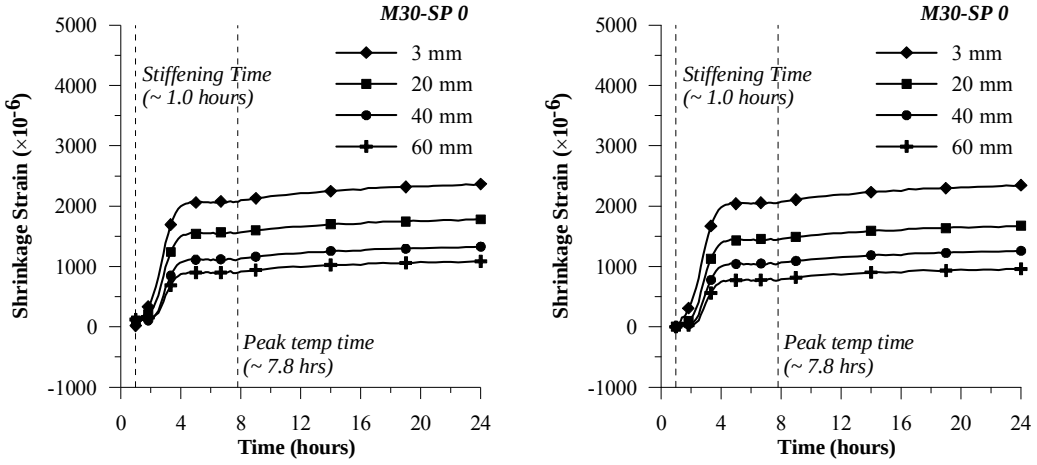

Figure 4.3 Early age shrinkage strain with respect to the depth from the top surface on unsealed mortar specimens cast with superplasticizer dosage of 0% starting from (a) 30 minutes after water was added to the mixture, and (b) stiffening time respectively

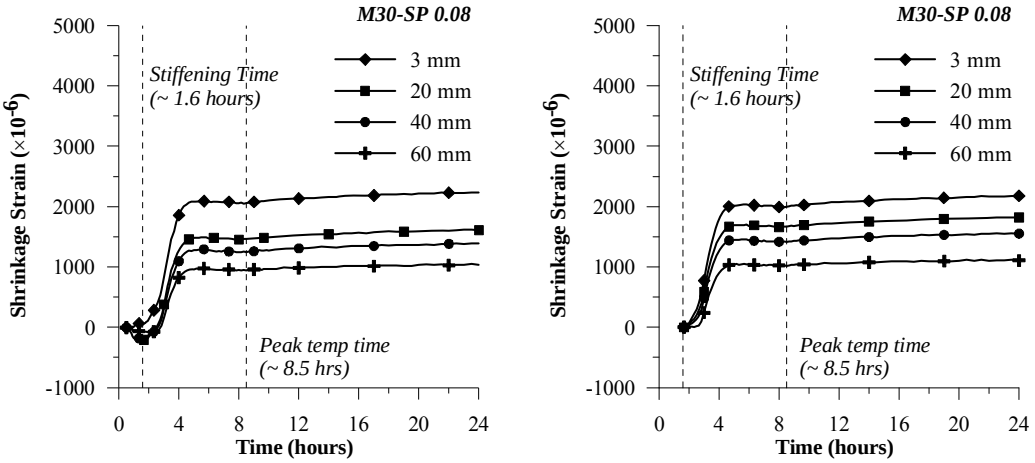

Figure 4.4 Early age shrinkage strain with respect to the depth from the top surface on unsealed mortar specimens cast with superplasticizer dosage of 0.08% starting from (a) 30 minutes after water was added to the mixture, and (b) stiffening time respectively

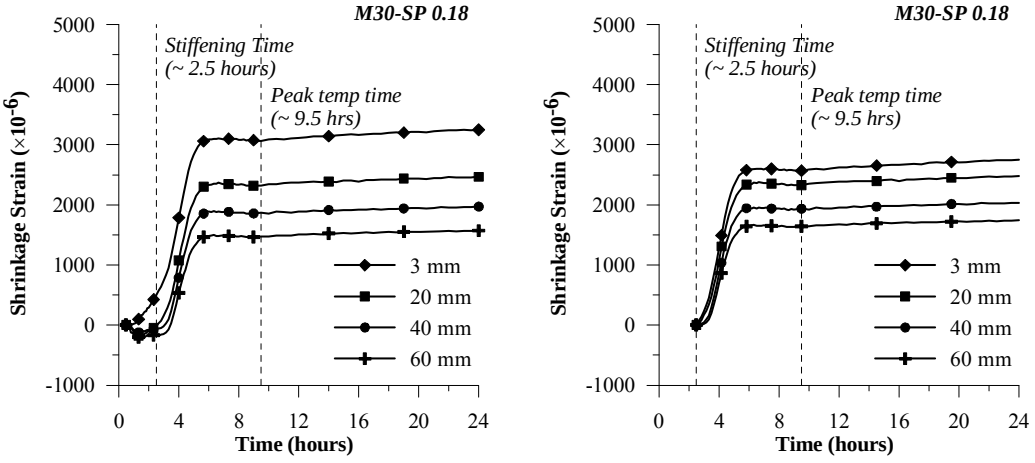

Figure 4.5 Early age shrinkage strain with respect to the depth from the top surface on unsealed mortar specimens cast with superplasticizer dosage of 0.18% starting from (a) 30 minutes after water was added to the mixture, and (b) stiffening time respectively

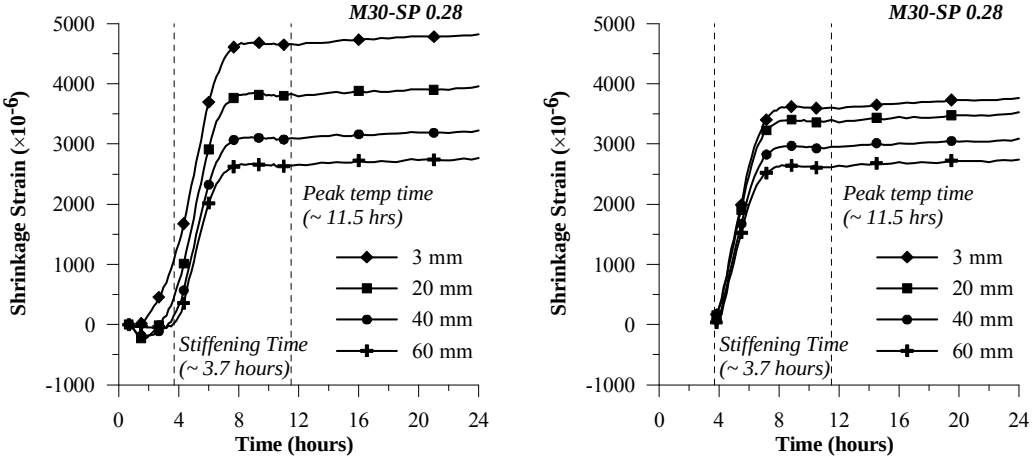

(a) *(b)*

Figure 4.6 Early age shrinkage strain with respect to the depth from the top surface on unsealed mortar specimens cast with superplasticizer dosage of 0.28% starting from (a) 30 minutes after water was added to the mixture, and (b) stiffening time respectively

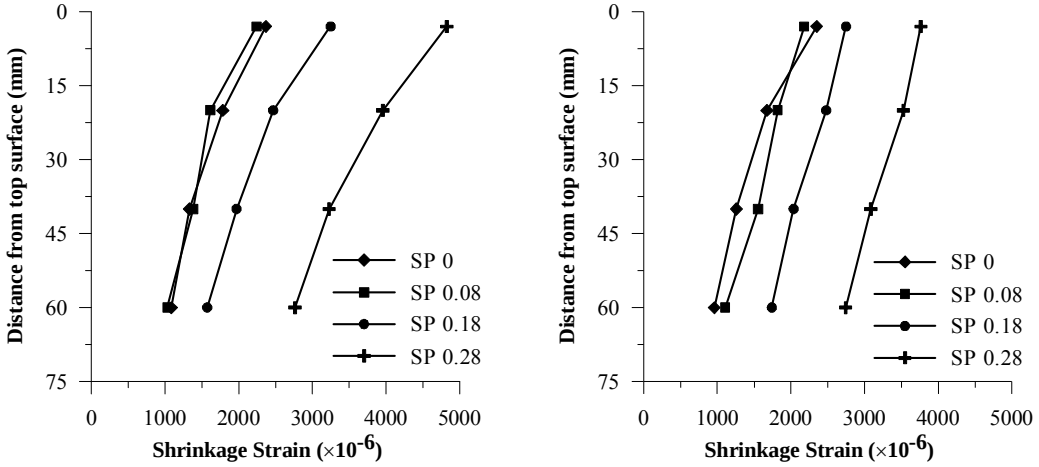

(a) *(b*

Figure 4.7 Plotting of early age shrinkage strains with respect to the depth from the top exposed surface of mortar mixtures with different superplasticizer dosages at 24 hours after adding water to the mixture, starting from (a) 30 minutes after adding water to the mixture, and (b) stiffening time respectively

4.3.2 Effect of Aggregate Volume

The effect of different aggregate volume on the variation of early age shrinkage strain with respect to the depth from the top exposed surface was studied on mortar specimens cast with a water-to-cementitious ratio of 0.30. The fine aggregates were varied from 36% to 55% by volume. To bring each mortar mixture to a target workability of approximately 110%, different amounts of superplasticizer had to be used. The resulting workability based on the flow method, as can be seen in *Table 4.3*, varied between 80% and 140%. The results also showed that the stiffening time, the initial setting, and the final setting time were delayed in the mortar specimens with higher aggregate volumes. This retardation can be attributed mainly to the use of higher dosages of superplasticizer.

Table 4.3 Mixture properties of mortar with different aggregate volume

Mixture	w/c	Agg. vol.	Workability	Stiffening time (hrs)	Initial set (hrs)	Final set (hrs)	Peak temp time (hrs)
M30-AG36	0.30	36%	110%	1.5	3	3.9	6.3
M30-AG45	0.30	45%	140%	2.0	3.5	4.4	8.0
M30-AG50	0.30	50%	80%	2.0	3.3	4.5	7.7
M30-AG55	0.30	55%	140%	4.0	5.6	7.0	10.5

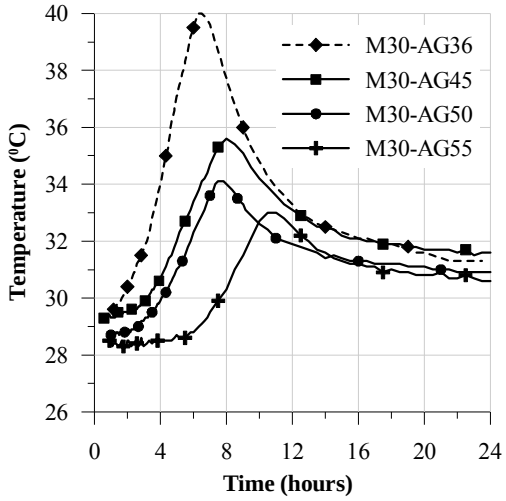

Figure 4.8 Temperature development of mortar mixtures with different aggregate volumes

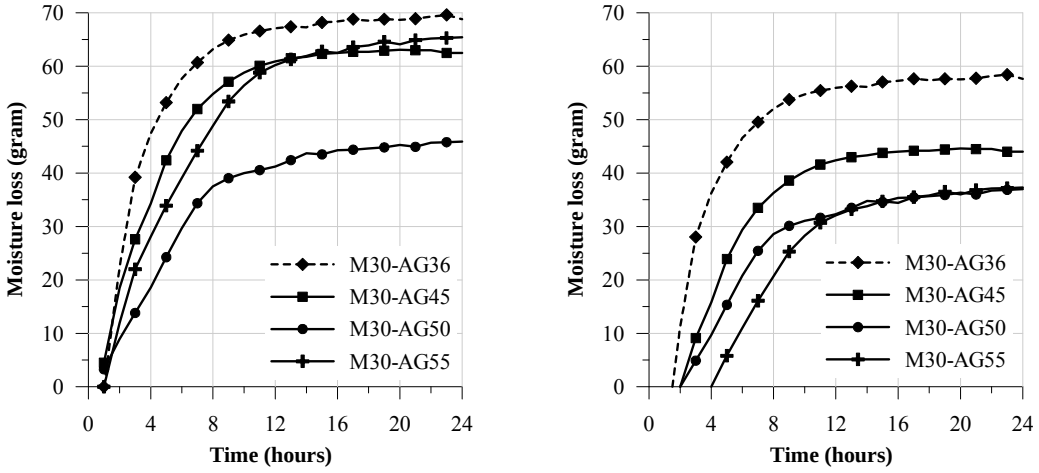

Figure 4.9 Moisture loss measurement for mortar specimens with different aggregate volumes starting from (a) 30 minutes after adding water to the mixture, and (b) stiffening time up to 24 hours after adding water to the mixture

The temperature development of mortar specimens cast with different aggregate volumes during the first 24 hours after adding water to the mixture is shown in *Figure 4.8*. As

expected, the results showed that the higher aggregate volumes resulted in a decrease in the peak temperature reached. In the mortar specimens cast with an aggregate volume of 36%, 45%, 50%, and 55%, the maximum temperature reached was 40^0C, 35.5^0C, 34^0C, and 33^0C respectively. The lower peak temperature observed can be attributed to the lower cement content available for hydration in the mortar specimens with higher aggregate volumes. A delay in the peak temperature time was also observed in the mortar specimens with higher aggregate volumes. This delay in the temperature rise was consistent with the delay in the stiffening time or the setting time as tested on the companion mortar cubes.

The total moisture loss for these mortar specimens plotted starting either from 30 minutes after adding water to the mixture or from the stiffening time up to the 24 hours after adding water to the mixture are shown in *Figure 4.9*. The results suggested that the total moisture loss decreased with a higher aggregate volume. Less mixing water available in the mortar mixtures with a higher aggregate volume may be a possible reason for the reduction in the total moisture loss. One exception was noted; despite had the reduced amount of mixing water, the mortar specimens with an aggregate volume of 55% (i.e. M30-AG55) registered higher moisture loss as compared to that monitored for the M30-AG50. The significant higher total moisture loss of the M30-AG55 specimens can be attributed to a significant longer stiffening time leading to a longer transitional stage experienced by the M30-AG55 mortar specimens.

Figure 4.10 to *Figure 4.13* show the early age shrinkage strains monitored at different depths from the top exposed surface of the mortar specimens cast with different aggregate volumes starting either from 30 minutes or from stiffening time up to 24 hours after adding water to the mixture. As expected, the results showed that the moisture loss affected the shrinkage strains throughout the depth of the mortar specimens. Starting from 30 minutes after adding water to the mixture, it can be seen that the shapes of the shrinkage strains-versus-time plots were similar and decreased with the depth from the top exposed surface. In addition, it is also noted that in the mortar specimens cast with an aggregate volume of 55% (i.e. M30-AG55), the shrinkage strains developed rapidly during the plastic stage. When the stiffening time

occurred at 4 hours after water was added to the mixture, "absolute" shrinkage strains values of 1700 με, 1440 με, 1180 με, and 560 με was registered at the depths of 3, 20, 40, and 60 mm respectively. It can also be seen that if the results are plotted starting from the stiffening time, the difference between the early age shrinkage strains monitored near the top exposed surface and that monitored at deeper depths was reduced with higher aggregate volumes.

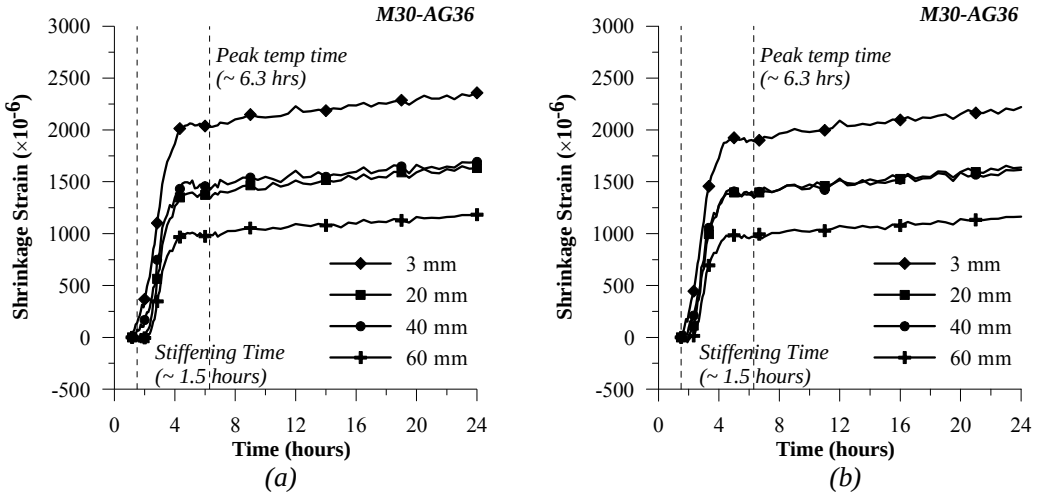

Figure 4.10 Early age shrinkage strain with respect to the depth from the top surface on unsealed mortar specimens cast with aggregate volume of 36% starting from (a) 30 minutes after water was added to the mixture, and (b) stiffening time respectively

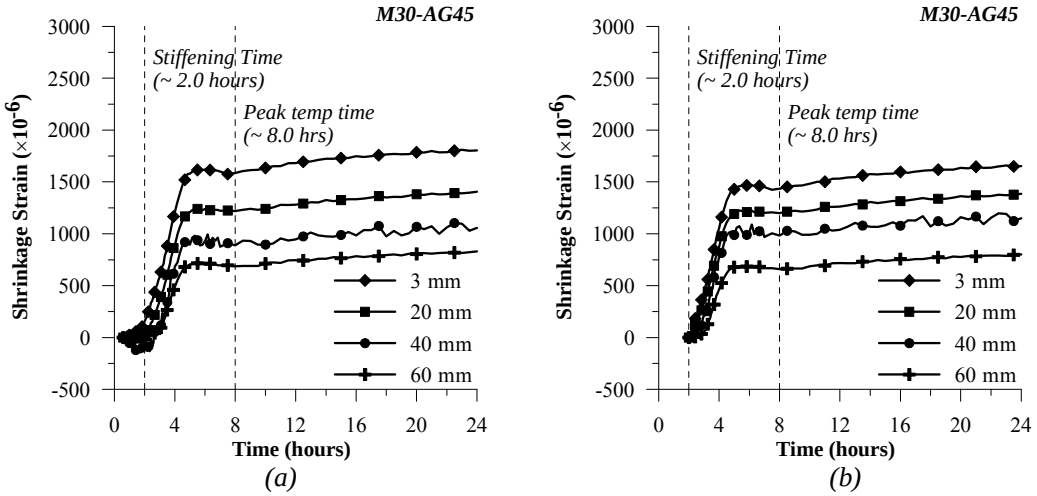

Figure 4.11 Early age shrinkage strain with respect to the depth from the top surface on unsealed mortar specimens cast with aggregate volume of 45% starting from (a) 30 minutes after water was added to the mixture, and (b) stiffening time respectively

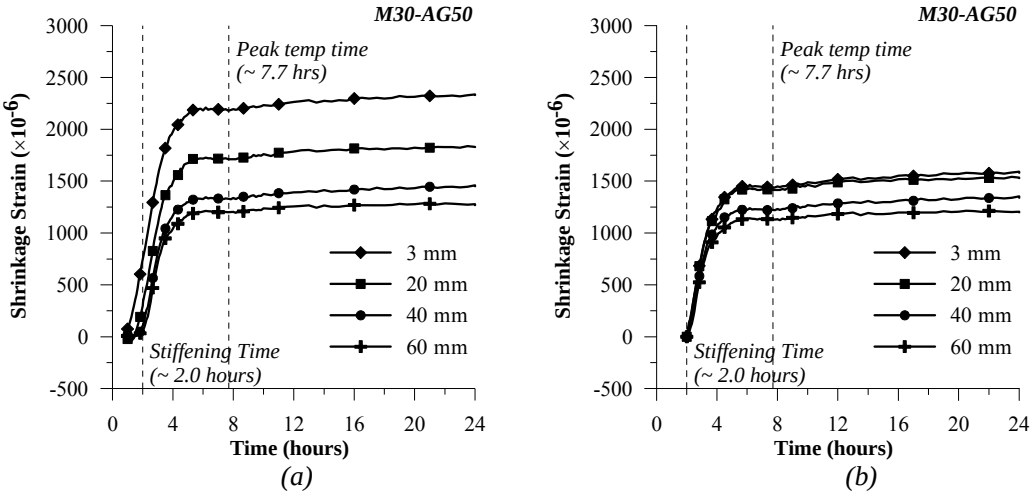

Figure 4.12 Early age shrinkage strain with respect to the depth from the top surface on unsealed mortar specimens cast with aggregate volume of 50% starting from (a) 30 minutes after water was added to the mixture, and (b) stiffening time respectively

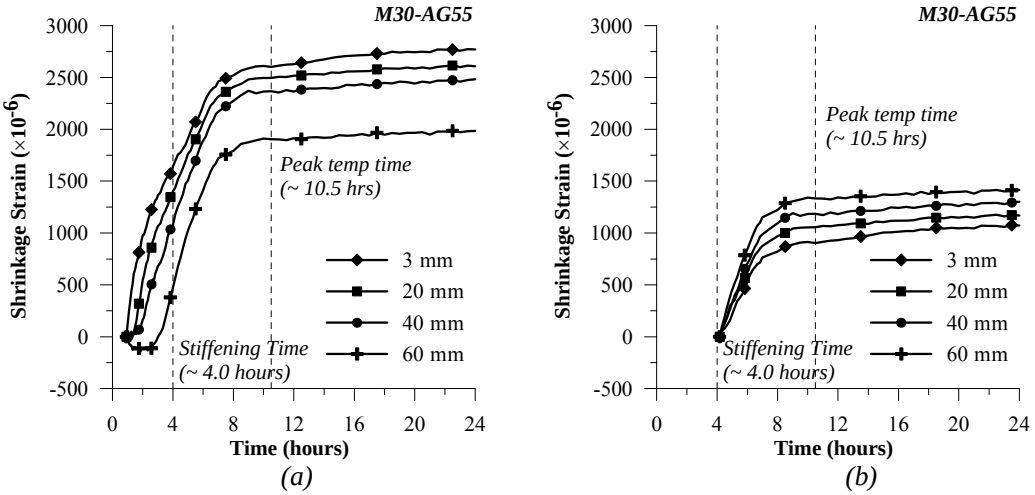

Figure 4.13 Early age shrinkage strain with respect to the depth from the top surface on unsealed mortar specimens cast with aggregate volume of 55% starting from (a) 30 minutes after water was added to the mixture, and (b) stiffening time respectively

In order to investigate the effect of aggregate volume more clearly, shrinkage strains-versus-distance from the top surface at 24 hours after adding water to the mixture were plotted, starting either from 30 minutes after adding water to the mixture or from the stiffening time. These plots are shown in *Figure 4.14* and *Figure 4.15* respectively. Starting from 30 minutes after adding water to the mixture, the results showed that the mortar specimens cast with an

aggregate volume of 45% (i.e. M30-AG45) registered the lowest "absolute" shrinkage strains values while the mortar specimens cast with an aggregate volume of 55% (i.e. M30-AG55) registered the highest "absolute" shrinkage strains values. This result showed that for the mortar specimens tested, the effects of aggregate restraint may also be tempered with the effects of superplasticizer. The coupled effect of aggregate restraint and superplasticizer was clearly shown in the case of mortar specimens cast with aggregate volume of 36% and 50%. In the M30-AG50 mortar specimens, the higher restraining effect of aggregate seemed to have been offset by the use of a higher dosage of superplasticizer. As a result, the M30-AG50 mortar specimens registered comparable "absolute" shrinkage strains value to that of the M30-AG36 mortar specimens. For lower dosages of superplasticizer, the effect of superplasticizer is expected to be less significant. A comparison between the results of the M30-AG36 and M30-AG45 mortar specimens showed that the "absolute" shrinkage strains decreased with a higher aggregate volume.

A comparison of shrinkage strains plotted starting from the stiffening time is shown in *Figure 4.15*. The higher restraining effect due to higher aggregate volumes was clearly observed especially near the top exposed surface. The results showed that a higher aggregate volume reduced the early age shrinkage strains monitored near the top exposed surface. At a depth of 3 mm from the top exposed surface, the mortar specimens cast with aggregate volume of 36%, 45%, 50%, and 55% registered absolute shrinkage strains values of 2220 με, 1650 με, 1530με, and 1070 με respectively. On the other hand, the early age shrinkage strains monitored at the depths of 60 mm showed interesting result. While a reduction was observed when the aggregate volume was increased from 36% to 45%, an increase in the early age shrinkage strains was observed when the aggregate volume was increased from 45% to 50% or 55%. As mentioned previously, one possible explanation of the higher shrinkage strains observed at deeper depths is due to the use of a higher dosage of superplasticizer in the mortar mixtures cast with aggregate volume of 50% or 55%.

In addition, the results also showed that the "absolute" shrinkage strains value decreased more gradually with the depth from the top surface in the mortar specimens with

higher aggregate volumes. In the mortar specimens cast with aggregate volume of 55% (i.e. M30-AG55), the "absolute" shrinkage strains value monitored near the exposed top surface registered lower values compared to that monitored near the base of the specimens. This result suggests that a "skin layer" effect may have taken place with an increase in the aggregate volume. As shown in *Figure 4.16*, in the mortar specimens tested, the negative capillary pressure due to evaporation may consolidate the internal structure of the mortar specimens with higher aggregate volumes, bringing the solid particles (i.e. cement particles and fine aggregates) closer to each other especially near the top exposed surface. The contact between these solid particles may provide an internal solid skeleton resulting in higher internal restraint in the "skin layer". With the higher internal restraint and less moisture available for hydration, the shrinkage strain monitored may thus show reductions when compared to shrinkage strains monitored at deeper depths. At deeper depth, the distance between the solid particles as well as the hydration process may be less affected. It is expected that at such condition, a refinement of microstructure due to hydration may cause the mortar specimens to register higher shrinkage strains.

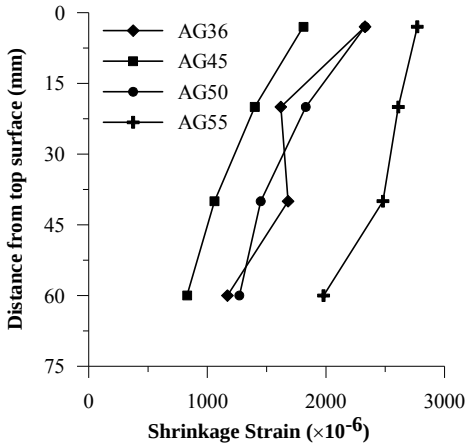

Figure 4.14 Plotting of early age shrinkage strains with respect to the depth from the top exposed surface of mortar mixtures with different aggregate volumes at 24 hours after adding water to the mixture, starting from 30 minutes after adding water to the mixture

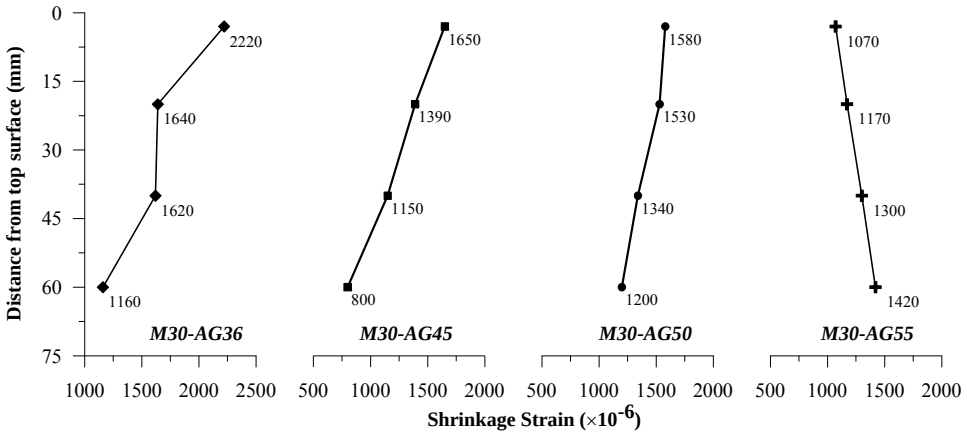

Figure 4.15 Plotting of early age shrinkage strains with respect to the depth from the top exposed surface of mortar mixtures with different aggregate volumes at 24 hours after adding water to the mixture, starting from stiffening time

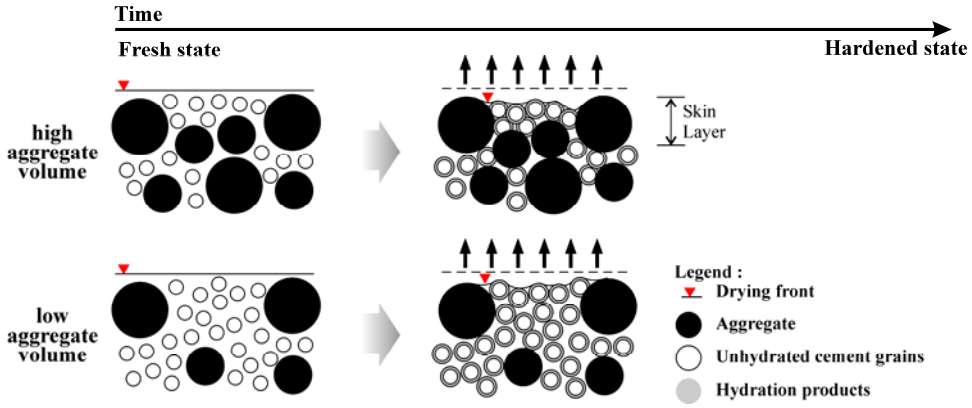

Figure 4.16 Drying sequence for mortar mixture with different aggregate volumes when exposed to drying environment at early ages

4.3.3 Effect of Water-to-Cementitious Ratio

The effect of water-to-cementitious ratio on the variation of early age shrinkage strains with respect to the depth from the top exposed surface was studied on mortar and concrete specimens cast with different water-to-cementitious ratios ranging between 0.20 and 0.45. The aggregate volume was kept at 50% and 65% by volume for the mortar and concrete mixtures respectively. To achieve the target workability, different amounts of superplasticizer had to be used. As can be seen in *Table 4.4*, the resulting mortar workability based on the flow method varied between 80% and 140%, whereas the slump for the concrete mixtures varied between 90

mm and 165 mm. The results also showed that the stiffening time, the initial setting, and the final setting time were delayed longer in the mortar and concrete mixtures with lower water-to-cementitious ratios. This retardation can be attributed mainly to the use of higher dosages of superplasticizer.

Table 4.4 Mixture properties of mortar and concrete mixtures with different w/c ratios

Mixture	w/c	Agg. vol.	Workability	Stiffening time (hrs)	Initial set (hrs)	Final set (hrs)	Peak temp time (hrs)
M20	0.20	50%	110%	14.8 / 3.7*	12.8	17.9	21.7
M25	0.25	50%	140%	3.5	5.0	7.0	9
M30	0.30	50%	80%	2.0	3.3	4.5	7.5
M35	0.35	50%	90%	2.0	3.2	4.6	8.5
M45	0.45	50%	110%	2.0	3.6	4.9	9
C25	0.25	65%	110 mm	5.2	6.2	8.3	12
C35	0.35	65%	165 mm	3.1	4.8	6.1	10.3
C45	0.45	65%	90 mm	2.6	3.6	4.8	8.4

Note: * stiffening time monitored near the exposed surface

The temperature development of mortar and concrete specimens cast with different water-to-cementitious ratios during the first 24 hours after adding water to the mixture are shown in *Figure 4.17(a)* and *Figure 4.17(b)* respectively. As expected, the results showed that the specimens cast with lower water-to-cementitious ratios registered higher peak temperature. The peak temperature reached was 31.7^0C, 32.8^0C, 34.1^0C, and 34.4^0C for the mortar specimens cast with a water-to-cementitious ratio of 0.45, 0.35, 0.30, and 0.25 respectively. One exception was noted for the mortar specimens cast with water-to-cementitious ratio of 0.20 (i.e. M20). The M20 mortar specimens registered lower peak temperature compared to that monitored on mortar mixture specimens cast with a water-to-cementitious ratio of 0.25 (i.e. M25). The lower peak temperature reached in M20 mortar mixture could be attributed to several factors. First, the loss of moisture caused by evaporation during the very early ages may significantly reduce the water available for the hydration process. Second, due to the very low water-to-cementitious ratio of the M20 mortar specimens, the space between aggregate particles to be filled by hydration product are more limited. Third, the significant amount of superplasticizer used may have also

affected cement hydration in the M20 mortar specimens. A combination of these factors may have contributed to the lower peak temperature monitored.

In the case of concrete specimens tested, similar results were obtained. The peak temperature increased with a reduction in the water-to-cementitious ratio. The peak temperature reached was 32.9^0C, 33.6^0C, and 35.4^0C for the concrete specimens cast with a water-to-cementitious ratio of 0.45, 0.35, and 0.25 respectively. Similarly, a delay in the peak temperature time was also observed. This delay was consistent with the delay observed in the stiffening and initial setting times.

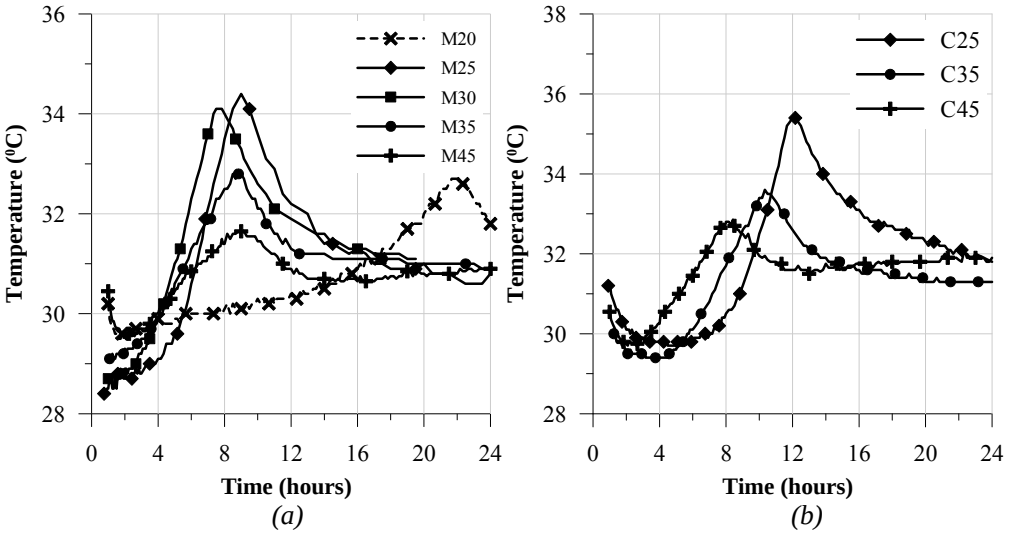

Figure 4.17 Temperature development of (a) mortar specimens, and (b) concrete specimens cast with different water-to-cementitious ratios

The moisture loss measurements for these mortar and concrete specimens starting either from 30 minutes or from the stiffening time up to the 24 hours after adding water to the mixture are shown in *Figure 4.18* and *Figure 4.19* respectively. It can be seen that the plot of moisture loss-versus-time increased more gradually with a reduction in the water-to-cementitious ratio. The total moisture loss monitored at 24 hours after adding water to the mixture also decreased with a reduction in water-to-cementitious ratio for the mortar and concrete specimens tested. The reduction in the total moisture loss may be attributed to the fact that less water was present in the specimens cast with lower water-to-cementitious ratios.

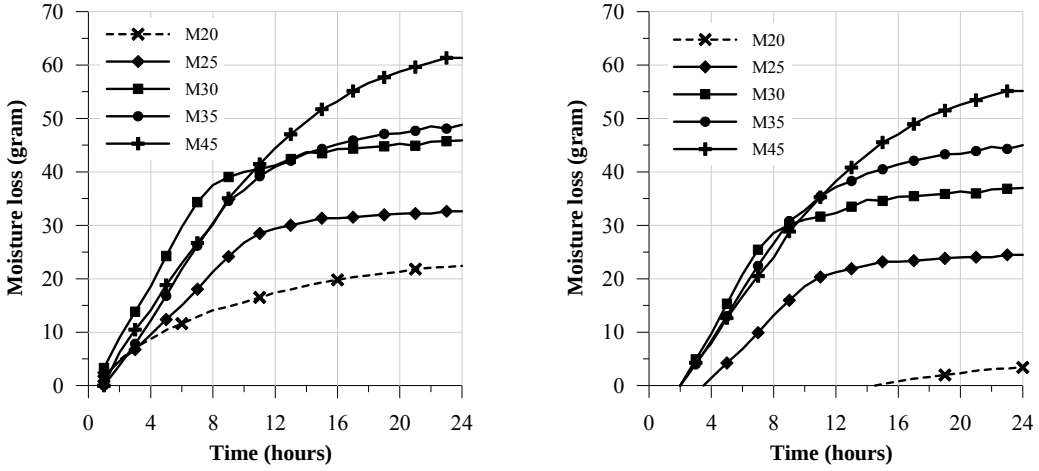

(a) *(b)*

Figure 4.18 Moisture loss measurement for mortar specimens with different water-to-cementitious ratios starting from (a)30 minutes after adding water to the mixture, and (b) stiffening time up to 24 hours after adding water to the mixture

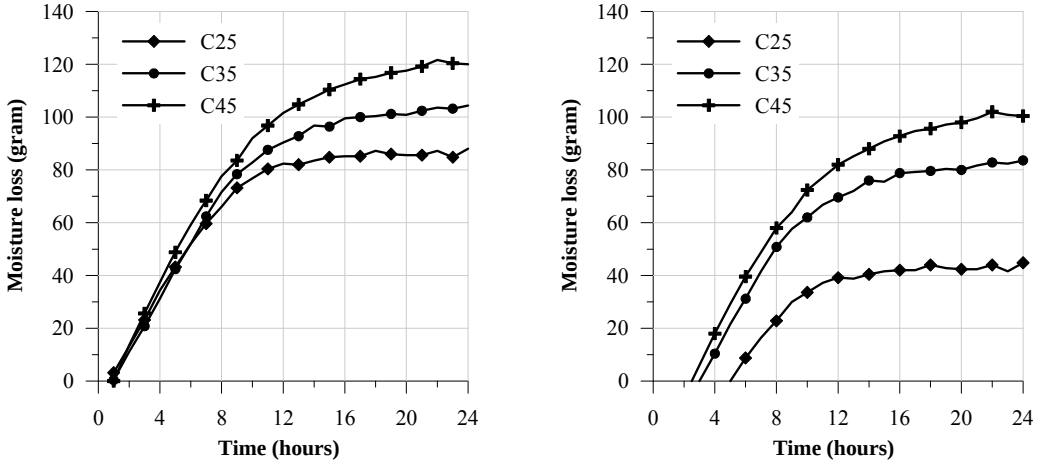

(a) *(b)*

Figure 4.19 Moisture loss measurement for concrete specimens with different water-to-cementitious ratios starting from (a) 30 minutes after adding water to the mixture, and (b) stiffening time up to 24 hours after adding water to the mixture

In the case of mortar specimens cast with different water-to-cementitious ratios, the early age shrinkage monitored at various depths from the top exposed surface starting either from 30 minutes after adding water to the mixture or from the stiffening time up to 24 hours after adding water to the mixture are shown in *Figure 4.20* to *Figure 4.24*. Whether plotted from 30 minutes after adding water to the mixture or from the stiffening time, the results clearly showed different shrinkage strains at different depths from the top exposed surface. The results

also showed that the plots of early age shrinkage strain at various depths versus time were rather similar. Starting from 30 minutes after adding water to the mixture, it can be seen that shrinkage strains near the top exposed surface started to develop earlier as expected. Thus significantly higher shrinkage strains were monitored near the exposed surface of the mortar specimens. Similarly, starting from the stiffening time, it can be seen that the early age shrinkage strains developed more rapidly near the top exposed surface as compared to that monitored near the base of the specimens with the exception of the M25 mortar specimens. The different behavior observed for the M25 mortar specimens will be discussed later.

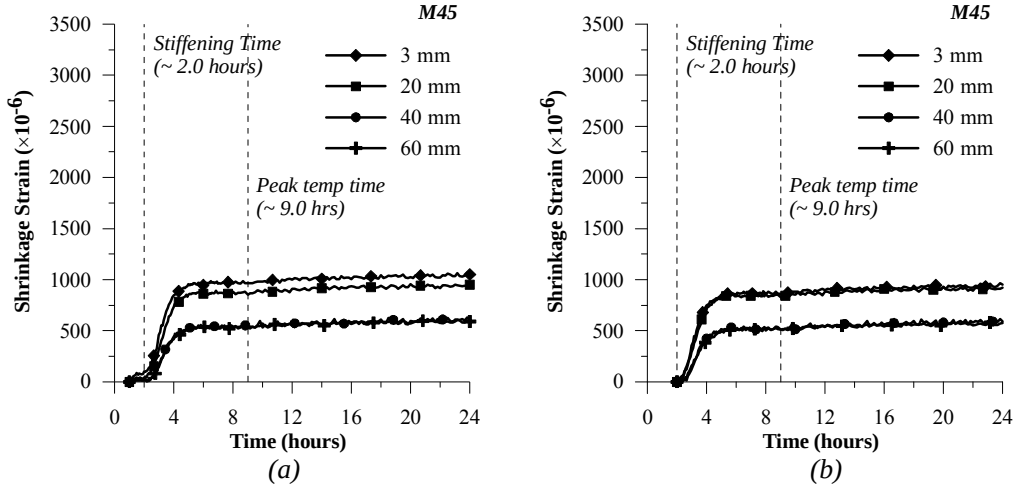

Figure 4.20 Early age shrinkage strain with respect to the depth from the top surface on unsealed mortar specimens cast with water-to-cementitious ratio of 0.45 starting from (a) 30 minutes after water was added to the mixture, and (b) stiffening time respectively

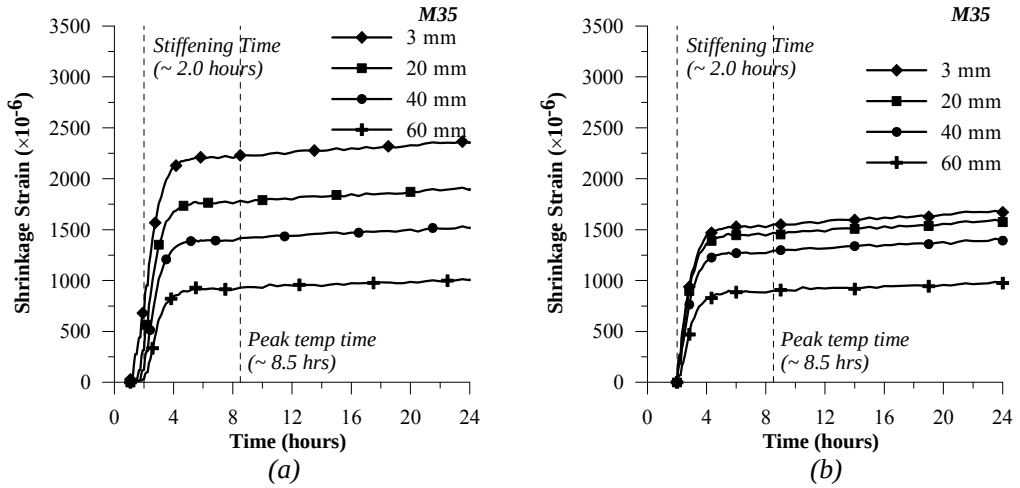

Figure 4.21 Early age shrinkage strain with respect to the depth from the top surface on unsealed mortar specimens cast with water-to-cementitious ratio of 0.35 starting from (a) 30 minutes after water was added to the mixture, and (b) stiffening time respectively

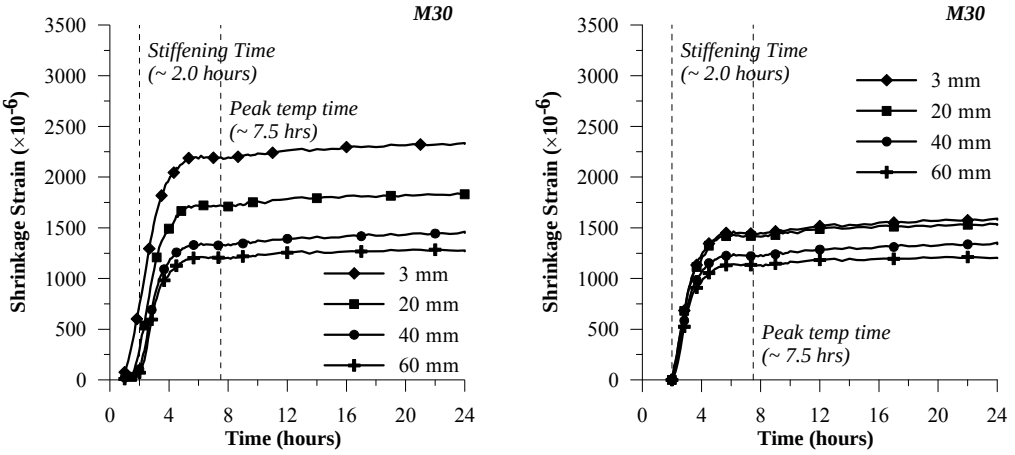

Figure 4.22 Early age shrinkage strain with respect to the depth from the top surface on unsealed mortar specimens cast with water-to-cementitious ratio of 0.30 starting from (a) 30 minutes after water was added to the mixture, and (b) stiffening time respectively

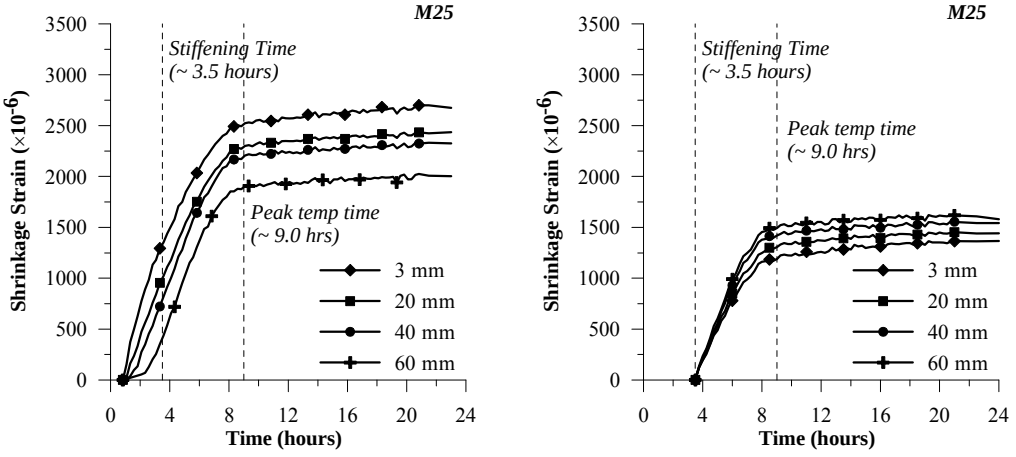

Figure 4.23 Early age shrinkage strain with respect to the depth from the top surface on unsealed mortar specimens cast with water-to-cementitious ratio of 0.25 starting from (a) 30 minutes after water was added to the mixture, and (b) stiffening time respectively

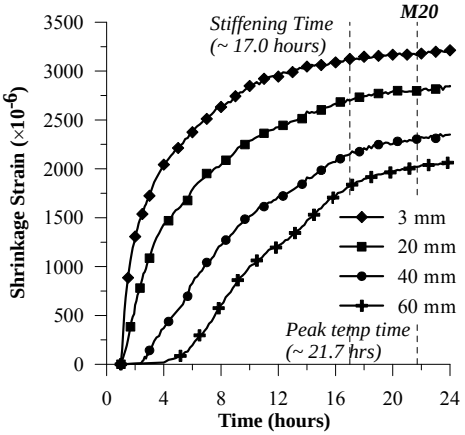

Figure 4.24 Early age shrinkage strain with respect to the depth from the top surface on unsealed mortar specimens cast with water-to-cementitious ratio of 0.20 starting from 30 minutes after water was added to the mixture

In order to investigate the effect of water-to-cementitious ratio more clearly, the shrinkage-time curves for the mortar specimens cast with a water-to-cementitious ratio of 0.45 or 0.25 may be characterized as following the plastic, transitional, and hardening stage as shown in *Figure 4.25*. The shrinkage strains monitored was zeroed at the beginning of each stage. It can be seen that during the plastic stage, the M25 mortar specimens registered significantly higher early age shrinkage strains especially near the top exposed surface as compared to the M45 mortar specimens. During the transitional stage, the results showed that reducing the water-to-cementitious ratio increased the early age shrinkage strains at all depths. The M25 mortar specimens registered higher shrinkage strains compared to that monitored in the M45 mortar specimens. The result also showed that during this transitional stage, different behaviors were observed for the M25 and M45 mortar specimens tested. The M45 mortar specimens registered a rapid increase in the shrinkage strains near the top exposed surface while a more gradual increase of shrinkage strains was monitored near the base of the specimens. On the other hand, when the water-to-cementitious ratio was reduced to 0.25, the opposite of the above was observed. The M25 mortar specimens showed a relatively more gradual increase in shrinkage strains near the top exposed surface and a more rapid increase in shrinkage strains near the base of the specimens. It can be seen that at the end of transition stage, the M25 mortar specimens registered "absolute" shrinkage strains values of 1180 με, 1300 με, 1410με, and 1470 με at the depths of 3, 20, 40, and 60 mm respectively, while the M45 mortar specimens registered "absolute" shrinkage strains values of 860 με, 830 με, 510με, and 520 με at the depths of 3, 20, 40, and 60 mm respectively. The difference in behavior of the M25 and M45 mortar mixtures could be attributed to the "skin layer" effect, mentioned previously in Chapter 2. During early ages, when the top surface was exposed to a dry environment, rigidity (i.e. stiffness) of the cementitious mixture near the top exposed surface may be affected. It is possible that within the "skin layer", the stiffness of the cementitious mixture increased rapidly compared to that of the interior. This increase in the cementitious mixture's stiffness would provide higher internal restraint locally thus reducing the early age shrinkage strains monitored.

Finally, during the hardening stage, the M45 and M25 mortar specimens showed behavior typical of a hardened mortar when exposed to a dry environment; the top exposed surface registered higher "absolute" shrinkage strains values compared to that monitored in the interior. In addition, the M25 mortar mixtures also registered higher shrinkage strains at all depths during this hardening stage. This can be attributed to contraction due to the reduction in temperature of the mortar specimens during the hardening stage. As the M25 mortar specimens registered higher temperature rise, a higher contraction as the temperature dropped (i.e. from the peak temperature monitored to the ambient temperature) is expected.

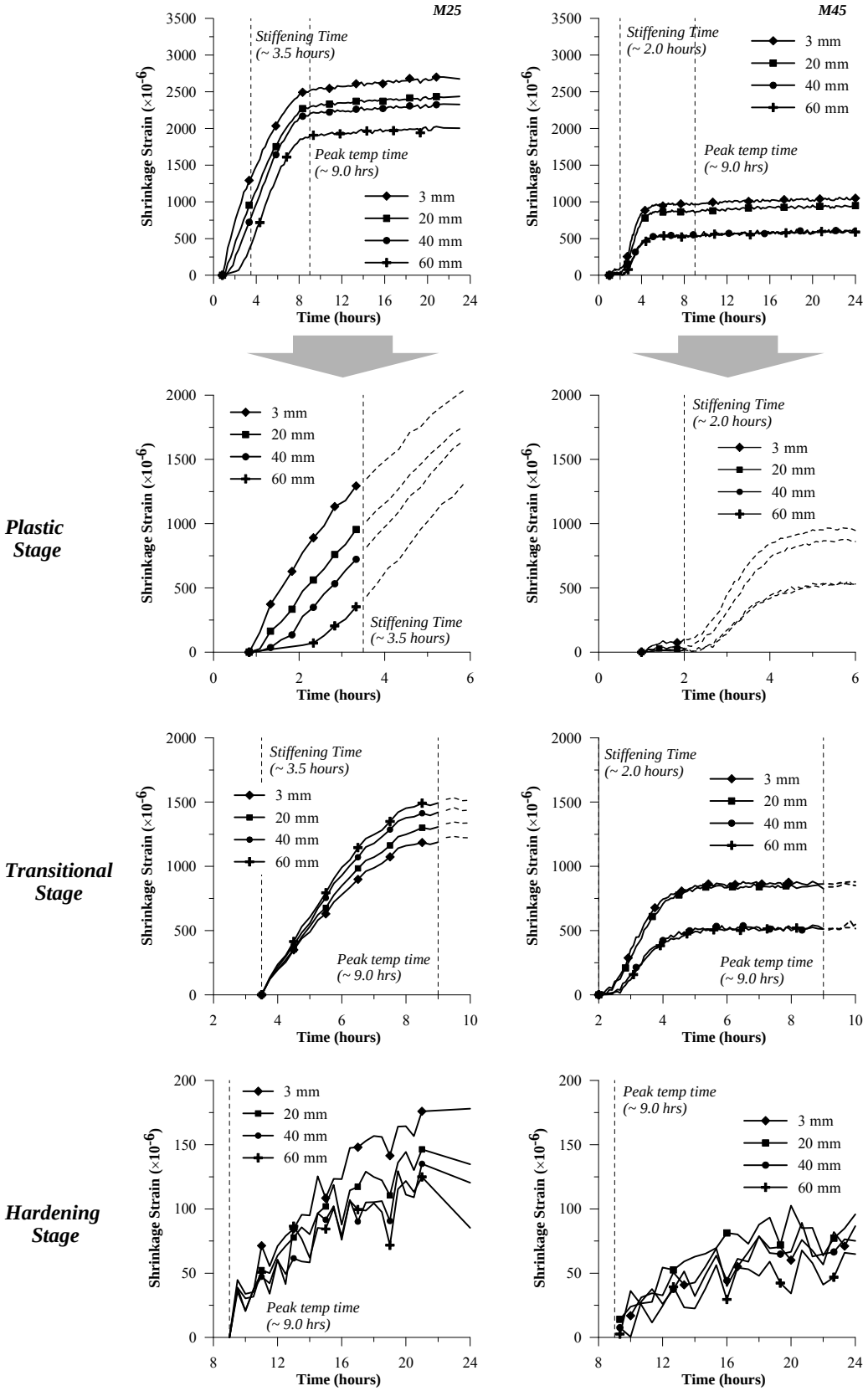

Figure 4.25 Shrinkage strains monitored at different depths on mortar specimens with water-to-cementitious ratio of 0.25 and 0.45 during plastic, transition, and hardening stages

The plots of shrinkage strains-versus-distance from the top surface at 24 hours after adding water to the mortar mixture of the mortar mixtures cast with different water-to-cementitious ratios starting either from 30 minutes after water was added to the mixture or from the stiffening time are shown in *Figure 4.26* and *Figure 4.27* respectively. As shown in *Figure 4.26*, the "absolute" shrinkage strains value at all depths increased with a reduction in the water-to-cementitious ratio. The "absolute" shrinkage strain at a depth of 3 mm from the top exposed surface registered a value of 1050 με, 2360 με, 2270 με, 2690 με, and 3200 με for the M45, M35, M30, M25, and M20 mortar specimens respectively; whereas the "absolute" shrinkage strain at a depth of 60 mm from the top exposed surface reached a value of 590 με, 1010 με, 1270 με, 2000 με, and 2060 με for the M45, M35, M30, M25, and M20 mortar specimens respectively. The higher "absolute" shrinkage strain values observed could be attributed to the delay in the stiffening time as well as to the higher shrinkage rate in the mortar specimens cast with lower water-to-cementitious ratios. With the stiffening time delayed, the shrinkage induced by moisture loss would be prolonged, resulting in higher "absolute" shrinkage strain values. In addition, the higher shrinkage rate of the mortar specimens cast with lower water-to-cementitious ratios could be attributed to the finer micro-pores and meso-pores in these mortar specimens. The removal of moisture or water from these pores would generate higher capillary stresses that eventually led to higher shrinkage strains.

As shown in *Figure 4.27*, the development of shrinkage strains at various depths from the top surface starting from the stiffening time showed that an increase in the "absolute" shrinkage strains value near the top exposed surface was observed when the water-to-cementitious ratio was lowered from 0.45 to 0.35. However, further reductions in the water-to-cementitious ratio to 0.30 and lower values resulted in a reduction in the "absolute" shrinkage strain monitored instead. At a depth of 3 mm from the top exposed surface, the mortar specimens cast with water-to-cementitious ratio of 0.35, 0.30, and 0.25 registered "absolute" shrinkage strains values of 1670 με, 1530 με, and 1370 με respectively. On the other hand, the early age shrinkage strain monitored near the base of the specimens showed that the "absolute"

shrinkage strains values increased with a reduction in the water-to-cementitious ratio. It can be seen that at a depth of 60 mm from the top exposed surface, the mortar specimens cast with a water-to-cementitious ratio of 0.45, 0.35, 0.30, and 0.25 registered an "absolute" shrinkage strain values of 580 με, 980 με, 1210 με, and 1580 με respectively. *Figure 4.27* also shows that the "absolute" value of shrinkage strains decreased more gradually with depth from the top exposed surface in the mortar mixtures with a lower water-to-cementitious ratio. Moreover, it can be seen that in the case of M25 mortar specimens, the "absolute" shrinkage strains monitored near the top exposed surface registered lower values compared to that monitored at deeper depths. This behavior seemed similar to that monitored in mortar specimens cast with high aggregate volume.

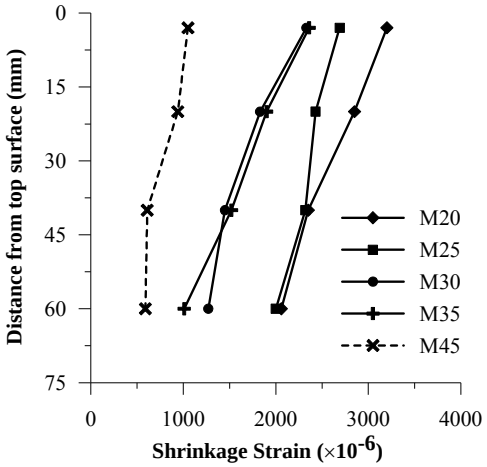

Figure 4.26 Plotting of early age shrinkage strains with respect to the depth from the top exposed surface of mortar specimens cast with different water-to-cementitious ratios at 24 hours after adding water to the mixture, starting from 30 minutes after adding water to the mixture

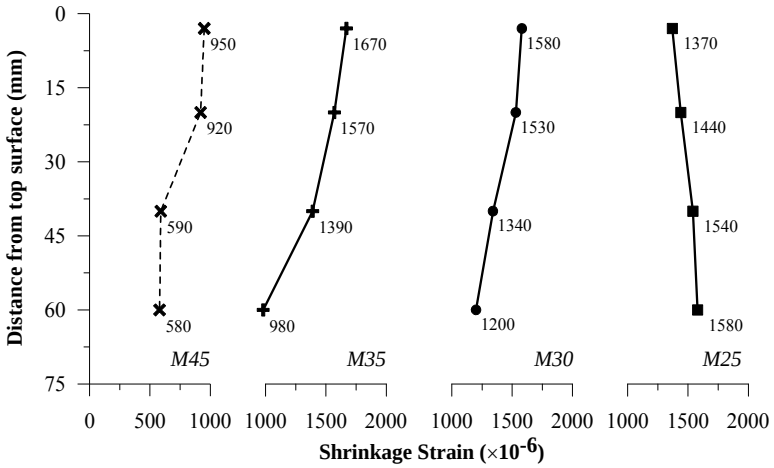

Figure 4.27 Plotting of early age shrinkage strains with respect to the depth from the top exposed surface of mortar specimens cast with different water-to-cementitious ratios at 24 hours after adding water to the mixture, starting from stiffening time

In the case of concrete specimens cast with a water-to-cementitious ratio of 0.45, 0.35, and 0.25 tested, behavior similar to that of the mortar specimens were observed. As can be seen in *Figure 4.28* to *Figure 4.30*, the early age shrinkage strains monitored at the depths of 3, 20, 40, 60, and 80 mm from the top exposed surface starting from 30 minutes up to 24 hours after adding water to the concrete mixture showed that the moisture loss during the early ages affected the shrinkage strains throughout the depth of the concrete specimens. The effect of moisture loss on the shrinkage strains at different depths also became more significant with a reduction in the specimen's water-to-cementitious ratio. As shown in *Figure 4.31*, it can be seen that during the plastic stage, the shrinkage strains monitored at all depths in the C25 concrete specimens increased rapidly compared to that monitored in the C45 concrete specimens. When the stiffening time occurred in the concrete specimens, the C25 concrete specimens registered "absolute" shrinkage strains values of 1950 με, 1700 με, 1530 με, 1260 με, and 990 με at the depth of 3, 20, 40, 60, and 80 mm respectively. While the C45 concrete specimens registered "absolute" shrinkage strains values of 560 με, 370 με, 280 με, 150 με, and 80 με at the depth of 3, 20, 40, 60, and 80 mm respectively.

During the transitional stage, good agreement with that monitored for the mortar specimens were also observed in concrete specimens cast with lower water-to-cementitious ratios. It can be seen in *Figure 4.31* that the C45 concrete specimens registered a relatively rapid

increase in the shrinkage strains near the top exposed surface and a more gradual increase in shrinkage strains near the base of the specimens. On the other hand, the C25 concrete specimens showed a more rapid increase in shrinkage strains near the base of the specimens. As mentioned previously, the different behavior of the C25 and C45 concrete mixtures could be attributed to the "skin layer" effect.

During the hardening stage, as expected the top exposed surface layer of hardened concrete registered higher "absolute" shrinkage strains values compared to that monitored in the interior, was observed especially in the C25 concrete specimens. The results also showed agreement with that obtained for the mortar specimens. The C25 concrete specimens registered higher shrinkage strains at all depths during this hardening stage. As mentioned previously, the higher shrinkage strains monitored for the C25 concrete specimens can be attributed to the more significant contraction due to a higher temperature drop upon hardening.

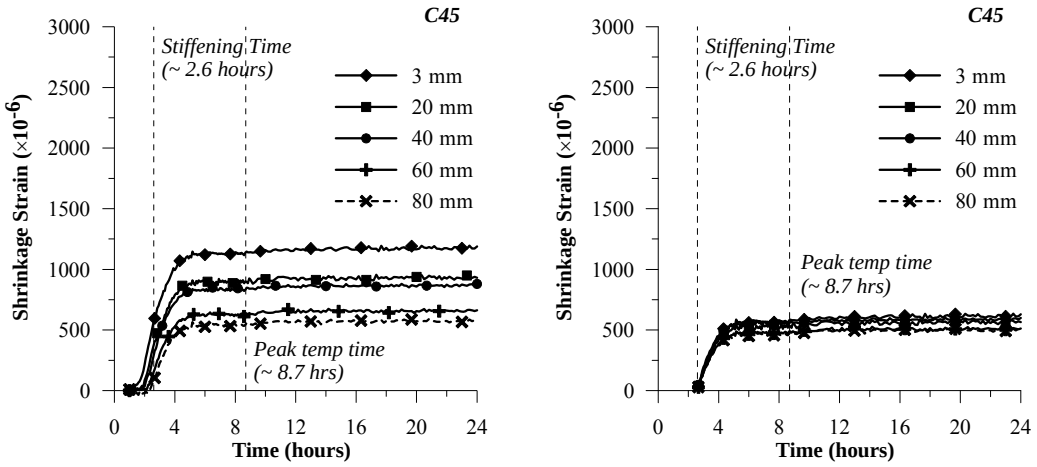

Figure 4.28 Early age shrinkage strain with respect to the depth from the top surface on unsealed concrete specimens cast with water-to-cementitious ratio of 0.45 starting from (a) 30 minutes after water was added to the mixture, and (b) stiffening time respectively

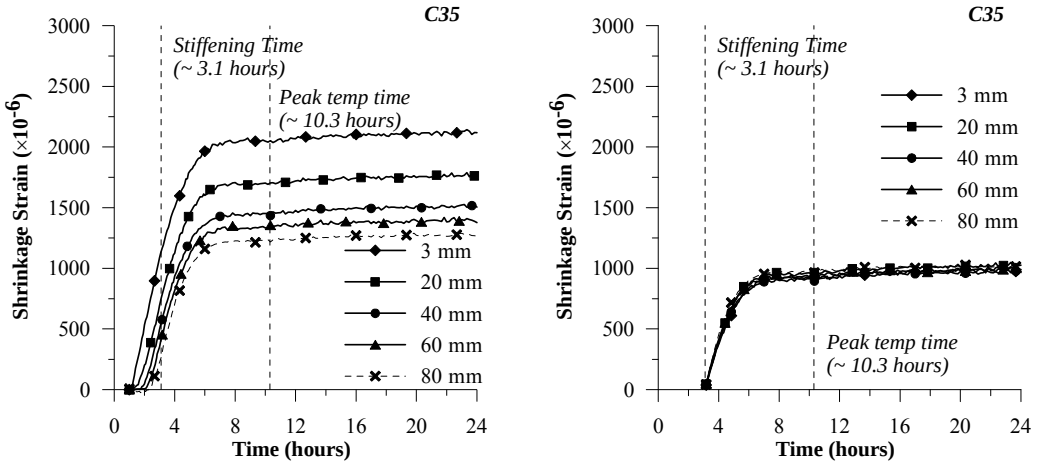

(a) *(b)*

Figure 4.29 Early age shrinkage strain with respect to the depth from the top surface on unsealed concrete specimens cast with water-to-cementitious ratio of 0.35 starting from (a) 30 minutes after water was added to the mixture, and (b) stiffening time respectively

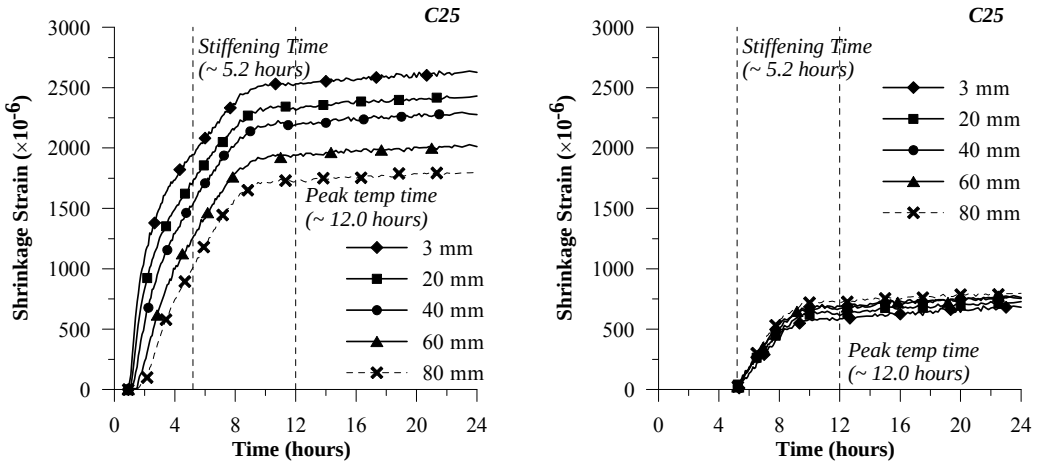

(a) *(b)*

Figure 4.30 Early age shrinkage strain with respect to the depth from the top surface on unsealed concrete specimens cast with water-to-cementitious ratio of 0.25 starting from (a) 30 minutes after water was added to the mixture, and (b) stiffening time respectively

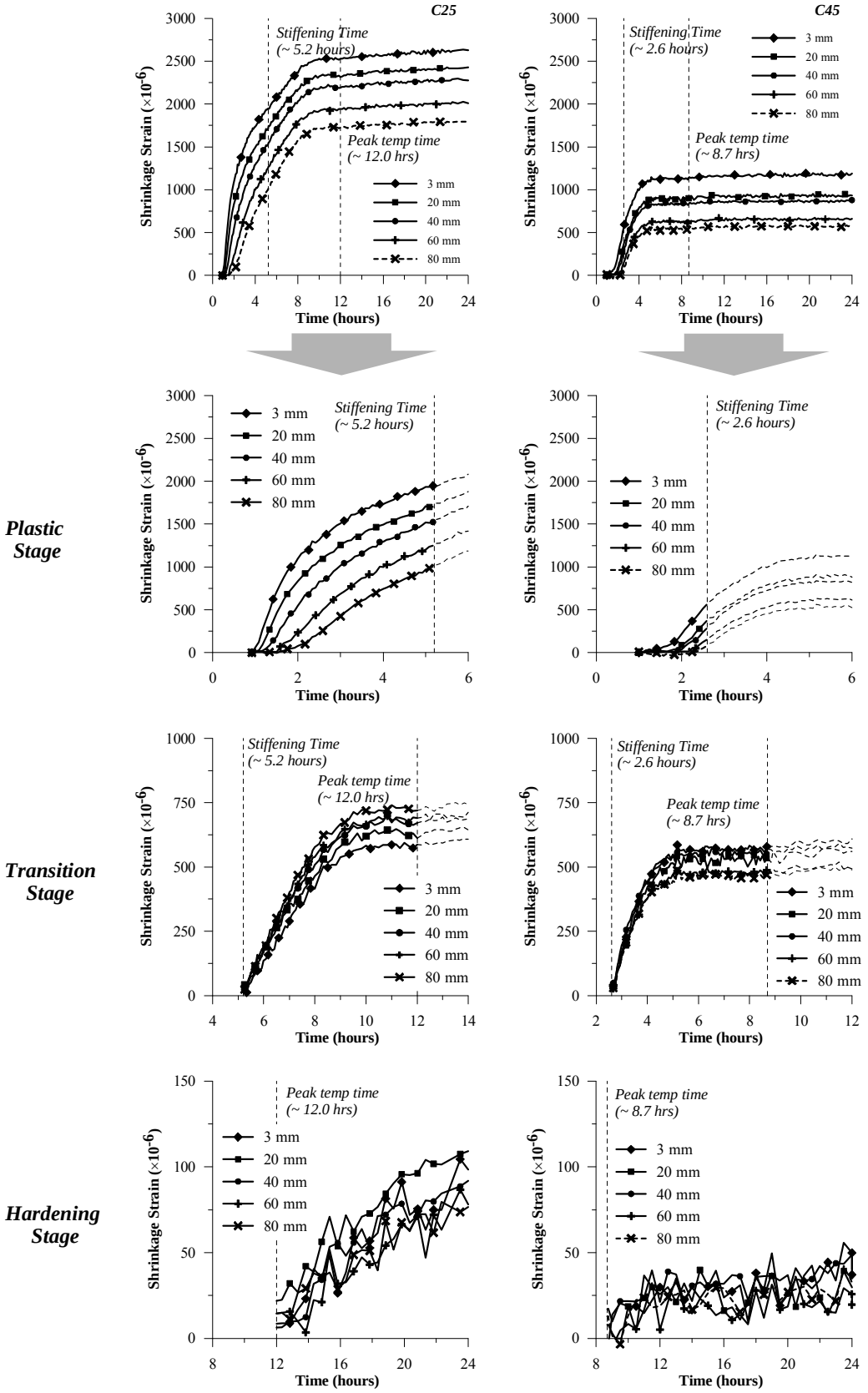

Figure 4.31 Shrinkage strains monitored at different depths on concrete specimens with water-to-cementitious ratio of 0.25 and 0.45 during plastic, transitional, and hardening stages

The plots of shrinkage strains-versus-distance from the top surface at 24 hours after adding water to the mixture, starting either from 30 minutes after adding water to the mixture or from the stiffening time is shown in *Figure 4.32*. Starting from 30 minutes after adding water to the mixture, the results showed that the highest "absolute" shrinkage strain values was observed near the top exposed surface and decreased with the depth from the top exposed surface. The results also showed that the "absolute" shrinkage strains values at all depths increased with a reduction in the water-to-cementitious ratio. The "absolute" shrinkage strain at a depth of 3 mm from the top exposed surface reached a value of 1180 με, 2120 με, and 2630 με for the C45, C35, and C25 concrete specimens respectively; while the "absolute" shrinkage strain at a depth of 60 mm from the top exposed surface reached a value of 580 με, 1270 με, and 1790 με for the C45, C35, and C25 concrete specimens respectively. The increase in the shrinkage strains monitored, as discussed previously, can be attributed to the delay in the stiffening time as well as to the higher shrinkage rate in concrete specimens cast with lower water-to-cementitious ratios.

Using the stiffening time as the TZV, *Figure 4.32(b)* shows that different plots of shrinkage strains-versus-distance from the top exposed surface were obtained for concrete specimens cast with different water-to-cementitious ratios. In the C45 concrete specimens, the "absolute" shrinkage strains values gradually decreased with depth from the top exposed surface. However, when the water-to-cementitious ratio was reduced to 0.35, the shrinkage strains "absolute" value was observed to be similar at all depths of the concrete specimen. Finally, in the C25 concrete mixture, the "absolute" shrinkage strains value gradually increased with depth from the top exposed surface. In addition, similar to that monitored in the mortar specimens, the "absolute" shrinkage strain values monitored in the concrete specimens increased when the water-to-cementitious ratio was lowered from 0.45 to 0.35. However, further reductions in the water-to-cementitious ratio to 0.30 or lower values resulted in a reduction in the "absolute" shrinkage strain values monitored at all depths. This reduction in the "absolute" shrinkage strain

values, as mentioned previously, may be linked to the "skin layer" effect developed in cementitious specimens cast with lower water-to-cementitious ratios.

Overall, the results obtained for the mortar and concrete specimens cast with different water-to-cementitious ratios showed that a reduction in the water-to-cementitious ratio led to an increase in the early age shrinkage strains monitored especially during the plastic stage. In addition, the results also showed that below a certain water-to-cementitious ratio, a "skin layering" effect may have taken place resulting in lower shrinkage strains monitored near the top exposed surface. As the surface layer dried out at a much faster rate than water could migrate up from below the surface, the surface layer may develop higher stiffness and accompanied by slower hydration resulting in lower "absolute" shrinkage strains being registered. In the present study, this phenomenon was clearly discernable in the mortar and concrete specimens cast with a water-to-cementitious ratio of 0.25. The phenomenon did not seem to be predominant in the case of the mortar specimens cast with higher water-to-cementitious ratios. It is possible that in the case of mortar specimens cast with a higher water-to-cementitious ratio, more moisture could migrate up from interior to replenish the moisture lost from the top exposed surface.

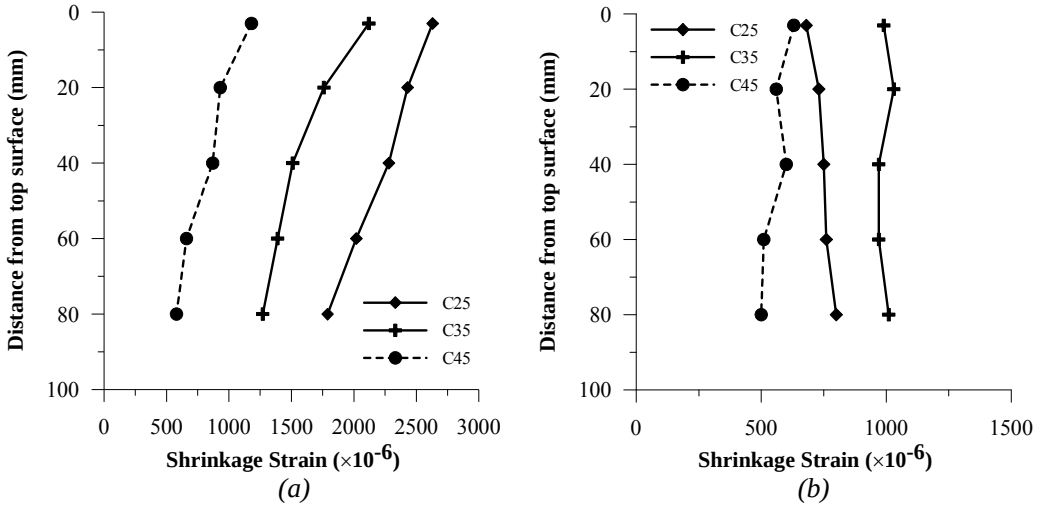

Figure 4.32 Plotting of early age shrinkage strains with respect to the depth from the top exposed surface of concrete specimens cast with different water-to-cementitious ratios at 24 hours after adding water to the mixture, starting from (a) 30 minutes after adding water to the mixture, and (b) stiffening time respectively

4.3.4 Effect of Silica Fume

The effect of silica fume as a cement replacement on the variation of early age shrinkage strains with respect to the depth from the top exposed surface was studied on mortar and concrete specimens cast with a water-to-cementitious ratio of 0.30. The silica fume content was varied from 5% to 15% by weight of cement. The aggregate volume was kept at 50% and 65% by volume for the mortar and the concrete mixtures respectively.

Table 4.5 Mix properties of mortar and concrete mixtures with different silica fume contents

Mixture	w/c	Agg. Vol. %	Workability	Stiffening Time hrs	Initial set hrs	Final set hrs	Peak Temp time Hrs
M30-SF0	0.30	50%	80%	2.0	3.3	4.5	7.5
M30-SF5	0.30	50%	140%	2.7	4.2	5.4	9
M30-SF7.5	0.30	50%	136%	2.4	3.9	5.1	8.6
M30-SF10	0.30	50%	135%	3.2	4.7	6.1	10.1
C30-SF0	0.30	65%	80 mm	2.1	3.8	5.4	9.4
C30-SF5	0.30	65%	165 mm	2.4	5.1	6.9	11
C30-SF10	0.30	65%	165 mm	4.1	6.1	7.8	11.5
C30-SF15	0.30	65%	200 mm	5.5	6.9	8.4	13.5

Table 4.5 provides a summary of the experimentally determined physical properties of the mortar and concrete mixtures. The resulting mortar workability based on the flow method varied between 80% and 140%, while the slump for the concrete mixtures varied between 80 mm and 200 mm. Due to the higher dosages of superplasticizer used in the mixtures with silica fume, a longer delay in the stiffening time, the initial setting, and the final setting time was observed.

The temperature development of mortar and concrete mixtures cast with different silica fume contents during the first 24 hours after adding water to the mixture are shown in *Figure 4.33*. The results showed that the peak temperature in both mortar and concrete mixtures reduced with an increase in silica fume content. In addition, the peak temperature was also delayed in the specimens with higher silica fume contents. The delay in the time to reach peak temperature was consistent with the delay in the setting time as tested using the penetration resistance method.

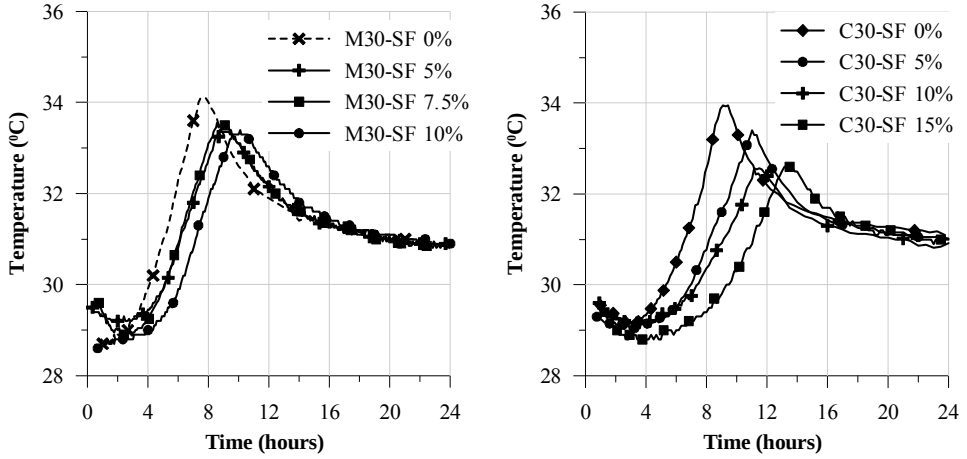

(a) *(b)*

Figure 4.33 Temperature development of (a) mortar specimens, and (b) concrete specimens cast with different silica fume contents

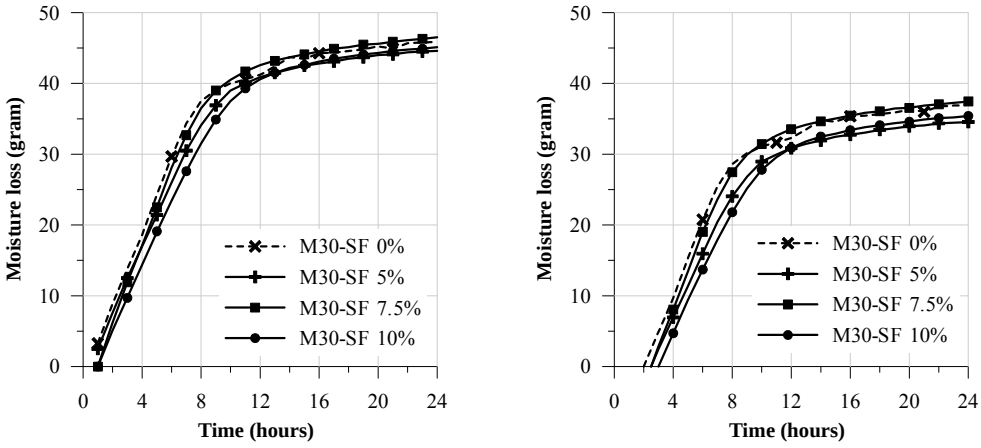

(a) *(b)*

Figure 4.34 Moisture loss measurement for mortar specimens with different silica fume contents starting from (a) 30 minutes after adding water to the mixture, and (b) stiffening time up to 24 hours after adding water to the mixture

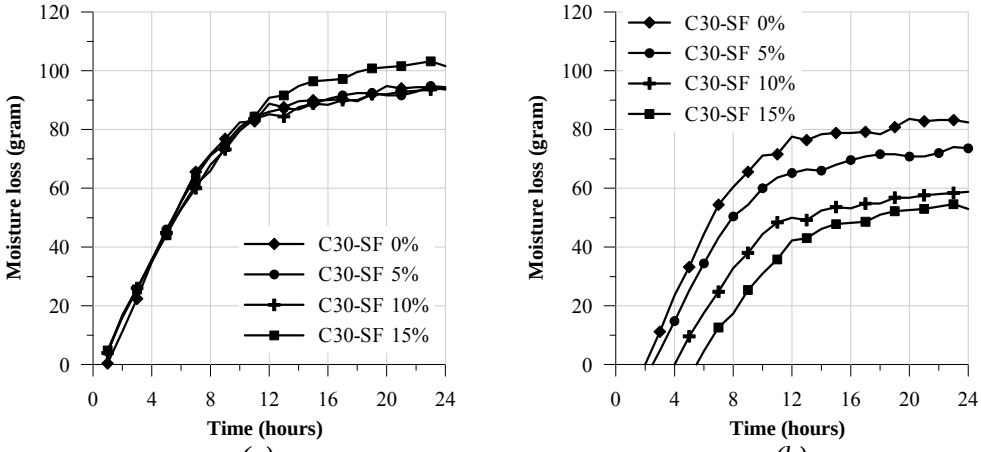

(a) *(b)*

Figure 4.35 Moisture loss measurement for concrete specimens with different silica fume contents starting from (a) 30 minutes after adding water to the mixture, and (b) stiffening time up to 24 hours after adding water to the mixture

The moisture loss development of the mortar and concrete specimens cast with different silica fume contents starting either from 30 minutes after adding water to the mixture or from the stiffening time up to the 24 hours after adding water to the mixture are shown in *Figure 4.34* and *Figure 4.35* respectively. Despite the delay in the stiffening time observed for the mortar and concrete specimens cast with silica fume, the results showed that there was no significant difference in the total moisture loss monitored. At the end of testing period (i.e. 24 hours after adding water to the mixture), a total moisture loss of 45.9 gr, 44.6 gr, 46.5 gr, and 45.1 gr was monitored on mortar specimens cast with silica fume content of 0%, 5%, 7.5%, and 10% respectively. In the case of concrete specimens, only concrete specimens cast with a silica fume content of 15% registered higher total moisture loss while the rest were rather similar. The rather similar total moisture loss monitored may be attributed to the reduced bleeding expected in cementitious mixtures with silica fume. According to Neville (2003), the addition of silica fume reduces bleeding in cementitious materials due to its high fineness. As the bleed water is reduced, less water will be available for evaporation.

In the case of mortar specimens cast with different silica fume contents, the plots of early age shrinkage monitored at various depths from the top exposed surface starting either from 30 minutes after adding water to the mixture or from the stiffening time up to 24 hours after adding water to the mixture are shown in *Figure 4.36* to *Figure 4.39*. The results showed that the addition of silica fume changed the mortar's response when subjected to a dry environment at an early age. It can be seen in mortar specimens cast with silica fume, more rapid increase of shrinkage strains was monitored at all depths from the top exposed surface. Moreover, it can be seen that in mortar specimens with a higher silica fume content, early age shrinkage strains monitored in the interior gradually approached a comparable value to that monitored near the top exposed surface.

In order to illustrate the effect of silica fume more clearly, the shrinkage-time curves for the mortar specimens cast with silica fume contents of 0% and 7.5% were divided into the plastic, transitional, and hardening stages as shown in *Figure 4.40*. The results showed that

during the plastic stage, the shrinkage strains monitored near to the top surface up to a depth of 40 mm from the top surface were significantly increased with higher silica fume contents. On the other hand, the results showed that the inclusion of silica fume increased the shrinkage strains in the interior and near the base of the mortar specimens during the transitional stage. At the end of transitional stage, the M30-SF7.5 mortar specimens registered "absolute" shrinkage strains values of 1270 με, 1320 με, 1450με, and 1580 με at the depths of 3, 20, 40, and 60 mm respectively. Finally, during the hardening stage, the results showed that there was only a slight increase in the "absolute" shrinkage strain values monitored in the mortar specimens cast with silica fume replacements. This small increase in the shrinkage strain during the hardening stage is to be expected as the silica fume has yet to be significantly activated to change the mortar structure. Nevertheless, the results of the M30-SF0 and M30-SF7.5 mortar specimens showed behavior typical of a hardened mortar when exposed to dry environment; the mortar layer near the top exposed surface registered higher "absolute" shrinkage strains values compared to that monitored in the interior.

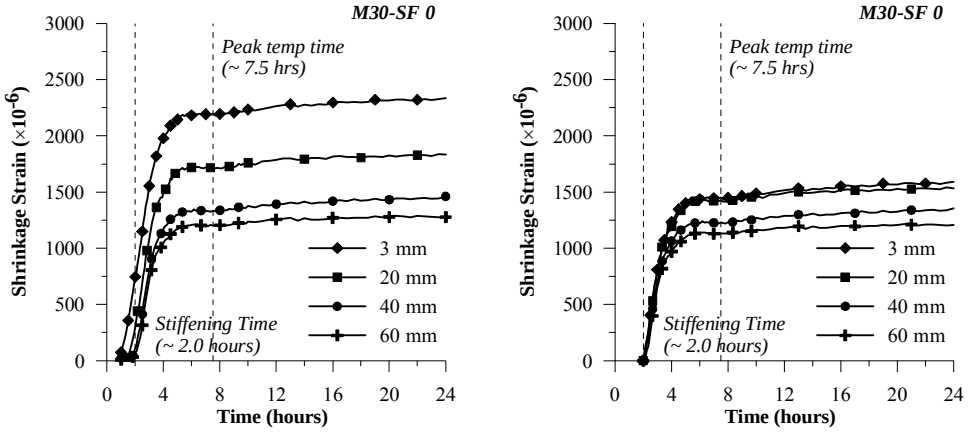

Figure 4.36 Early age shrinkage strain with respect to the depth from the top surface on unsealed mortar specimens cast with silica fume content of 0% starting from (a) 30 minutes after water was added to the mixture, and (b) stiffening time respectively

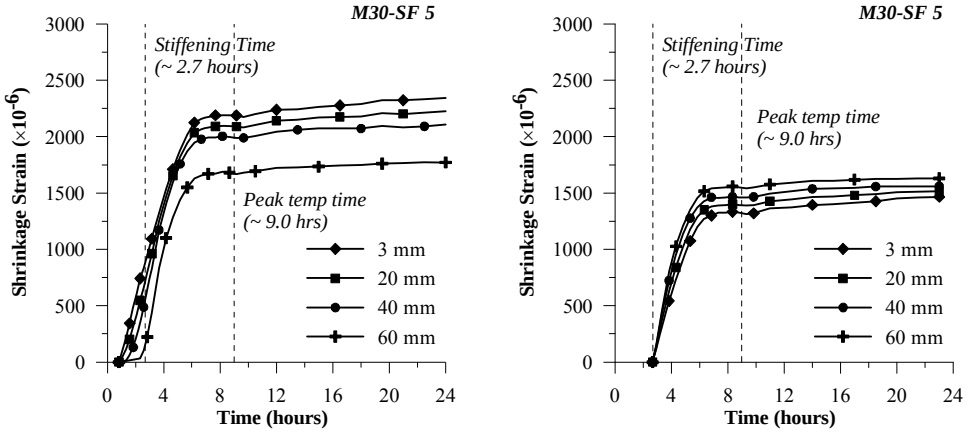

(a) *(b)*

Figure 4.37 Early age shrinkage strain with respect to the depth from the top surface on unsealed mortar specimens cast with silica fume content of 5% starting from (a) 30 minutes after water was added to the mixture, and (b) stiffening time respectively

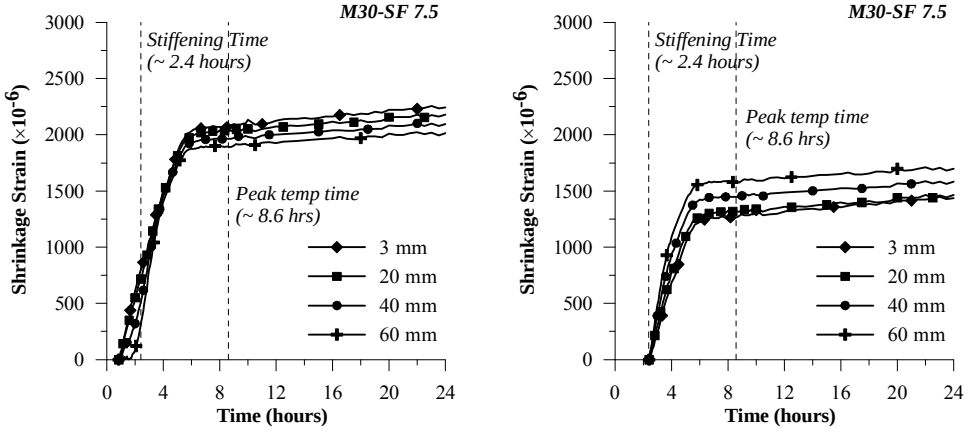

(a) *(b)*

Figure 4.38 Early age shrinkage strain with respect to the depth from the top surface on unsealed mortar specimens cast with silica fume content of 7.5% starting from (a) 30 minutes after water was added to the mixture, and (b) stiffening time respectively

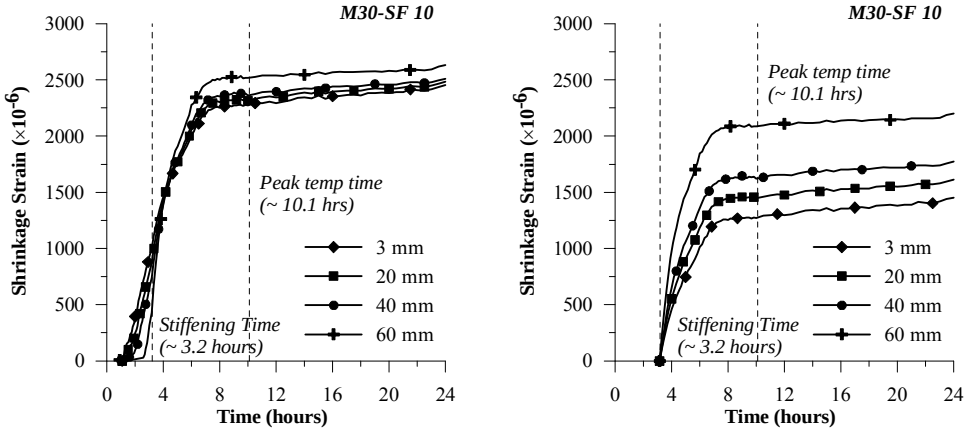

(a) *(b)*

Figure 4.39 Early age shrinkage strain with respect to the depth from the top surface on unsealed mortar specimens cast with silica fume content of 10% starting from (a) 30 minutes after water was added to the mixture, and (b) stiffening time respectively

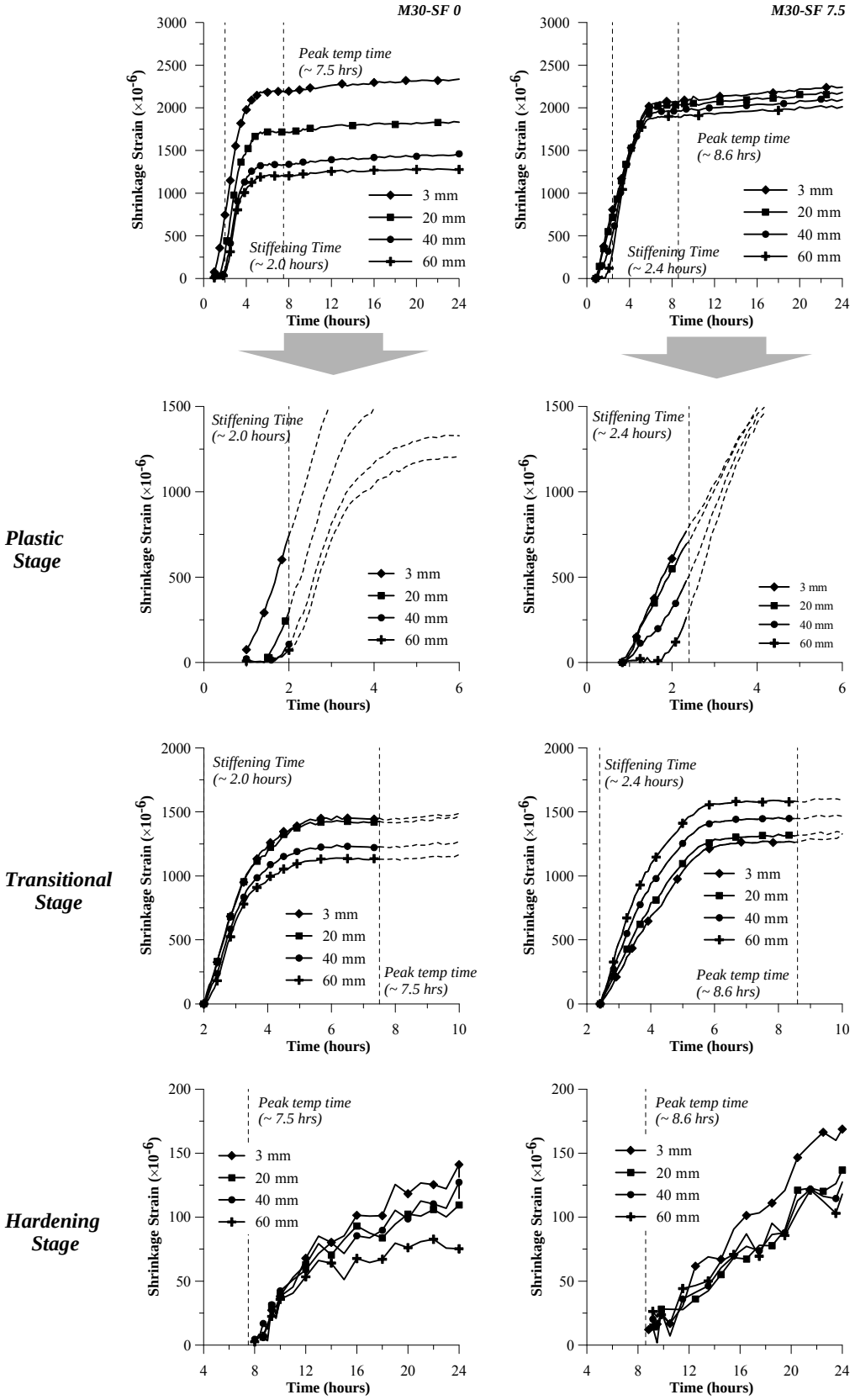

Figure 4.40 Shrinkage strains monitored at different depths on mortar specimens with silica fume content of 0% and 7.5% during plastic, transitional, and hardening stages

The plots of shrinkage strains-versus-distance from the top surface at 24 hours after adding water to the mixture with the starting time either from 30 minutes after adding water to the mixture or from the stiffening time are shown in *Figure 4.41* and *Figure 4.42* respectively. As shown in *Figure 4.41*, the results showed that starting from 30 minutes after adding water to the mixture, the mortar specimens cast with higher silica fume contents only registered a slight increase in the "absolute" shrinkage strain values near the top exposed surface. It can be seen that at a depth of 3 mm from the top surface, an "absolute" shrinkage strain value of 2270 με, 2350 με, 2240 με, and 2440 με was monitored for the mortar mixtures cast with a silica fume content of 0%, 5%, 7.5%, and 10% respectively. However, in the interior, the higher silica fume contents significantly increased the "absolute" shrinkage strain values. It can be seen that at a depth of 60 mm from the top surface, for the mortar specimens tested, the mortar specimens cast with a silica fume content of 10% registered "absolute" shrinkage strain values more than double that monitored on mortar specimens without any inclusion of silica fume. Moreover, the results also showed that a gradual change in the plots of shrinkage strains-versus-distance from the top surface was observed with increasing silica fume content. In the mortar specimens without any replacement of silica fume (i.e. M30-SF0), the "absolute" shrinkage strains value decreased rapidly with depth from the top exposed surface. On the other hand, when a 5% or 7.5% by weight of cement was replaced by silica fume, the "absolute" shrinkage strain values decreased more gradually with depth from the top exposed surface. For the highest silica fume content of 10%, the "absolute" shrinkage strains values increased more gradually with the depth from the top exposed surface.

As mentioned previously, shrinkage strains-versus-distance from the top exposed surface at 24 hours after adding water to the mixture may also be plotted with the TZV taken as the stiffening time. As shown in *Figure 4.42*, it can be seen that a slight decrease in the "absolute" shrinkage strains value with increasing silica fume replacement was observed at a depth of 3 mm from the top exposed surface. On the other hand, a significant increase in the "absolute" shrinkage strains values with increasing silica fume content was observed near the

base of the specimens. At a depth of 60 mm from the top exposed surface, an increase of about 36%, 40%, and 82% in the "absolute" shrinkage strains value were registered for the mortar specimens cast with a silica fume content of 5%, 7.5%, and 10% respectively. The results also showed that the 'absolute" shrinkage strains values increased with the depth from the top surface in the mortar specimens cast with silica fume.

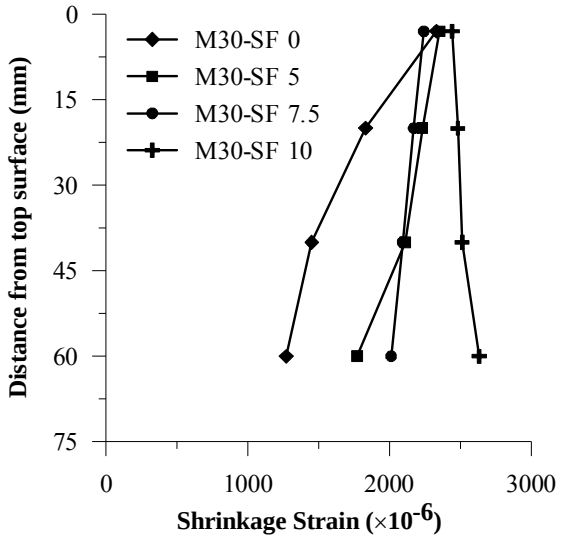

Figure 4.41 Plotting of early age shrinkage strains with respect to the depth from the top exposed surface of mortar specimens cast with different silica fume contents at 24 hours after adding water to the mixture, starting from 30 minutes after adding water to the mixture

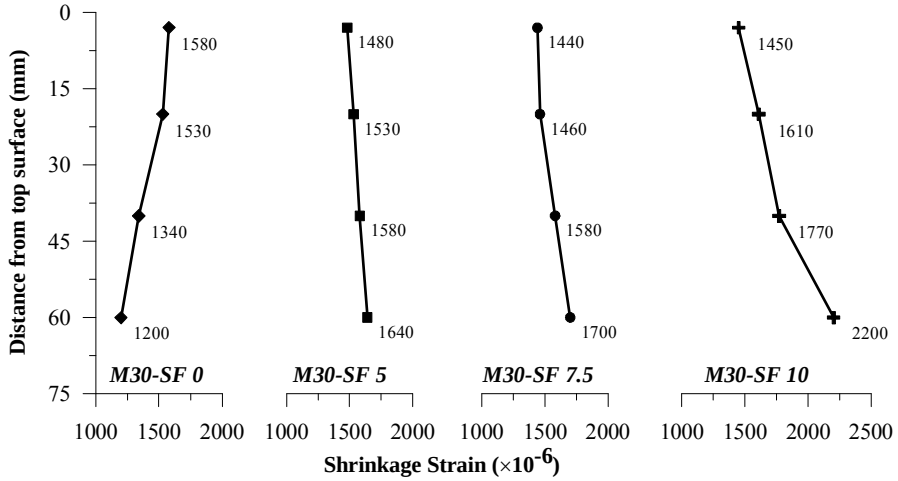

Figure 4.42 Plotting of early age shrinkage strains with respect to the depth from the top exposed surface of mortar specimens cast with different silica fume contents at 24 hours after adding water to the mixture, starting from stiffening time

In the case of concrete specimens cast with different silica fume contents, the early age shrinkage strains monitored at different depths from the top exposed surface starting either from 30 minutes after adding water to the mixture or from the stiffening time up to 24 hours after adding water to the mixture are shown in *Figure 4.43* to *Figure 4.46*. Similar to that monitored in the mortar specimens tested, it can be seen that a significant increase in the early age shrinkage strains in the interior was observed for concrete specimens cast with a higher silica fume content.

A comparison of shrinkage strain development during the plastic, transitional, and hardening stages for the concrete specimens cast with silica fume content of 0% and 15% is shown in *Figure 4.47*. It can be seen that during the plastic stage, a significant increase in the shrinkage strains was monitored with an increase in the silica fume content. This significant increase in the early age shrinkage strains could be attributed to the delay in the stiffening time as well as to the higher shrinkage rate in the concrete specimens cast with silica fume. During the transitional stage, it can be seen that for the C30-SF0 and C30 SF15 concrete specimens, the early age shrinkage strains gradually increased with the depth from the top exposed surface. Moreover, it can be seen that the difference between the "absolute" shrinkage strains value monitored at a depth of 3 mm and 60 mm also increased with an increase in the silica fume content. At the end of the transitional stage, the difference in the "absolute" shrinkage strains value was about 170 με and 360 με for concrete specimens cast with silica fume content of 0% and 15% respectively. Finally, at the hardening stage, the results showed that there was no significant difference in the "absolute" shrinkage strains value monitored in the concrete specimens cast with 15% and without silica fume replacements. Nevertheless, the results showed that the concrete layer near the top exposed surface registered a slightly higher "absolute" shrinkage strains values compared to that monitored in the interior and near the base of the specimens.

The plots of shrinkage strain-versus-distance from the top surface at 24 hours after adding water to the mixture for concrete specimens cast with different silica fume contents, starting from 30 minutes after adding water to the mixture is shown in *Figure 4.48*. The results

showed that the increase in the "absolute" shrinkage strain values was more prominent when the silica fume content was increased from 0% to 5%. However, when the silica fume content was increased to 10% or 15%, there was only a slight increase in the shrinkage strains monitored at all depths as compared to that of the C30-SF5 concrete specimens.

Figure 4.49 shows the plots of shrinkage strains-versus-distance from the top exposed surface at 24 hours after adding water to the mixture with the TZV taken as the stiffening time. A comparison between the C30-SF0 and C30-SF5 concrete specimens showed that the "absolute" shrinkage strain values increased with the addition of silica fume. It can be seen that an increase of about 400 με to 600 με at all depths was monitored for the C30-SF5 concrete specimens as compared to that of the C30-SF0 concrete specimens. However, the results also showed that when the silica fume contents was increased to 10% or 15% (i.e. C30-SF10 or C30-SF15), the "absolute" shrinkage strains values monitored at various depths were either slightly lower or comparable to that of the C30-SF0 concrete specimens. This could be explained by the moisture loss measurements as shown in *Figure 4.35*. The measurement of the total moisture loss starting from the stiffening time showed that in the case of the concrete specimens tested, a lower total moisture loss was observed for concrete specimens cast with higher silica fume contents. However, the results showed that the concrete specimens cast with higher silica fume contents registered comparable "absolute" shrinkage strain values, thus implying that the rate of shrinkage strain seemed to increase with the inclusion of silica fume.

Figure 4.49 also shows that in the case of the concrete specimens tested, the 'absolute" shrinkage strains values increased with depth from the top surface. Moreover, it can be seen that the difference between the "absolute" shrinkage strain values monitored at a depth of 3 mm and 60 mm from the top exposed surface also increased with an increase in the silica fume content.

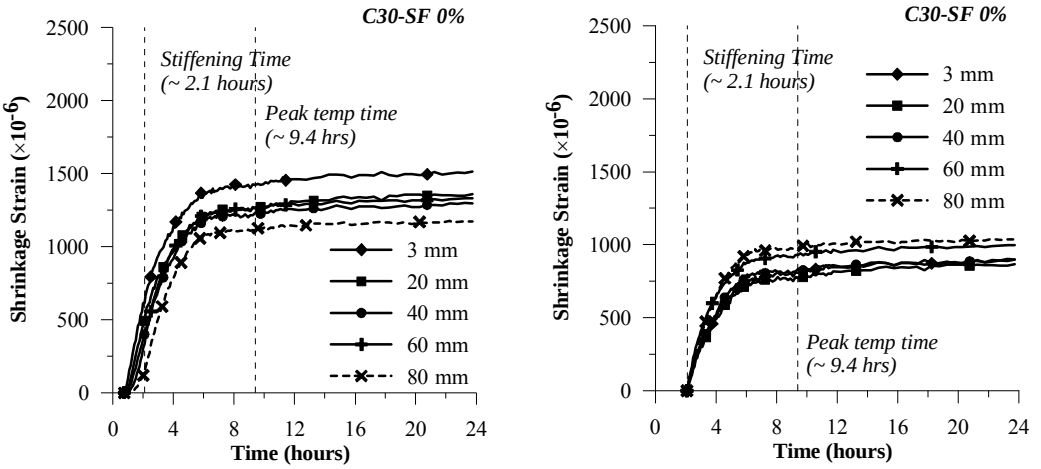

Figure 4.43 Early age shrinkage strain with respect to the depth from the top surface on unsealed concrete specimens cast with silica fume content of 0% starting from (a) 30 minutes after water was added to the mixture, and (b) stiffening time respectively

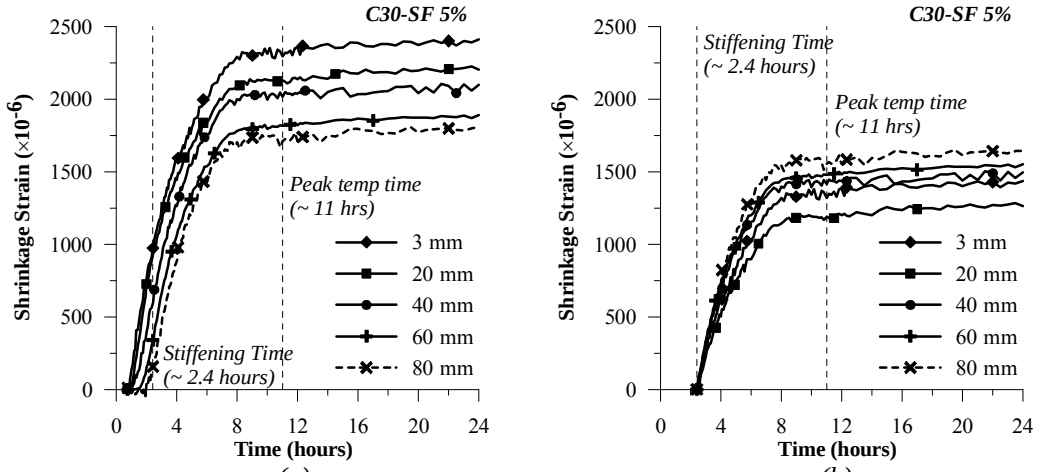

Figure 4.44 Early age shrinkage strain with respect to the depth from the top surface on unsealed concrete specimens cast with silica fume content of 5% starting from (a) 30 minutes after water was added to the mixture, and (b) stiffening time respectively

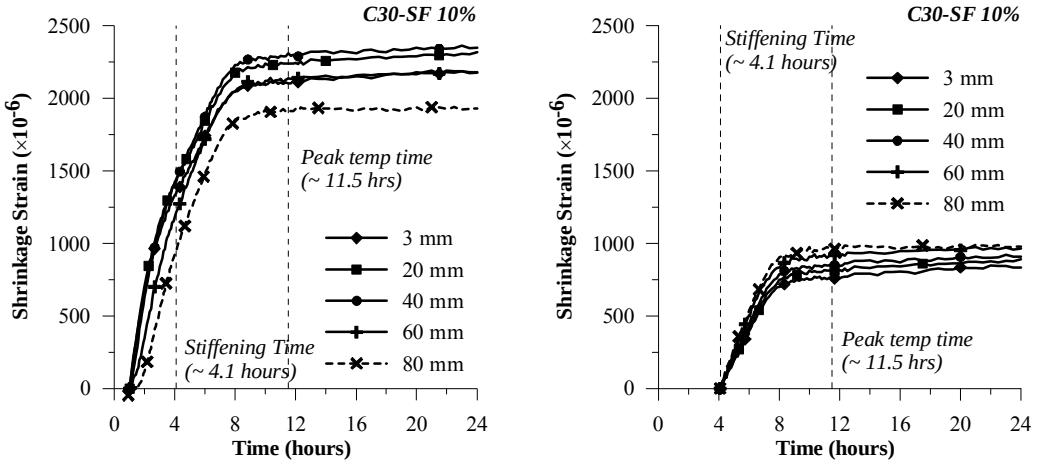

Figure 4.45 Early age shrinkage strain with respect to the depth from the top surface on unsealed concrete specimens cast with silica fume content of 10% starting from (a) 30 minutes after water was added to the mixture, and (b) stiffening time respectively

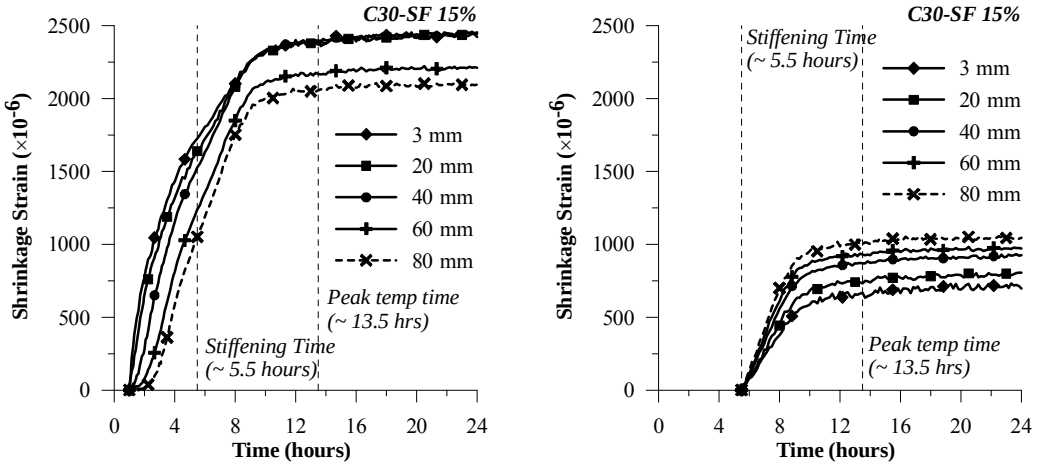

Figure 4.46 Early age shrinkage strain with respect to the depth from the top surface on unsealed concrete specimens cast with silica fume content of 15% starting from (a) 30 minutes after water was added to the mixture, and (b) stiffening time respectively

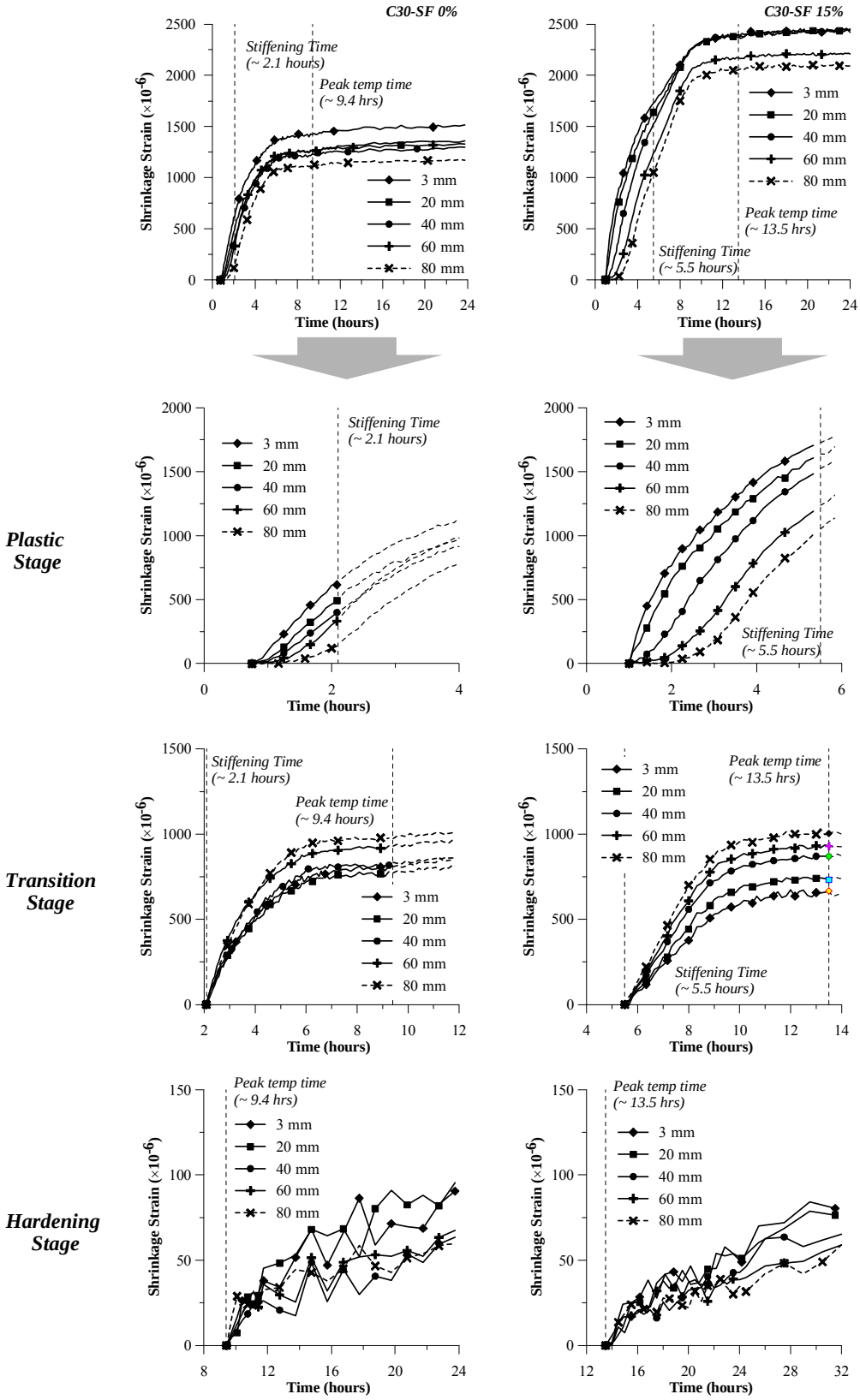

Figure 4.47 Shrinkage strains monitored at different depths on concrete specimens with silica fume content of 0% and 15% during plastic, transitional, and hardening stages

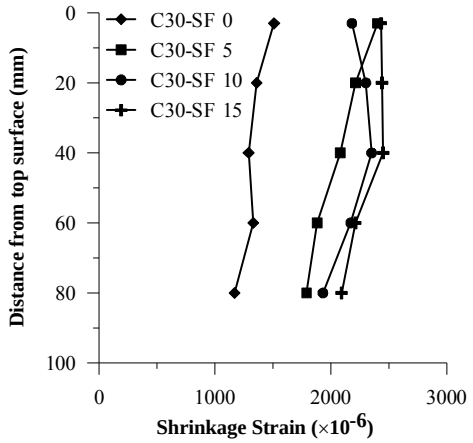

Figure 4.48 Plotting of early age shrinkage strains with respect to the depth from the top exposed surface of concrete specimens cast with different silica fume contents at 24 hours after adding water to the mixture, starting from 30 minutes after adding water to the mixture

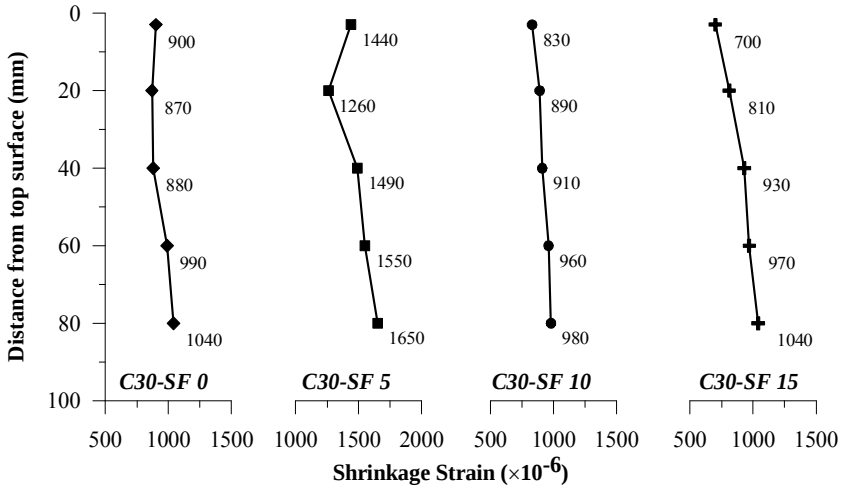

Figure 4.49 Plotting of early age shrinkage strains with respect to the depth from the top exposed surface of concrete specimens cast with different silica fume contents at 24 hours after adding water to the mixture, starting from the stiffening time

Based on the results obtained for the mortar and the concrete specimens cast with different silica fume contents, the effect of silica fume was found to be more predominant during the very early ages, i.e. during the plastic and transitional stages. During the plastic stage, as mentioned previously, the inclusion of silica fume resulted in a rapid development of shrinkage strains across the specimen's depth. This rapid increase in the shrinkage strains can be attributed to the delay in the stiffening time as well as the higher shrinkage rate in cementitious mixtures with silica fume. With a longer time to reach the stiffening time, higher shrinkage

strain would be developed during the plastic stage. Moreover, the "filling" effect of the silica fume particles could also contribute to the higher shrinkage rate observed. As shown in *Figure 4.50*, with a denser microstructure associated with cementitious mixtures cast with silica fume, the inter-particles spacing in these mixtures may be reduced significantly. As the evaporation and hydration proceed, the reduction in the inter-particles spacing will contribute to high negative capillary pressure. The high negative capillary pressures may significantly increase the shrinkage of the cementitious material.

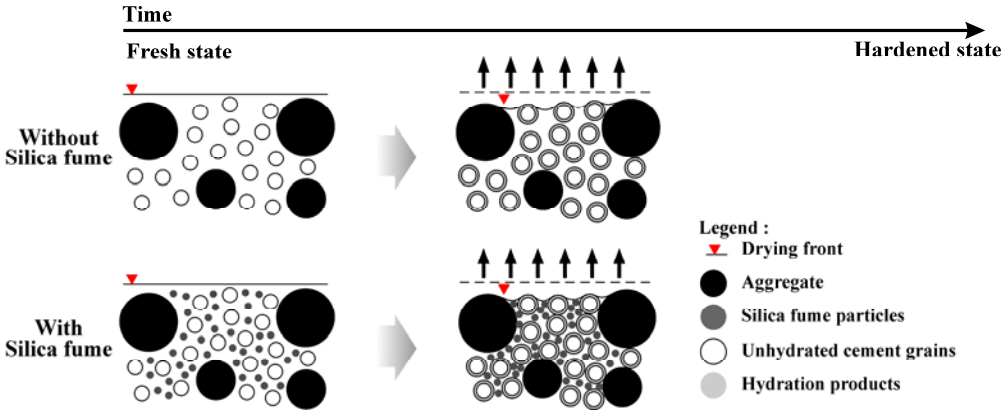

Figure 4.50 Drying sequence for cementitious mixture with and without silica fume when exposed to drying environment at early ages

In the case of the mortar and the concrete specimens tested in the present study, the moisture loss due to evaporation during the transitional stage may result in a rather complex process. First, as discussed earlier, the evaporation may create high negative capillary pressure in the cementitious mixture cast with silica fume that may lead to high shrinkage strains. Second, this high capillary pressure may also significantly consolidate both the cement particles and aggregates, causing these particles to be in contact with each other, and creating "skin layer" near the top exposed surface. Once the "skin layer" is formed, the subsequent evaporation and hydration may increase the stiffness of the "skin layer" thus the cementitious mixture will be able to resist the shrinkage strains induced by the high negative capillary pressure. Third, evaporation may also reduce available free water for hydration especially near the top exposed surface. As a result, less shrinkage due to self-desiccation may be expected. Due to the

aforementioned conditions, similar "absolute" shrinkage strain values for the cementitious mixture cast with different silica fume contents may be observed near the top exposed surface at 24 hours after adding water to the mixture.

4.4 Summary

This chapter discussed several mixtures parameters that influence the development of early age drying shrinkage within the first 24 hours after adding water to the mixture. Based on experimental studies carried out, the following conclusions could be drawn:

1. The addition of superplasticizers significantly increased the early age shrinkage strains monitored at all depths during the first 24 hours after adding water to the mixture. The increase in the shrinkage strains monitored can be attributed to the delay in the stiffening time as well as the prolonged transitional stage.

2. The higher aggregate volume, as expected, led to higher internal restraints within the cementitious specimens. Moreover, while it was typically observed in early age drying shrinkage monitoring that the "absolute" shrinkage strain values decreased with depth from the top exposed surface of prism specimens, in the case of mortar prism specimens cast with the highest aggregate volume (i.e. 55%), opposite results were observed. The "absolute" shrinkage strain values monitored near the exposed top surface registered lower values compared to those monitored near the base of the prism specimens. This high internal restraint led to a "skin layer" effect being included near the top exposed surface.

3. The reduction in the water-to-cementitious ratio significantly increased the early age shrinkage strains monitored during the plastic stage. In addition, a "skin layer" effect may also have taken place below a certain water-to-cementitious ratio. As the surface layer dried out at much faster rate than could be replaced by water migrating from below, the surface layer may develop higher stiffness as well as lower hydration resulting in less "absolute" shrinkage strain values. In the preset study, this phenomenon was clearly discernable in the mortar and concrete specimens cast with a water-to-cementitious ratio of 0.25. The phenomenon did not seem to be predominant for the mortar and concrete specimens cast with higher water-to-cementitious

ratios. Perhaps there was more moisture migration from below, replenishing the loss of moisture from the top exposed surface.

4. For the cementitious specimens cast with similar water-to-cementitious ratio, the inclusion of silica fume significantly increased the early age shrinkage strains monitored, especially during the plastic and transitional stages. This can be attributed to the denser microstructure in the mortar and concrete specimens cast with silica fume as well as the delay in the stiffening time. During the transitional stage, the development of shrinkage strain near the top exposed surface was influenced by stiffening of the surface layer or the "skin layer" effect. As a result of this "skin layer" effect, similar "absolute" shrinkage strain values for the cementitious mixtures cast with different silica fume contents was observed near the top exposed surface at 24 hours after adding water to the mixture. Nevertheless, in the interior, shrinkage strains were observed to increase with an increase in the silica fume content.

Chapter 5 EARLY AGE SHRINKAGE OF HIGH PERFORMANCE CONCRETE IN BONDED CONCRETE OVERLAY

5.1 Introduction

The technique of casting a new cementitious layer on top of an old concrete substrate is frequently applied in the area of concrete repair and retrofitting. In such composite systems, the durability of the repaired structure depends on the interaction between the new and the old concrete at the interface as well as the durability of the new concrete layer (Xu (1999)). In such repair work, it is recognized that the properties of the old substrate layer may have a significant influence on the bond at the interfacial layer. These include surface roughness, soundness, cleanliness, and moisture condition prior to the application of the new concrete layer [Wall and Shrive (1988), Austin et al. (1995), Xu (1999), Climaco and Regan (2001), Kyaw (2007)]. It is also important to note that at the same time, some of the substrate properties namely substrate roughness and moisture condition may also influence the durability of the new concrete layer (Xu (1999)). As the surface of the substrate gets rougher, higher restraints are provided by the substrate and consequently, relatively higher stresses develop within the new concrete material which may lead to premature cracking. Simultaneously, the moisture condition of the old substrate layer may also influence the durability of the new concrete layer. Xu (1999) postulated that the early age shrinkage of the new concrete layer would be higher due to water absorption by the substrate layer in contact with the newly cast cementitious layer at the interface. In addition, the water absorbed by the substrate layer may also induce early age expansion of the adjacent substrate layer that can lead to de-lamination at the interface between the two layers. Subsequent study by Kyaw (2007) showed results which contradicted postulations by Xu (1999). As the substrate layer absorbed water from the new concrete layer, the newly cast concrete layer on composite systems did not shrink as much as newly cast monolithic specimen. This anomaly

was attributed to the restraint effect provided by the substrate surface in contact with the newly cast cementitious layer.

In the literature, two types of failure in a composite system, often reported are cracking and de-lamination of the new layer (Xu (1999), Carlswärd (2006), Kyaw (2007)). Both phenomena are usually reported to be caused by internal stresses due to shrinkage of the new concrete layer coupled with shrinkage differences between the new concrete layer and the old substrate. The assessment cracking of the new concrete layer due to its shrinkage, both at the microscopic and macroscopic levels, has been extensively reported in the literature (Xu (1999), Bisschop and van Mier (2002), Kim and Weiss (2003), Pease et al. (2004), Banthia and Gupta (2009)). At the microscopic level, the presence of microcracks has been documented experimentally by using optical and scanning electron microscopy (Xu (1999), Bisschop and van Mier (2002)) as well as by using acoustic emission sensors (Kim and Weiss (2003), Pease et al. (2004)). At the macroscopic level, the development of macrocracks in the new concrete layer has been documented by Carlswärd (2006) and Banthia and Gupta (2009). A study by Carlswärd (2006) on composite specimens after 5 days of sealed-moist curing reported the occurrence of cracks with widths in the range of 0.05 to 0.6 mm on the surface of the new concrete layer. Another study by Banthia and Gupta (2009) on composite specimens exposed to a dry environment of 50^0C and 5% RH as soon as the casting was completed, showed that plastic shrinkage cracks started to develop rapidly during the first three hours after adding water to the mixture. At 20 hours after adding water to the mixture, the cracks width monitored was in the range of 0.4 to 1.8 mm. The occurrence of de-lamination at the interface between the concrete substrate and the new concrete layer was also reported by Xu (1999), Shin and Lange (2004) and Carlswärd (2006). An earlier study by Xu (1999) noted that after a period of moist curing, cracks with widths in the range of 0.1 to 0.6 mm were observed at the interface between the old substrate and the new concrete layer. Another study by Shin and Lange (2004) starting from 1 day after casting showed that de-lamination was observed at the edges of the composite specimens after 2 days exposure to a dry environment. A more recent study by Carlswärd (2006) reported that the de-lamination on composite slab specimens was also apparent from

visual inspection. Despite the numerous studies on cracking and de-lamination of composite specimens, it is important to note that most of the studies were carried out after a period of curing in which the influence of very early age shrinkage strains during the first 24 hours after adding water to the mixture was not included.

In this chapter, the development of early age shrinkage strain with respect to the depth from the top exposed surface of composite prism specimens by direct measurement is investigated with emphasis on the first 24 hours after adding water to the mixture. The influence of substrate surface preparation and moisture condition prior to the application of the new concrete layer is studied along with an assessment of cracking and de-lamination due to early age shrinkage during the first 24 hours after adding water to the mixture.

5.2 Methodology and Mix Compositions

In this investigation, the image analysis technique as described in Chapter 3 was used for monitoring the variation of early age shrinkage strain with respect to the depth from the top surface of the composite prism specimens. The temperature readings were monitored on the same specimen via a thermocouple with an automatic data logger with a sensitivity of 0.1^0C. The workability of concrete mixture was determined according to the slump test method (ASTM-C143/C143M-09 (2009)) respectively. The slump of concrete mixture was measured just after the mixing process was completed (i.e. within 10 to 15 minutes after water was added to the mixture). The assessment of stiffening time was performed by using the S-wave reflection technique as discussed previously in Chapter 2. After the casting was finished, all the specimens were placed in the temperature and humidity controlled room maintained at 30 ± 0.5^0C and 65 ± 2 % for the entire duration of the experiment.

Table 5.1 shows a summary of concrete mixture proportions used in the present study. The substrate concrete layer was cast with a water-to-cementitious ratio of 0.50 while two different concrete mixtures were prepared for the new concrete layer. These two concrete mixtures representative of a high performance concrete and a normal strength concrete respectively, were prepared with water-to-cementitious ratios of 0.25 and 0.45 respectively. The

substrate cast with w/c ratio of 0.50 was used since the focus of the present study is to investigate the effect of substrate surface preparation and substrate moisture absorption on the development of early age shrinkage and cracking (i.e. delamination) development of the new overlay mixtures. In such cases, the effect of substrate moisture absorption can be observed more clearly since it is expected that the substrate cast with high w/c ratio will absorb more moisture as compared to that of substrate cast with low w/c due to their inherent properties. Nevertheless, it should be noted that in the actual practice, the requirement for elastic and dimensional compatibility will dictate the selection of the repairs/overlay materials.

In all concrete mixtures, type I Portland cement with Blaine fineness of 365 m^2/kg was used. Crushed granite with a maximum size of 12.5 mm and a specific gravity of 2.60 was used as coarse aggregates. The fine aggregates used was natural sand with fineness modulus and specific gravity of 2.80 and 2.60 respectively. Both coarse and fine aggregates were prepared according to the requirement specified in ASTM-C33-08 (2008). The total volume of the aggregates was kept between 62% and 65% by volume. A commercially available high-range water-reducing admixture[5] with a specific gravity of 1.125 and a solid content of about 35.5% by weight was used in the concrete mixtures to achieve target workability. This chemical admixture conform to ASTM-C494/C494M-08a (2008) as a type F and G (retarding) admixture.

Table 5.1 Mix proportion of concrete mixtures

Mixture	w/c	Agg. vol.	Water, kg/m^3	Cement, kg/m^3	Fine Agg. kg/m^3	Coarse Agg. kg/m^3	HRWRA	
							lt/m^3	by cement mass (%)
C25 – New concrete layer	0.25	65%	144	588	790	900	4.42	0.30
C45 – New concrete layer	0.45	65%	196	436	790	900	0.66	0.06
C50 – Old substrate layer	0.50	62%	224	448	736	873	0	0.00

[5] ADVA 181N, W.R. Grace Pte. Ltd. Singapore

5.2.1 Shrinkage monitoring and crack opening (de-lamination) measurement

Two types of shrinkage strains were monitored in the present study; free shrinkage strains and restrained shrinkage. The restrained shrinkage was monitored on composite specimen comprised of 50 mm thick substrate and 50 mm thick new concrete layer. The shrinkage strains monitored on composite specimens were compared to free shrinkage strains monitored on monolithic specimens, which had thicknesses equal to the thickness of the new concrete layer (i.e. 50 mm).

Figure 5.1 shows a composition of the composite specimens and the locations of targets on the composite specimens. The targets used for the new concrete layer were exactly the same to that described earlier in Chapter 3, while the target used for the substrate layer comprises of a plastic disc topped with a 4 mm square inked target. This target was directly epoxy-glued on the surface of the concrete substrate. The shrinkage strains of the new concrete layer were monitored at a depth of 3, 20, and 40 mm from the top surface of composite specimen, while the shrinkage strains of the substrate layer were monitored at a depth of 60, 75, and 90 mm from the top surface of composite specimen. Two surface treatments, sealed and unsealed surface, were performed on the new concrete layer. The sealed and unsealed surfaces represented, respectively, "adequately cured" and "inadequately cured" specimens.

The cracks on the surface of the new concrete layer and the de-lamination development at the interface between the new concrete and substrate layers were monitored by means of the image analysis technique. Two approaches were carried out in the image analysis technique. In the first approach, images of cracks were captured as they develop. The cracks images were obtained by demolding the composite specimens at a specific time and capturing images of the cracks or the de-laminations manually from the top or the side of the specimen by using a digital microscope (i.e. VMS-004) with a 20× magnification. Subsequently, the composite specimen was cut by a concrete cutter according to the cutting configuration as shown in *Figure 5.2*. After cutting, each section was carefully examined under stereomicroscope (i.e. Leica MZ8) with a maximum magnification of 50× for closer inspection of cracks and de-laminations. In this investigation, a similar procedure to that developed by Qi et al. (2003) was performed to

quantify the cracks widths. This includes: 1) acquiring the image of cracks by using either digital microscope or stereomicroscope, 2) extracting the cracks contour in the binary image by means of intensity thresholding, 3) image cleaning, 4) grid subtraction, and 5) cracks width measurement. *Figure 5.3(a)* shows a typical gray-scaled image of a crack which occurred at the interface between the new concrete and substrate layers. As reported in an earlier study by Qi et al. (2003), the image of the crack would have a certain range of gray level intensities that were different from the surrounding area. This change in gray level intensity is shown in *Figure 5.3(b)* for the line "A" shown in the original image. It can be seen that the crack typically had lower gray level intensities compared to that of the surrounding area. Based on these intensities, a threshold value was taken to be the average value of the intensities of the crack area and the surrounding area. The resulting binary image after the thresholding process is shown in *Figure 5.3(c)*. Subsequently, image cleaning process was performed to remove unwanted pores or craters while at the same time preserving the crack's features (i.e. *Figure 5.3(d)*). For crack width measuring purpose, a series of predetermined vertical lines were superimposed on the crack image. This step allowed the crack width to be determined at consistently spaced locations along the length of the crack (i.e. *Figure 5.3(e)*). In this investigation, depending on the magnification used, the resolution of the test set-up ranged between 5 and 15 μm/pixel.

In the second approach, the development of de-laminations or cracks at the interface was monitored by the same target used for the early age shrinkage monitoring. As shown in *Figure 5.4*, the occurrence of de-lamination and the cracks width development were assessed by calculating the distance between two targets located near the interface of the new concrete and substrate layers at a specific time (D_i). The present test set-up allows the cracks width to be measured at two locations, i.e. at a distance of 25 mm and 75 mm from the edge of the prism specimens. Given the ability of image analysis technique to resolve the movement of target in sub-pixels value, the resolution of the present test set-up is approximately 4 μm.

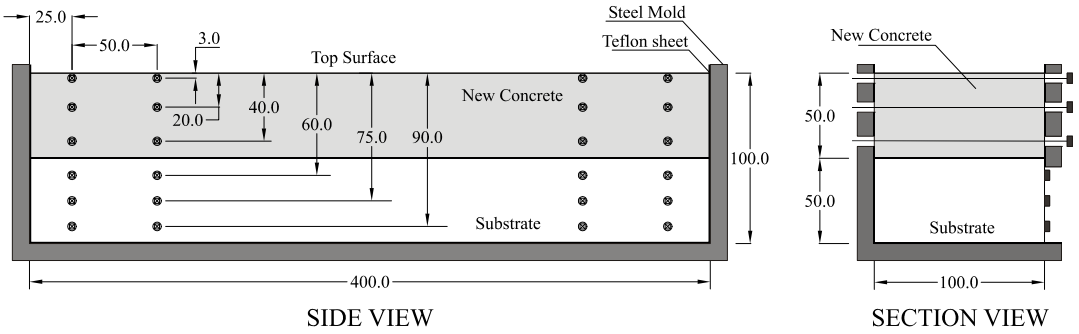

Figure 5.1 Composition and location of targets in the composite specimens (mm)

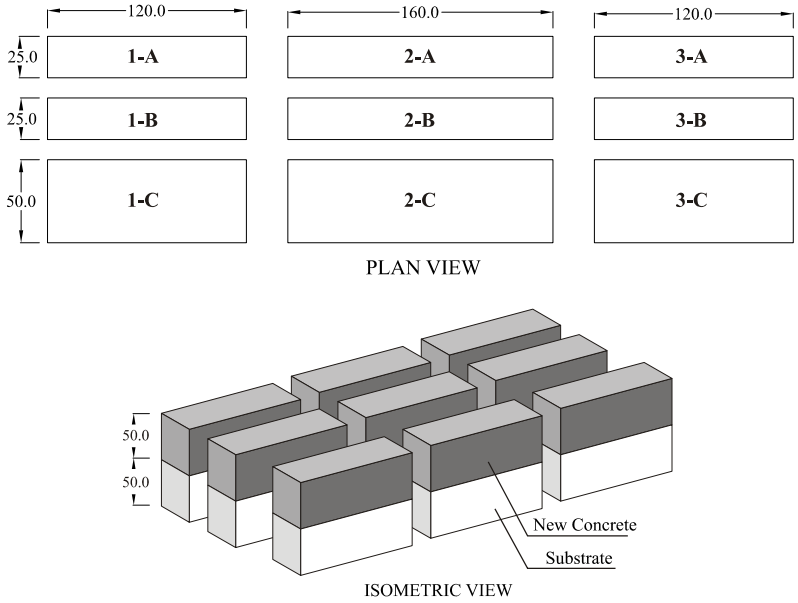

Figure 5.2 Cutting configuration of the composite specimen (mm)

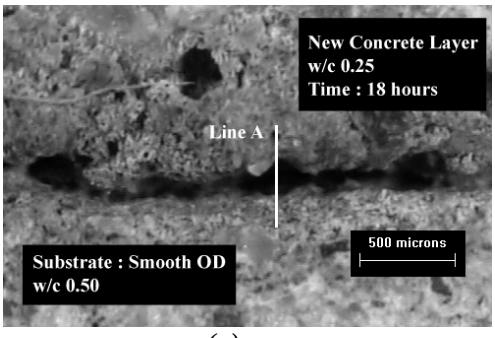

(a)

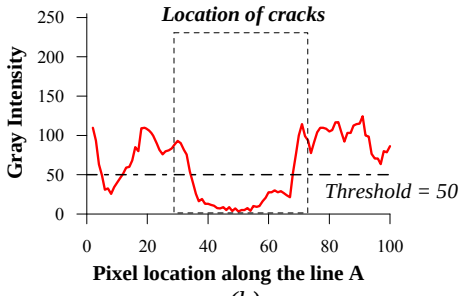

(b)

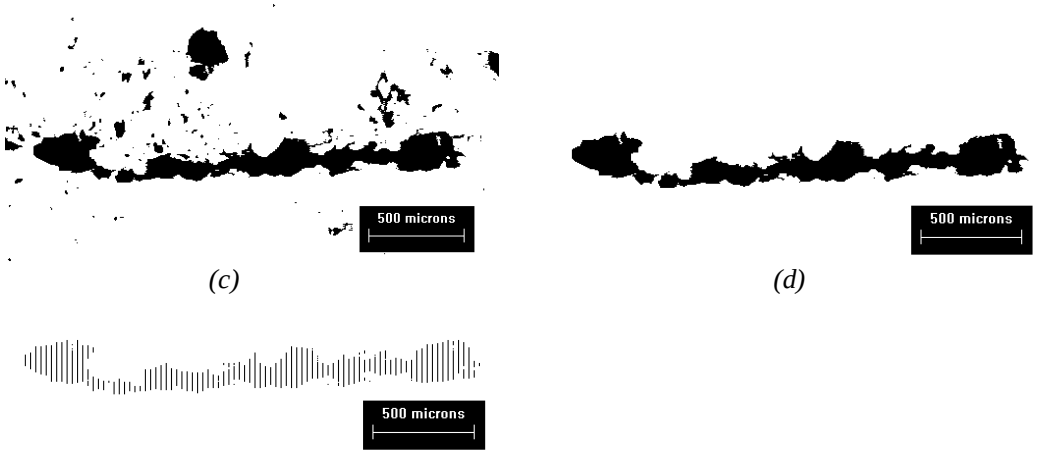

(c) *(d)*

(e)

Figure 5.3 Image analysis procedures for quantifying the crack width at interface; (a) original image,(b) selection of threshold value, (c) binary image after thresholding process, (d) binary image after cleaning process, and (e) binary image after imposing a series of predetermined vertical lines

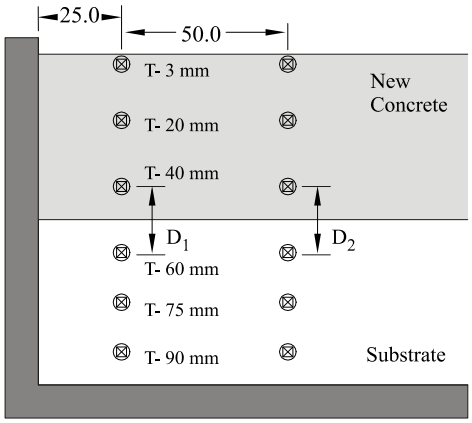

SIDE VIEW

Figure 5.4 The target used for monitoring the crack and de-lamination

5.2.2 Substrate preparation

In the present study, the concrete substrate used was at least 3 months old at the time of the placement of the new concrete layer to make sure that most of its drying shrinkage had taken place. This concrete substrate was firstly cast and de-molded the next day before being moist-cured for 28 days. After moist curing, it was allowed to dry in the temperature and relative humidity controlled room at 30 ± 0.5^0C and $65 \pm 2\%$ for at least 90 days.

Prior to the casting of the new concrete layer, the concrete substrate was prepared with three different moisture conditions; oven-dry (OD), pre-wetted surface (SW), and saturated surface dry (SSD). For the substrate with OD condition, the substrate was firstly placed in an oven at a temperature of 105 ± 5^0C for a duration of 24 hours. After heating, the substrate was allowed to cool down for about 2 hours before all the surfaces were sealed using an aluminium tape except one surface that will be in contact with the fresh new concrete layer. Finally, the substrate was allowed to cool down to room temperature for about 22 hours before casting of the new concrete layer.

The SW and SSD substrates were prepared in the same manner as the OD substrates, but were subjected to water-ponding for 1 hour and 24 hours prior to the casting of the new concrete layer respectively. The surface of the SW and SSD substrate was mopped dry to remove the excess moisture just before casting of the new concrete layer.

In order to investigate the influence of substrate surface roughness on shrinkage of the new concrete layer, two different surface conditions were prepared; smooth surface and rough surface. The smooth surface was obtained from casting against the mould face while the rough surface was obtained by creating a series of "U" groove of about 5 mm width and 5 mm deep on the surface of the smooth substrate. As shown in *Figure 5.5*, centre-to-centre spacing between these grooves was approximately 20 mm. This rough substrate has been determined to have arithmetical mean roughness (R_a) of 17.45 mm and the differences between the highest peak and the deepest valley (R_{max}) of 50.35 mm.

Figure 5.5 Substrate with rough surface used in present investigation

5.3 Results and Discussion

In the present study, two assumptions were made as follows:

- In the free shrinkage strains monitoring on monolithic specimens, as layers of Teflon sheet and plastic wrap were placed between the newly cast cementitious material and the steel mold, minimum restraint effect (i.e. minimum friction and no bonding strength) was assumed to occur at the interface of the newly cast cementitious material and the steel mold. In the case of composite specimens cast with smooth substrate, restraint effects in terms of friction and bond between the newly cast cementitious material and the substrate was assumed to occur at the interface. Similarly, in the case of composite specimens cast with rough surface, higher restraint effects as compared to that provided by the substrate with smooth surface was assumed to occur at the interface between the newly cast cementitious material and the substrate. This higher restraint effects was due to mechanical interlocking arising from the presence of grooves.

- Similar assumption was made for the water absorption by the substrate. The substrate with oven-dry condition (i.e. OD substrate) was expected to have the highest absorption capacity. While the substrate with saturated surface dry condition (i.e. SSD substrate) was expected to have the minimum water absorption capacity. The absorption capacity of the pre-wetted substrate (i.e. SW substrate) was expected to be in between of that of the OD and SSD substrates. In the case of the monolithic specimens, as the bottom part was sealed by plastic wrap, no water movement was considered.

5.3.1 Substrate deformation

The effect of substrate moisture absorption on its deformation is clearly shown in *Figure 5.6* and *Figure 5.7* for the C25 and C45 composite specimens respectively. The OD substrates which were expected to have the highest moisture absorption, registered the highest expansion among the three substrates. The results also showed that during the first few hours after casting of the new concrete layer, the expansion of the OD substrates reduced with distance from the interface. A rapid expansion was registered at a distance of 10 mm from the interface (i.e. at a depth of 60 mm from the top surface of composite specimen), while a more gradual increase in expansion was registered at a distance of 40 mm from the interface (i.e. at a depth of 90 mm from the top surface of composite specimen). In the case of SW and SSD substrates, the results showed that the SW and SSD substrates still registered a slight expansion during the first few hours after casting of the new concrete layer, followed by a contraction up to the end of the testing period. A comparison between SW and SSD substrates also showed that the SW substrates registered a slightly higher expansion as compared to that monitored for the SSD substrates especially in the C25 composite specimens.

In the case of the composite specimens tested, although the expansion of the substrate was mostly attributed to its moisture absorption, the expansion and contraction registered by the substrates could also be affected by the variation in the temperature of the substrate. As shown in *Figure 5.6* and *Figure 5.7*, the temperature monitoring at the mid-height of substrate thickness showed that most of the substrates registered a temperature increase of about 1.5^0C

before finally cooling down with time. This increase in the substrate temperature could be attributed to heat transferred from the hydration reaction of the new concrete layer. As the substrate temperature increases, the substrate expands. Simultaneously, when the substrate temperature starts to decrease, the substrate shrinks. As can be seen in *Figure 5.6* and *Figure 5.7*, the effect of temperature variation on substrate deformation was clearly shown in the substrates with SSD condition.

The substrate deformation measurement also showed that at later ages, the bottom portion of the substrate registered either similar or higher rate of expansion as compared to that monitored near the interface. Considering the test set-up in which both ends of the composite specimen were left free to move, the results showed that the early age shrinkage of the new concrete layer was sufficient to induce "curling" behavior in the composite specimens tested. This "curling" behavior of composite specimens was also reported by Kyaw (2007).

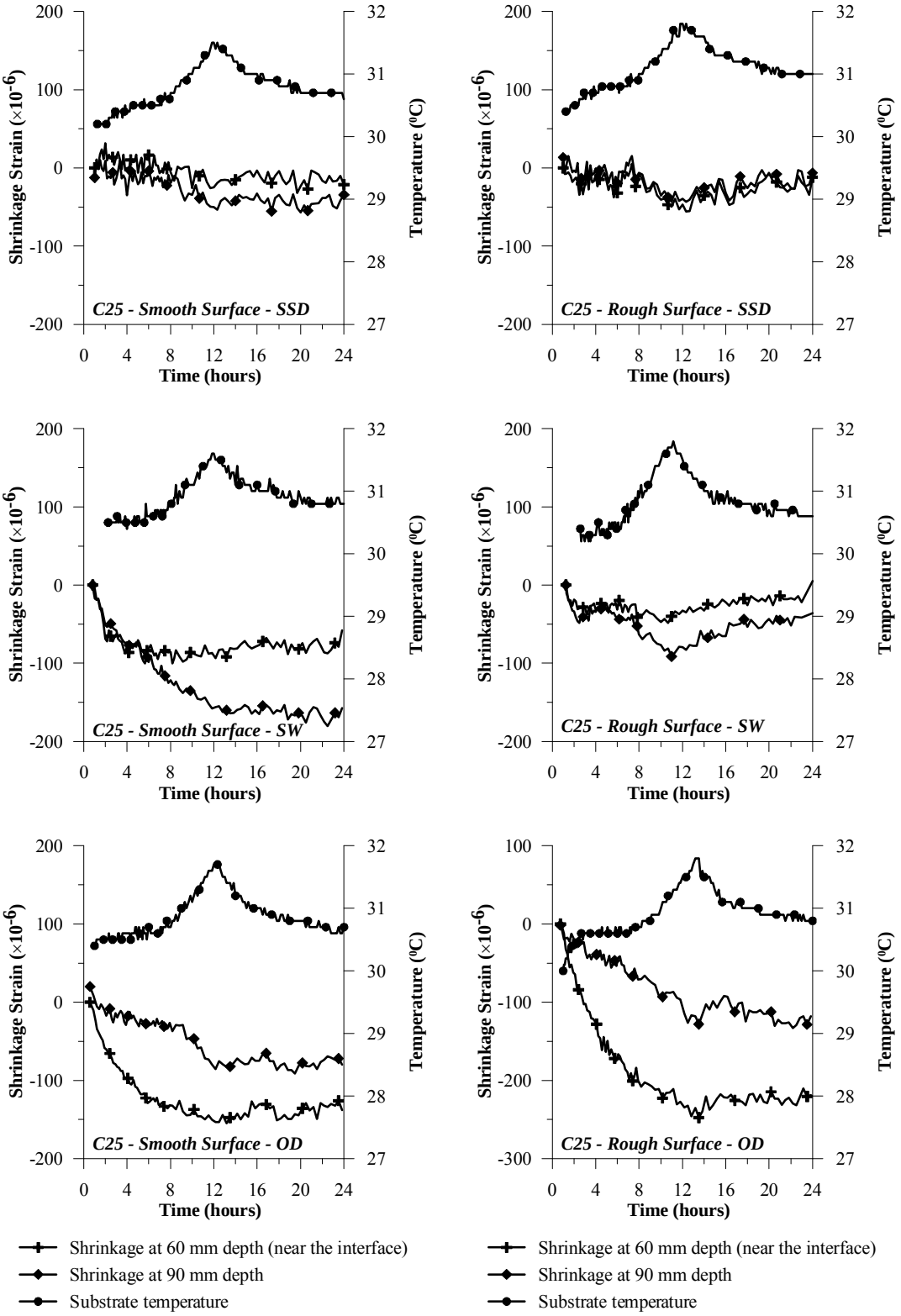

Figure 5.6 Substrate deformations monitored at a depth of 60 mm and 90 mm from the top surface of composite specimens with different moisture conditions, for both smooth and rough surfaces (new concrete layer w/c ratio 0.25; sealed top surface).

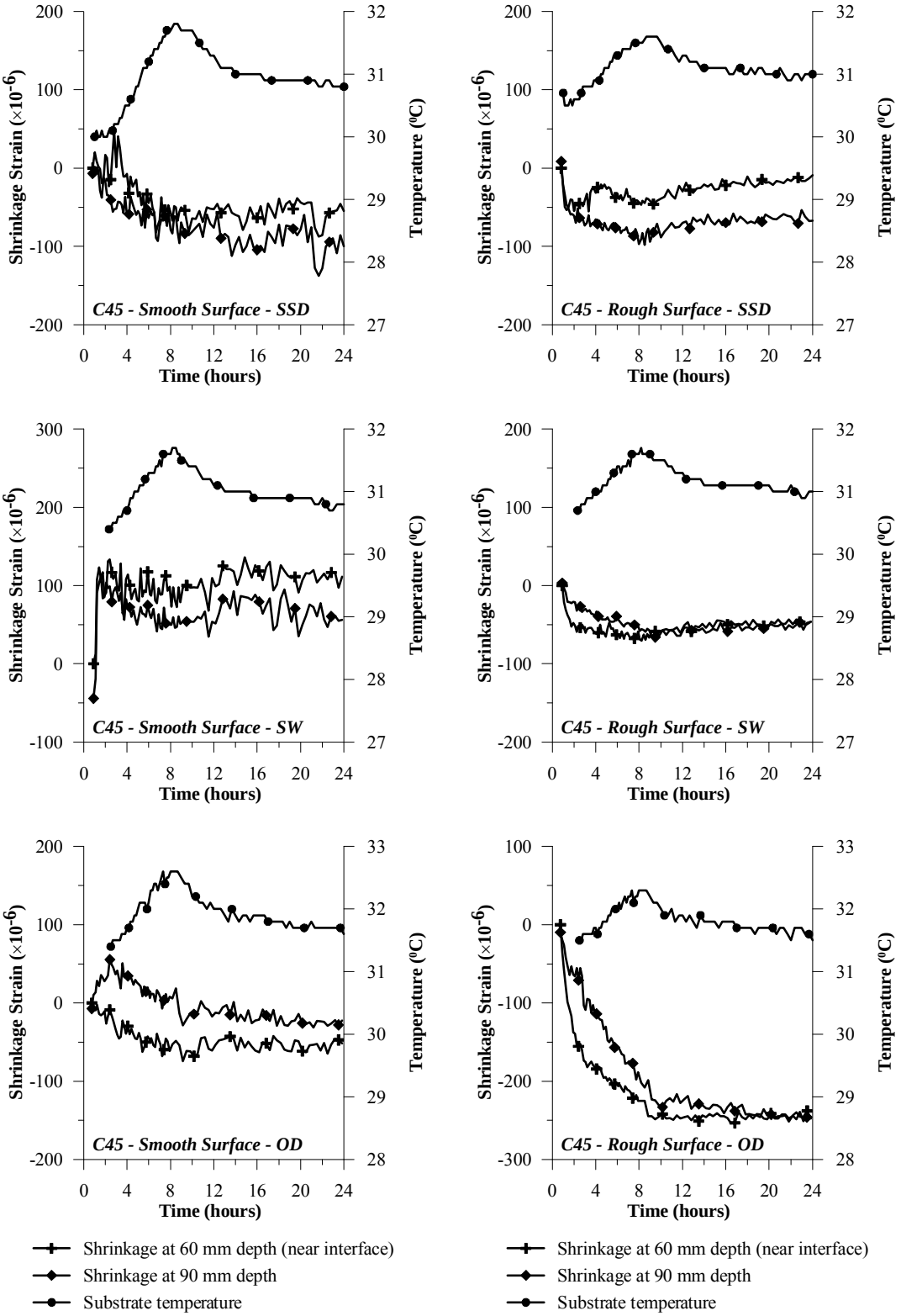

Figure 5.7 Substrate deformations monitored at a depth of 60 mm and 90 mm from the top surface of composite specimens with different moisture conditions, for both smooth and rough surfaces (new concrete layer w/c ratio 0.45; sealed top surface)

5.3.2 Temperature development of the new concrete layer

The temperature development of the C25 and C45 concrete specimens, both for monolithic and composite specimens with either sealed or unsealed top surface during the first 24 hours after adding water to the mixture, are shown in *Figure 5.8* and *Figure 5.9* respectively. The temperature reading is taken at the mid-height of the specimen thickness (i.e. 25 mm from the top surface of the new concrete layer). The results showed that there was no significant difference in the temperature development between the 50 mm thick monolithic specimens and the composite specimens with different substrate moisture conditions.

The effect of sealing the top surface to the temperature rise of the new concrete layer was also noticeable in both C25 and C45 concrete specimens. In the case of the unsealed concrete specimens, the temperature of the new concrete mixture decreased during the first few hours before it started to increase with time. Moreover, it can be seen that the peak temperature registered by the unsealed concrete specimens was also about 1^0C or 2^0C lower compared to that monitored for the companion sealed concrete specimens.

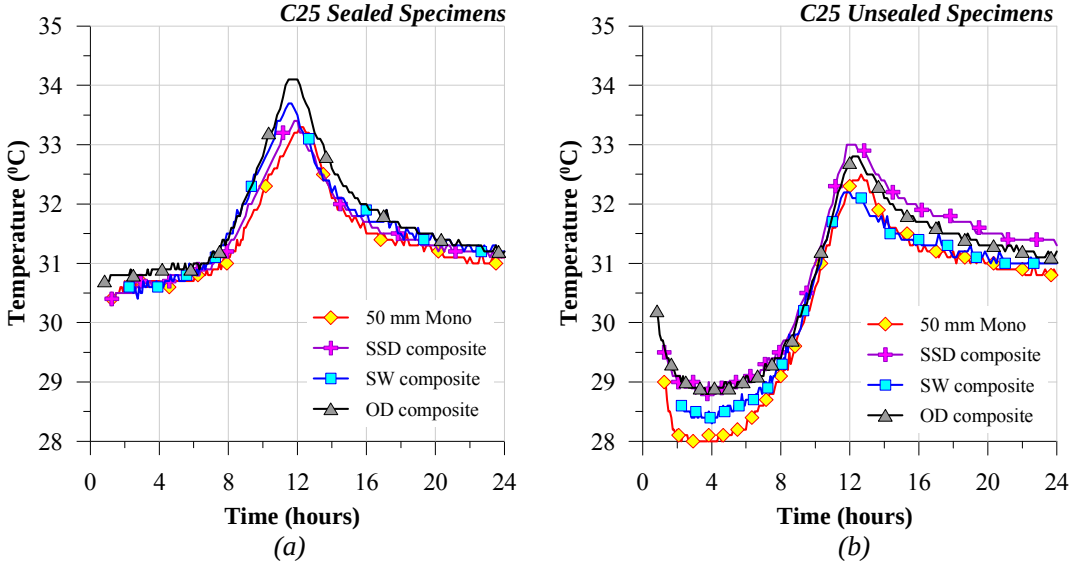

Figure 5.8 Temperature development of C25 new concrete layer with (a) sealed, and (b) unsealed top surface during the first 24 hours after adding water to the mixture.

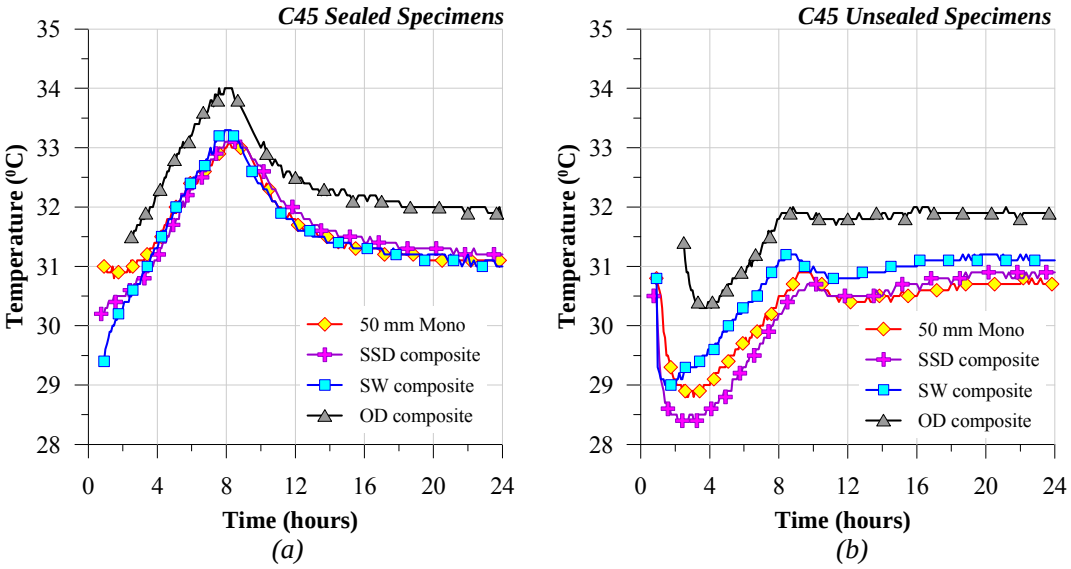

Figure 5.9 Temperature development of C45 new concrete layer with (a) sealed, and (b) unsealed top surface during the first 24 hours after adding water to the mixture.

5.3.3 Composite specimens with sealed top surface

5.3.3.1 Effect of substrate surface roughness

In order to investigate the influence of substrate surface roughness on early age shrinkage of the new concrete layer, a comparison was made between the monolithic specimen and the SSD composite specimens. In addition, another comparison was also made between the shrinkage strains monitored on the new concrete layer cast on smooth and rough substrates.

Table 5.2 and *Table 5.3* shows the "absolute" shrinkage strains values monitored at 24 hours after adding water to the mixture on the sealed monolithic and composite specimens for C25 and C45 new concrete layer respectively. The shrinkage strain was "zeroed" at the stiffening time. Comparing the "absolute" shrinkage strain values monitored on the 50 mm thick monolithic specimens with that monitored on the new concrete layer cast on SSD substrate with smooth surface, both the C25 and C45 new concrete layer showed a similar trend; lower "absolute" shrinkage strains values or expansion were monitored on the composite specimens. It seems that with the friction provided by the substrates along with minimal water migration towards the saturated substrates, the shrinkage of the new concrete layer would not exceed the shrinkage strains of the corresponding monolithic specimens.

A comparison between the shrinkage strains monitored on the new concrete layer cast on smooth and rough substrates showed that there was no significant difference in the "absolute" shrinkage strain values monitored for the new concrete layer cast on SSD substrate with smooth and rough surfaces. On the other hand, the new concrete layer cast on either SW or OD substrates clearly showed a reduction in the shrinkage strains with rougher substrates. Moreover, based on the results obtained, it seems that the restraining effect of substrate may not only influence the early age shrinkage strain of the new concrete layer near the interface but this influence extends also up to the top surface of the new concrete layer. It can be seen that in the case of the C25 new concrete layer cast on OD substrate, the 'absolute" shrinkage strains values monitored near the interface (i.e. at a depth of 40 mm from the top surface of composite specimens) decreased from 100 με to 20 με. Near the top surface of the composite specimens (i.e. at a depth of 3 mm from the top surface), a reduction was also observed. The "absolute" shrinkage strains value decreased from 350 με to 240 με.

Table 5.2 Effect of substrate surface roughness on "absolute" shrinkage strains values at 24 hours after adding water to the mixture (new concrete layer cast with w/c of 0.25 and sealed top surface)

Depth from the top surface (mm)	Shrinkage strains values (με)						
	Monolithic (50 mm)	SSD Substrate		SW Substrate		OD Substrate	
		Smooth	Rough	Smooth	Rough	Smooth	Rough
3	110	40	20	370	230	350	240
20	100	20	20	260	170	260	140
40	100	10	20	130	110	100	20

Table 5.3 Effect of substrate surface roughness on "absolute" shrinkage strains values at 24 hours after adding water to the mixture (new concrete layer cast with w/c of 0.45 and sealed top surface)

Depth from the top surface (mm)	Shrinkage strains values (με)						
	Monolithic (50 mm)	SSD Substrate		SW Substrate		OD Substrate	
		Smooth	Rough	Smooth	Rough	Smooth	Rough
3	0	-70	-30	220	240	210	100
20	-10	-40	-10	250	150	180	50
40	0	-40	-30	130	80	40	-20

In order to investigate the effect of substrate roughness on the early age shrinkage of the new concrete layer more clearly, the shrinkage-versus-time curves of the monolithic and composite specimens were plotted and divided into three stages as discussed previously in Chapter 4 (i.e. plastic, transitional, and hardening stages). As shown in *Figure 5.10* and *Figure 5.11*, in the case of sealed monolithic and sealed composite specimens with SSD substrate, the results showed that the effect of substrate roughness was not significant. It can be seen that during the plastic, transition, and hardening stages, comparable shrinkage strains were monitored for the monolithic and composite specimens with either smooth or rough surfaces. The results implied that the new concrete layer cast on SSD substrate shrank as much as the companion 50 mm thick monolithic specimens.

In the case of composite specimens cast with SW and OD substrates, the effect of substrate roughness on the early age shrinkage strain of the new concrete layer was much clearer. As shown in *Figure 5.12* to *Figure 5.15*, significantly lower shrinkage strains were clearly observed at all depths in composite specimens cast with a rough substrate. From closer inspection, the effect of substrate roughness was more significant during the plastic and transitional stages. It can be seen that a more gradual increase in shrinkage strains was observed on composite specimens cast with a rough substrate during these stages. At the hardening stage, the effect of substrate roughness was less apparent. It can be seen that comparable shrinkage strains were monitored for composite specimens cast with either smooth or rough substrates.

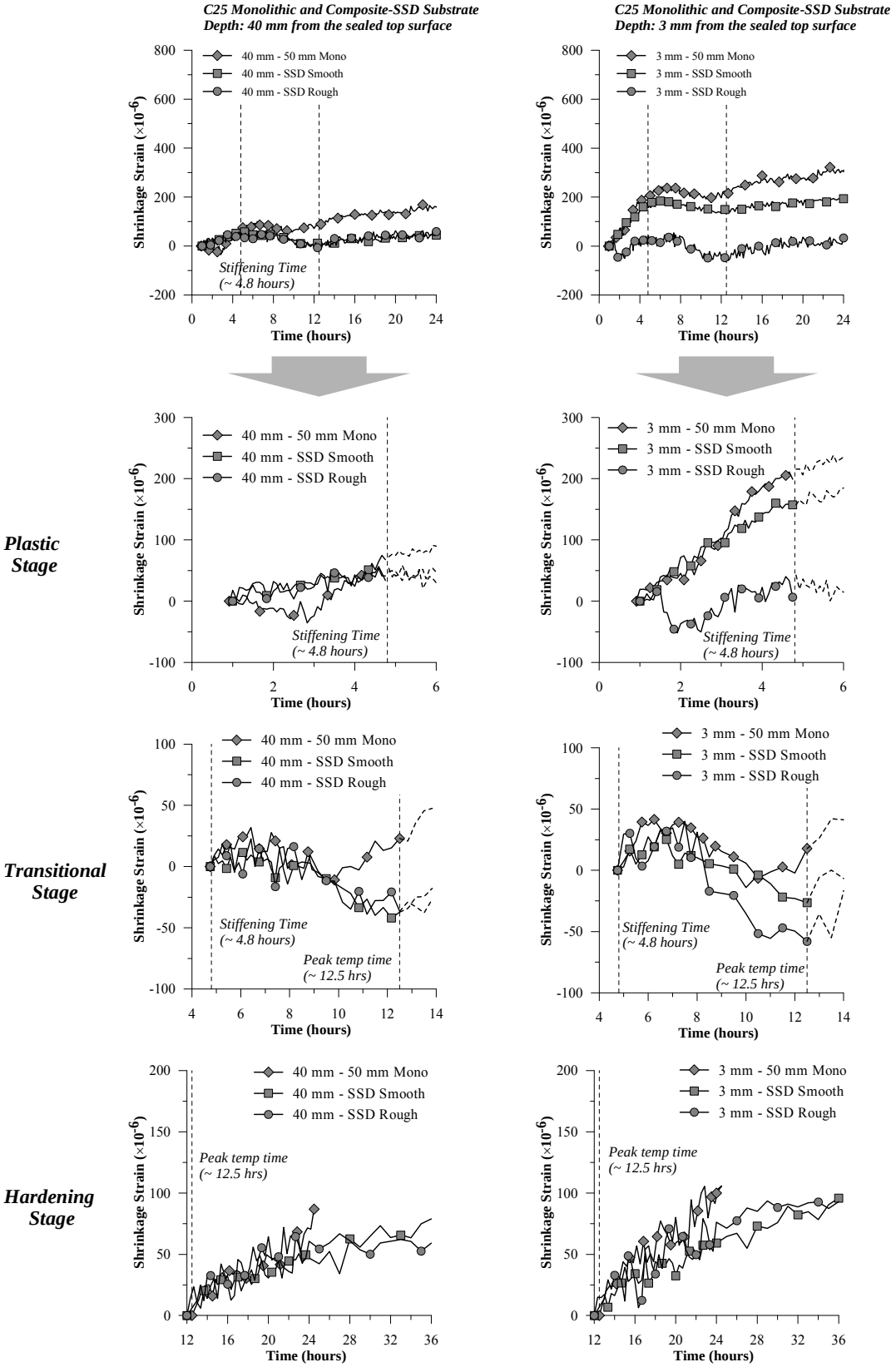

Figure 5.10 Early age shrinkage strains monitored at a depth of 40 mm and 3 mm from the top surface of the sealed monolithic and sealed composite specimens with SSD substrate during plastic, transitional, and hardening stages (new concrete layer w/c = 0.25).

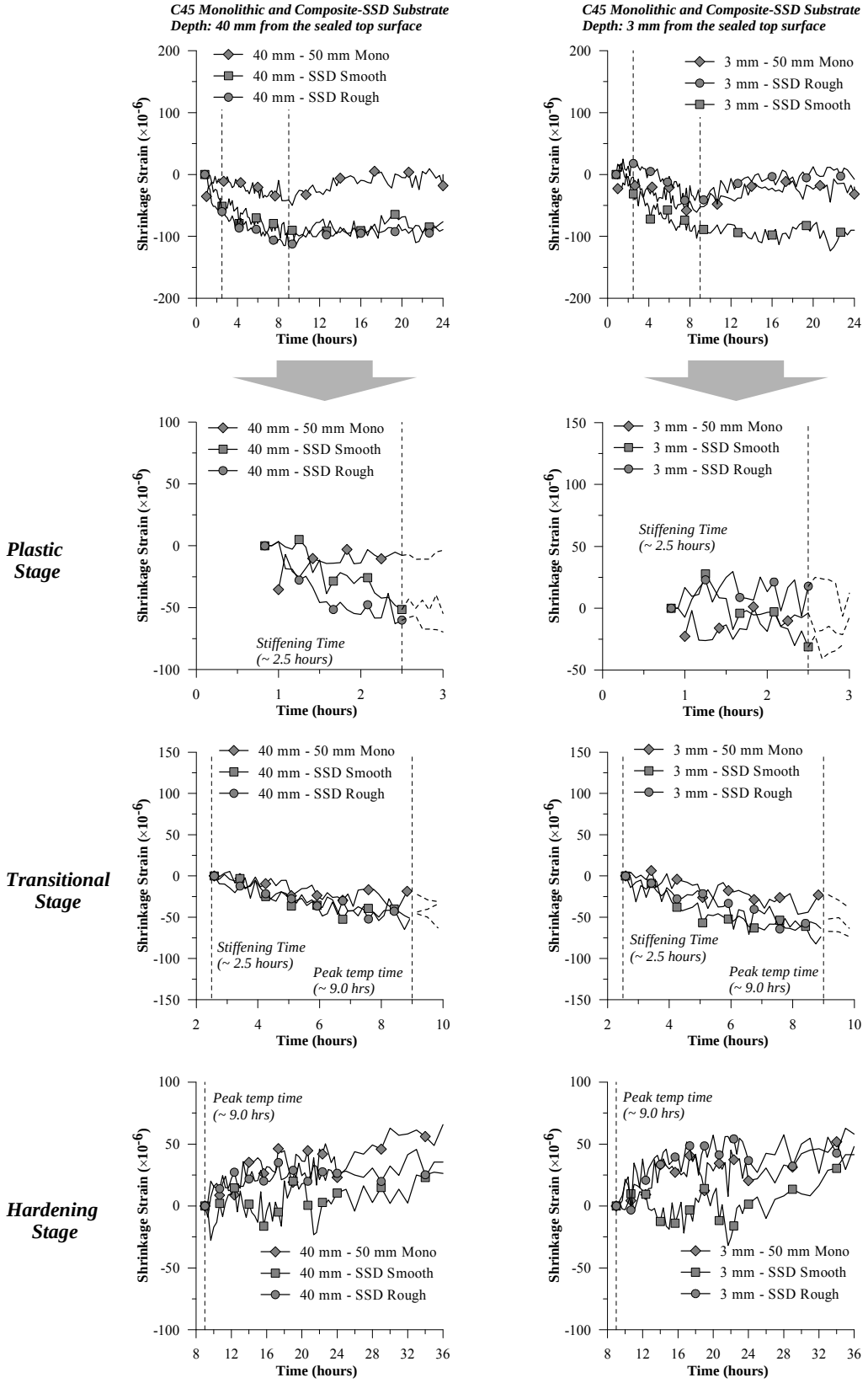

Figure 5.11 Early age shrinkage strains monitored at a depth of 40 mm and 3 mm from the top surface of the sealed monolithic and sealed composite specimens with SSD substrate during plastic, transitional, and hardening stages (new concrete layer w/c = 0.45).

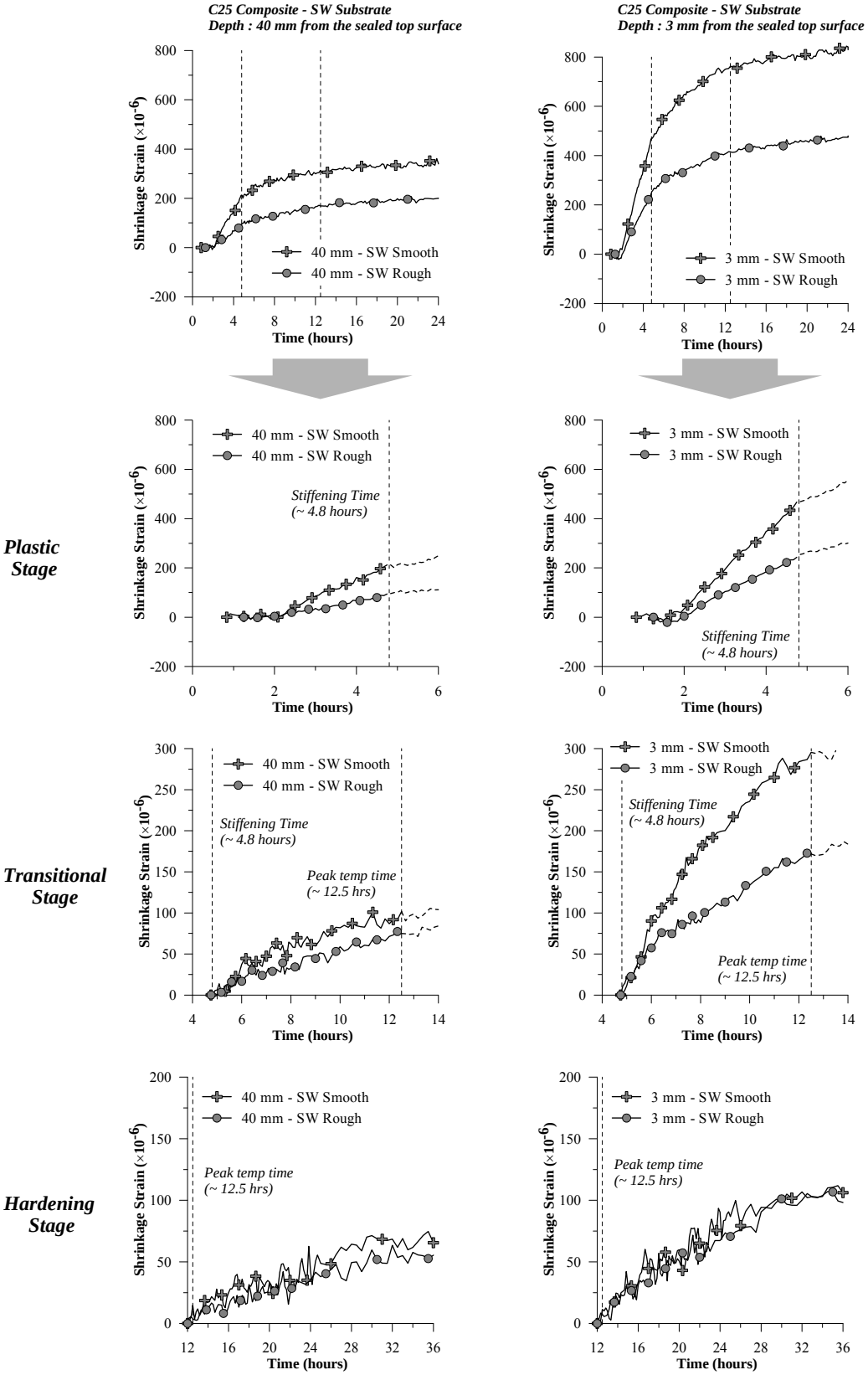

Figure 5.12 Early age shrinkage strains monitored at a depth of 40 mm and 3 mm from the top surface of the sealed composite specimens with SW substrate during plastic, transitional, and hardening stages (new concrete layer w/c = 0.25).

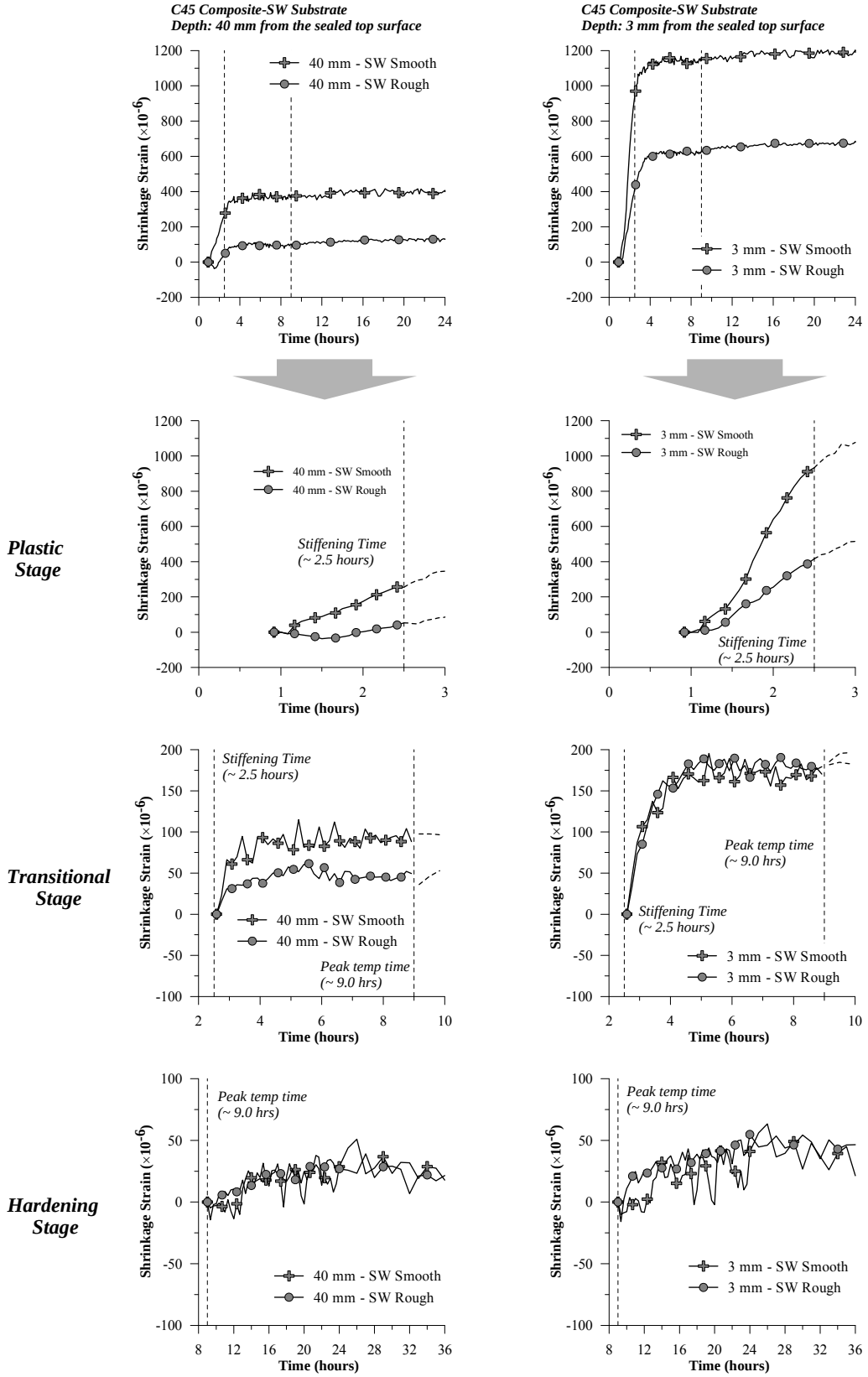

Figure 5.13 Early age shrinkage strains monitored at a depth of 40 mm and 3 mm from the top surface of the sealed composite specimens with SW substrate during plastic, transitional, and hardening stages (new concrete layer w/c = 0.45).

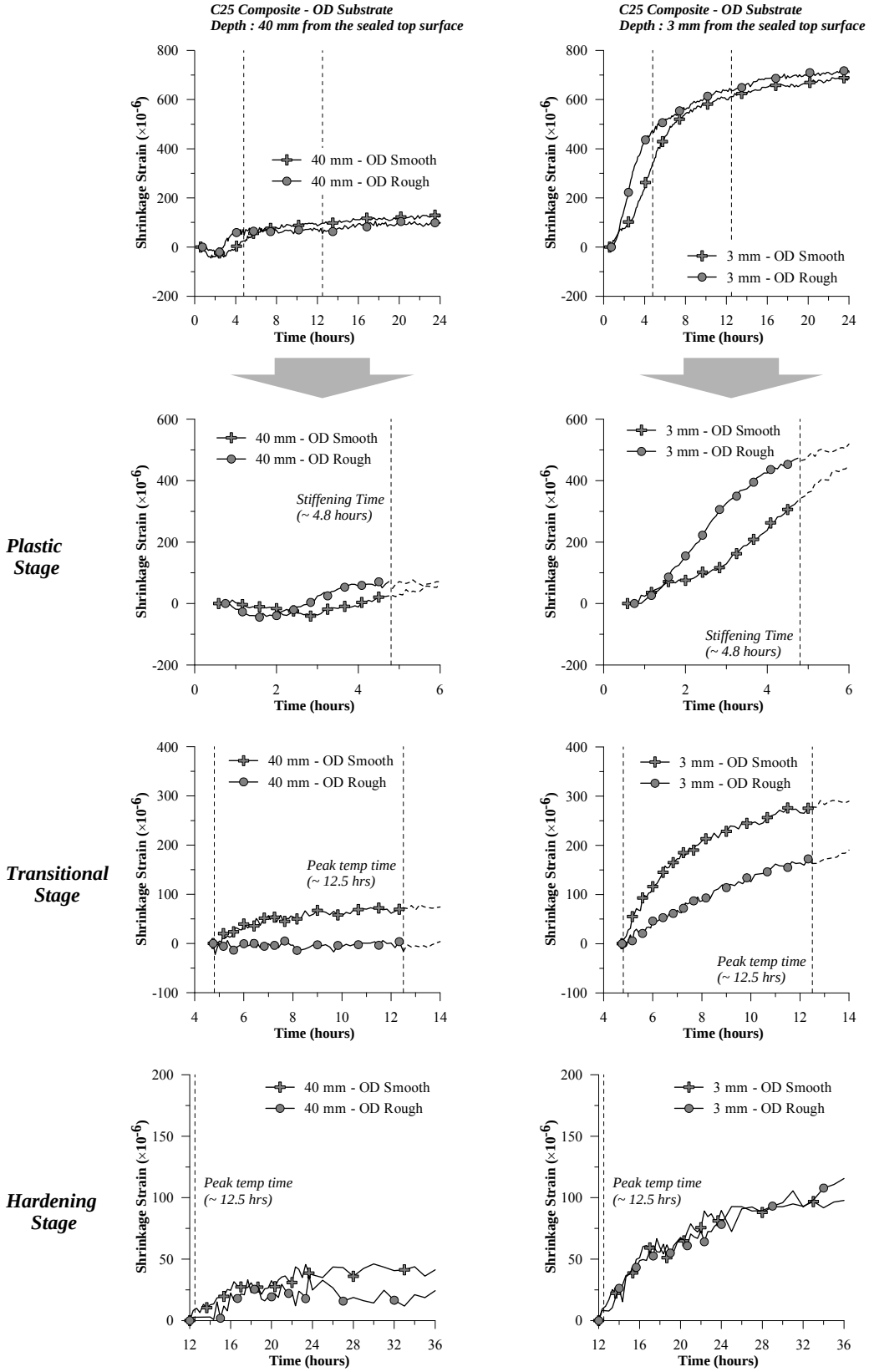

Figure 5.14 Early age shrinkage strains monitored at a depth of 40 mm and 3 mm from the top surface of the sealed composite specimens with OD substrate during plastic, transitional, and hardening stages (new concrete layer w/c = 0.25).

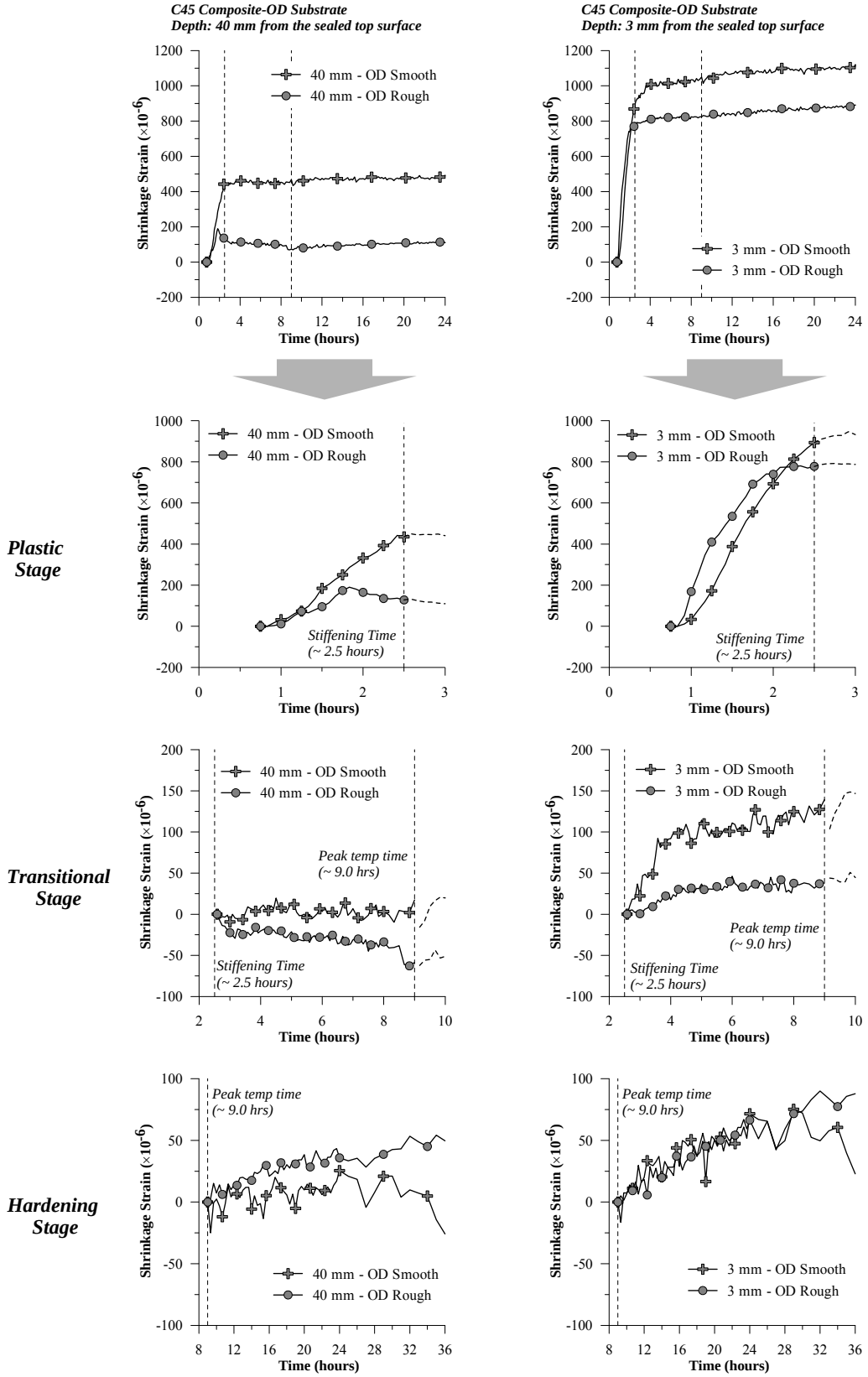

Figure 5.15 Early age shrinkage strains monitored at a depth of 40 mm and 3 mm from the top surface of the sealed composite specimens with OD substrate during plastic, transitional, and hardening stages (new concrete layer w/c = 0.45).

5.3.3.2 Effect of substrate moisture absorption

The influence of substrate moisture absorption was assessed by comparing the shrinkage development of the C25 and C45 new concrete layer cast on substrate with different moisture conditions respectively (i.e. SSD – saturated surface dry, SW – substrate with pre-wetted surface, and OD – oven dry substrate). As shown in *Table 5.4* and *Table 5.5*, the results showed that in the case of the C25 and C45 new concrete layer tested, the effect of substrate moisture absorption on the early age shrinkage of the new concrete layer was significant. It can be seen that the "absolute" shrinkage strains values monitored on the new concrete layer were much higher in the composite specimens with either SW or OD substrate as compared to the corresponding composite specimens with SSD substrate.

Table 5.4 Effect of substrate moisture condition on "absolute" shrinkage strains values at 24 hours after adding water to the mixture (new concrete layer cast with w/c of 0.25 and sealed top surface)

Depth from the top surface (mm)	Shrinkage strains values (με)						
	Monolithic (50 mm)	Smooth Substrate			Rough Substrate		
		SSD	SW	OD	SSD	SW	OD
3	110	40	370	350	20	230	240
20	100	20	260	260	20	170	140
40	100	10	130	100	20	110	20

Table 5.5 Effect of substrate moisture condition on "absolute" shrinkage strains values at 24 hours after adding water to the mixture (new concrete layer cast with w/c of 0.45 and sealed top surface)

Depth from the top surface (mm)	Shrinkage strains values (με)						
	Monolithic (50 mm)	Smooth Substrate			Rough Substrate		
		SSD	SW	OD	SSD	SW	OD
3	0	-70	220	210	-30	240	100
20	-10	-40	250	180	-10	150	50
40	0	-40	130	40	-30	80	-20

In the case of the C25 new concrete layer, the result showed that when the substrate moisture conditions was changed from SSD to SW condition, the "absolute" shrinkage strain values monitored at a depth of 40 mm from the top surface (i.e. near the interface) increased from 10 με to 130 με and from 20 με to 110 με for the smooth and rough substrate respectively.

Similarly, the "absolute" shrinkage strains values monitored at a depth of 3 mm from the top surface (i.e. near the interface) also increased from 40 με to 370 με and from 20 με to 230 με for the smooth and rough substrate respectively. The increase in the early age shrinkage strains was also observed in the case of C45 new concrete layer. It can be seen in the C45 new concrete layer cast on substrate with smooth surface, the results showed that the "absolute" shrinkage strains values monitored at a depth of 3 mm and 40 mm from the top surface increased from -70 με to 220 με and from -40 με to 130 με respectively.

In the case when the substrate moisture conditions was changed from SW to OD conditions, the results showed that comparable "absolute" shrinkage strain values were monitored at a depth of 3 mm from the top surface. However, at a depth of 20 mm from the top surface and also near the interface (i.e. at a depth of 40 mm from the top surface), a reduction in the "absolute" shrinkage strains were monitored. It can be seen that in the case of the C25 new concrete layer, the "absolute" shrinkage strains monitored near the interface decreased from 130 με to 100 με and from 110 με to 20 με for the smooth and rough substrates respectively.

In order to investigate the effect of substrate moisture conditions on the early age shrinkage of the new concrete layer more clearly, the shrinkage-time curves of monolithic and composite specimens were plotted and divided into three stages (i.e. plastic, transitional, and hardening stages). The results for the C25 and C45 new concrete layer are shown in *Figure 5.16* to *Figure 5.19*. The results showed that during the plastic stage, the new concrete layer cast on SSD substrate registered comparable shrinkage strains vis-à-vis that monitored for the 50 mm monolithic specimens. This indicated that in the case of sealed specimens, there seems to be negligible moisture migration to the SSD substrate. It can also be seen that the shrinkage strains of the new concrete layer developed more rapidly when cast against dryer substrates. In the case of the C25 new concrete layer cast on OD substrate, a slight expansion at a depth of 40 mm from the top surface was observed during the plastic stage. It is possible that the expansion registered in the C25 new concrete layer may have been caused by the expansion of the substrate. As shown previously in *Figure 5.6*, the substrate with OD conditions registered a relatively high expansion due to moisture absorption during the plastic stage. This expansion

may exert an expansionary influence on the C25 newly cast concrete layer in contact with this substrate, resulting in a net expansion being registered during the plastic stage.

In the subsequent stage, i.e. transitional stage, the new concrete layer cast on SSD substrate registered slightly lower shrinkage strains as compared to that monitored for the 50 mm thick monolithic specimens. As discussed previously, the lower shrinkage strain values could be caused by the restraining effect of the substrate surface. On top of this, the shrinkage strain monitored for the new concrete layer cast on substrate with SW and OD conditions showed that the new concrete layer which was cast on SW substrate registered a relatively higher shrinkage strains at a depth of 40 mm from the top surface (i.e. near the interface) as compared to that monitored for the new concrete layer cast on the OD substrate. The new concrete layer cast on the OD substrate itself, registered comparable shrinkage strains vis-à-vis the new concrete layer cast on SSD substrate. Similarly, at the depth of 3 mm from the top surface, the results also showed that the new concrete layer which was cast on the SW substrate registered a shrinkage strains which is either higher or comparable to that monitored for the new concrete layer cast on OD substrate. These results indicated that the 1-hour pre-wetting procedure performed on the SW substrate was not enough to eliminate the moisture absorption by the SW substrates. In addition, the results also indicate that the new concrete layer cast on the SW substrate may experience a bond failure at the interface as indicated by the much higher shrinkage strains developed near the interface. This will be elaborated more in the next section which deals with unsealed composite specimens.

In the last stage, i.e. hardening stage, given the accuracy of the present image analysis technique of about ± 12 με, the results showed that the effect of substrate moisture absorption was less apparent. No significant difference in the shrinkage strains of the new concrete layer cast on substrates with the three different substrate moisture conditions was observed.

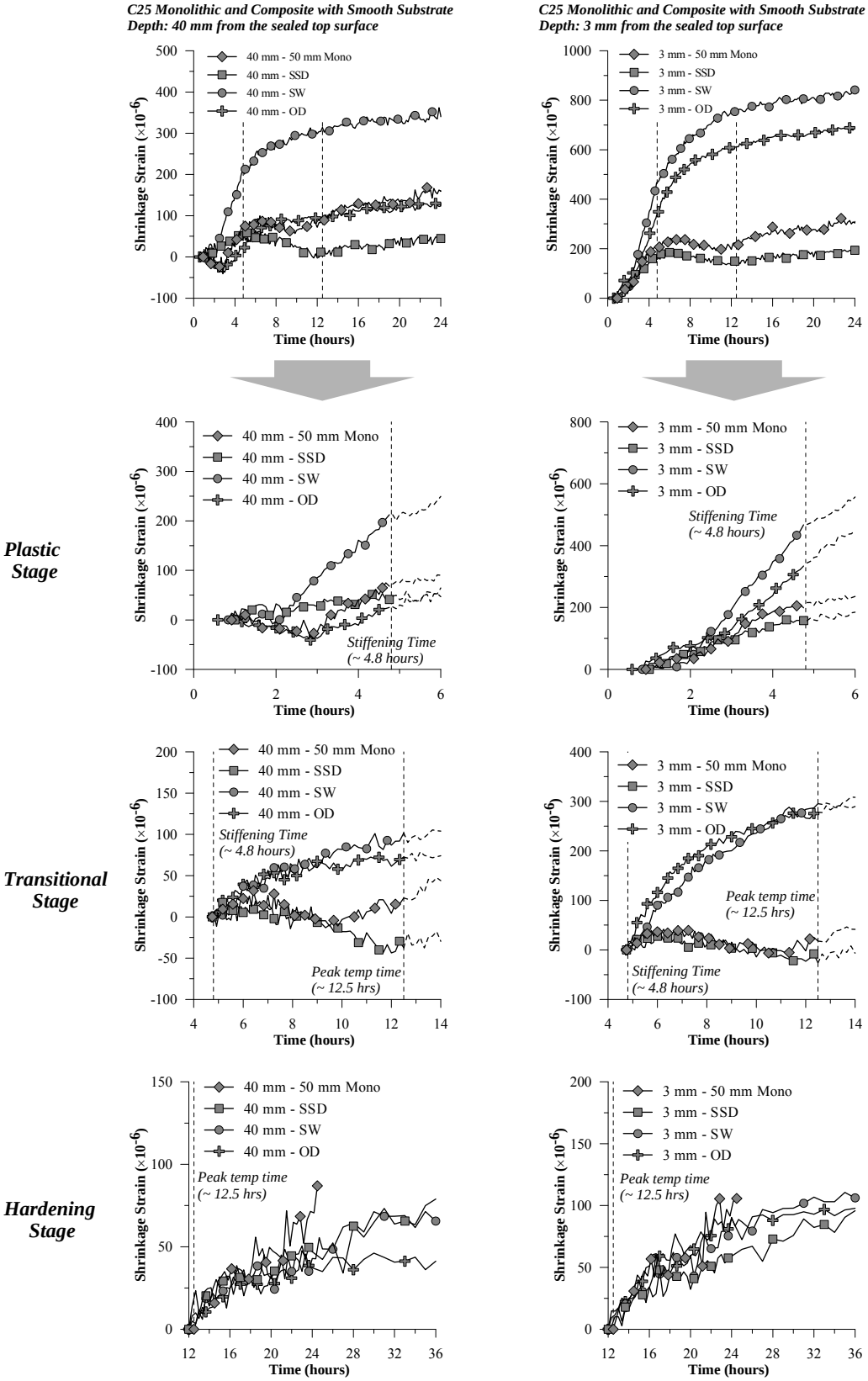

Figure 5.16 Early age shrinkage strains monitored at a depth of 40 mm and 3 mm from the top surface of the sealed monolithic and sealed composite specimens cast on substrate with smooth surface during plastic, transitional, and hardening stages (new concrete layer w/c = 0.25).

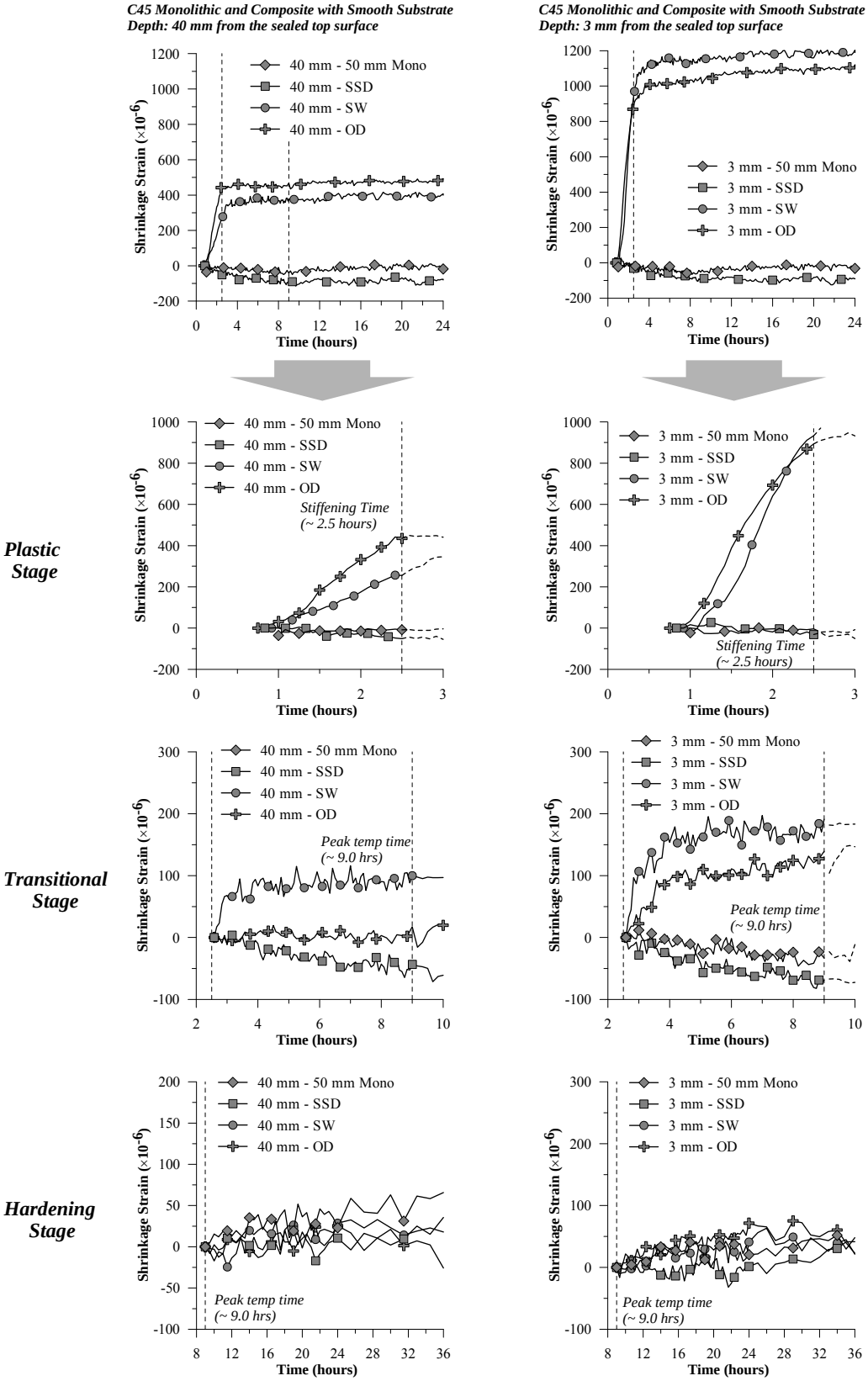

Figure 5.17 Early age shrinkage strains monitored at a depth of 40 mm and 3 mm from the top surface of the sealed monolithic and sealed composite specimens cast on substrate with smooth surface during plastic, transitional, and hardening stages (new concrete layer w/c = 0.45).

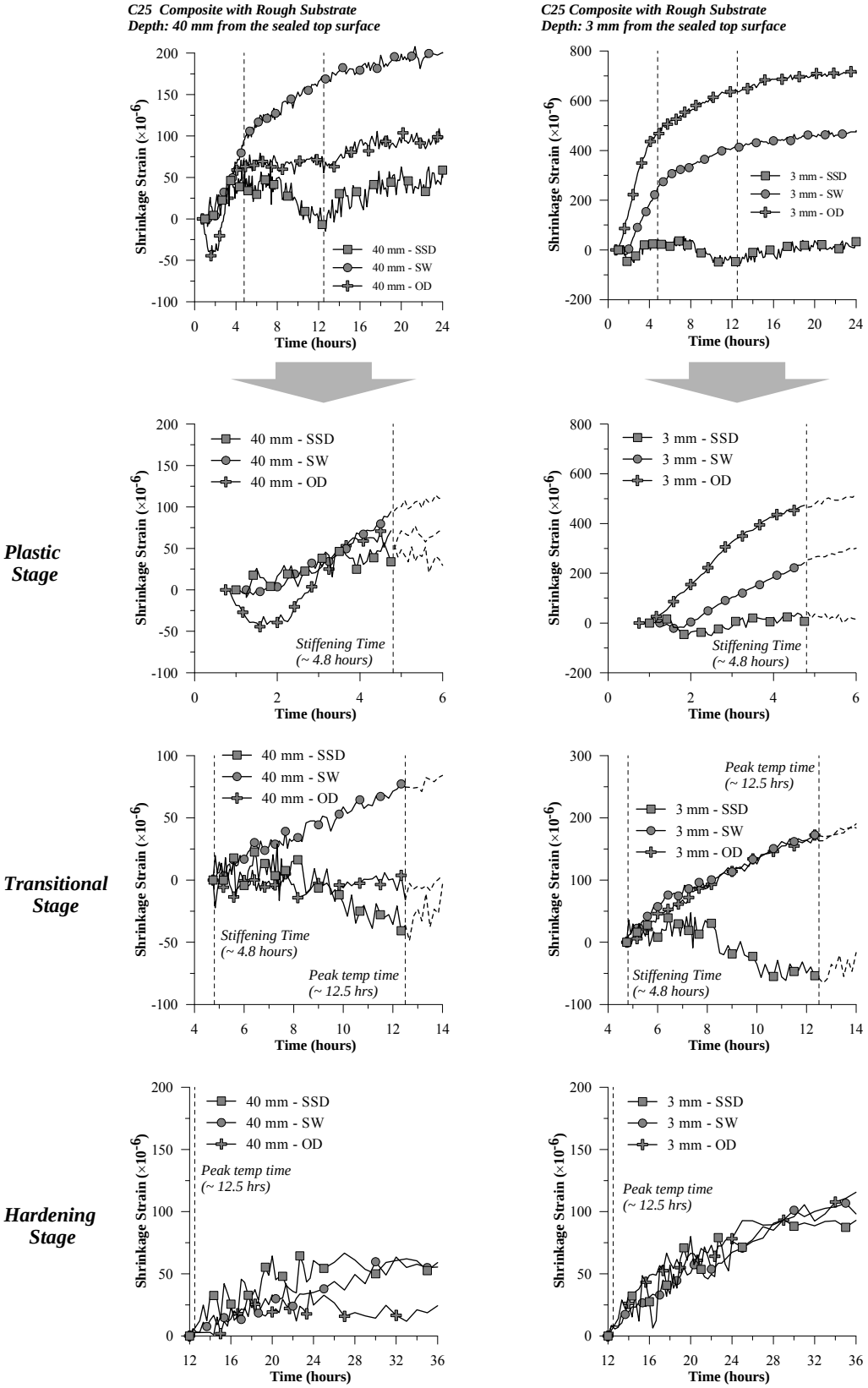

Figure 5.18 Early age shrinkage strains monitored at a depth of 40 mm and 3 mm from the top surface of the sealed monolithic and sealed composite specimens cast on substrate with rough surface during plastic, transitional, and hardening stages (new concrete layer w/c = 0.25).

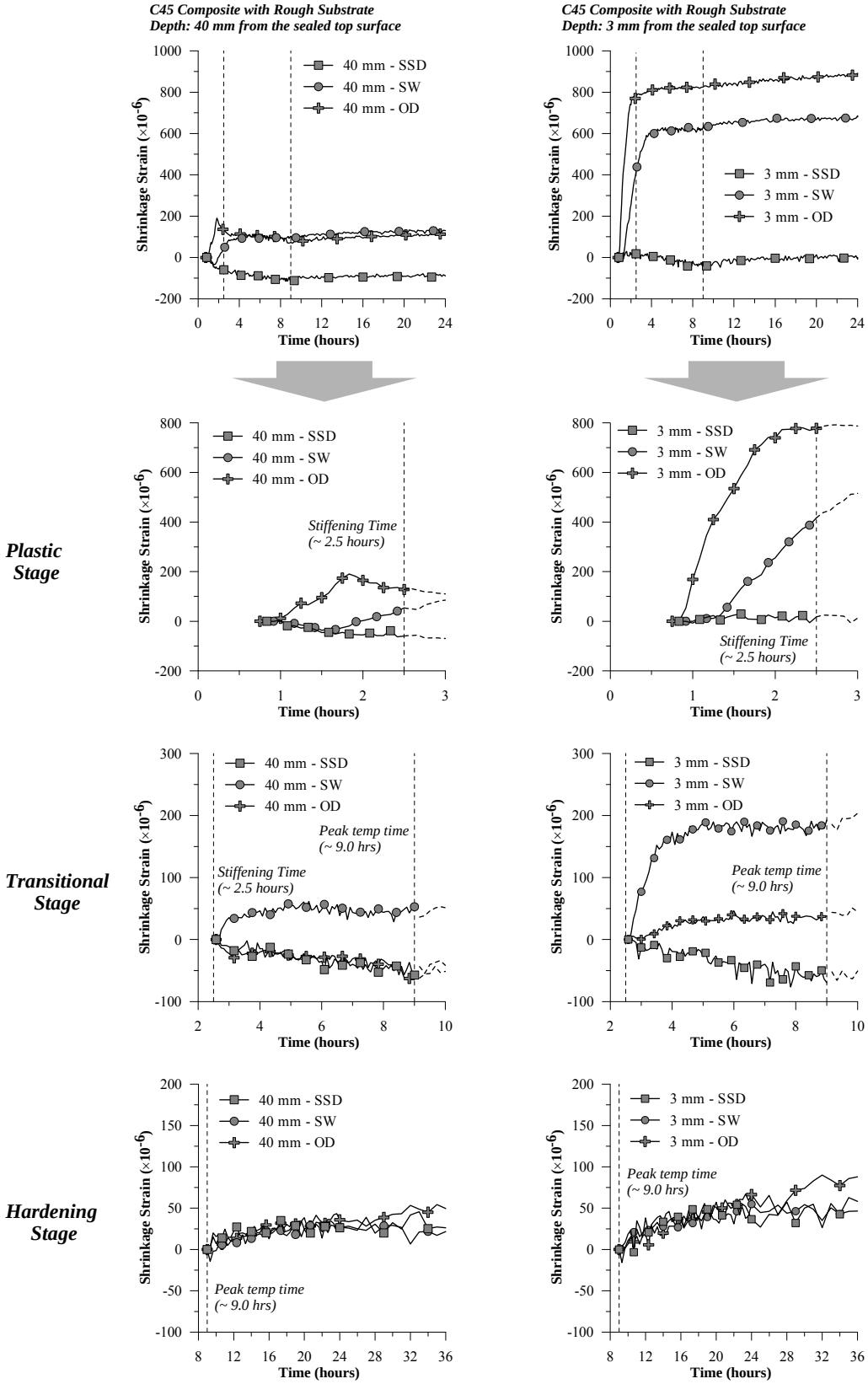

Figure 5.19 Early age shrinkage strains monitored at a depth of 40 mm and 3 mm from the top surface of the sealed monolithic and sealed composite specimens cast on substrate with rough surface during plastic, transitional, and hardening stages (new concrete layer w/c = 0.45).

5.3.4 Composite specimens with exposed top surface

5.3.4.1 Effect of substrate surface roughness

Table 5.6 and *Table 5.7* shows the "absolute" shrinkage strains values monitored at 24 hours after adding water to the mixture on the unsealed monolithic and composite specimens comprising a new C25 and C45 concrete layer cast on top of a smooth and rough substrates respectively. The shrinkage strain was "zeroed" at the stiffening time. Comparing the "absolute" shrinkage strain values monitored on the 50 mm thick monolithic specimens with that monitored on the new concrete layer cast on the SSD substrate with smooth surface, both the C25 and C45 new concrete layer showed that a significant reduction in the "absolute" shrinkage strains values was monitored on the composite specimens. As expected, the reduction was more significant near the interface as the new concrete layer was restrained through bonding with the substrate. These results implied that even with a smooth surface, restraint afforded by the substrate surface seems to be sufficient to reduce the early age "absolute" shrinkage strains of the new concrete layer.

In the case of the new concrete layer cast on substrate with either smooth or rough surfaces, the shrinkage monitoring showed that the restraining effect of substrate roughness was more apparent near the top surface of the composite specimen. While near the interface (i.e. at a depth of 40 mm from the top surface), the results showed that the new concrete layer registered a comparable "absolute" shrinkage strain values regardless of the substrate roughness.

Table 5.6 Effect of substrate surface roughness on "absolute" shrinkage strains values at 24 hours after adding water to the mixture (new concrete layer cast with w/c of 0.25 and unsealed top surface)

Depth from the top surface (mm)	Shrinkage strains values (με)						
	Monolithic (50 mm)	SSD Substrate		SW Substrate		OD Substrate	
		Smooth	Rough	Smooth	Rough	Smooth	Rough
3	600	420	300	350	300	250	180
20	630	290	260	250	250	180	100
40	690	120	120	140	140	60	30

Table 5.7 Effect of substrate surface roughness on "absolute" shrinkage strains values at 24 hours after adding water to the mixture (new concrete layer cast with w/c of 0.45 and unsealed top surface)

Depth from the top surface (mm)	Shrinkage strains values (με)						
	Monolithic (50 mm)	SSD Substrate		SW Substrate		OD Substrate	
		Smooth	Rough	Smooth	Rough	Smooth	Rough
3	1220	270	250	330	180	210	140
20	1230	240	190	190	110	180	80
40	1170	120	110	110	150	-30	30

Figure 5.20 to *Figure 5.25* show plots of shrinkage strains-versus-time curves during plastic, transitional, and hardening stages of the unsealed monolithic specimens and composite specimens cast on substrate with different surface roughness. A comparison between the 50 mm thick monolithic specimens and composite specimens with SSD substrate, as shown in *Figure 5.20* and *Figure 5.21* for the C25 and C45 new concrete layer respectively, showed that the new concrete layer which cast on SSD substrate with smooth surface registered a significantly lower shrinkage strains at all depths compared to that monitored for the 50 mm thick monolithic specimens reduction especially during the plastic and transitional stages. On the other hand, when the SSD substrate surface was changed from smooth to rough, the results seem to indicate that there was only a slight reduction in the early age shrinkage strains observed near the interface and near the top exposed surface. In the subsequent stage, i.e. the hardening stage, it was found that there was no significant difference in the shrinkage strains monitored for the monolithic specimens and the new concrete layer in the composite specimens. This implied that the new concrete layer shrank as much as the monolithic specimens.

In the case of unsealed composite specimens with SW and OD substrates, the results showed that the early age shrinkage strains monitored at all depths for the C25 new concrete layer were reduced with a rough substrate. Similar to that of the unsealed composite specimens with SSD substrate, the reduction observed for the C25 new concrete layer was more apparent during the plastic and transitional stages. It can also be seen that the reduction was more significant near the top exposed surface. However, in the case of C45 new concrete layer, an

exception was noted. As shown in *Figure 5.23* and *Figure 5.25*, it can be seen that the new concrete layer cast on the rough substrate registered higher shrinkage strains during the plastic and transitional stages as compared to that monitored for the new concrete layer cast on the smooth substrate. Although this was unexpected, this may be due to the higher bond at the interface of the composite specimens with smooth substrate. With a higher bond at the interface between the new concrete layer and the concrete substrate, lower shrinkage strains would be monitored. In the subsequent stage, i.e. hardening stage, the results for both the C25 and C45 new concrete layers showed that the effect of substrate roughness was less apparent. It can be seen that there was no significant difference between the shrinkage strains monitored in the composite specimen with smooth and rough substrates.

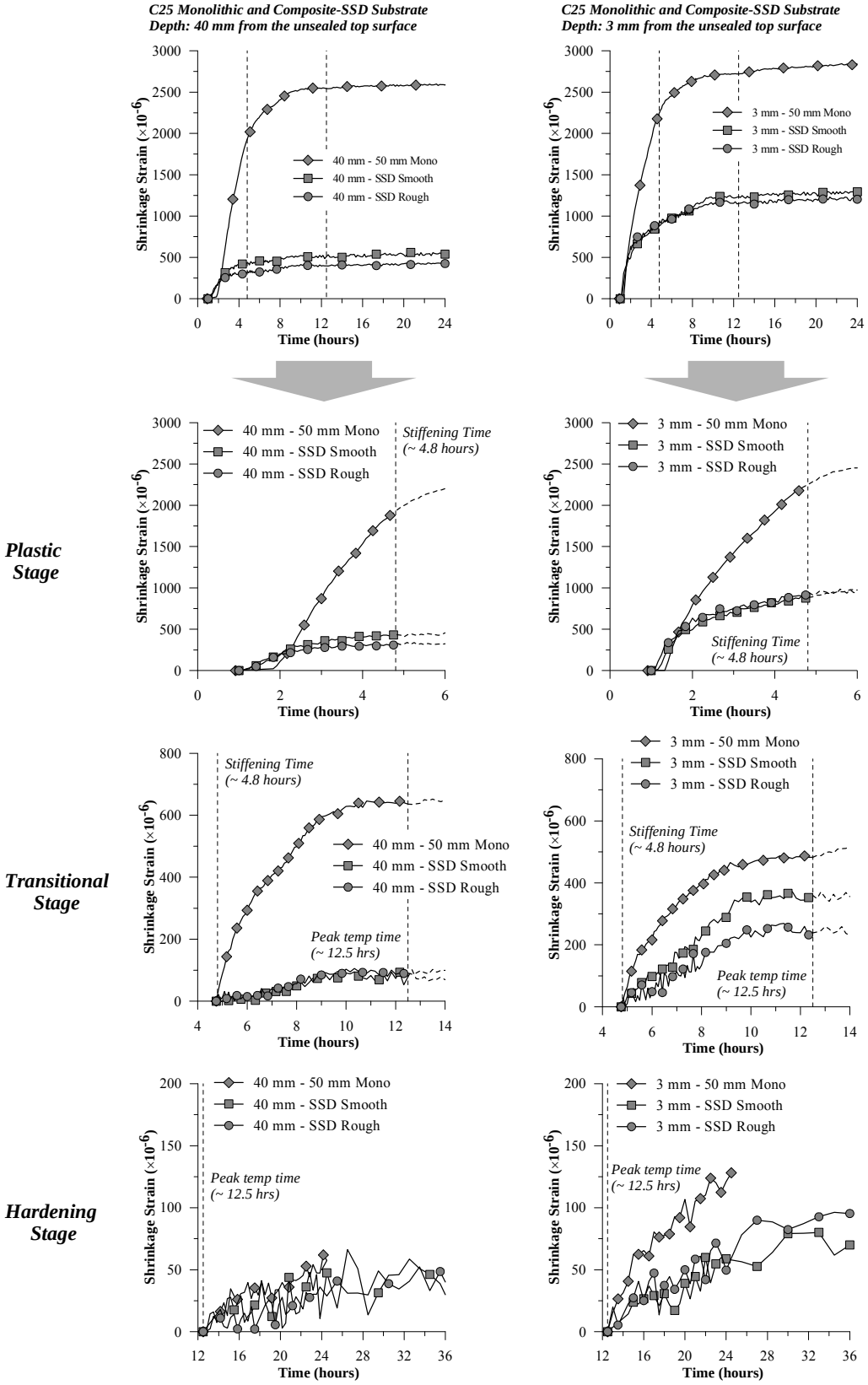

Figure 5.20 Early age shrinkage strains monitored at a depth of 40 mm and 3 mm from the top surface of the unsealed monolithic and unsealed composite specimens with SSD substrate during plastic, transitional, and hardening stages (new concrete layer w/c = 0.25).

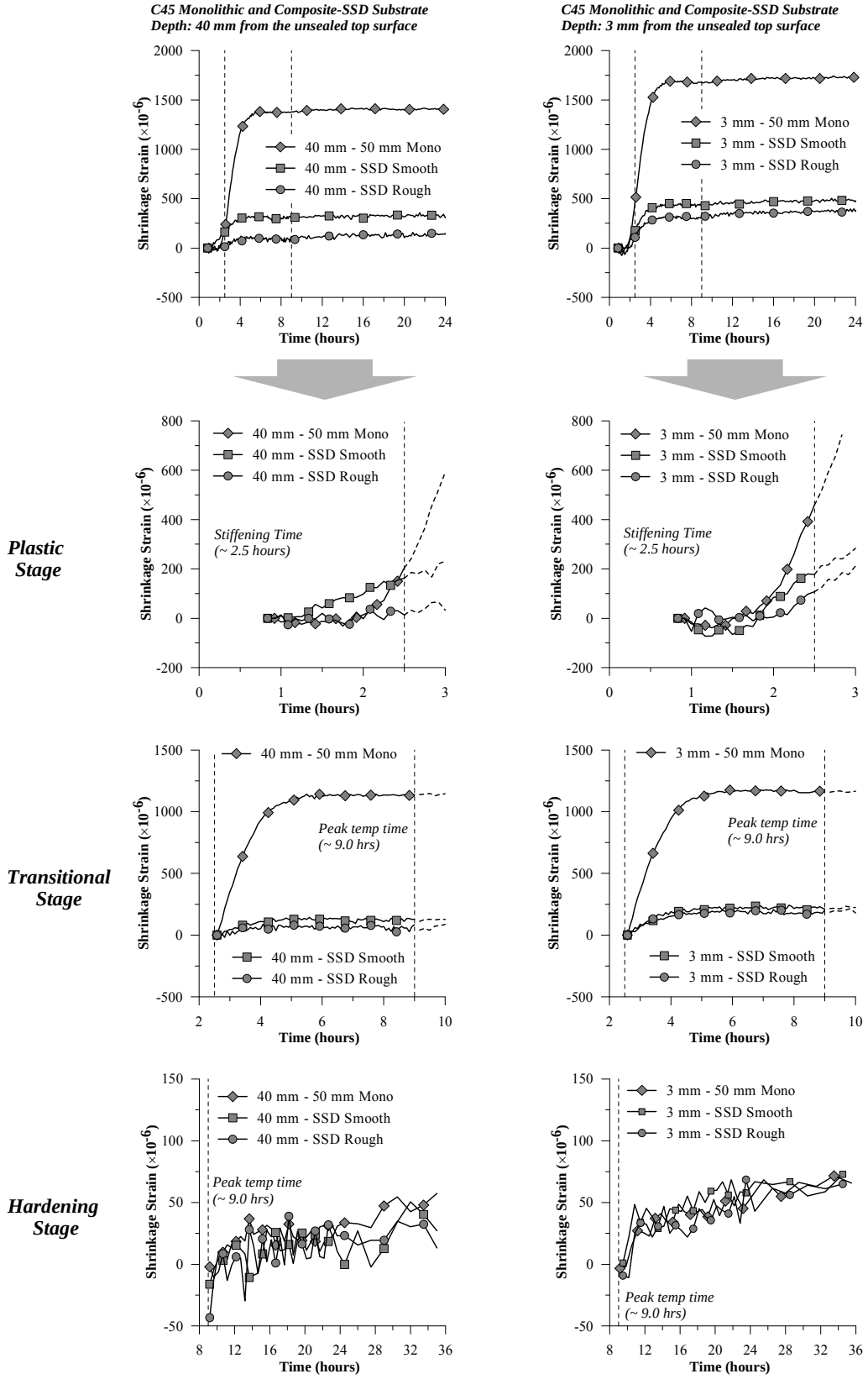

Figure 5.21 Early age shrinkage strains monitored at a depth of 40 mm and 3 mm from the top surface of the unsealed monolithic and unsealed composite specimens with SSD substrate during plastic, transitional, and hardening stages (new concrete layer w/c = 0.45).

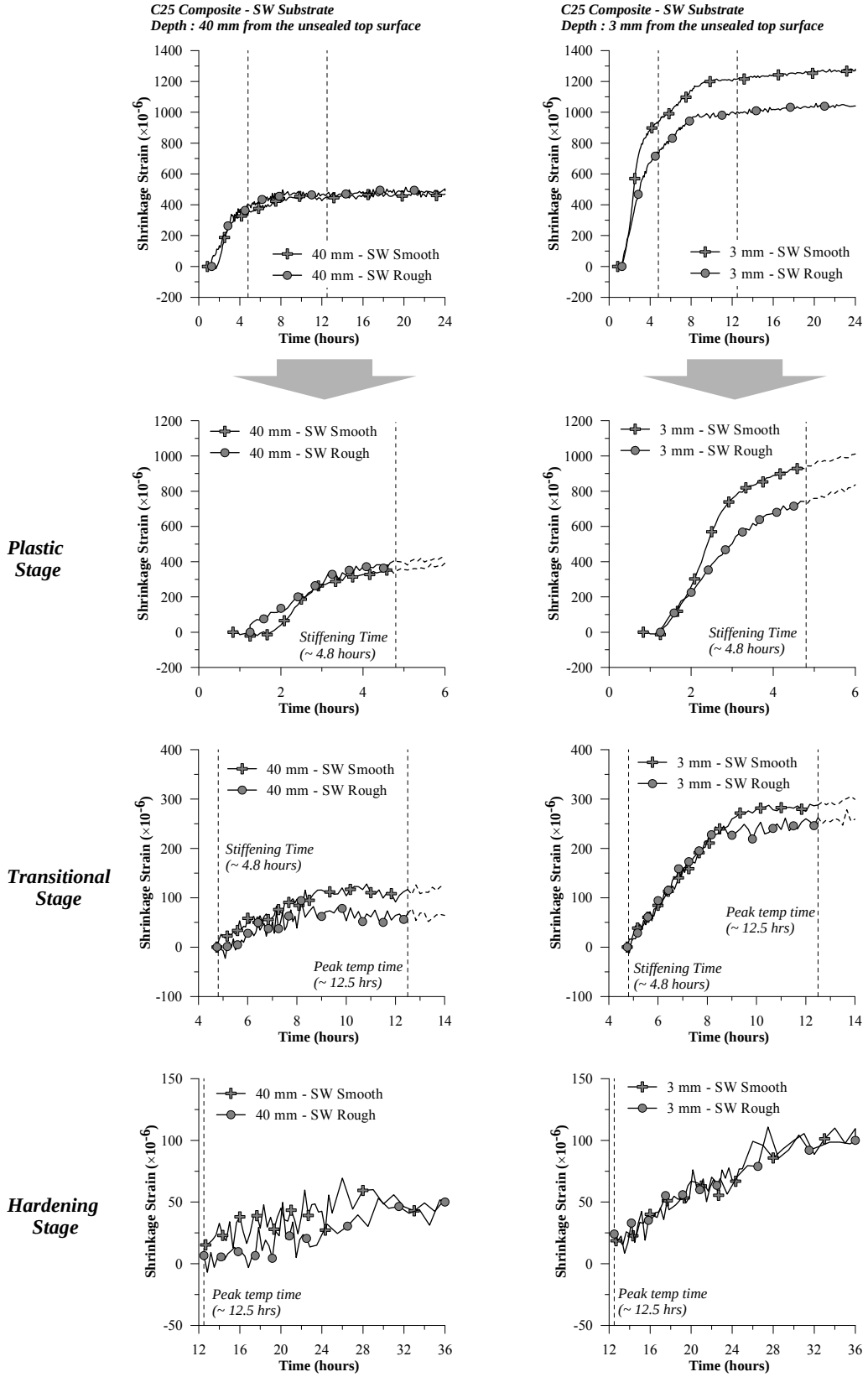

Figure 5.22 Early age shrinkage strains monitored at a depth of 40 mm and 3 mm from the top surface of the unsealed composite specimens with SW substrate during plastic, transitional, and hardening stages (new concrete layer w/c = 0.25).

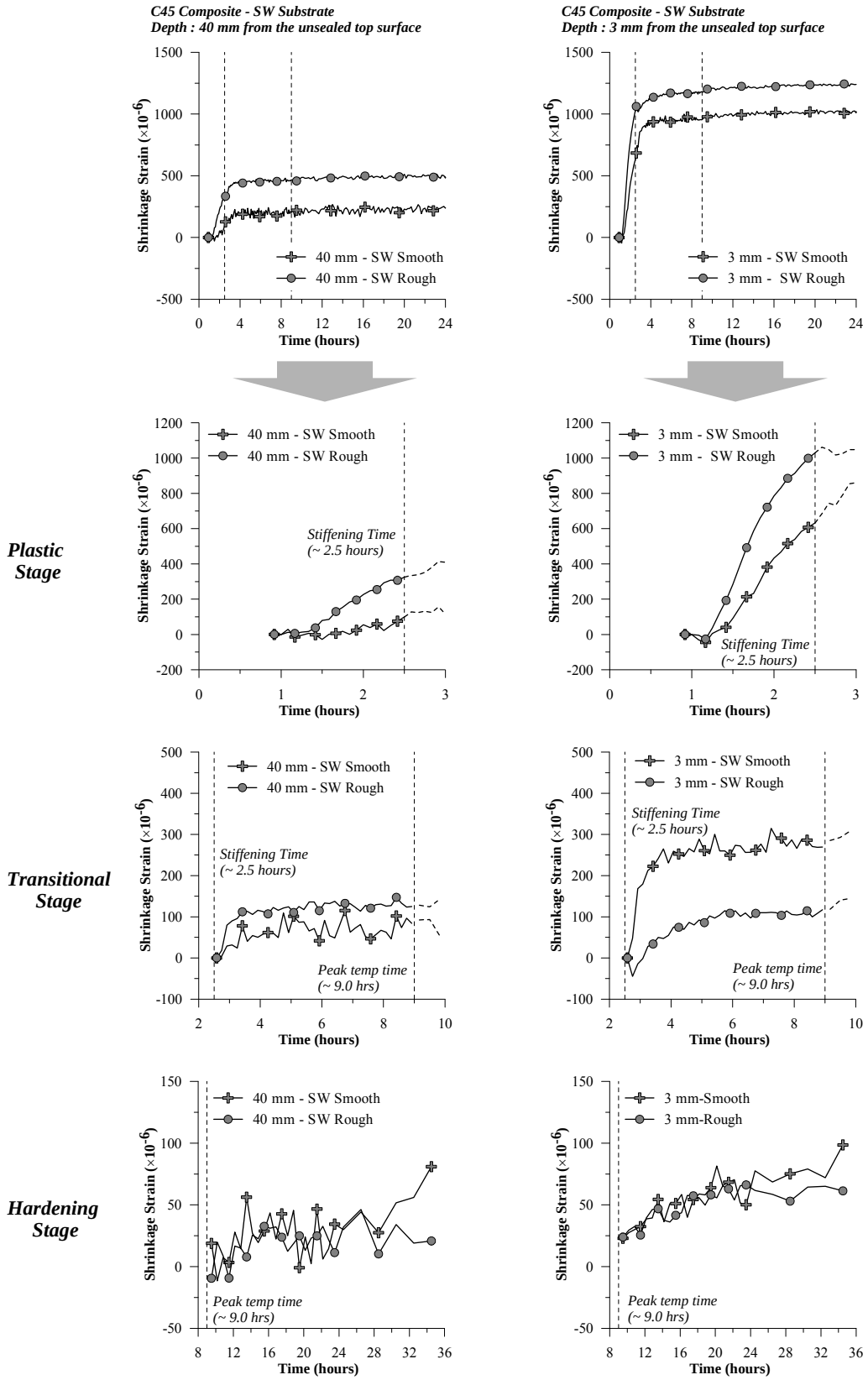

Figure 5.23 Early age shrinkage strains monitored at a depth of 40 mm and 3 mm from the top surface of the unsealed composite specimens with SW substrate during plastic, transitional, and hardening stages (new concrete layer w/c = 0.45).

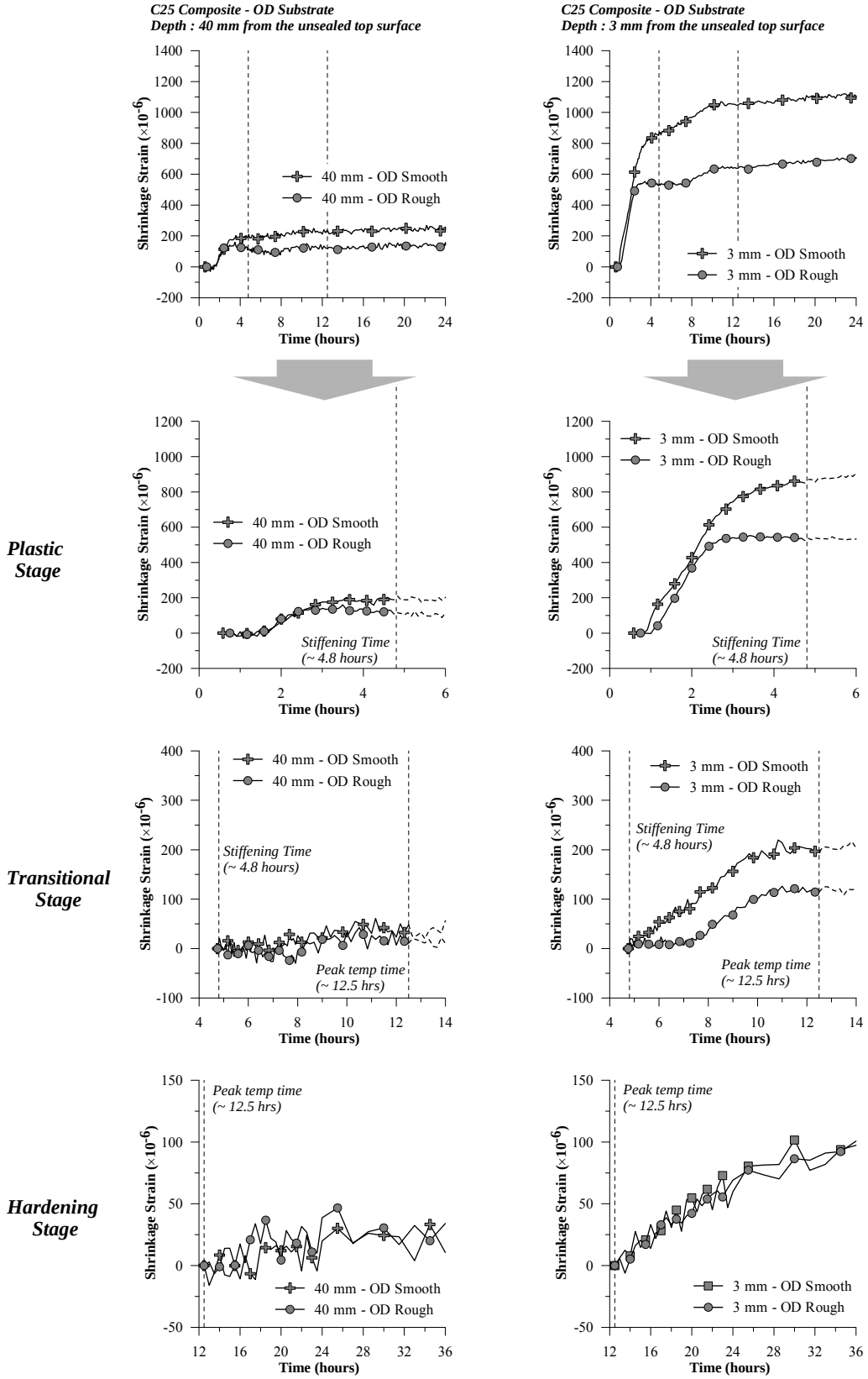

Figure 5.24 Early age shrinkage strains monitored at a depth of 40 mm and 3 mm from the top surface of the unsealed composite specimens with OD substrate during plastic, transitional, and hardening stages (new concrete layer w/c = 0.25).

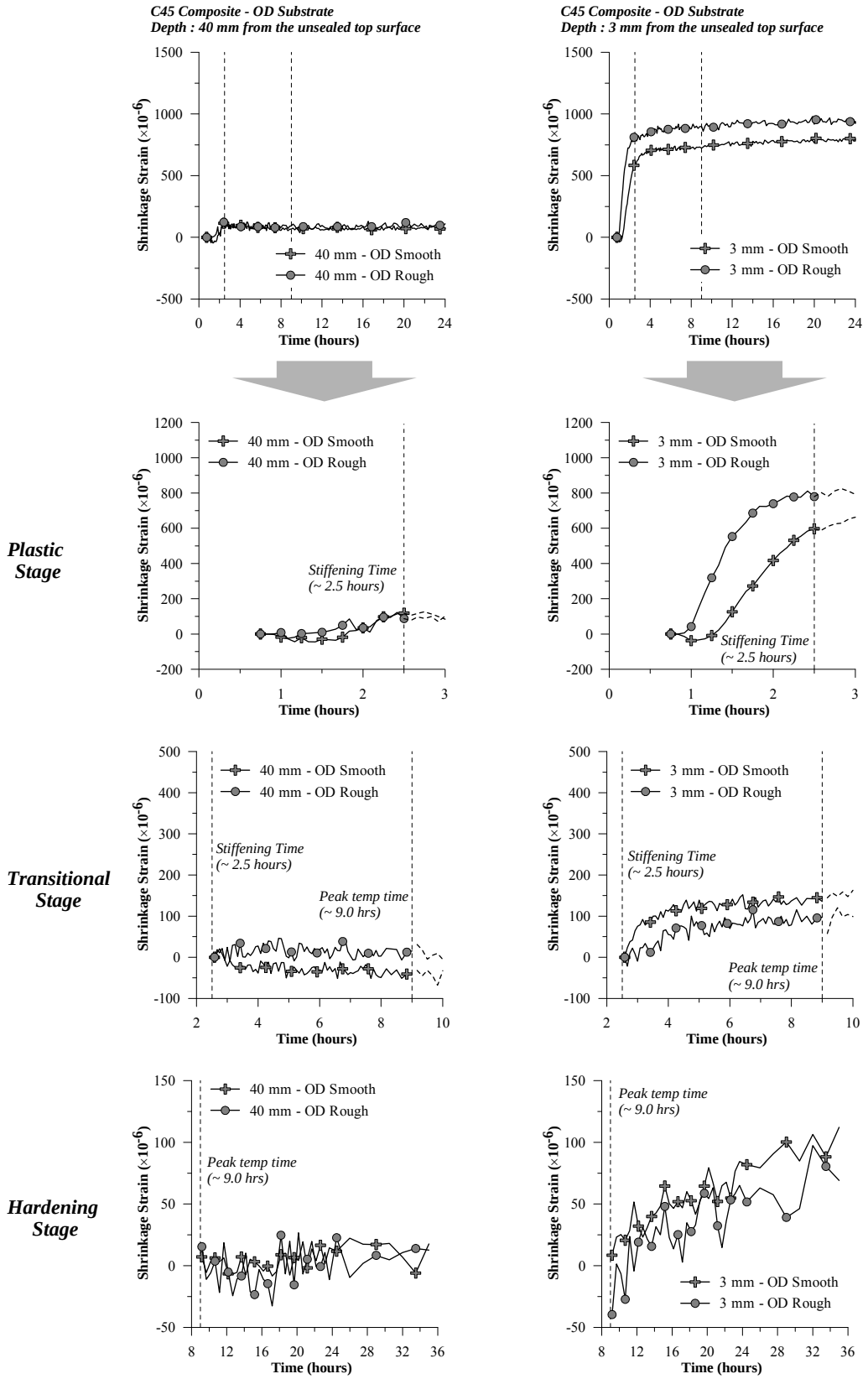

Figure 5.25 Early age shrinkage strains monitored at a depth of 40 mm and 3 mm from the top surface of the unsealed composite specimens with OD substrate during plastic, transitional, and hardening stages (new concrete layer w/c = 0.45).

5.3.4.2 Effect of substrate moisture absorption

In the case of unsealed composite specimens, the influence of substrate moisture absorption on the early age shrinkage strains of the new concrete layer was assessed by comparing the shrinkage development of the C25 and C45 new concrete layer cast on substrate with different moisture conditions respectively. A comparison between the monolithic specimens and the composite specimens with SSD substrate was also made.

Table 5.8 Effect of substrate moisture condition on "absolute" shrinkage strains values at 24 hours after adding water to the mixture (new concrete layer cast with w/c of 0.25 and unsealed top surface)

Depth from the top surface (mm)	Shrinkage strains values (με)						
	Monolithic (50 mm)	Smooth Substrate			Rough Substrate		
		SSD	SW	OD	SSD	SW	OD
3	600	420	350	250	300	300	180
20	630	290	250	180	260	250	100
40	690	120	140	60	120	140	30

Table 5.9 Effect of substrate moisture condition on "absolute" shrinkage strains values at 24 hours after adding water to the mixture (new concrete layer cast with w/c of 0.45 and unsealed top surface)

Depth from the top surface (mm)	Shrinkage strains values (με)						
	Monolithic (50 mm)	Smooth Substrate			Rough Substrate		
		SSD	SW	OD	SSD	SW	OD
3	1220	270	330	140	250	180	140
20	1230	240	190	80	190	110	80
40	1170	120	110	30	110	150	30

As shown in *Table 5.8* and *Table 5.9*, a comparison between the 50 mm thick monolithic unsealed specimens and the new concrete layer cast on SSD substrate with smooth surface showed that significantly lower "absolute" shrinkage strains values were observed in the new concrete layer, indicating that in the case of unsealed composite specimens with SSD substrate, there seems to be negligible moisture migration to the SSD substrate.

A comparison between unsealed composite specimens with different substrate moisture conditions indicated that the "absolute" shrinkage strains values at all depths of the new concrete layer decreased with dryer substrates. This behavior was observed for both the C25 and

C45 new concrete layers. It can be seen that in the case of the C25 new concrete layer cast on smooth substrate with SSD, SW, and OD substrate, the 'absolute" shrinkage strains monitored near the interface (i.e. at a depth of 40 mm from the top exposed surface) registered a value of 120 με , 140 με, and 60 με respectively. At a depth of 3 mm from the top exposed surface, a similar trend was observed. The C25 new concrete layer cast on smooth substrate with SSD, SW, and OD substrate registered "absolute" shrinkage strain values of 420 με, 370 με, and 250 με respectively. These results are particularly important since it usually expected that since the OD substrate has the highest moisture absorption; it should give rise to higher shrinkage strains in the new concrete layer.

Based on the results obtained, it seemed that in the case of unsealed composite specimens, the moisture absorption by a dry substrate may exacerbate the effect of evaporation, causing the new concrete layer to stiffen at an earlier time. This mechanism may result in lower shrinkage strains being registered in the new concrete layer cast on OD substrate. In addition, in the case of SSD and SW substrate, analogous to that of the Interfacial Tansition Zone of cement paste and aggregate (i.e. ITZ), there is a possibility of an "interfacial zone" being formed at the interface between the newly cast concrete and the substrate layer. In this interfacial zone, an increase in the local water-to-cementitious ratio may occur thus creating a porous layer with low bonding strength that may act as a "sliding layer" for the new concrete layer. This result is in agreement with a previous study reported by Morgan (1996). It was reported that an excessively wet surface (i.e. defined as a surface conditions that would wet when a hand is drawn over it) would result in a high local water-to-cementitious ratio at the bond interface and thus may have a more damaging effect on the bond strength. The formation of "interfacial zone" may also explain the results obtained for the sealed composite specimens with SW substrate. As discussed previously in Chapter 5.3.3.2, the new concrete layer cast on SW substrate registered an increase in the shrinkage strains monitored near the interface when compared to that monitored for the composite specimens with OD substrate. Due to the formation of this "interfacial zone" in the composite specimens with SW substrate, the new concrete layer could shrink more compared to the same mixtures cast on OD substrate.

Figure 5.26 to *Figure 5.29* show plots of shrinkage strain-versus-time curve during plastic, transitional, and hardening stages of the unsealed monolithic specimens and composite specimens cast on substrate with different moisture conditions. As shown in *Figure 5.26* and *Figure 5.27*, the new concrete layer cast on SSD substrate with smooth surface registered a significantly lower shrinkage strains as compared to that monitored for the 50 mm thick monolithic specimens especially during the plastic and transitional stages. This indicated that the moisture absorption of SSD substrate was negligible and the restraining effect of the substrate at the interface was more dominant during these stages. In the case of the new concrete layer cast on the smooth substrate with different moisture conditions, the results showed that a more gradual increase in the shrinkage strains was observed with dryer substrates. A similar result was also observed in the case of the new concrete layer cast on the rough substrate, as shown in *Figure 5.28* and *Figure 5.29*. This behavior, as mentioned previously, could be attributed to the stiffening of the new concrete layer arising from the absorption of moisture from the newly cast concrete layer by the OD substrate and to the possibility of the "interfacial zone" formation at the interface of SSD and SW substrates.

In the last stage, i.e. hardening stage, given the accuracy of the present image analysis technique of about ± 12 με, the results showed that the effect of substrate moisture absorption was less apparent. The present results showed that there was no significant difference in the shrinkage strains monitored for composite specimens cast with the three different substrate moisture conditions.

.

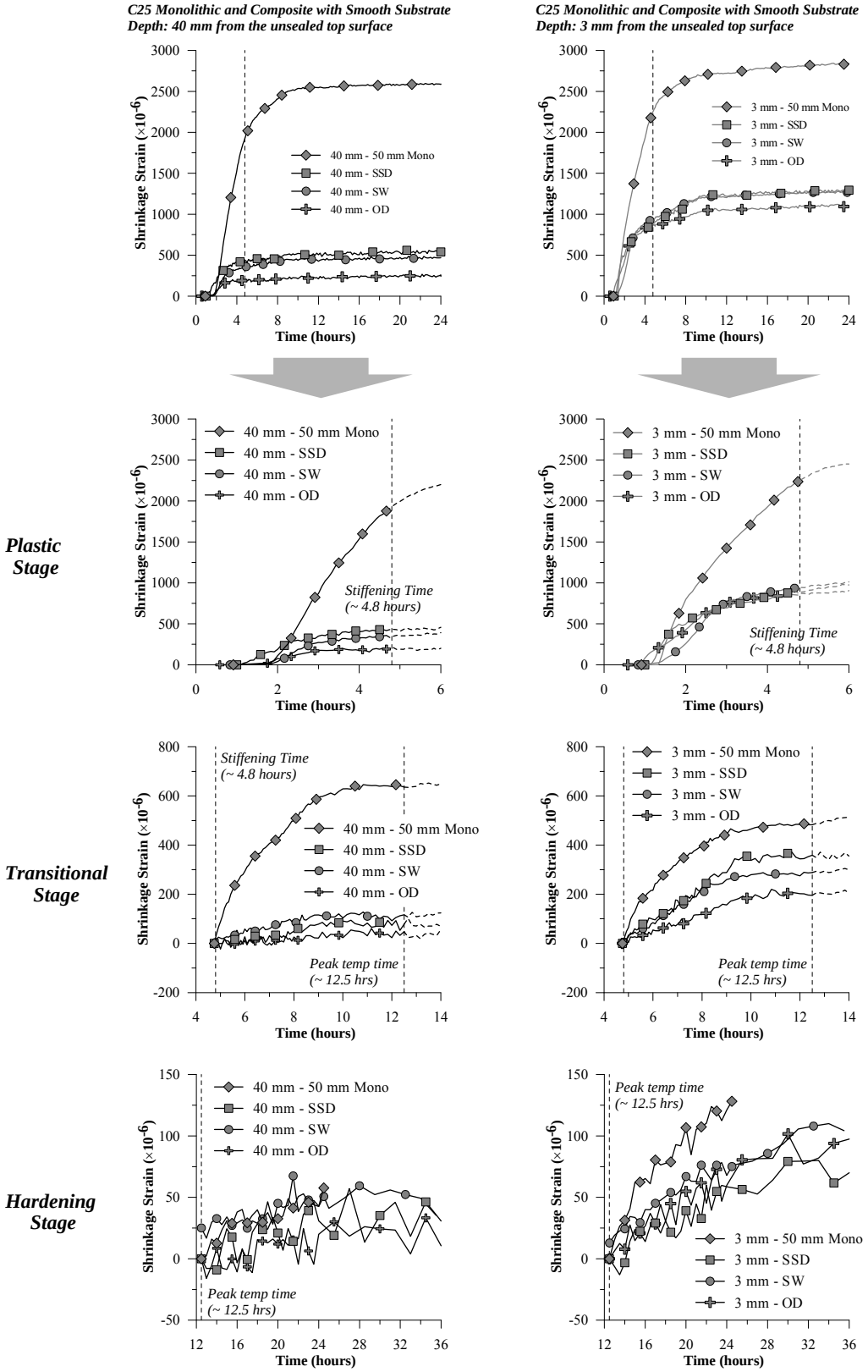

Figure 5.26 Early age shrinkage strains monitored at a depth of 40 mm and 3 mm from the top surface of the unsealed monolithic and unsealed composite specimens cast on substrate with smooth surface during plastic, transitional, and hardening stages (new concrete layer w/c = 0.25).

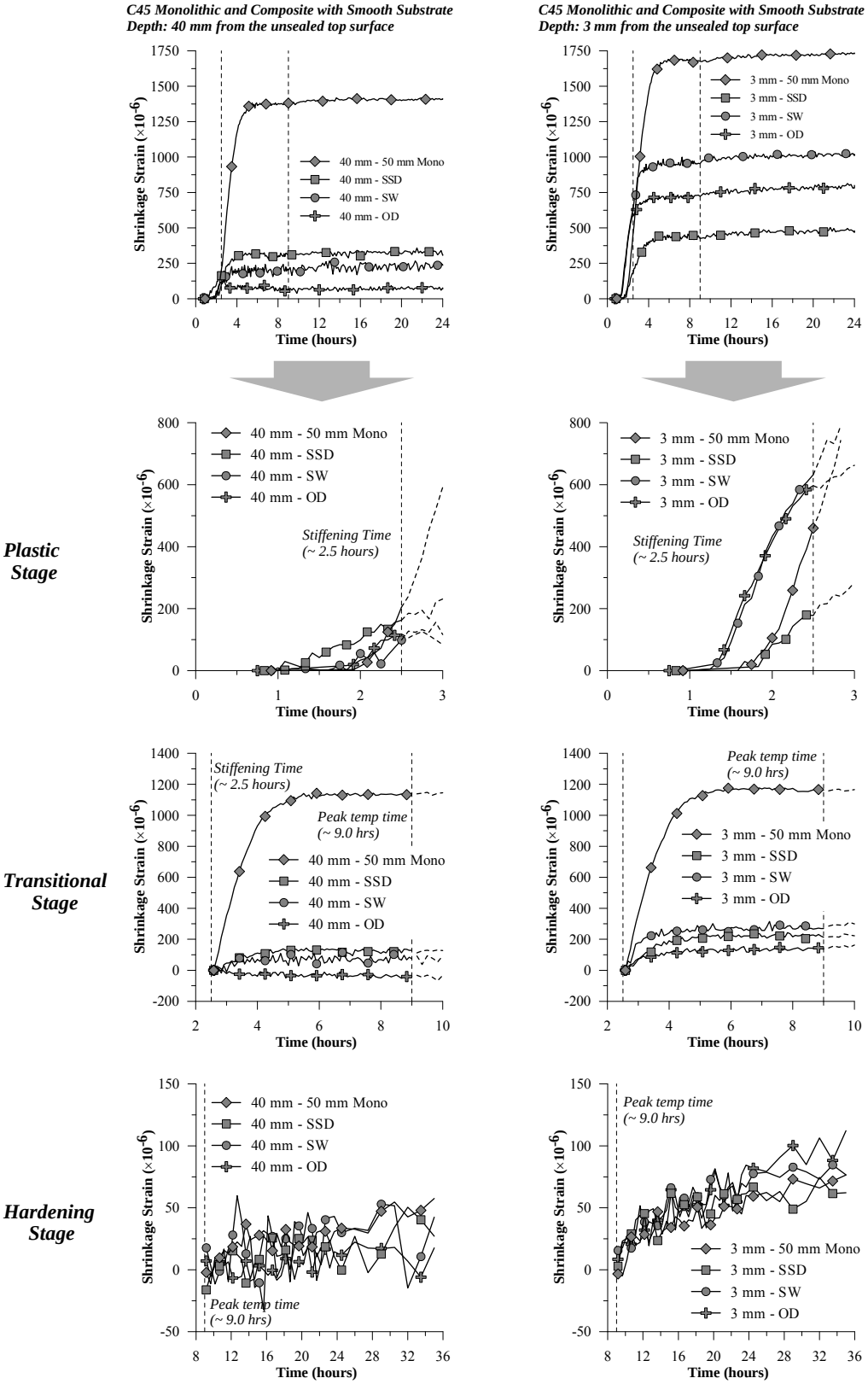

Figure 5.27 Early age shrinkage strains monitored at a depth of 40 mm and 3 mm from the top surface of the unsealed monolithic and unsealed composite specimens cast on substrate with smooth surface during plastic, transitional, and hardening stages (new concrete layer w/c = 0.45).

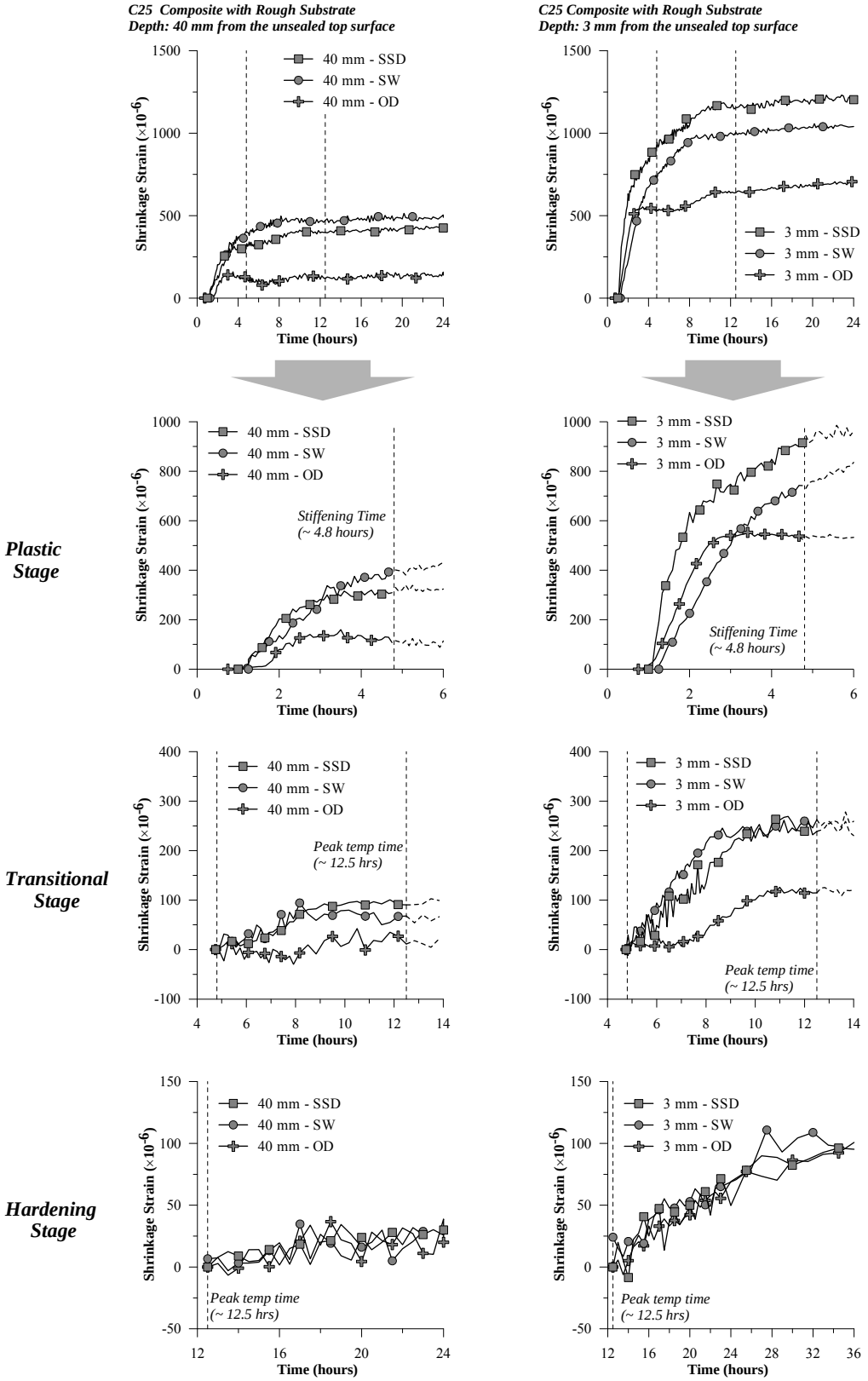

Figure 5.28 Early age shrinkage strains monitored at a depth of 40 mm and 3 mm from the top surface of the unsealed monolithic and unsealed composite specimens cast on substrate with rough surface during plastic, transitional, and hardening stages (new concrete layer w/c = 0.25).

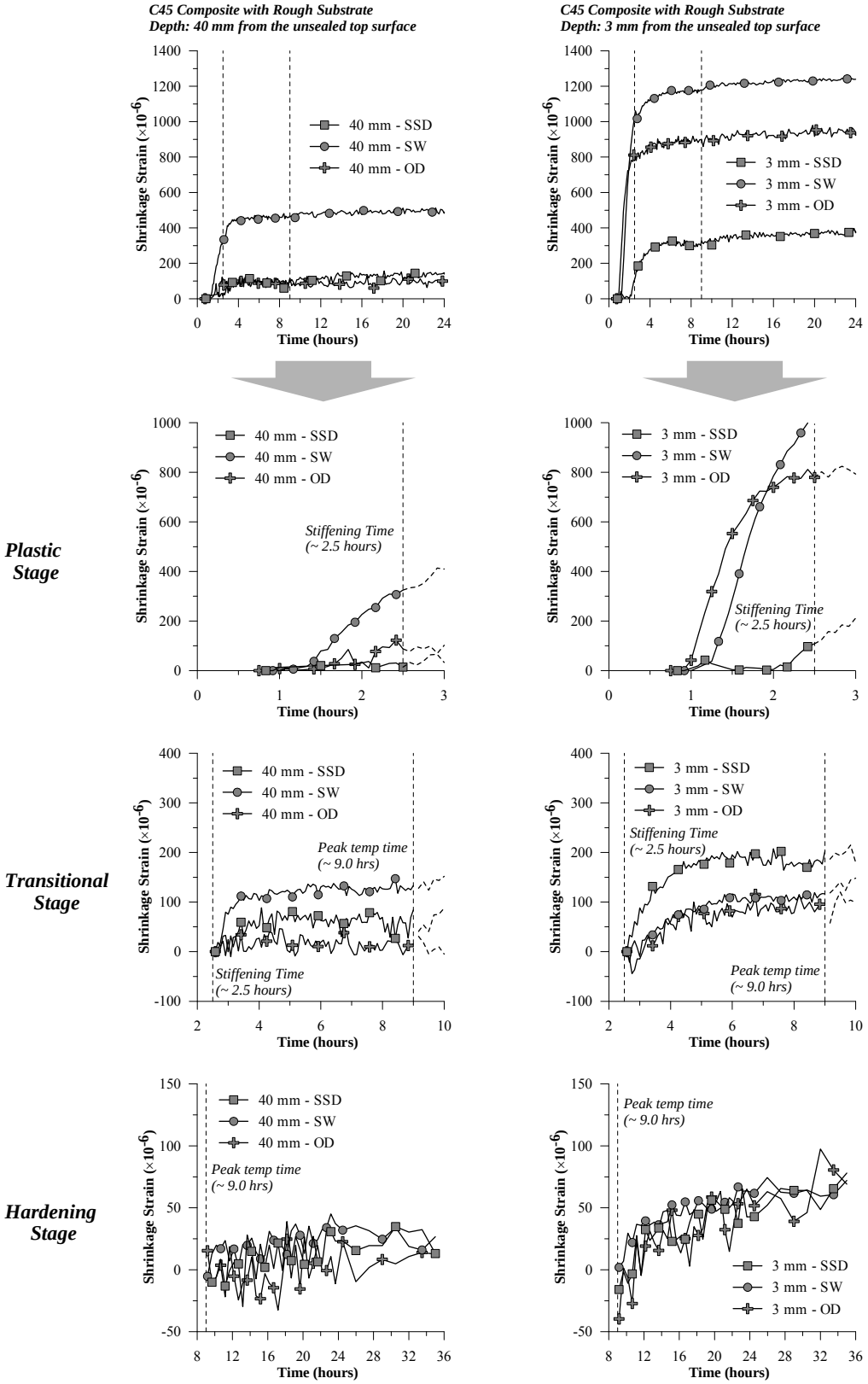

Figure 5.29 Early age shrinkage strains monitored at a depth of 40 mm and 3 mm from the top surface of the unsealed monolithic and unsealed composite specimens cast on substrate with rough surface during plastic, transitional, and hardening stages (new concrete layer w/c = 0.45).

5.3.5 Assessment of early age crack and de-lamination

As mentioned previously, two kinds of failure in composite systems due to early age shrinkage strain that are often reported are cracking and de-lamination of the new concrete layer. In the present study, there were no cracks visible to the naked eye on the top surface of the new concrete layer. The absence of surface crack could be attributed to several factors. First, the tensile creep and stress relaxation of the new concrete layer. It is well known that during early ages of cementitious material, it undergoes significant tensile creep and stress relaxation (Weiss et al. (1998),Cusson and Hoogeveen (2007)). Second, the lack of restraint at both ends of the composite specimen may also contribute to the absence of surface cracks. As the restraint was provided only at the bottom of the new concrete layer through interface bonding with the substrate concrete, this restraint may not be sufficient to induce surface cracks. Third, the size of the composite specimens used in the present investigation may not be sufficient to result in the formation of surface cracks.

On other hand, the occurrence of de-lamination or cracks at the interface was clearly observed in the composite specimens tested in the present study. *Figure 5.30* to *Figure 5.37* show images of interface near the ends of the C25 composite specimens. The substrate used was OD substrate with either the smooth or rough surfaces. The image was taken using the digital microscope (i.e. VMS-004) from the side of the specimen immediately after demolding at 6, 12, 18, and 24 hours after adding water to the new concrete mixture. The results showed that partial de-lamination at the interface was clearly visible as early as about 6 hours after adding water to the mixture especially in the composite specimens cast with smooth substrate. After initial observation from the top and the side of the composite specimens, the specimens were cut open. The cutting of composite specimen at 6 hours after adding water to the mixture could not be accomplished since the new concrete layer had not attained sufficient stiffness and bond strength at the interface. Due to this reason, the wet-cutting was only performed at the age of 12 hours and beyond. *Figure 5.38* to *Figure 5.40* show the de-lamination observed near the edge of the C25 composite specimens at 12, 18, and 24 hours after adding water to the new concrete mixture respectively. It can be seen that for both composite specimens cast with the smooth and

rough substrates, partial de-lamination at the interface between the two concrete layers was clearly visible.

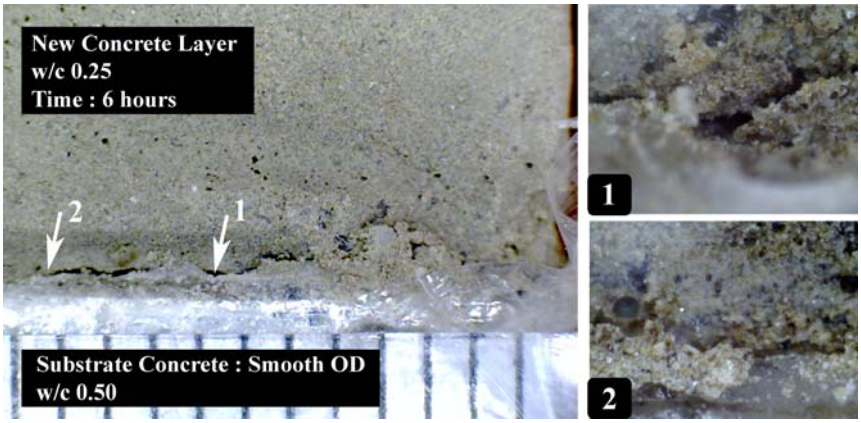

Figure 5.30 De-lamination at the interface of the unsealed composite specimen monitored from the side of the specimen at 6 hours after adding water to the mixture (OD substrate with smooth surface)

Figure 5.31 De-lamination at the interface of the unsealed composite specimen monitored from the side of the specimen at 12 hours after adding water to the mixture (OD substrate with smooth surface)

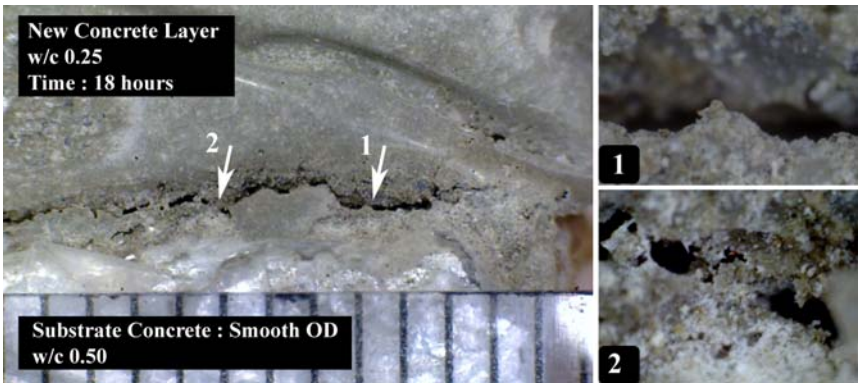

Figure 5.32 De-lamination at the interface of the unsealed composite specimen monitored from the side of the specimen at 18 hours after adding water to the mixture (OD substrate with smooth surface)

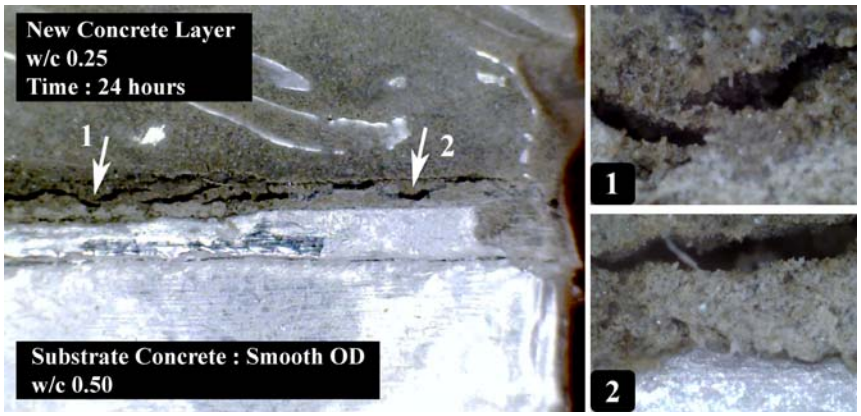

Figure 5.33 De-lamination at the interface of the unsealed composite specimen monitored from the side of the specimen at 24 hours after adding water to the mixture (OD substrate with smooth surface)

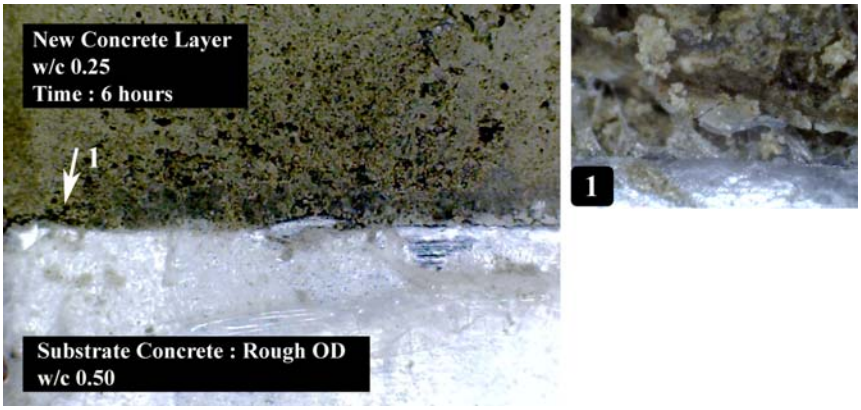

Figure 5.34 De-lamination at the interface of the unsealed composite specimen monitored from the side of the specimen at 6 hours after adding water to the mixture (OD substrate with rough surface)

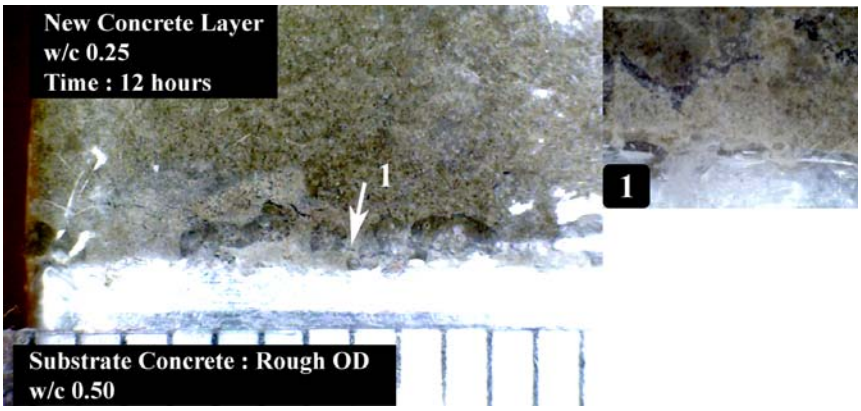

Figure 5.35 De-lamination at the interface of the unsealed composite specimen monitored from the side of the specimen at 12 hours after adding water to the mixture (OD substrate with rough surface)

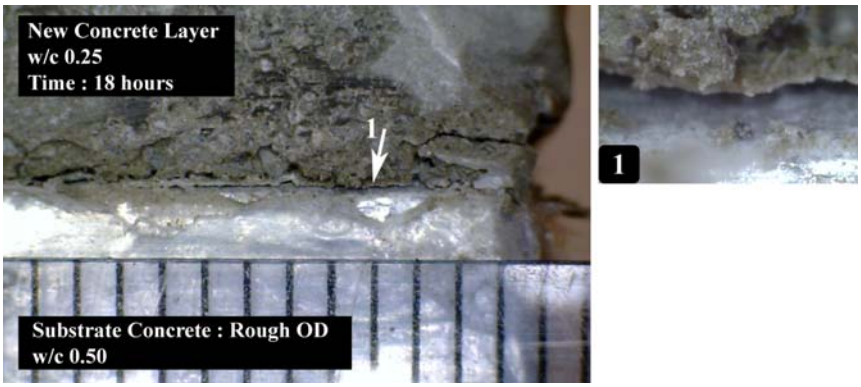

Figure 5.36 De-lamination at the interface of the unsealed composite specimen monitored from the side of the specimen at 18 hours after adding water to the mixture (OD substrate with rough surface)

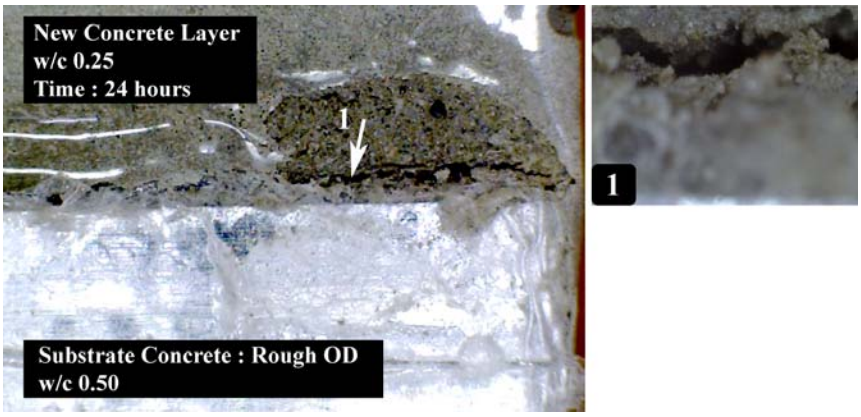

Figure 5.37 De-lamination at the interface of the unsealed composite specimen monitored from the side of the specimen at 24 hours after adding water to the mixture (OD substrate with rough surface)

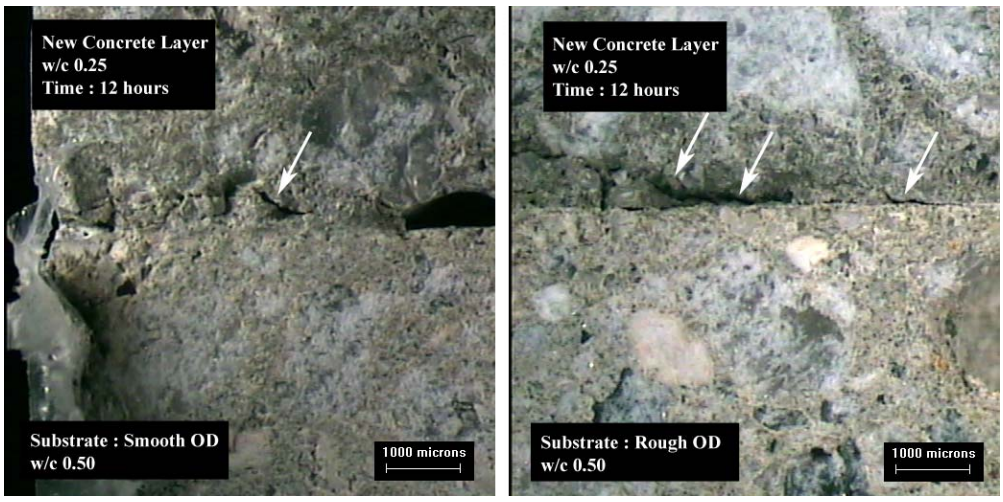

(a) *(b)*

Figure 5.38 De-lamination at the interface of the unsealed composite specimen with (a) smooth, and (b) rough substrate monitored from the cutting section of the specimen at 12 hours after adding water to the mixture

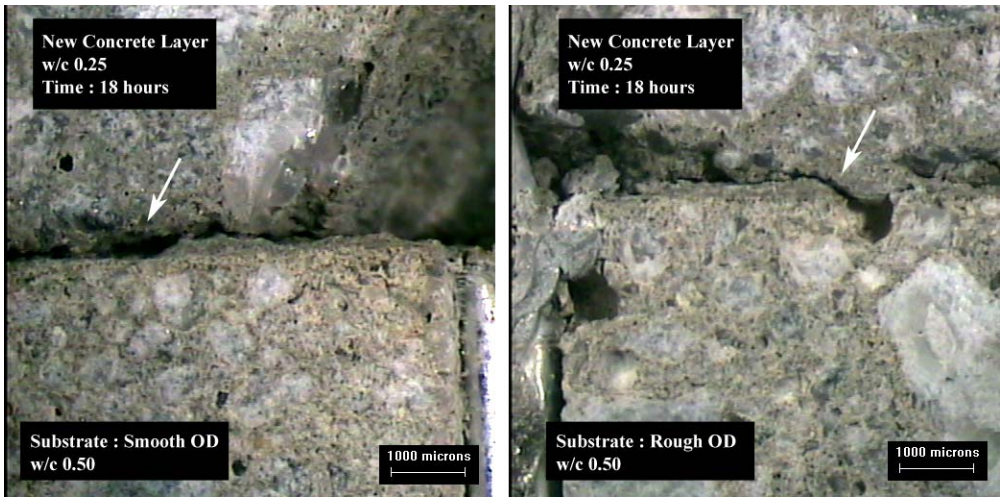

(a) *(b)*

Figure 5.39 De-lamination at the interface of the unsealed composite specimen with (a) smooth, and (b) rough substrate monitored from the cutting section of the specimen at 18 hours after adding water to the mixture

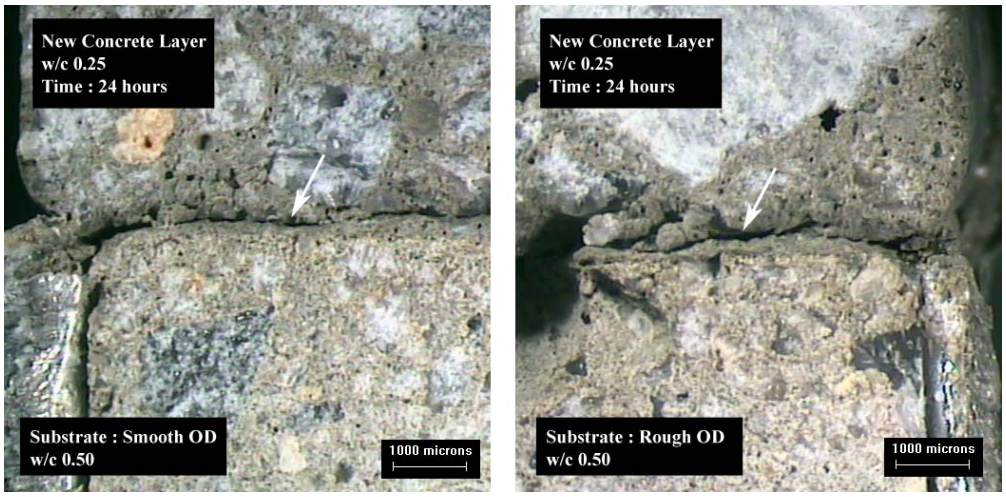

(a) *(b)*

Figure 5.40 De-lamination at the interface of the unsealed composite specimen with (a) smooth, and (b) rough substrate monitored from the cutting section of the specimen at 24 hours after adding water to the mixture

As mentioned previously, two approaches for measuring the crack widths by using the image analysis technique are possible. In the first approach, the crack widths were measured using the crack images captured. While in the second approach, the crack widths were measured by making use of the same target used for early age shrinkage monitoring.

Table 5.10 shows the results of crack width monitored at the interface between the two concrete layers by using the first approach. In this approach, an average and a maximum crack width at a distance of 10 to 20 mm from the ends of the composite specimens were measured

through the crack images taken from the side or from the cut cross-section of the composite specimens. Based on the results obtained, it can be seen that both the average and the maximum cracks widths increased with time. Although this approach was able to quantify cracks width, it is important to note that it may not be able to provide continuous information on how the cracks or de-lamination at the interface develop with time. In addition, some difficulties associated with this approach are noted. First, identifying the crack width may prove to be quite challenging as the cracks may be discontinuous along the length of the cracks. This discontinuity may affect the crack width measurement. Second, the wet-cutting process prior to the assessment of cracks or de-lamination may induce either additional cracks or the closure of cracks due to energy release through the cutting process. Third, the approach required a crack image to be taken either from the side of the composite specimens or from the cut cross-section of the composite specimens at a specific time. This may not be practical since time is always needed for sample preparation and the cutting process.

Table 5.10 Cracks width measurement from microscope & stereomicroscope

	Smooth Substrate				**Rough Substrate**			
Time	Crack width (μm) from side surface		Crack width (μm) from cut section		Crack width (μm) from side surface		Crack width (μm) from cut section	
	Average	Maximum	Average	Maximum	Average	Maximum	Average	Maximum
6 hrs	63	188	-	-	-	-	-	-
12 hrs	52	125	72	156	60	292	64	286
18 hrs	84	267	106	316	98	357	87	453
24 hrs	88	263	85	237	85	400	66	224

Note: cracks were measured at a distance of 10 to 20 mm from the ends of prism specimens.

In order to overcome these problems, the cracks width or the de-lamination was measured using the same targets used for early age shrinkage monitoring. Using the same composite specimens with images of the cracks taken from the side or from the cut cross-section of the composite specimens, the cracks width or the de-lamination development at the interface of the composite specimen was monitored by calculating the increase in the distance between a pair of targets located near the interface. In this approach, it was assumed that the increase in the

distance between the two targets would be equal to the increase in width of crack observed at the interface of the composite specimens. *Figure 5.41* show the typical development of cracks at the interface of the C25 unsealed composite specimens. It can be seen that the cracks developed rapidly from the start of the casting of the new concrete layer up to the time when the stiffening time of the new concrete layer occurred. After the stiffening time, a more gradual increase in the crack width was observed. In addition, the crack width measurement also showed that the targets located at 25 mm from the ends of the composite specimen registered wider cracks widths compared to those monitored using targets located at 75 mm from the ends of the composite specimens. This was expected since the de-lamination would start from the ends of the composite specimens and progressed into the middle portion of the composite specimens.

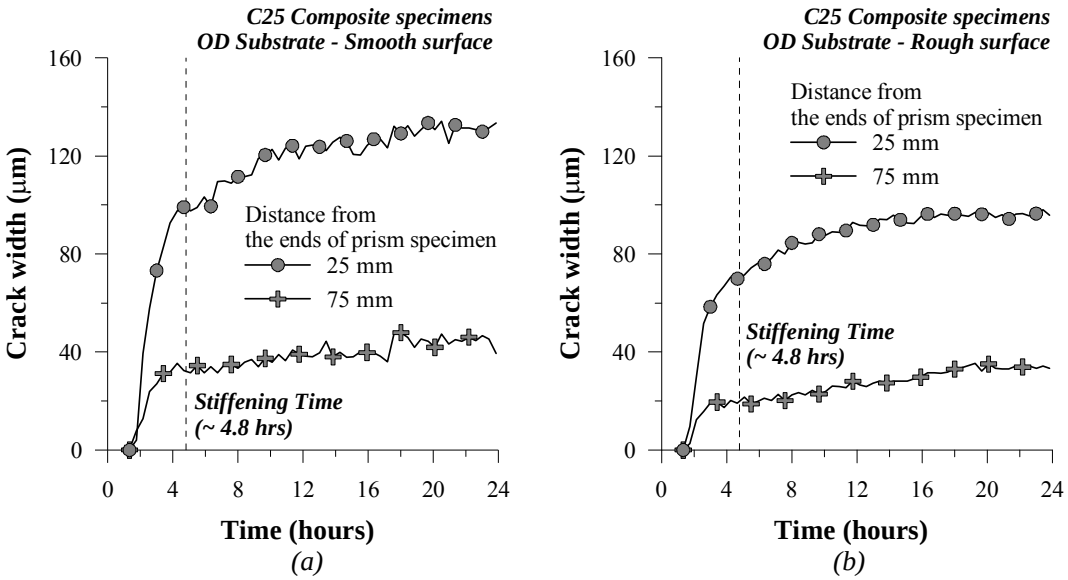

Figure 5.41 Cracks width monitored at the interface of C25 unsealed composite specimens with (a) smooth substrate, and (b) rough substrate during the first 24 hours after adding water to the mixture.

Repeatability of the cracks width measurements using the targets located near the interface were summarized in *Table 5.11*. Comparing the results of two similar composite specimens, it can be seen that the crack widths measured are in agreement. Considering the resolution of the present testing setup of about 4 μm as well as the possible variation in the composite specimens itself, a difference about 7 to 15 μm in the crack widths measured for the two composite specimens seems reasonable.

Comparing the crack widths measured using the crack images with those measured using the targets near the interface, it can be observed that the crack widths measured using the targets near the interface were generally wider than those measured using the crack images. This was not unexpected since it was assumed that the increase in the distance of these targets would correspond to the widening of the crack width at the interface. This may not be true in all cases. It was possible that several thin cracks parallel to the interface may develop within the two pair of targets monitored, thus the targets measured the "total" increase in crack width instead of the increase in individual crack width. Nevertheless, crack widths monitoring using the targets mounted near the interface may be more useful for assessing the development of cracks or de-lamination of the new concrete layer cast on different types of substrates.

Table 5.11 Repeatability of cracks widths measurement using a same target used for early age shrinkage monitoring

	Smooth substrate				**Rough substrate**			
	Crack width measured at 25 mm from the ends of specimen (μm)		Crack width measured at 75 mm from the ends of specimen (μm)		Crack width measured at 25 mm from the ends of specimen (μm)		Crack width measured at 75 mm from the ends of specimen (μm)	
Time	1st specimen	2nd specimen	1st specimen	2nd specimen	1st specimen	2nd specimen	1st specimen	2nd specimen
4.8 hrs	82	99	48	33	71	70	42	19
6 hrs	88	102	51	32	75	76	42	20
12 hrs	110	123	59	39	87	93	49	27
18 hrs	114	130	61	46	89	96	49	34
24 hrs	-	131	-	45	-	95	-	34

Note: + Measurement was started at about 30 minutes after adding water to the mixture
+ Location of the targets = 25 mm or 75 mm from the ends of 400 mm long prism specimen

5.3.5.1 Effect of Substrate Surface Preparations and Moisture Conditions

In the present study, the effect of substrate surface preparation and its moisture conditions on the development of de-lamination at the interface of composite specimens were investigated. *Table 5.12* to *Table 5.15* shows the cracks width measured at the interface of C25 and C45

composite specimens with either smooth or rough substrates. The "absolute" crack width values were measured at 24 hours after adding water to the new concrete layer.

Comparing the "absolute" cracks width values measured on composite specimens with smooth and rough substrates, the results showed that the composite specimens with smooth substrate generally registered wider cracks compared to that with a rough substrate. As expected, the composite specimens with a smooth substrate exhibit higher risks of de-lamination at the interface. In the composite specimens with a rough substrate, the grooves may provide mechanical interlocking that inhibits the occurrence and development of de-lamination and also prevents the cracks from developing further into the middle section of the composite specimens. As shown in *Figure 5.42*, a manual inspection from the cut cross-section of composite specimens showed that the cracks were apparent only towards the ends of the specimens up to the first groove which was located at about 20 mm from both ends of the composite specimens.

The effect of substrate moisture conditions on cracks development was also found to be significant. It can be seen that wider cracks were observed in all the composite specimens with the oven-dry (i.e. OD) substrate. In addition, the results also showed that water-ponding for about 1 hour prior to the casting of the new concrete layer did not significantly reduce the risk of partial de-lamination at the interface. The results of composite specimens with the SW substrate showed that the crack widths measured at the interface was only slightly narrower than that monitored on the composite specimens with the OD substrate.

Comparing the sealed and unsealed composite specimens, the results also indicated that sealing the top surface of the new 50 mm thick concrete layer may not be sufficient to reduce the risk of de-lamination at the interface, as moisture absorption by the substrate may cause the sealed composite specimens to register crack widths at the interface comparable with that monitored on the unsealed composite specimens. It can be seen from the results that in the case of both the C25 and C45 composite specimens with SW and OD substrates, the sealed and unsealed composite specimens registered comparable "absolute" cracks width values irrespective of the substrate roughness.

Table 5.12 Cracks width measurement of C25 sealed composite specimens

	Smooth substrate		**Rough substrate**	
Substrate moisture condition	Crack width at 25 mm (μm)	Crack width at 75 mm (μm)	Crack width at 25 mm (μm)	Crack width at 75 mm (μm)
SSD	0.0	3.0	7.0	7.0
SW	105.0	56.0	12.0	3.0
OD	136.0	63.0	95.0	42.0

Table 5.13 Cracks width measurement of C25 unsealed composite specimens

	Smooth substrate		**Rough substrate**	
Substrate moisture condition	Crack width at 25 mm (μm)	Crack width at 75 mm (μm)	Crack width at 25 mm (μm)	Crack width at 75 mm (μm)
SSD	37.0	23.0	22.0	0.0
SW	121.0	71.0	69.0	21.0
OD	130.0	73.0	82.0	23.0

Table 5.14 Cracks width measurement of C45 sealed composite specimens

	Smooth substrate		**Rough substrate**	
Substrate moisture condition	Crack width at 25 mm (μm)	Crack width at 75 mm (μm)	Crack width at 25 mm (μm)	Crack width at 75 mm (μm)
SSD	2.0	6.0	11.0	11.0
SW	42.0	20.0	34.0	8.0
OD	55.0	26.0	73.0	31.0

Table 5.15 Cracks width measurement of C45 unsealed composite specimens

	Smooth substrate		**Rough substrate**	
Substrate moisture condition	Crack width at 25 mm (μm)	Crack width at 75 mm (μm)	Crack width at 25 mm (μm)	Crack width at 75 mm (μm)
SSD	40.0	25.0	0.0	0.0
SW	64.0	20.0	47.0	29.0
OD	102.0	41.0	48.0	13.0

Note : SSD : water ponding for 24 hours prior to casting the new layer
SW : water ponding for 1 hour prior to casting the new layer
OD : oven-dry substrate

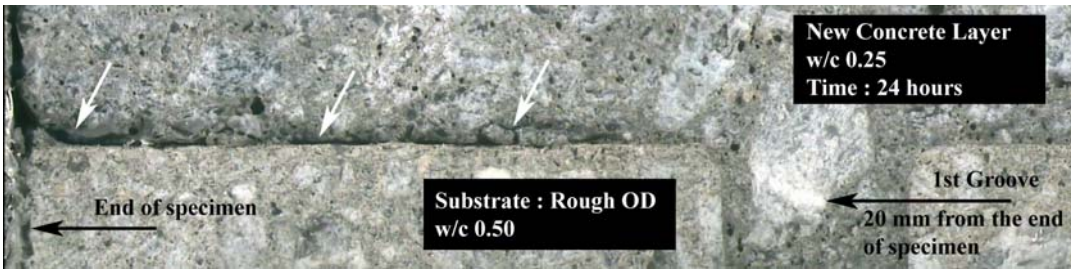

Figure 5.42 De-lamination at the interface of the composite specimen with rough substrate monitored from the cutting section of the specimen at 24 hours after adding water to the mixture

5.4 Summary

This chapter discusses the effect of substrate roughness and its moisture conditions on the development of early age shrinkage of a new concrete layer cast on top of old concrete substrate. In addition, the assessment of early age cracking and de-lamination due to early age shrinkage during the first 24 hours after adding water to the mixture was also performed. Based on experimental studies carried out, the following conclusions could be drawn:

1. The restraining effect of substrate surface roughness on early age shrinkage strains of the newly cast concrete layer was found to be significant at all depth, i..e both near the interface and near the top surface of a 50 mm thick new concrete layer.

2. The results showed that the restraining effect of substrate surface roughness was mainly observed during the plastic and transitional stages. While during the hardening stage, the restraining effect of substrate roughness was less apparent. In addition, the early age shrinkage strains monitored during the hardening stage were similar for both monolithic and composite specimens, suggesting that the new concrete layer shrank as much as the monolithic specimens.

3. The moisture conditions of the substrate concrete prior to the casting of the new concrete layer significantly influenced the early age shrinkage strain development of the 50 mm thick new concrete layer. The effect of substrate moisture absorption on the early age shrinkage development of the new concrete layer was also observed mainly in the plastic and transitional stages. Based on the results of the sealed and unsealed composite prism specimens, it is postulated that in the case of SSD and SW substrates, a presence of “interfacial zone” at the interface between the newly cast concrete and substrate layers may result in the formation of a

more porous layer with lower bonding strength. This more porous layer may act as a "sliding layer" and could give rise to slippage of the new concrete layer as indicated by higher "absolute" shrinkage strains values monitored. In addition, it also noted that the substrate moisture absorption may also exacerbate the effect of evaporation since it may lead to earlier stiffening time of new concrete layer. This mechanism may result in lower shrinkage strains be registered in the new concrete layer cast on OD substrate.

4. In this investigation, the targets used for early age shrinkage monitoring can also be used for the continuous monitoring of de-lamination development at the interface of composite specimens during the first 24 hours after adding water to the mixture with reasonable accuracy. This approach eliminates several difficulties associated with cracks width measurement such as the need to cut open the specimen to view the crack itself, the need for locating the cracks being formed, capturing images of cracks, and identifying the crack contour. In addition, the new approach may be more useful for assessing the development of cracks or de-lamination of the new concrete layer cast on different types of substrates.

5. The development of de-lamination on the composite specimens due to early age shrinkage strain during the first 24 hours after adding water to the mixture was clearly observed in the present study. The composite specimens with smooth substrate generally registered wider cracks compared to those with rough substrate. In the composite specimens with the roughened substrate, the presence of the groove seems to provide a higher mechanical interlocking as well as preventing the cracks from extending further towards the middle section of the composite specimens. The substrate moisture condition prior to the casting of the new concrete layer also plays a significant role in the de-lamination development at the interface. The results showed that a significant increase in the crack widths was observed in composite specimens with the SW and OD substrate. In addition, the results also suggested that sealing the top surface of the new 50 mm thick concrete layer may not be sufficient to reduce the risk of de-lamination at the interface, as moisture absorption by the substrate may cause the sealed composite specimens to register crack widths at the interface comparable with that monitored on the unsealed composite specimens.

Chapter 6 CONCLUSIONS AND RECOMMENDATIONS

6.1 Findings and Conclusions

This study is aimed at obtaining a better understanding of early age shrinkage of high performance cementitious mixtures monitored through test conducted on monolithic and composite prism specimens. More specifically, issues pertaining to the selection of "time zero value" (i.e. TZV) for early age shrinkage monitoring were discussed. The image analysis technique was modified in order that early age shrinkage strains may be monitored with respect to the depth from the top surface of cementitious prism specimen with acceptable accuracy. Simultaneously, the influence of material constituents on the development of shrinkage strains within prism specimens exposed to a dry environment from an early age was studied. The influence of substrate preparation on early age shrinkage strains and cracking (i.e. delamination) during the first 24 hours after adding water to the newly cast cementitious mixtures in composite prism specimens was also presented. The findings provide a better understanding of early age shrinkage of high performance cementitious mixtures cast monolithically and as a two layer composite prism specimen.

The main contribution of the present study can be summarized as follows:

1. S-wave reflection loss was shown to be a suitable method for selecting "time zero" value or TZV for early age shrinkage monitoring as it able to detect solid particles connectivity - the time when the cementitious mixture starts to develop its stiffness. The S-wave reflection loss could also be applied directly on various cementitious materials being tested from paste to concrete mixtures. Furthermore, the possibility of using the S-wave reflection loss technique to obtain stiffening time to be used as the TZV within the timeline along which early age shrinkage of cementitious materials occurs under both sealed and unsealed curing conditions had also been shown.

2. The results of mortar specimens tested in the present study seemed to show that for sealed specimens, a similar stiffening time occurred throughout the depth of the mortar specimens. On the other hand, in the case of unsealed mortar specimens, it was found that the stiffening time tends to vary with depth depending on the water-to-cementitious ratio of the mortar mixture used. In the case of mortar specimens cast with water-to-cementitious ratio of 0.20, a much earlier stiffening time especially near the top exposed surface.

3. For several gauge lengths tested (i.e. 75, 150, 200, and 250 mm) in the present study, the effect of gauge length used on the early age shrinkage strains monitored was found to be negligible in the case of sealed mortar prism specimens. However, a gauge length of less than 200 mm may not be suitable for unsealed prism specimens. The corresponding "absolute" shrinkage strain values were found to be lower than those obtained based on a nominal gauge length of 250 mm. The reduction in the "absolute" shrinkage strain values monitored when using shorter gauge lengths primarily occurred during the plastic stage, prior to the occurrence of the stiffening time. After the stiffening time, the "absolute" shrinkage strains value was less affected by the gauge length used. In this regard, it is recommended that gauge lengths in the order of 200 to 250 mm be used for early age shrinkage monitoring of typical prism specimens, especially unsealed prism specimens.

4. The present study showed that the image analysis technique can be used to monitor early age shrinkage strains with respect to the depth from the trowelled surface of monolithic mortar and concrete prism specimens starting as early as 30 minutes after adding water to the mixture with acceptable accuracy. This technique can be applied for either sealed prism specimens (generally used for autogenous shrinkage monitoring) or unsealed prism specimens (typical of those used for early age drying shrinkage monitoring). The results showed that as expected, the early age shrinkage strains monitored were relatively uniform across the whole cross section of the sealed prims specimen. On the other hand, the early age shrinkage strains varied significantly with depth from the exposed top surfaces of the unsealed prism specimens especially when adopting a chronologically earlier TZV.

5.

6. Experimental study on the influence of several mixture parameters on early age drying shrinkage strains of prism specimens showed that inclusion of superplasticizers significantly increased the early age shrinkage strains monitored at all depths during the first 24 hours after adding water to the mixture. The increase in the shrinkage strains monitored can be attributed to the side effect of HWRA in delaying the stiffening time as well as prolonging the transitional stage.

7. While it was typically observed in early age drying shrinkage monitoring that the "absolute" shrinkage strain values decreased with depth from the top exposed surface of prism specimens, in certain circumstances, such as in the case of mortar prism specimens cast with the higher aggregate volume, lower water-to-cementitious ratio, and/or with inclusion of silica fume, opposite behavior was observed. The "absolute" shrinkage strain values monitored near the exposed top surface might register lower values compared to those monitored near the base of the prism specimens. This opposite behavior could be attributed to the "skin layer" effect. As the top surface was exposed to a dry environment at such early ages, rigidity (i.e. stiffness) of the cementitious mixture near the top exposed surface may be affected. It is possible that within the "skin layer", the stiffness of the cementitious mixture increased rapidly compared to that of the interior. This increase in the cementitious mixture's stiffness would provide higher internal restraint locally thus reducing the early age shrinkage strains monitored.

8. The effect of substrate surface preparation and its moisture content prior the application of new concrete overlay on early age shrinkage strains of the new concrete layer was found to be significant both near the interface and within a 50 mm thick new concrete layer. In addition, based on the results of the sealed and unsealed composite prism specimens, it is postulated that in the case of SSD and SW substrates, a presence of "interfacial zone" at the interface between the newly cast concrete and substrate layers may result in the formation of a more porous layer with lower bonding strength. This more porous layer may act as a "sliding layer" and could give rise to slippage of the new concrete layer as indicated by higher "absolute" shrinkage strains values monitored. In addition, it also noted that the substrate moisture absorption may also exacerbate the effect of evaporation since it may lead to earlier

stiffening time of new concrete layer. This mechanism may result in lower shrinkage strains be registered in the new concrete layer cast on OD substrate.

9. The present study also showed that the same targets used for early age shrinkage monitoring can also be used for the continuous monitoring of de-lamination development at the interface of the composite prism specimens. It was found that composite specimens with smooth substrate generally registered wider cracks compared to those with a rougher substrate. In the composite specimens with the roughened substrate, the presence of the grooves seemed to provide higher mechanical interlocking and seemed to result in reduced propagation of cracks with time. The substrate moisture condition prior to the casting of the new concrete layer also played a significant role in the de-lamination development observed at the interface. The results showed that a significant increase in the crack widths was observed in composite specimens with the SW and OD substrate.

6.2 Recommendation for further study

The following are some suggestion for future research to obtain more insights on the early age shrinkage behavior of high performance cementitious mixtures:

1. The finding obtained from the assessment of the stiffening time via the shear-wave reflection loss technique is limited to rather low water-to-cementitious ratio mixtures cast with type I normal OPC. In the future, further study regarding the stiffening time of cementitious mixtures cast with other types of binders, as well as cementitious mixtures incorporating mineral and chemical admixtures should be carried out. In addition, as the present study was limited to the assessment of stiffening time in rather thin sections, the results of using thick / mass cementitious sections should be investigated in the future.

2. In this investigation, it is postulated that the water redistribution as well as the formation of a “skin layer” may significantly affect the occurrence of the stiffening time and the development of early age shrinkage strains in the unsealed prism specimens tested. In the future, analytical or numerical approaches can be carried out in order to shed more light on this issue.

3. Dealing with early age shrinkage monitoring, it is realized that there is still a need for some means of standardization to interpret the actual early age shrinkage strain values monitored using the various methods currently available for use. In the present investigation, a comparison was only made between early age shrinkage strains monitored using image analysis technique and those monitored using laser sensors. Perhaps future studies can be conducted on specimens tested using other early age shrinkage monitoring technique in order to shed more light on this particular issue. Nevertheless, it is important to note that a comprehensive understanding needs to take into account the various underlying and influencing factors arising from the adoption of a specific size of specimen, duration of monitoring, exposure conditions, mixture properties (w/c ratios, aggregate volume, etc.) and constituent materials (superplasticizers, silica fume, fly ash, GGBS, etc.).

4. It is realized that using prism specimen may not be representative of a number of field applications. Thus further test should be conducted to simulate actual field applications e.g. using specimens of various geometric dimensions, etc. This kind of information would be useful for estimating shrinkage strains that could be taken into consideration to meet the requirements of serviceability limit states during the design stage. In addition, it is possible to use the image analysis in order to investigate the restrained shrinkage behaviour of cementitious materials using a typical specimen of various geometric dimension, such as slab, etc. This information would be useful to assess the cracking risk of such cementitious material.

5. Although Chapter 4 provided a description on the influence of several key parameters such as superplasticizers, water-to-cementitious ratio, aggregate volume, and silica fume on the shrinkage development with respect to the depth from the top exposed surface of prism specimens, the influence of temperature, relative humidity and wind speed on early age drying shrinkage has not been fully investigated.

6. In the present investigation, only a few configurations of composite specimens were tested. Further tests are required to achieve a better understanding of early age shrinkage in composite specimens with other geometric and dimensional properties. In addition, an analytical

approach could be developed in order to shed more light on the behaviour of such composite systems.

REFERENCES

Abel, J. D. and Hover, K. C. (2000). "Field Study of the Setting Behavior of Fresh Concrete." Cement, Concrete and Aggregates **22**(2): 95-102.

Aggelis, D. G. and Philippidis, T. P. (2004). "Ultrasonic wave dispersion and attenuation in fresh mortar." NDT and E International **37**(8): 617-631.

Al-Amoudi, O. S. B., Abiola, T. O. and Maslehuddin, M. (2006). "Effect of superplasticizer on plastic shrinkage of plain and silica fume cement concretes." Construction and Building Materials **20**(9): 642-647.

Al-Amoudi, O. S. B., Maslehuddin, M. and Abiola, T. O. (2004). "Effect of type and dosage of silica fume on plastic shrinkage in concrete exposed to hot weather." Construction and Building Materials **18**(10): 737-743.

Al-Saleh, S. A. and Al-Zaid, R. Z. (2006). "Effect of drying conditions, admixtures and specimen size on shrinkage strains." Cement and Concrete Research **36**: 1985-1991.

Almusallam, A. A. (2001). "Effect of environmental conditions on the properties of fresh and hardened concrete." Cement and Concrete Composites **23**(4-5): 353-361.

ASTM-C33-08 (2008). "Standard Specification for Concrete Aggregates," ASTM C 33 / C33M-08. Annual Book of ASTM Standards. West Conshohocken, PA, American Society for Testing Materials. **04.02**.

ASTM-C143/C143M-09 (2009). "Standard Test Method for Slump of Hydraulic-Cement Concrete" ASTM C 143/C 143M-09. Annual Book of ASTM Standards, American Society for Testing Materials. **04.02**.

ASTM-C157/C157M-04 (2004). "Standard Test Method for Length Change of Hardened Hydraulic-Cement Mortar and Concrete," ASTM C 157/C 157M-04. Annual Book of ASTM Standards, American Society for Testing Materials. **04.02**.

ASTM-C191 (2004). "Standard Test Methods for Time of Setting of Hydraulic Cement by Vicat Needle," ASTM C 191-04b. Annual Book of ASTM Standards, American Society for Testing Materials. **04.02**.

ASTM-C403/403M (2008). "Standard Test Method for Time of Setting of Concrete Mixtures by Penetration Resistance," ASTM C 403/ C 403M-08. Annual Book of ASTM Standards, American Society for Testing Materials. **04.02**.

ASTM-C490-04 (2004). "Standard Practice for Use of Apparatus for the Determination of Length Change of Hardened Cement Paste, Mortar, and Concrete," ASTM C 490-04. Annual Book of ASTM Standards, American Society for Testing Materials. **04.02**.

ASTM-C494/C494M-08a (2008). "Standard Specification for Chemical Admixtures for Concrete," ASTM C494 / C494M - 08a
Annual Book of ASTM Standards, American Society for Testing Materials. **04.02**.

ASTM-C1437-07 (2007). "Standard Test Method for Flow of Hydraulic Cement Mortar," ASTM C 1437-07. Annual Book of ASTM Standards, American Society for Testing Materials. **04.01**.

Austin, S., Robins, P. and Pan, Y. (1995). "Tensile bond testing of concrete repairs." Materials and Structures **28**(5): 249-259.

Aïtcin, P.-C. (1999). Autogenous shrinkage measurement. Proceedings of the International Workshop on Autogenous Shrinkage of Concrete, Hiroshima, Japan, E & FN Spon.

Aïtcin, P.-C. (2001). High-Performance Concrete. New York, E & FN Spon.

Aïtcin, P.-C. and Neville, A. M. (2003). How the Water-cement Ratio Affects Concrete Strength. Concrete International. **25:** 51-58.

Banthia, N. and Gupta, R. (2009). "Plastic shrinkage cracking in cementitious repairs and overlays." Materials and Structures **42**(5): 567-579.

Bisschop, J. and van Mier, J. G. M. (2002). "How to study drying shrinkage microcracking in cement-based materials using optical and scanning electron microscopy?" Cement and Concrete Research **32**(2): 279-287.

Bjøntegaard, Ø., Hammer, T. A. and Sellevold, E. J. (2004). "On the Measurement of Free Deformation of Early Age Cement Paste and Concrete." Cement and Concrete Composites **26**: 427-435.

Bjøntegaard, Ø. and Sellevold, E. J. (2000). Interaction between Thermal Dilation and Autogenous Deformation in HPC. Proceedings of the International RILEM Workshop on Shrinkage of Concrete: Shrinkage 2000, France, Paris, RILEM.

Bjøntegaard, Ø. and Sellevold, E. J. (2004). Effects of Silica Fume and Temperature on Autogenous Deformation of High Performance Concrete Farmington HIlls, MI, American Concrete Institute.

Boivin, S., Acker, P., Rigaud, S. and Clavaud, B. (1999). Experimental Assessment of Chemical Shrinkage of Hydrating Cement Pastes. Proceedings of the International Workshop on Autogenous Shrinkage of Concrete, Hiroshima, Japan, E & FN Spon.

Boumiz, A., Vernet, C. and Cohen-Tenoudji, F. (1996). "Mechanical Properties of Cement Pastes and Mortars at Early Ages: Evolution with time and degree of hydration." Advanced Cement Based Materials **3**: 94-106.

Brinker, C. J. and Scherer, G. W. (1990). Sol-gel science : the physics and chemistry of sol-gel processing Academic Press**:** 908 pp.

Bury, M. A., Bury, J. R. and Martin, D. (1994). Testing Effects of New Admixtures on Concrete Finishing. Concrete International. **16:** 26-31.

Calleja, J. (1953). "Determination of Setting and Hardening Time of High-Alumina Cements by Electrical Resistance Technique " ACI Journal **25**(3): 249-256.

Carlswärd, J. (2006). Shrinkage cracking of steel fibre reinforced self compacting concrete overlays, Luleå University of Technology. **PhD Thesis:** 250.

Christensen, B. (2006). Time of Setting. Significance of Tests and Properties of Concrete and Concrete Making Materials, ASTM STP 169D. West Conshohocken, PA, ASTM International**:** 86-98.

Climaco, J. C. T. S. and Regan, P. E. (2001). "Evaluation of bond strength between old and new concrete in structural repairs." Magazine of Concrete Research **53**(6): 377-390.

Cusson, D. and Hoogeveen, T. (2007). "An experimental approach for the analysis of early-age behaviour of high-performance concrete structures under restrained shrinkage." Cement and Concrete Research **37**(2): 200-209.

D'Angelo, R., Plona, T. J., Schwartz, L. M. and Coveney, P. (1995). "Ultrasonic measurements on hydrating cement slurries : Onset of shear wave propagation." Advanced Cement Based Materials **2**(1): 8-14.

Dierckx, P. (1993). Curve and Surface Fitting with Splines. Oxford, United Kingdom, Oxford University Press.

Esping, O. (2007). Early age properties of self-compacting concrete – Effects of fine aggregate and limestone filler. Göteborg, Sweden, CHALMERS University of Technology. **PhD Thesis:** 206.

Gartner, E. M., Young, J. F., Damidot, D. A. and Jawed, I. (2001). Hydration of Portland cement. Structure and Performance of Cements. P. Barnes and J. Bensted. New York, Spon Press**:** 565 pp.

Glišić, B. and Simon, N. (2000). "Monitoring of concrete at very early age using stiff SOFO sensor." Cement and Concrete Composites **22**(2): 115-119.

Grasley, Z. C., Lange, D. A. and D'Ambrosia, M. D. (2006). "Internal Relative Humidity and Drying Stress Gradients in Concrete." Materials and Structures **39**: 901-909.

Grosse, C. U. and Reinhardt, H. W. (2001). "Fresh Concrete Monitored by Ultrasound Methods." Otto-Graf-Journal **12**: 157-168.

Hammer, T. (2001). "Effect of silica fume on the plastic shrinkage and pore water pressure of high-strength concretes." Materials and Structures **34**(5): 273-278.

Hammer, T. A. (1999). Test Methods for Linear Measurement of Autogenous Shrinkage Before Setting. Proceedings of the International Workshop on Autogenous Shrinkage of Concrete, Hiroshima, Japan, E & FN Spon.

Hammer, T. A. (2002). Why is High Strength Concrete so Susceptible to Cracking before Setting 6th International Symposium on Utilization of High Strength / High Performance Concrete, Leipzig.

Hobbs, D. W. (1974). "Influence of Aggregate Restraint on the Shrinkage of Concrete." ACI Journal Proceedings **71**(9): 445-450.

Holt, E. E. (2001). Early Age Autogenous Shrinkage of Concrete. Finland, Technical research Centre of Finland.

Holt, E. E. (2002). Very early age autogenous shrinkage: Governed by chemical shrinkage or selfdesiccation? Proceedings of the 3rd International Research Seminar on Self-desiccation and its Importance in Concrete Technology, TVBM-3104, Lund.

Holt, E. E. and Leivo, M. (1999). Autogenous Shrinkage at Very Early Ages. Proceedings of the International Workshop on Autogenous Shrinkage of Concrete, E & FN Spon.

Ishikawa, M., Imamoto, K., Watanabe, H. and Ito, M. (2000). Evaluation of autogenous shrinkage of concrete based on mechanical properties of the cement paste matrix.

Control of cracking in early age concrete : proceedings of the International Workshop on Control of Cracking in Early Age Concrete, Sendai, Japan.

JCI (1999). Autogenous Shrinkage of Concrete. Proceedings of the International Workshop on Autogenous Shrinkage of Concrete, Hiroshima, Japan.

Jensen, O. M. and Hansen, P. F. (1996). "Autogenous deformation and change of the relative humidity in silica fume-modified cement paste." ACI Materials Journal **93**(6): 539-543.

Kaufmann, J., Winnefeld, F. and Hesselbarth, D. (2004). "Effect of the addition of ultrafine cement and short fiber reinforcement on shrinkage, rheological and mechanical properties of Portland cement pastes." Cement and Concrete Composites **26**(5): 541-549.

Keating, J., Hannant, D. J. and Hibbert, A. P. (1989). "Correlation between Cube Strength, Ultrasonic Pulse Velocity and Volume Change for Oil Well Cement Slurries." Cement and Concrete Research **19**(5): 715-726.

Kim, B. and Weiss, W. J. (2003). "Using acoustic emission to quantify damage in restrained fiber-reinforced cement mortars." Cement and Concrete Research **33**(2): 207-214.

Kim, J. K. and Lee, C. S. (1998). "Prediction of Differential Drying Shrinkage in Concrete." Cement and Concrete Research **28**: 985-994.

Kyaw, M.-L. (2007). Early Age Shrinkage and Bond at Interface Between Repair Material and Concrete Substrate. Civil Engineering. Singapore, National University of Singapore. **PhD Thesis:** 252.

Lafhaj, Z., Goueygou, M., Djerbi, A. and Kaczmarek, M. (2006). "Correlation between porosity, permeability and ultrasonic parameters of mortar with variable water / cement ratio and water content." Cement and Concrete Research **36**(4): 625-633.

Lee, H. K., Lee, K. M., Kim, Y. H., Yim, H. and Bae, D. B. (2004). "Ultrasonic in-situ Monitoring of Setting Process of High Performance Concrete." Cement and Concrete Research **34**: 631-640.

Li, Z., Wei, X. and Li, W. (2003). "Preliminary interpretation of portland cement hydration process using resistivity measurements." ACI Materials Journal **100**(3): 253-257.

Li, Z., Xiao, L. and Wei, X. (2007). "Determination of concrete setting time using electrical resistivity measurement." Journal of Materials in Civil Engineering **19**(5): 423-427.

Loukili, A., Chopin, D., Khelidj, A. and Le Touzo, J.-Y. (2000). "New approach to determine autogenous shrinkage of mortar at an early age considering temperature history." Cement and Concrete Research **30**(6): 915-922.

Lura, P., Pease, B., Mazzotta, G. B., Rajabipour, F. and Weiss, J. (2007). "Influence of shrinkage-reducing admixtures on development of plastic shrinkage cracks." ACI Materials Journal **104**(2): 187-194.

Meddah, M. S., Aitcin, P.-C. and Petrov, N. (2006). A New Approach for the Determination of the Starting Point of Autogenous Shrinkage Strains (ASS). Seventh CANMET/ACI International Conference on Durability of Concrete. V. M. Malhotra**:** 473-484.

Mehta, P. K. and Monteiro, J. M. (1993). Concrete: Structure, Properties and Materials, 2nd Edition, Prentice Hall, Inc.

Mindess, S., Young, J. F. and Darwin, D. (2003). Concrete, Prentice Hall.

Miyazawa, S. and Tazawa, E.-c. (2001). Autogenous Shrinkage of Cementitious Material at Early Ages. Proceedings of the International Workshop on Control of Cracking in Early Age Concrete, Sendai, Japan, Sendai, Japan.

Morgan, D. R. (1996). "Compatibility of concrete repair materials and systems." Construction and Building Materials **10**(1): 57-67.

Morioka, M., Hori, A., Hagiwara, H., Sakai, E. and Diamon, M. S. (1999). Measurement of Autogenous Length Change by Laser Sensor Equipped with Digital Computer System. Proceedings of the International Workshop on Autogenous Shrinkage of Concrete, Hiroshima, Japan, E & FN Spon.

Neville, A. M. (2003). Properties of Concrete. England, Pearson Prentice Hall.

Olken, P. and Rostasy, F. S. (1994). A Practical Planning Tool for the Simulation of Thermal Stresses and for the Prediction of Early Thermal Cracks in Massive Concrete Structures Proceedings of RILEM Symposium: Thermal Cracking in Concrete at Early Age E & FN Spon.

Ong, K. C. G. and Kyaw, M.-L. (2006). "Application of Image Analysis to Monitor Very Early Age Shrinkage." ACI Materials Journal **103**: 169-176.

Ozturk, T., Rapoport, J., Popovics, J. S. and Shah, S. P. (1999). "Monitoring the Setting and Hardening of Cement Based Materials with Ultrasound " Concrete Science and Engineering **1**: 83-91.

Pease, B., Hossain, A. B. and Weiss, J. (2004). Quantifying Volume Change, Stress Development, and Cracking Due to Early-Age Autogenous Shrinkage ACI SP-220. O. M. Jensen, D. P. Bentz and P. Lura. Farmington HIlls, MI, American Concrete Institute**:** 23-38.

Perez-Pena, M. and Roy, D. M. (1989). "Influence of Chemical Composition and Inorganic Admixtures on the Electrical Conductivity of Hydrating Cement Pastes " Materials Research **4**(1): 215-223.

Pessiki, S. P. and Carino, N. J. (1988). "Setting Time and Strength of Concrete Using the Impact-Echo Method." ACI Materials Journal **85**: 389-399.

Popovics, S., Rose, J. L. and Popovics, J. S. (1990). "Behavior of ultrasonic pulses in concrete." Cement and Concrete Research **20**(2): 259-270.

Qi, C., Weiss, J. and Olek, J. (2003). "Characterization of plastic shrinkage cracking in fiber reinforced concrete using image analysis and a modified Weibull function." Materials and Structures **36**(6): 386-395.

Radocea, A. (1994). "Model of plastic shrinkage." Magazine of Concrete Research **46**(167): 125-132.

Rapoport, J., Popovics, J. S., Subramaniam, K. V. and Shah, S. P. (2000). "Using Ultrasound to Monitor Stiffening Process of Concrete with Admixtures." ACI Materials Journal **97**: 675-683.

Reinhardt, H., Große, C. and Herb, A. (2000). "Ultrasonic monitoring of setting and hardening of cement mortar—A new device." Materials and Structures **33**(9): 581-583.

Reinhardt, H. W. and Grosse, C. U. (1996). Setting and Hardening of Concrete Continuosly Monitored by Elastic Waves. Proceedings of the International RILEM Conference: Production Methods and Workability of Concrete, Paisley, Scotland, RILEM.

Rose, J. L. (1999). Ultrasonic waves in solid media. New York, Cambridge University Press.

Sant, G., Lura, P. and Weiss, J. (2006). "Measurement of Volume Change in Cementitious Materials at Early Ages " Transportation Research Board **1979**: 21-29.

Sant, G., Rajabipour, F., Lura, P. and Weiss, J. (2006). Examining time-zero and early age expansion in pastes containing shrinkage reducing admixtures (SRA's). 2nd International RILEM Symposium on Advances in Concrete through Science and Engineering, RILEM Publications SARL.

Savitsky, A. and Golay, M. J. E. (1964). "Smoothing and differentiation of data by simplified least squares procedure." Analytical Chemistry **36**(8): 1627 - 1639.

Sayers, C. M. and Dahlin, A. (1993). "Propagation of Ultrasound Through Hydrating Cement Pastes at Early Times." Advanced Cement Based Materials **1**: 12-21.

Schindler, A. K. (2004). Prediction of Concrete Setting. RILEM International Symposium on "Advances in Concrete Through Science and Engineering", Evaston, Illinois, RILEM.

Shin, H.-C. and Lange, D. A. (2004). "Effects of shrinkage and temperature in bonded concrete overlays." ACI Materials Journal **101**(5): 358-364.

Slowik, V., Schlattner, E. and Klink, T. (2004). "Experimental investigation into early age shrinkage of cement paste by using fibre Bragg gratings." Cement and Concrete Composites **26**(5): 473-479.

Springenschmidt, R., Breitenbucker, R. and Mangold, M. (1994). Development of the Cracking Frame and Tempereture Stress Testing Machine. Proceedings of RILEM Symposium: Thermal Cracking in Concrete at Early Age E & FN Spon.

Stepisnik, J., Lukac, M. and Kocuvan, I. (1981). "Measurement of cement hydration by ultrasonics." American Ceramic Society Bulletin **60**(4): 481-483.

Subramaniam, K. V., Lee, J. and Christensen, B. (2005). "Monitoring the setting behavior of cementitious materials using one-sided ultrasonic measurements." Cement and Concrete Research **35**: 850-857.

Takada, K., Van Breugel, K., Koenders, E. A. B. and Kaptija, N. (1999). Experimental Evaluation of Autogenous Shrinkage of Lightweight Aggregate Concrete. Proceedings of the International Workshop on Autogenous Shrinkage of Concrete, Hiroshima, Japan, E & FN Spon.

Tazawa, E.-c. and Miyazawa, S. (1995). "Chemical Shrinkage and Autogenous Shrinkage of Hydrating Cement Paste." Cement and Concrete Research **25**: 288-292.

Tazawa, E.-c. and Miyazawa, S. (1999). Effect of Constituents and Curing Condition on Autogenous Shrinkage of Concrete. Proceedings of the International Workshop on Autogenous Shrinkage of Concrete, Hiroshima, Japan, E & FN Spon.

Tazawa, E.-c. and Miyazawa, S. (2001). Autogenous Shrinkage: Present Understanding and Future Research Needs. Proceedings of the International Workshop on Control of Cracking in Early Age Concrete, Sendai, Japan, E & FN Spon.

Voigt, T. (2005). The Application of an Ultrasonic Shear Wave Reflection Method for Nondestructive Testing of Cement-Based Materials at Early Ages, Books on Demand GmbH.

Voigt, T., Grosse, C. U., Sun, Z., Shah, S. P. and Reinhardt, H. W. (2005). "Comparison of Ultrasonic Wave Transmission and Reflection Measurement with P- and S-waves on Early Age Mortar and Concrete " Materials and Structures **38**: 729-738.

Voigt, T. and Shah, S. P. (2003). Nondestructive Monitoring of Setting and Hardening of Portland Cement Mortar with Sonic Methods. Proceedings of the Sixth International Symposium on Non-Destructive Testing in Civil Engineering (NDT-CE 2003), Berlin, Germany.

Voigt, T., Ye, G., Sun, Z., Shah, S. P. and van Breugel, K. (2005). "Early age microstructure of Portland cement mortar investigated by ultrasonic shear waves and numerical simulation." Cement and Concrete Research **35**(5): 858-866.

Wahba, G. (1990). Spline Models for Observational Data Philadelphia, PA, SIAM.

Wall, J. S. and Shrive, N. G. (1988). "Factors Affecting Bond Between New and Old Concrete." ACI Materials Journal **85**(2): 117-125.

Wei, X. and Li, Z. (2005). "Study on hydration of Portland cement with fly ash using electrical measurement." Materials and Structures/Materiaux et Constructions **38**(277): 411-417.

Weiss, J. (2002). Experimental Determination of the "Time Zero" t_0 (Maturity-Zero M_0). RILEM Technical Committee 181-EAS: Early Age Cracking in Cementitious Systems.

Weiss, W. J., Sheissl, A. and Shah, S. P. (1998). Shrinkage cracking potential, permeability and strength of HPC: Influence of W/C, silica fume, latex and shrinkage reducing admixture. Int. Symp. on High Performance and Reactive Powder Concrete, Sherbrooke, Canada.

Whiting, N. M. and Snyder, M. B. (2003). "Effectiveness of Portland Cement Concrete Curing Compounds." Transportation Research Record(1834): 59-68.

Wong, A. C. L., Childs, P. A., Berndt, R., Macken, T., Gang-Ding, P. and Gowripalan, N. (2007). "Simultaneous measurement of shrinkage and temperature of reactive powder concrete at early-age using fibre Bragg grating sensors." Cement and Concrete Composites **29**(6): 490-497.

Xiao, L. and Li, Z. (2008). "Early-age hydration of fresh concrete monitored by non-contact electrical resistivity measurement." Cement and Concrete Research **38**(3): 312-319.

Xu, W. (1999). Durability of Repaired Structure. Civil Engineering, National University of Singapore. **PhD Thesis:** 291.

Zhang, M. H., Tam, C. T. and Leow, M. P. (2003). "Effect of water-to-cementitious materials ratio and silica fume on the autogenous shrinkage of concrete." Cement and Concrete Research **33**(10): 1687-1694.